



TESIS DOCTORAL

OXIDACIÓN FOTOCATALÍTICA DE HERBICIDAS EN AGUA
MEDIANTE RADIACIÓN DE BAJA ENERGÍA. APLICACIÓN DE
CATALIZADORES, OZONO Y PROMOTORES PEROXÍDICOS

PHOTOCALYTIC OXIDATION OF AQUEOUS HERBICIDES WITH
RADIATION OF LOW ENERGY. APPLICATION OF CATALYSTS,
OZONE AND PEROXIDIC PROMOTERS

RAFAEL RODRÍGUEZ SOLÍS

Departamento de Ingeniería Química y Química Física

Conformidad de los directores

Fdo.: F. Javier Rivas Toledo

Fdo.: Olga Gimeno Gamero

Fdo.: José Luis Pérez Bote

2017



TESIS DOCTORAL

OXIDACIÓN FOTOCATALÍTICA DE HERBICIDAS EN AGUA
MEDIANTE RADIACIÓN DE BAJA ENERGÍA. APLICACIÓN DE
CATALIZADORES, OZONO Y PROMOTORES PEROXÍDICOS

PHOTOCALYTIC OXIDATION OF AQUEOUS HERBICIDES WITH
RADIATION OF LOW ENERGY. APPLICATION OF CATALYSTS,
OZONE AND PEROXIDIC PROMOTERS

**Memoria presentada para optar al Grado de
Doctor con mención Internacional**

RAFAEL RODRÍGUEZ SOLÍS

Departamento de Ingeniería Química y Química Física

Badajoz, 2017

A mis hermanos Inma y Alejandro

El presente trabajo ha sido realizado bajo la concesión de una beca de Iniciación a la Investigación para no doctores (Acción II) encuadrada en el 'Plan de Iniciación a la Investigación, Desarrollo Tecnológico e Innovación de la Universidad de Extremadura 2012'; y el posterior disfrute de un contrato de formación de personal predoctoral otorgado por la Consejería de Empleo, Empresa e Innovación del Gobierno de Extremadura, cofinanciado con Fondo Social Europeo (FSE), referencia de la ayuda PD12058. Asimismo, este trabajo ha sido posible gracias al apoyo económico sufragado por los proyectos de investigación de la Junta de Extremadura, GRU10012 y GR15033; y del CICYT a través de los proyectos CTQ2012-35789-C02-01 (*'Preparación de catalizadores y su aplicación en la eliminación de contaminantes refractarios de aguas residuales mediante ozonación fotocatalítica'*) y CTQ2015-64944-R (*'LED y fotocatalizadores polifuncionales basados en grafeno y estructuras metal-orgánicas para el tratamiento de aguas por ozonación fotocatalítica'*), sufragados con fondos FEDER. Por último, también agradecer al MINECO por la financiación recibida en la red de Excelencia FOTOCAT, acción de dinamización CTM2015-71054-REDT (*'Nuevos materiales y reactores fotocatalíticos para la eliminación de microcontaminantes y patógenos'*).



AGRADECIMIENTOS

La realización de esta tesis no ha sido fácil. Ni rápida. Sin embargo, con esfuerzo y sacrificio, el trabajo sale adelante. Han sido muchos los obstáculos, que gracias a todos los que aquí abajo menciono, se han podido sortear.

En primer lugar me gustaría agradecer al investigador principal del grupo *TRATAGUAS*, el Dr. Fernando J. Beltrán Novillo, por brindarme la oportunidad de desarrollar esta tesis en su equipo de trabajo. También, agradecer a todos los integrantes del grupo que en mayor o menor medida también han arrojado su granito de arena.

Siguiendo el orden cronológico, mostrar mi especial agradecimiento a mi *padre científico* o director de tesis, el Dr. F. Javier Rivas Toledo. No sólo por adoptarme desinteresadamente, porque los hijos pueden salirle a uno rebeldes, o no; sino también por la confianza depositada en las incontables ocasiones, o la libertad proporcionada para desarrollar el trabajo. Paciencia, mucha paciencia. Al final, pienso que no nos ha quedado un trabajo tan feo como pensábamos. Enhorabuena. También a los codirectores, el Dr. Jose Luis Pérez Bote y la Dra. Olga Gimeno Gamero, que han completado la labor de dirección, y enriquecido el trabajo con su ayuda y conocimientos.

Me gustaría mencionar la ayuda aportada desde la secretaría del Vicerrectorado de Investigación de esta, nuestra Universidad, y desde el Servicio de Recursos para la Investigación Científica de la Secretaría General de Ciencia y Tecnología de la Junta de Extremadura, nombre actualizado a 27 de febrero de 2017. Con tantos cambios uno se obnubila. Cualquier becario sabe de quiénes hablo, Isabel Rocha Gómez y Manuela del Río Montero, guías y protectoras de becarios desconsolados. El papeleo en España nunca fue gratificante, ni ágil, como ya lo denunciaba Larra en su *Vuelva usted mañana*.

Nada más bajar al laboratorio a trabajar, la palabra gracias se hace ya habitual. Los compañeros, bautizados como *researcheros del Sotelo*, ¿a quién le surgiría tan feliz idea?, conforman una segunda familia. Ya sea por actitud u obligación, las horas pasadas, en fin, ya me entendéis, que uno acaba cogiéndoles cariño. Y menos mal que es así, porque de otra forma se hace duro, y aburrido, trabajar. En casi seis años, y como en la propia vida en la que unos van y otros vienen, alguno aquí se reirá, no han sido pocos los individuos con los que he podido compartir muchísimos recuerdos.

Comencemos por el laboratorio 1, con los bautizados recientemente como *tratagüitas*. ¡Qué bien se me da esto de inventar! Nada más cacharrear, Azahara fue la primera en prestar su ayuda desinteresada en labores como dónde está este vial, cómo se colocan los reactivos, o cómo proceder para analizar. E instauró la moda de los vídeos de tesis. Por aquellos tiempos, andaba también Gracy, siempre corriendo y resoplando con su peculiar flequillo hacia atrás. Pero, a ver quién le decía nada a la *jefa del laboratorio*, cargo que nadie volvió seriamente a desempeñar. Diego vino a hacer las Españas, y se marchó a su América natal. Tranquilo pero trabajador, siempre el último en cerrar el laboratorio. Con Diego recuerdo innúmeras anécdotas, relacionadas con, sobre todo, su castellano antiguo, o los brackets a los que tanto cariño les había cogido que no se los quería ni quitar. ¿Juan José? Eso no es aquí, se han equivocado. Ah, Sagasti sí. Me enseñó a destripar aparatos cual experto que sabe lo que está desmontado, a hacer señales en los tornillos para no apretar de más, a cómo colocar el teflón en las piezas a roscar, y un sinfín más de tareas rutinarias de bricomanía para laboratorio. El tubo naranja hasta nos quedó bonito. Ana, o Ana Rey desde hace algún tiempo para diferenciar, constituye la voz sabia a la que consultar en caso de duda. Todo aquel que haya tenido la oportunidad de trabajar contigo sabe de qué hablo. No hace falta que diga más. Como última incorporación sería llegó Ana María, o AnaMari para abreviar. A AnaMari hay mucho que agradecer dado que está dispuesta siempre a dejar lo suyo para ayudar. O tranquilizar, porque cuando uno se adapta a su ritmo, las cosas se ven diferente. Ánimo que te queda menos. Te dejamos la labor de transmisión de conocimientos y tradiciones de becario padre a becario hijo. De vez en cuando, Eva nos premia con su presencia por el laboratorio, con un *jur jur* por aquí, y un *jur jur* por allá, embriagándonos con su particular alegría y vitalidad. Y..., no es que me olvide de alguien, le dejo para un párrafo individual. También he de mencionar a todos aquellos, con los que aunque en menor extensión, he compartido gratos momentos. No me olvidaré del día en el que tras romper el pozo, Almudena dijo: 'se está aguantando para no llorar'. De Ángel heredé espacio y material. Se desprendió del, si no raudo ordenador, del huequecito que este ocupaba. Así me instalé junto a la impresora. Algunas tardes, cargada de galletas de mantequilla, era posible percibir un rastro inconfundible de perfume. Era Mercedes, siempre transmitiendo sonrisas y positividad.

Para evitar conflictos, a los de *enfrente* en párrafo aparte. Aunque nos separe el pasillo, las incursiones interlaboratorio, han sido frecuentes y obligadas. Siempre hubo alguna excusa para un pastelito y juntarnos todos. Gracias a todos. A Elena por ser tan así, tan tú, en fin, tan achuchable. Además de polivalente. Desde *close friend* en la escuela de idiomas a compañera de

congresos accidentados. Y siempre con una envidiable sonrisa en la cara. No diré mucho más que no te quiero hacer llorar. También tenemos, digo teníamos, a Francisco Casas. Quizás le recuerden más como Paco y Medio, Paco Canales, Paco McClure, Paco Jiménez, y muchos más nombres que quedan por llegar. Luego, cerca de la puerta se sentaba, esta chica... ummm, ¿cómo se llamaba? Patricia Palo dicen quienes la conocían. Después de irse Patri, María Jesús instaló su estufa bajo el ordenador, siempre encendida ya fuera enero o septiembre. De vez en cuando venía Mar desde el edificio Eladio Viñuela, donde fue desterrada en sus inicios, proclamándose reina de las algas. Después han ido saliendo y entrando, para volver a salir, Bea, Virginia, Miriam que sigue los pasos acelerados de Sagasti, o Anabel.

‘¿Habéis avisado a Nuria?’ Esa era la frase habitual en todas las reuniones dulceras. En el laboratorio del rincón, se situaba Nuria. O la chica kínder, como la llegamos a bautizar. Nuria era de especial utilidad cuando se necesitaba calibrar los rotámetros o había algún problema con los gases. Gracias.

Ahora sí, es tu turno. Empezamos esta aventura universitaria allá por el 2005, y junto con Ana García Calle nos hicimos casi inseparables. Luego Ana se nos fue para Barcelona, y nos quedamos nosotros por la Universidad. ¿Qué puedo decir de Estefanía? Tantos años han dado para entendernos tanto... Si trabajamos bien de forma individual, en equipo ya no hay quien nos gane. Darte las gracias por aguantarme, digo aguantarnos, ayudar, entenderme, y sobre todo, saber sin tener que preguntar... en fin. No sé ni qué escribirte. Eso sí, lo de trabajar juntos en el futuro ni hablar. Es broma. Ojalá.

Y de forma inesperada, me fui a Almería. ‘Solo pide que no se mueva la falla tectónica que por ahí es habitual’, me dijo Javi. Me gustaría mostrar mi más sincera gratitud a la Dra. Ana Agüera López de la Universidad de Almería, con quien tuve la oportunidad de compartir dos meses en el CIESOL. Del trabajo codo con codo entre catedrática y becario, en el recién estrenado TripleTOF 5600+, aprendí mucho no, muchísimo. Muchas gracias por tu cercanía e implicación. Allí me topé también con grandes compañeros que me acogieron con los brazos abiertos. Agradecer a Anita, o Ana Belén, que dejó su trabajo aparcado para poder sacar adelante el ajeno. Fuiste una gran anfitriona, dentro y fuera del laboratorio. A Marina, nervio puro, con toques de locura y adrenalina. A Alejandro, preparando su petate para marchar a Chile; a Gracia con quien me sentí tan identificado; y, a Samira, que siempre andaba dispuesta a trastear y darle al asunto un toque de diversión. Gracias a todos aquellos compañeros con los que compartí andanzas y se me olvide nombrar.

Agora é o momento de mudar de língua. Devo ter nas minhas raízes algum antepassado português, de modo a explicar a minha paixão por esta terra e cultura. Daí que o Rafa fosse três meses para terras trasmontanas. Gostava

imenso de agradecer ao Dr. José Alcides Silvestre Peres, por me ter acolhido na *UTAD* e nas suas dependências laboratoriais, dispondo tudo à minha vontade. Graças ao Nelson, que partilhou a casa comigo. Lembro-me com saudades daquelas noites de *Barbarians* e das jantaradas quer com butelo quer com *paella*, ou no *Tralha*, além de me ensinar a apreciar o vinho tinto. És um rapaz porreiro e trabalhador. Obrigado. Quanto aos colegas de laboratório, hei de agradecer a todas as bolseiras uma vez que fizeram simples a minha integração na sua rotina de convívio universitário. Sinto-me em dívida com a Leonor, que não só fez com que me integrasse na equipa, como confiu em mim como se fosse mais um amigo de há muito tempo. Parabéns pela tua atitude e a tua força para desenvolveres o trabalho de investigação. Precisa-se de mais pessoas como tu. O toque chique e simpático foi aportado, sem dúvida nenhuma, pela Juliana, mulher com maiúsculas onde as houver. A equipa foi completada com a Sandrine, a Veronique e a Miriam. Os almoços, se bem que não tivessem muito siso, foram de certeza com muito riso. Assim é que é! Confirmando é isso que dizem de quem parte leva saudades, e quem fica saudades tem. Obrigadíssimo. Cá têm um amigo para o que precisarem.

Me gustaría también agradecer a todos los profesores que a lo largo de mi vida educativa han conseguido que hoy llegue hasta este escalón. Desde los *profes* del colegio Lope de Vega, pasando por el IES Zurbarán y la Universidad de Extremadura. Especial mención para los profesores del Dpto. de Ingeniería Química y Química Física, que me introdujeron en el apasionante mundo de la Ingeniería Química. Enhorabuena por el gran trabajo desarrollado.

También me gustaría agradecer a mi familia y amigos por estar ahí en todos los momentos en los que los he necesitado. Especial mención a mis hermanos, a los que dedico esta tesis, y son mi debilidad; así como a mi amiga Guada, que aunque pase más o menos tiempo siempre está en primera línea de la batalla dispuesta a escucharme, entenderme y aconsejarme.

Es la 1:06 y la redacción de estas líneas alcanza su cenit más sentimental y personal. Gracias tesis por estos años de trabajo que han servido también para encontrarnos, Rafa, para conocerte a mí mismo, tus sueños y por qué luchar para caminar. Ya no le hagáis mucho caso este *viejoven*, que solo sabe relatar. Dicen, ahí fuera, que tras cada amanecer, surge del horizonte un nuevo día que esconde trepidantes oportunidades aún por explorar. Adelante. ¡Muchas gracias!

No soy nada.

Nunca seré nada.

No puedo querer ser nada.

Aparte de esto, tengo en mí todos los sueños del mundo.

(Tabaquería, Fernando Pessoa)

INDEX

RESUMEN	11
SUMMARY	19
CHAPTER ONE. Introduction and objectives	25
1.1. Presentation	27
1.2. Global water situation. Water crisis: scarcity and pollution	27
1.2.1. Importance of water in life	27
1.2.2. Water as resource	28
<i>Domestic use</i>	31
<i>Industrial use</i>	32
<i>Agricultural use</i>	32
1.3. Pesticides as emerging contaminants. The model compounds used in this thesis	33
1.3.1. Emerging organic microcontaminants	33
1.3.2. Pesticides as pollutants in agriculture	34
1.3.3. The herbicides studied in this thesis	37
<i>MCPA: aryloxyalkanoic acid derivative</i>	37
<i>Clopyralid (CLO), picloram (PIC) and triclopyr (TRI): pyridine herbicides</i>	39
<i>Diuron (DIU): phenylurea</i>	41
<i>Tembotrione (TEMB): triketone</i>	42
<i>Metazachlor (METAZ): chloroacetamide</i>	43
<i>Tritosulfuron (TRITO): sulphonylurea</i>	44
<i>Ethofumesate (ETHO): benzofuran</i>	45
1.4. Advanced oxidation processes (AOPs) as emerging technology for oxidation of aqueous emerging contaminants	46

1.4.1. Photocatalytic oxidation	48
1.4.2. Ozonation and photocatalytic ozonation	51
1.4.3. Monoperoxysulfate and photocatalytic oxidation in the presence of monoperoxysulfate	55
<i>Oxidation with monoperoxysulfate and monoperoxysulfate decomposition into sulfate radicals</i>	55
<i>Photocatalytic oxidation in the presence of monoperoxysulfate</i>	57
1.5. Specific objectives	59
References	60
CHAPTER TWO. Experimental Section	75
2.1. Materials & chemicals	77
2.2. Experimental setups and procedures	79
2.2.1. Photocatalytic processes setup with UVA lamps	79
2.2.2. Photocatalytic processes setup with UVA LEDs	81
2.2.3. Photocharacterization of the radiation source. Chemical actinometry	82
2.2.4. Kinetic determinations	84
<i>Determination of the direct rate constant with molecular ozone by homogeneous competitive experiments in semicontinuous or discontinuous mode</i>	84
<i>Determination of the rate constant with hydroxyl radical through H₂O₂ decomposition with UVC radiation</i>	86
2.3. Methods for aqueous analyses	87
2.3.1. Aqueous herbicides concentration by High Performance Liquid Chromatography with UV detection (LC-HPLC-UV)	88
2.3.2. Transformation Products by Liquid Chromatography coupled to a Quadrupole Time-of-Flight Mass Spectrometer (LC-QTOF-MS)	89
2.3.3. Total Organic Carbon (TOC) and Inorganic Carbon (IC)	90
2.3.4. Inorganic and organic anions by Ionic Chromatography	91
2.3.5. Dissolved ozone concentration	91
2.3.6. Hydrogen peroxide concentration	92

<i>Hydrogen peroxide at low concentrations (<math>5 \times 10^{-5} \text{ M}</math>)</i>	92
<i>Hydrogen peroxide at high concentrations (<math>5 \times 10^{-5} - 10^{-3} \text{ M}</math>)</i>	93
2.3.7. Monoperoxy sulfate concentration	94
2.3.8. Aqueous iron (II) concentration	94
2.3.9. Aqueous cobalt concentration	95
<i>Determination of aqueous cobalt by atomic absorption spectroscopy</i>	95
<i>Spectrophotometric determination of aqueous cobalt</i>	96
2.3.10. Total polyphenol content	96
2.3.11. Chemical Oxygen Demand (COD)	97
2.3.12. Biological Oxygen Demand (BOD)	97
2.3.13. Toxicity tests	98
<i>Acute toxicity to Daphnia parvula and Culex pipiens larvae</i>	98
<i>Vibrio Fischeri toxicity assay</i>	98
<i>Phytotoxicity assays with Lactuca Sativa and Solanum Lycopersicum</i>	99
2.3.14. Turbidity	100
2.3.15. pH and temperature	100
2.3.16. Conductivity	100
2.4. Catalysts' synthesis and characterization	101
2.4.1. Catalysts' synthesis	101
<i>Bare & nitrogen-doped titanium dioxide (TiO_2 & N-TiO_2)</i>	101
<i>Lanthanum-cobalt perovskites (LaCoO_3)</i>	101
<i>Lanthanum-cobalt perovskites coupled to titanium dioxide (LaCoO_3-TiO_2)</i>	102
2.4.2. Techniques for analysis and characterization of catalysts	102
<i>Scanning Electron Microscopy (SEM)</i>	103
<i>Transmission Electron Microscopy (TEM)</i>	104
<i>X-Ray Diffraction (XRD)</i>	104
<i>X-Ray Photoelectron Spectroscopy (XPS)</i>	105
<i>Diffuse Reflectance Spectroscopy UV-visible (DRS-UV-vis)</i>	106

<i>Wavelength Dispersive X-Ray Fluorescence (WDXRF)</i>	107
<i>Nitrogen adsorption isotherms. BET area determination</i>	107
<i>ThermoGravimetry and Differential Thermal Analysis coupled to Mass Spectrometry (TG-DTA-MS)</i>	109
<i>pH of point zero charge (pH_{pzc})</i>	109
References	110
CHAPTER THREE. PAPER ONE. Photocatalytic elimination of aqueous 2-methyl-4-chloropheoxyacetic acid in the presence of commercial and nitrogen-doped TiO₂	113
3.1. Introduction	115
3.2. Materials and methods	116
3.2.1. Photoreactor and procedure	116
3.2.2. Materials	117
3.2.3. Analysis	118
3.2.4. Catalyst characterization	118
3.3. Results and discussion	118
3.3.1. Experiments carried out with pure MCPA: influence of TiO ₂ doping	118
3.3.2. Experiments carried out with commercial MCPA: influence of calcination temperature	121
3.3.3. Experiments carried out with commercial MCPA: influence of the ratio N:Ti in the synthesis process	122
3.3.4. Preliminary kinetics tests	123
<i>Influence of free hydroxyl radical scavengers</i>	124
<i>Influence of electron donors (hole reacting substances)</i>	125
<i>Influence of ¹O₂ reacting substances</i>	126
<i>Influence of quinonic substances</i>	126
<i>Influence of HO₂[•]/O₂^{•-} scavengers</i>	127
<i>Influence of oxygen concentration</i>	127
3.3.5. The proposed mechanism	127
3.4. Conclusions	135

References	135
CHAPTER FOUR. PAPER TWO. Photocatalytic ozonation of 4-chloro-2-methylphenoxyacetic acid and its reaction intermediate 4-chloro-2-methylphenol	139
4.1. Introduction	141
4.2. Experimental	142
4.2.1. Photoreactor and procedure	142
4.2.2. Materials	143
4.2.3. Analysis	143
4.2.4. Ecotoxicity bioassays with <i>Daphnia parvula</i> and <i>Culex pipiens larvae</i>	144
4.3. Results and discussion	144
4.3.1. Preliminary experiments: technologies comparison	144
4-Chloro-2-methylphenoxyacetic acid oxidation	144
4-Chloro-2-methylphenol oxidation	146
4.3.2. The system UVA/TiO ₂ /O ₃ . Operating variables effect	148
Catalyst concentration	148
MCPA concentration	150
pH influence	152
4.3.3. Detected intermediates and toxicity	152
4.4. Conclusions	156
References	157
CHAPTER FIVE. PAPER THREE. Photocatalytic ozonation of clopyralid, picloram and triclopyr. Kinetics, toxicity and influence of operational parameters	161
5.1. Introduction	163
5.2. Experimental	164
5.2.1. Photoreactor and procedure	164
5.2.2. Materials	165
5.2.3. Analysis	165
5.2.4. Ecotoxicity bioassays with <i>Daphnia parvula</i> and <i>Culex pipiens larvae</i>	166

5.3. Results and discussion	166
5.3.1. Technologies comparison	166
5.3.2. Photocatalytic ozonation. Influence of variables	173
<i>Catalyst concentration</i>	173
<i>Catalyst reuse</i>	174
<i>Initial herbicide concentration</i>	176
5.3.3. Photocatalytic ozonation of commercial clopyralid. Toxicity evolution	178
5.4. Conclusions	180
References	181
CHAPTER SIX. PAPER FOUR. Photocatalytic ozonation of pyridine-based herbicides by N-doped titania	183
6.1. Introduction	185
6.2. Experimental	187
6.2.1. Photoreactor and procedure	187
6.2.2. Materials	188
6.2.3. N-doped titania synthesis	188
6.2.4. Catalyst characterization	188
6.2.5. Analysis	189
6.2.6. Ecotoxicity bioassays with <i>Daphnia parvula</i>	190
6.2.7. Acute fitotoxicity assays	190
6.3. Results and discussion	191
6.3.1. Photocatalytic oxidation. Activity of catalysts with different Ti:N ratios	191
6.3.2. Ozonation and photocatalytic ozonation. Activity of catalysts with different Ti:N ratios	192
6.3.3. Photocatalytic ozonation. Stability and characterization of TiO ₂ _1:1.6 catalyst	194
<i>UV-vis absorption spectra</i>	195
<i>BET area</i>	196
<i>X-ray diffraction</i>	196

<i>X-ray photoelectron spectroscopy</i>	198
<i>Scanning electron microscopy/Transmission electron microscopy</i>	198
<i>Thermal gravimetry-differential temperature analysis-mass spectrometry</i>	199
6.3.4. Photocatalytic ozonation. Toxicity and fitotoxicity of treated samples	200
6.4. Conclusions	202
References	203
CHAPTER SEVEN. PAPER FIVE. Ozonation, photocatalysis and photocatalytic ozonation of diuron. Intermediates identification	207
7.1. Introduction	209
7.2. Materials and methods	210
7.2.1. Chemicals	210
7.2.2. Experimental setup and procedure	211
7.2.3. Photocatalyst synthesis	211
7.2.4. Analytical methods	212
7.2.5. Ecotoxicity assays	213
7.3. Results	213
7.3.1. Efficiency of ozonation, photocatalysis and photocatalytic ozonation	213
7.3.2. Identification of TPs by LC-QTOF-MS/MS and ionic chromatography	217
7.3.3. Evolution of toxicity to <i>Vibrio Fischeri</i>	225
7.4. Conclusions	226
References	227
CHAPTER EIGHT. PAPER SIX. Monoperoxsulfate photocatalysis under 365 nm radiation. Direct oxidation and monoperoxsulfate promoted photocatalysis of the herbicide tembotrione	231
8.1. Introduction	233

8.2. Experimental	234
8.2.1. Materials	234
8.2.2. Analytical methods	234
8.2.3. Photoreactor setup and experimental procedure	235
8.3. Results and discussion	236
8.3.1. Monoperoxysulfate promoted experiments in the absence of light and photocatalyst	236
<i>Influence of initial Oxone® concentration</i>	236
<i>Influence of temperature</i>	238
<i>Influence of pH</i>	240
8.3.2. Oxone® promoted tembotrione photocatalysis	241
8.3.3. Tembotrione photocatalysis in the presence of Oxone®. Experimental design	243
8.4. Conclusions	245
References	246
CHAPTER NINE. PAPER SEVEN. Removal of aqueous metazachlor, tembotrione, tritosulfuron and ethofumesate by heterogeneous monoperoxysulfate decomposition on lanthanum-cobalt perovskites	251
9.1. Introduction	253
9.2. Experimental	254
9.2.1. Materials	254
9.2.2. Catalyst synthesis and characterization	254
9.2.3. Experimental setup and procedure	255
9.2.4. Analytical methods	256
9.3. Results and discussion	256
9.3.1. Operating variables influence	256
<i>pH influence and cobalt leaching</i>	256
<i>Oxone concentration</i>	258
<i>Catalyst concentration influence</i>	260
<i>Catalyst stability</i>	262
<i>Scavengers influence</i>	263

9.3.2. Catalyst characterization	265
9.4. Conclusions	270
Supplementary data	272
References	275
CHAPTER TEN. PAPER EIGHT. Synergism between monoperoxysulfate and LaCo₃-TiO₂ photocatalysis for oxidation of herbicides. Operational variables and catalyst characterization assessment	279
10.1. Introduction	281
10.2. Experimental	283
10.2.1. Chemicals	283
10.2.2. Catalyst synthesis and characterization	283
10.2.3. Photoreactor and procedure	284
10.2.4. Analytical methods	285
10.3. Results & discussion	286
10.3.1. Effect of the ratio LaCo ₃ -TiO ₂	286
10.3.2. Monoperoxysulfate concentration effect	288
10.3.3. Influence of catalyst concentration	291
10.3.4. pH influence	292
10.3.5. Temperature influence	294
10.3.6. Catalyst stability	295
10.3.7. Phytotoxicity evolution	296
10.3.8. Catalyst characterization	298
10.4. Conclusions	302
Supplementary material	303
References	307
CHAPTER ELEVEN. PAPER NINE. Integrated aerobic biological-chemical treatment of winery wastewater diluted with urban wastewater. LED based photocatalysis in the presence of monoperoxysulfate	311
11.1. Introduction	313
11.2. Experimental section	315
11.2.1. Reagents	315

11.2.2. Wine Wastewater and analytical procedures_____	315
11.2.3. Biological treatment with activated sludge_____	316
11.2.4. LED photoreactor system_____	317
11.3. Results and discussion_____	318
11.3.1. Aerobic Biological treatment of DWW_____	318
11.3.2. Chemical post-treatment of biologically processed DWW____	323
11.4. Conclusions_____	328
References_____	329
CHAPTER TWELVE. Conclusions_____	333

RESUMEN

La presente tesis doctoral ha sido desarrollada dentro de la actividad investigadora del grupo *TRATAGUAS*, en el departamento de Ingeniería Química y Química Física de la Universidad de Extremadura. La actividad investigadora del grupo *TRATAGUAS* se centra en la búsqueda de nuevos Procesos de Oxidación Avanzada (POAs) con efectos beneficiosos en la eliminación de contaminantes en agua, calificados como contaminantes emergentes, cuya existencia es una consecuencia de los hábitos de consumo actuales. En este sentido, los esfuerzos del grupo se han centrado en los procesos fotocatalíticos, concretamente en aquellos combinados con ozono u otros agentes oxidantes que aportan un efecto sinérgico. El proyecto en el que esta tesis ha sido principalmente encuadrada se titula '*Preparación de catalizadores y su aplicación en la eliminación de contaminantes refractarios de aguas residuales mediante ozonación fotocatalítica*', referencia CTQ2012/35789/C02-01, financiado por el CICYT de España y fondos FEDER.

La escasez y contaminación del agua es un problema de preocupación global como puede extraerse de la atención prestada en las políticas del agua. Debido al crecimiento exponencial de la población y la expansión de los hábitos tecnológicos del estilo de vida actual, se precisa nueva legislación que apoye la conservación de recursos hídricos para un adecuado suministro de agua. Los microcontaminantes emergentes en agua son un claro ejemplo de una de las consecuencias que los hábitos de vida actuales. Estos contaminantes llamados *emergentes* generan preocupación debido a su potencial toxicidad y destino ambiental. No obstante, estos microcontaminantes se han detectado en niveles de concentración considerado demasiado bajo para producir efectos negativos significativos a corto plazo en sistemas acuáticos. La mayor parte acaba en el medioambiente, y otros atraviesan los procesos de tratamiento biológicos de las plantas de tratamiento de aguas donde permanecen inalterados, frecuentemente debido a su naturaleza no biodegradable o refractaria. Por todas estas razones, el trabajo aquí presentado proviene de la necesidad de investigar tecnologías emergentes, como los tratamientos basados en POAs, para eliminar contaminantes que no son eliminados en las plantas de tratamiento convencionales.

Para un mejor entendimiento, la memoria de esta tesis se ha dividido en dos partes bien diferenciadas, ambas basadas en el estudio de procesos fotocatalíticos con radiación UVA. La primera parte se centra en el estudio del proceso de fotocátalisis y ozonación fotocatalítica aplicando titanía comercial, Degussa P25, así como titanía dopada con nitrógeno (N-TiO₂) y sin dopar sintetizadas en el laboratorio. En la segunda parte se desarrolla el uso de monopersulfato combinado, o no, con el proceso de fotocátalisis o catálisis heterogénea; aplicando dióxido de titanio comercial Degussa P25, perovskita de lantano y cobalto (LaCoO₃), o perovskita de lantano y cobalto acoplada a dióxido de titanio (LaCoO₃-TiO₂). En todos los casos, se han considerado como microcontaminantes herbicidas de diferente naturaleza y carácter recalcitrante.

En primer lugar, se estudió el dopado de dióxido de titanio con nitrógeno para la oxidación fotocatalítica del ácido 4-cloro-2-metilfenol (MCPA), comparando los resultados con los obtenidos en presencia de titanía sin dopar y dopada con nitrógeno (N-TiO₂), así como el comercial Degussa P25. En el proceso de síntesis, basado en método sol-gel, se observó que las variables más influyentes en la actividad fotocatalítica fueron el porcentaje de agente dopante (urea o trietilamina, principalmente) y la temperatura de calcinación. Aunque en ningún caso se mejoró la fotoactividad del comercial Degussa P25 con ningún catalizador sintetizado en el laboratorio, sí se apreció una mejora de la fotoactividad al dopar con nitrógeno. El N-TiO₂ con mejor actividad fotocatalítica fue caracterizado mediante técnicas de microscopía electrónica de barrido (SEM, *Scanning Electron Microscopy*), microscopía electrónica de transmisión (TEM, *Transmission Electron Microscopy*) y fotoespectroscopía de rayos X (XPS, *X-Ray Photoelectron Spectroscopy*). Ensayos cinéticos en presencia de diferentes inhibidores de especies oxidantes involucradas en el proceso fotocatalítico permitieron proponer un mecanismo de reacción pseudoempírico capaz de simular de forma aceptable el proceso en presencia del catalizador comercial P25. Este mecanismo subraya la importancia de radicales hidroxilo, peroxiorgánicos orgánicos en la oxidación fotocatalítica de MCPA.

Una vez estudiada la oxidación fotocatalítica de MCPA, se abordó el proceso de ozonación fotocatalítica con titanía comercial. Así, se llevaron a cabo diferentes procesos de oxidación de MCPA en agua, tales como fotocátalisis en ausencia de oxígeno (UVA/TiO₂/N₂), ozonación (O₃), ozonación catalítica (TiO₂/O₃), fotocátalisis en presencia de oxígeno (UVA/TiO₂/O₂) y ozonación fotocatalítica (UVA/TiO₂/O₃). El MCPA fue eliminado fácilmente debido a su afinidad por el radical hidroxilo y la formación de radicales orgánicos en los procesos fotocatalíticos. Sin embargo, la ozonación

fotocatalítica fue el sistema más eficiente tanto en términos de velocidad de eliminación de MCPA como, y especialmente, en grado de mineralización. El MCPA no es altamente refractario al proceso de ozonación simple, y los procesos fotocatalíticos no producen mejoras significativas en la velocidad de eliminación del herbicida. No obstante, las diferencias fueron más significativas en cuanto a lo que el grado de mineralización y velocidad se refiere, alcanzándose los mejores resultados en el proceso de ozonación fotocatalítica. En los sistemas que combinan TiO_2 y radiación UVA se detectó como subproducto de oxidación el 4-cloro-2-metilfenol (CMP). Este compuesto es fácilmente oxidable después de ser generado a partir de MCPA en los procesos que envuelven el uso de ozono, tal y como prueba la constante de reacción directa entre CMP y ozono: $7,2 \cdot 10^4$, $4,4 \cdot 10^5$, $2,9 \cdot 10^6 \text{ M}^{-1}\text{s}^{-1}$ a pHs 4, 7 y 10 respectivamente. En el proceso de ozonación fotocatalítica de MCPA se identificaron mediante LC-QTOF-MS (*Liquid Chromatography coupled to Quadrupole Time-Of-Flight Mass Spectrometry*) productos de oxidación que corresponden principalmente a especies oxigenadas derivadas del compuesto inicial tras la pérdida de algunos grupos funcionales. No se apreció toxicidad de los mismos en *Daphnia parvula* y *Culex pipiens larvae* durante el proceso de ozonación fotocatalítica (concentración inicial de MCPA 5 mg L^{-1}). De hecho, fue necesario aumentar de forma considerable la concentración ($50\text{-}100 \text{ mg L}^{-1}$) para apreciar toxicidad aguda de los intermedios formados, que en cualquier caso fueron eliminados durante el proceso de oxidación.

La combinación de fotocatálisis y ozono fue estudiada con otros herbicidas más refractarios, como son los derivados de la familia de los piridínicos. Se aplicaron procesos de fotólisis UVA, fotocatálisis y ozonación fotocatalítica a la eliminación de tres herbicidas piridínicos: clopiralid, picloram y triclopir. Como fotocatalizador se consideró Degussa P25, en ensayos donde cada herbicida se usó por separado. Los tres herbicidas fueron altamente recalcitrantes a la ozonación directa, como las bajos valores de las constantes cinéticas de segundo orden calculadas demuestran ($\sim 20 \text{ M}^{-1} \text{ min}^{-1}$ para clopiralid y triclopir, y $105 \text{ M}^{-1} \text{ min}^{-1}$ para picloram). La combinación de ozono y fotocatálisis condujo a los mejores resultados dado que el proceso de degradación en este caso se desarrolla a través de la acción del radical hidroxilo, cuyas constantes de reacción de segundo orden con cada uno de los herbicidas fue de $0,73$, $3,80$ y $1,73 \cdot 10^9 \text{ M}^{-1} \text{ s}^{-1}$ para clopiralid, picloram y triclopir, respectivamente, a pH neutro. Se apreció un marcado efecto sinérgico tanto en la velocidad de eliminación de herbicidas como de mineralización. El seguimiento de los aniones formados durante los procesos

sugiere la dechloración como primera etapa en la ozonación fotocatalítica. La abertura del anillo aromático condujo a la acumulación de nitratos y la aparición de ácidos carboxílicos de cadena corta. Se analizó la toxicidad aguda frente a *Daphnia Parvula* y *Culex Pipiens* en el proceso de ozonación fotocatalítica de clopiralid, siendo posible observar que los primeros intermedios formados mostraron mayor toxicidad que el compuesto inicial, esto es el propio herbicida. Según avanzó el proceso, la toxicidad descendió hasta tomar valores insignificantes al final del proceso.

La ozonación fotocatalítica de los tres herbicidas piridínicos también fue investigada usando dióxido de titanio dopado con nitrógeno. Mezclas de clopiralid, triclopir y picloram se trataron mediante fotocatalisis con oxígeno u ozono. El dopado de la titania con nitrógeno fue realizado usando trietilamina en el método de síntesis sol-gel. En ensayos de oxidación fotocatalítica se determinó la cantidad de agente dopante óptima para el proceso. El catalizador de comportamiento óptimo en el proceso fotocatalítico también condujo a los mejores resultados de eliminación de mineralización en el proceso de ozonación fotocatalítica, cercano al 95% en 180 min bajo las condiciones experimentales consideradas. El dióxido de titanio dopado fue caracterizado mediante técnicas de adsorción de N₂, SEM, TEM, difracción de rayos X (XRD, *X-Ray Diffraction*), XPS, espectroscopía de reflectancia difusa UV-visible (DRS-UV-vis, *Diffuse Reflectance Spectroscopy UV-visible*) y termogravimetría con análisis térmico diferencial y espectrometría de masas (TG-DTA-MS, *ThermoGravimetry and Differential Thermal Analysis coupled to Mass Spectrometry*). Se apreció fase anatasa, con cristales de tamaño de 25 nm, y 1% de N superficial en el N-TiO₂ con mejor fotoactividad. La estabilidad fotocatalítica fue validada tras cinco ciclos de reacción consecutivos, no observándose pérdida relevante. La toxicidad, durante y después del tratamiento de ozonación fotocatalítica, fue evaluado mediante medidas de DBO, y exposición a *Daphnia Parvula*, y de forma alternativa a ensayos de fitotoxicidad de germinación de semillas de *Lactuca Sativa* y *Solanum Lycopersicum*. Inicialmente, aunque no se apreció toxicidad aguda de la mezcla inicial de herbicidas en el crustáceo *Daphnia Parvula*, esta incrementó en la etapa inicial del proceso de ozonación fotocatalítica. Una vez los compuestos iniciales fueron oxidados por completo, la toxicidad desapareció hasta valores inapreciables. Por otro lado, en los ensayos de fitotoxicidad no se apreció germinación de la muestra inicial de reacción, esto es, la mezcla inicial de herbicidas; y, gradualmente se fue apreciando crecimiento de la longitud de la radícula según avanzó el proceso de oxidación.

El último estudio relacionado con el proceso de ozonación fotocatalítica se centró en la identificación de los Productos Intermedios (PI) de oxidación. La identificación de los PI se llevó a cabo en los procesos de ozonación, fotocatálisis, y ozonación fotocatalítica de diurón. El fotocatalizador aplicado fue el N-TiO₂ que mejores resultados produjo previamente. El proceso de ozonación fotocatalítica no mejoró la velocidad de eliminación de diurón respecto a la ozonación simple; sin embargo, sí se observó un efecto sinérgico en la eliminación de Carbono Orgánico Total (COT). Se identificaron mediante LC-QTOF-MS 10 PI formados durante las tres tecnologías de oxidación estudiadas. Tanto el proceso de ozonación simple como el de ozonación fotocatalítica condujeron a la formación y completa eliminación de todos los PI. Por otro lado, la evolución de los ácidos carboxílicos de cadena corta generados sugiere que el elevado porcentaje de eliminación de COT en el proceso de ozonación fotocatalítica está unido a la elevada capacidad de oxidación de estos ácidos y la liberación de aniones cloruro y nitrato. La evolución de la toxicidad a la bacteria *Vibrio Fischeri* durante el proceso de ozonación fotocatalítica conllevó un incremento de la inhibición en el crecimiento de la bacteria, para luego descender según avanzaba el tiempo de reacción.

El segundo bloque de esta tesis, centrado en la oxidación fotocatalítica en combinación con monopersulfato (MPS), comenzó con el estudio de la oxidación del herbicida tembotriona aplicando MPS y fotocatálisis. En primer lugar, se evaluó la oxidación directa del herbicida con MPS, estudiando las variables más significativas que afectan al proceso: concentración inicial de MPS, pH y temperatura. Se apreció que el proceso siguió una cinética de orden 2/3 para MPS y primer orden para tembotriona. Se estimó un pH óptimo de trabajo en el entorno de condiciones neutras debido a la reactividad de las especies neutras y disociadas tanto de MPS como tembotriona. En segundo lugar, se evaluó la simbiosis de MPS y fotocatálisis, lo cual mejoró significativamente la velocidad de degradación de tembotriona y mineralización, si se comparan con el proceso en ausencia de MPS. Así, se alcanzó una degradación completa de tembotriona en 20 min aplicando 50 mg L⁻¹ de Degussa P25 y MPS 2 · 10⁻⁴ M. Bajo condiciones similares, se eliminó un 70% en 90 min. Para evaluar la importancia de algunas variables sobre el proceso fotocatalítico con MPS se realizó un diseño de experimentos tipo Plackett-Burman.

La capacidad de oxidación de monopersulfato también se estudió a través de la descomposición en radicales mediante catálisis heterogénea aplicando perovskita de lantano y cobalto (LaCoO₃). Este óxido mixto se usó como

catalizador en la descomposición heterogénea para la eliminación de una mezcla de cuatro herbicidas (metazacloro, tembotriona, tritosulfurón y etofumesato). Se evaluó la influencia del pH, concentración inicial de MPS y catalizador. De los resultados obtenidos se apreció que una vez el MPS se adsorbe en la superficie del catalizador, donde tiene lugar la descomposición en radicales altamente oxidantes que reaccionan con los herbicidas en disolución. La estabilidad del catalizador se corroboró realizando ciclos consecutivos de reacción, apreciándose baja lixiviación de cobalto al medio y ausencia de pérdida significativa en actividad catalítica. Ensayos en presencia de inhibidores tales como el terbutanol, metanol y anión carbonato destacaron la importancia de la formación de radicales para una degradación de los herbicidas. Las partículas de LaCoO_3 fueron estudiadas usando diversas técnicas de caracterización de sólidos. Las microcopias SEM y TEM denotaron la presencia de nanopartículas, de forma esférica en su gran mayoría, con un área BET de $15,20 \text{ m}^2 \text{ g}^{-1}$. La presencia de estructura tipo perovskita se corroboró con diversas técnicas tales como XRF (*X-Ray fluorescence*, ratio atómico La:Co 1:1), XPS (estados de oxidación superficiales Co^{3+} y La^{3+}), y XRD (estructura tipo perovskita de fase romboédrica).

Se consideró el composite $\text{LaCoO}_3\text{-TiO}_2$ como fotocatalizador con doble vía de descomposición de monopersulfato en radicales. En primer lugar, debido a la descomposición fotocatalítica de MPS en las partículas de titanía; y en segundo lugar, a través la descomposición catalítica heterogénea sobre las partículas de perovskita. Este sistema fotocatalítico se aplicó a la mezcla previa de herbicidas (metazacloro, tembotriona, tritosulfurón y etofumesato). Se evaluaron el ratio $\text{LaCoO}_3\text{:TiO}_2$, la concentración de agente oxidante, la concentración de catalizador, el pH y la temperatura como principales variables que gobiernan el proceso. La completa oxidación de los herbicidas se produjo según las variables operacionales y su naturaleza recalcitrante. Se alcanzó un 55% de conversión de COT en el mejor de los sistemas (concentración de MPS 10^{-3} M). Ensayos de fitotoxicidad de germinación de *Lactuca Sativa* no mostraron inhibición tras 180 min del tratamiento fotocatalítico. Las propiedades del sólido de ratio Co:Ti=0.1:1 se estudiaron en técnicas SEM (agregados de LaCoO_3 unidos a partículas de TiO_2 de diversa forma y tamaño), XRF (6,1% de LaCoO_3), XPS (estados de oxidación superficiales Co^{3+} , La^{3+} y Ti^{4+}), XRD (anatasa, rutilo y LaCoO_3 romboédrico) y DRS-UV-vis (absorción en el rango visible con un TiO_2 de band gap 2,88 eV).

Finalmente, se estudió la aplicación de procesos fotocatalíticos combinados con MPS para la depuración de un efluente procedente de actividades vitivinícolas, previamente tratado biológicamente. Así, la

combinación secuencial de los procesos biológico y químico permitió la eliminación del contenido orgánico biodegradable y recalcitrante presente en este tipo de agua residual. Para ello, se realizó una oxidación biológica aerobia basada en fangos activados diluyendo el efluente original con agua urbana simulada. Primeramente, se realizó una aclimatación secuencial en la que se aumentó la carga vitivinícola de forma gradual. Se estudiaron ciertas variables de especial interés en el proceso de oxidación biológica, además de parámetros de diseño relacionados con la sedimentabilidad del fango. Una vez tratado el efluente biológicamente (reducción de Demanda Química de Oxígeno, DQO, en un 40-50% tras 8 horas), se continuó el tratamiento mediante procesos químicos basados en radiación UVA-LED, monopersulfato y fotocatalizadores. Así, se completó la reducción de la DQO remanente y una completa oxidación del contenido polifenólico, levemente oxidado en el proceso de fangos activos previo. De todas las opciones evaluadas, la combinación de MPS y el fotocatalizador $\text{LaCoO}_3\text{-TiO}_2$, con doble vía de descomposición de MPS a través de catálisis heterogénea y fotocatalisis, proporcionó los mejores resultados (95% de eliminación de polifenoles y 60% de reducción de DQO). En este sistema se estudió la influencia de la concentración de MPS y pH en la efectividad del proceso.

SUMMARY

The work of this doctoral thesis has been developed within the activity of the *TRATAGUAS* research group in the Department of Chemical Engineering and Physical Chemistry of the University of Extremadura. *TRATAGUAS* research activity has lately been concentrated on the search for new Advanced Oxidation Processes (AOPs) with beneficial effects in the elimination of new pollutants, named as emerging contaminants, whose existence is a consequence of current human consumption habits. In this sense, the efforts of the research group have been dedicated to photocatalytic processes, especially combined with ozone or other oxidant compounds presenting synergistic effect in the process. The project in which this thesis has mainly been framed was entitled '*Preparación de catalizadores y su aplicación en la eliminación de contaminantes refractarios de aguas residuales mediante ozonación fotocatalítica*', reference CTQ2012/35789/C02-01, financed by CICYT of Spain and FEDER funds.

Water scarcity and pollution is an issue of global concern which is drawing attention of water policies. Due to the exponential growth of population and the widespread application of modern life technology, conserving aqueous resources to supply water is increasingly difficult and requires new legislation for its support. Emerging aqueous micropollutants are a clear example of one of the consequences of current modern life in the environment. These labelled 'Emerging Contaminants' generate alarmingly concern caused by their potential toxicity and environmental fate; nevertheless, they are micropollutants as the reported concentration level is considered too low to cause short-term effects in aquatic ecosystems. Most of them are discharged to the environment, and others pass through biological-based water treatment plants where they keep unaltered, frequently due to their non-biodegradable and refractory nature. For all these reasons, the research here presented comes from the need of searching for emerging technologies, such as AOP-based processes, to remove new pollutants that are not satisfactorily treated in conventional water treatment plants.

This dissertation can be divided into two different blocks for a better understanding, both involving photocatalytic process under UVA radiation. The first part was concentrated on photocatalysis and photocatalytic ozonation

using commercial titania Degussa P25, and synthesized bare or nitrogen doped titania (N-TiO₂). The second part is focused on the use of monoperoxysulfate combined, or not, with photocatalysis or heterogeneous catalysis; applying commercial titania Degussa P25, lanthanum-cobalt perovskite (LaCoO₃), or lanthanum-cobalt perovskite joint to titania (LaCoO₃-TiO₂). In all cases, herbicides of different recalcitrance and nature were considered as organic micropollutants.

Nitrogen-doped titania was first explored as an active photocatalyst for the photocatalytic oxidation of 2-methyl-4-chlorophenoxyacetic acid (MCPA), and the results compared to those obtained in the presence of bare titania and commercial Degussa P25. In the synthesis process, based on sol-gel method, nitrogen doping percentage (using urea and trimethylamine, mainly) and calcination temperature have been considered as the most influential variables. Although in no case the results obtained with lab made catalysts improved the photoactivity of Degussa P25, N doping strengthens the photoactivity of synthesized undoped titania. N-doped TiO₂ with best results was characterized by Scanning Electron Microscopy (SEM), Transmission Electron Microscopy (TEM) and X-ray Photoelectron Spectroscopy (XPS) techniques. Some kinetic tests under different scavengers of the photocatalytic process led to the proposal of a pseudoempirical reaction mechanism capable of acceptably simulating the process in the presence of commercial Degussa P25. This mechanism outlined the role played by hydroxyl, peroxy and organic radicals in the photocatalytic oxidation of MCPA.

After the photocatalytic oxidation of MCPA has been studied, the photocatalytic ozonation was tackled. Hence, aqueous MCPA was treated by different oxidation systems for comparison purposes, like photocatalysis in the absence of oxygen (UVA/TiO₂/N₂), single ozonation (O₃), catalytic ozonation (TiO₂/O₃), photocatalysis in the presence of oxygen (UVA/TiO₂/O₂) and photocatalytic ozonation (UVA/TiO₂/O₃). MCPA was easily removed due to its affinity towards hydroxyl radicals and organic radical formed in photocatalytic processes. However, photocatalytic ozonation was the most efficient process in terms of both MCPA removal rate and especially mineralization. MCPA is not highly refractory to single ozonation, and photocatalytic processes do not produce significant improvements in MCPA removal rate. However, differences were more appreciable in terms of Total Organic Carbon (TOC) removal rate and extent, achieving the best results with photocatalytic ozonation. 4-Chloro-2-methyl phenol (CMP) was detected in those systems combining TiO₂ and UVA radiation. As the direct rate constant between CMP and molecular ozone corroborated ($7,2 \cdot 10^4$, $4,4 \cdot 10^5$,

$2,9 \cdot 10^6 \text{ M}^{-1} \text{ s}^{-1}$ at pHs 4, 7 y 10 respectively), CMP was completely oxidized after being generated from MCPA oxidation during processes involving the presence of ozone. Identified intermediates detected by Liquid Chromatography coupled to a Quadrupole Time-Of-Flight Mass Spectrometer (LC-QTOF-MS) in the photocatalytic ozonation applied to MCPA correspond to oxygenated species derived from the parent compound after loss of some substituting groups. No significant toxicity of intermediates was observed in *Daphnia parvula* and *Culex pipiens larvae* during photocatalytic ozonation treatment (initial MCPA concentration 5 mg L^{-1}). Actually, it was necessary to increase considerably initial MCPA concentration ($50\text{-}100 \text{ mg L}^{-1}$) to appreciate acute toxicity of intermediates, which was removed during the photocatalytic ozonation process.

The photocatalytic ozonation was further studied using more refractory herbicides, such as those from the pyridine family. Hence, UVA photolysis, photocatalysis and photocatalytic ozonation were applied to the elimination of three aqueous pyridine carboxylic acid herbicides: clopyralid, picloram and triclopyr. Degussa P25 was used as photocatalyst and herbicides were individually tested. All herbicides were highly recalcitrant to direct ozonation, as the calculated second order rate constant proved ($\sim 20 \text{ M}^{-1} \text{ min}^{-1}$ for clopyralid and triclopyr, and $105 \text{ M}^{-1} \text{ min}^{-1}$ for picloram). Combination of ozone and photocatalysis led to the best results since degradation is supposed to be developed by the action of hydroxyl radicals, whose calculated second order rate constants with HO^\bullet were 0.73 , 3.80 and $1.73 \cdot 10^9 \text{ M}^{-1} \text{ s}^{-1}$ corresponding to clopyralid, picloram and triclopyr respectively, at neutral pH. A synergistic effect was noticed in parent herbicides and TOC removals. The monitoring of released anions suggested dechlorination as the primary stage in the photocatalytic ozonation process. Ring opening led to the accumulation of nitrates and the appearance of some low weight carboxylic acids. Acute toxicity to *Daphnia Parvula* and *Culex Papiens* was analyzed during the photocatalytic ozonation of clopyralid, being possible to observe that first intermediates showed higher toxicity than the parent compound. As oxidation progressed, toxicity decreased until being negligible at the end of the process.

Photocatalytic ozonation of the three pyridinic herbicides was also investigated using nitrogen doped titania. Thus, a mixture of aqueous clopyralid, triclopyr and picloram was treated by photocatalysis with oxygen or ozone. Nitrogen doping of titania was carried out using triethylamine in a sol-gel method. A catalyst with an optimized N doping amount was found in the photocatalytic oxidation experiments series. This optimum photocatalyst also produced the best TOC removal rate in the photocatalytic ozonation, nearly

95% in 180 min under the experimental conditions tested. N-doped TiO₂ was characterized by N₂ adsorption isotherm, SEM, TEM, X-Ray Diffracton (XRD), XPS, Diffuse Reflectance Spectroscopy UV-visible (DRS-UV-vis) and ThermoGravimetry and Differential Thermal Analysis coupled to Mass Spectrometry (TG-DTA-MS) techniques. Anatase phase, with crystals of 25 nm of size, and 1% of superficial N was established in the N-TiO₂ with best photoactivity. The stability of the catalyst was assessed after five consecutive runs, and no relevant loss of photoactivity was detected. Toxicity, during and after the photocatalytic ozonation, was evaluated through Biological Oxygen Demand (BOD) measurements, exposition to *Daphnia Parvula* and alternatively, seed germination of *Lactuca Sativa* and *Solanum Lycopersicum*. Although no acute toxicity was initially appreciated from the parent compounds to the crustacean *Daphnia Parvula*, it increased at the earliest stage of the photocatalytic ozonation process. Once the parent compounds were totally degraded and dechlorination completed, toxicity decayed to negligible values. Phytotoxicity tests revealed no seed germination of parent compound, that is, before the photocatalytic oxidation process; and gradual increase of root length as the oxidation process proceeded.

A final study on the photocatalytic ozonation was focused on Transformation Product (TP) identification. TPs identification was carried out during the ozonation, photocatalysis and photocatalytic ozonation of diuron. The photocatalyst applied was the N-TiO₂ that previously produced the best results. Diuron elimination in the photocatalytic ozonation was not enhanced if compared to single ozonation; however, TOC removal was significantly improved. Ten TPs generated during the application of the three technologies were tentatively identified by Liquid Chromatography-Quadrupole Time-Of-Flight Mass Spectrometry (LC-QTOF-MS/MS). Single ozonation and photocatalytic ozonation led to the formation and complete elimination of all by-products. Low weight carboxylic acids evolution suggests that high TOC removal in photocatalytic ozonation was linked to its capacity to oxidize small oxygenated compounds and release inorganic chloride and nitrate. Toxicity evolution to the bacteria *Vibrio Fischeri* in photocatalytic ozonation displayed an increase of inhibition at the initial stages, followed by a decrease of this parameter as the reaction progressed.

Moving to the second part of this thesis, focused on the photocatalytic oxidation involving monoperoxysulfate (MPS), the oxidation of the herbicide tembotrione was studied using MPS and photocatalysis. Firstly, the direct oxidation of tembotrione by MPS was assessed, studying the variables affecting the process (initial MPS concentration, pH and temperature). The

process followed 2/3 and first orders regarding MPS and tembotrione concentrations, respectively. Optimal pH was located around circumneutral conditions due to the reactivity of neutral/dissociated species of both MPS and tembotrione. Secondly, the combination of MPS and photocatalysis was applied, improving significantly tembotrione and mineralization rate abatements, if compared to runs conducted in the absence of MPS. For example, tembotrione total abatement was achieved in 20 min when 50 mg L^{-1} of titania and $2 \cdot 10^{-4} \text{ M}$ of MPS were used. TOC conversion was roughly 70% in 90 min under similar operating conditions. In order to evaluate the importance of some variables in MPS photocatalytic process, an experimental design (Plackett-Burman) was considered.

Monoperoxysulfate oxidation capacity through heterogeneous radical decomposition was studied using lanthanum-cobalt perovskites. LaCoO_3 oxide was applied as catalyst for the heterogeneous decomposition of MPS in the removal of a mixture of four herbicides (metazachlor, tembotrione, tritosulfuron and ethofumesate). The influence of pH, initial MPS concentration and catalyst load were assessed. After MPS being absorbed onto the perovskite surface, a breakage led to the formation of powerful oxidizing radicals which react with herbicides in solution. Catalyst stability was tested by means of consecutive reuse cycles with no appreciable loss of activity and low cobalt leaching at circumneutral pH. Assays in the presence of scavengers such as *tert*-butyl alcohol, methanol and carbonate outlined the importance of radical formation in the herbicide degradation. LaCoO_3 particles were studied by diverse solid characterization techniques. SEM and TEM microscopies showed the presence of nanosized material, mostly spherical shaped, with $15.20 \text{ m}^2 \text{ g}^{-1}$ of BET area. LaCoO_3 perovskite structure was corroborated by diverse techniques such as XRF (X-Ray Fluorescence, La:Co atomic ratio of 1:1), XPS (superficial Co^{3+} and La^{3+} oxidation states), and XRD (rhombohedral LaCoO_3 phase).

The coupled $\text{LaCoO}_3\text{-TiO}_2$ composite was considered as photocatalyst with double route of monoperoxysulfate activation. Firstly, through photocatalytic MPS decomposition due to titania; and secondly, through MPS heterogeneous decomposition onto LaCoO_3 particles. This photocatalytic system was applied to the previous studied aqueous mixture of herbicides (metazachlor, tembotrione, tritosulfuron and ethofumesate). $\text{LaCoO}_3\text{:TiO}_2$ ratio, oxidant concentration, catalyst load, pH and temperature were evaluated as the main variables dominating the process. Herbicides were completely oxidized depending on the operational variables and their recalcitrant nature. 55% of TOC conversion was reached in the best case (MPS concentration of 10^{-3} M).

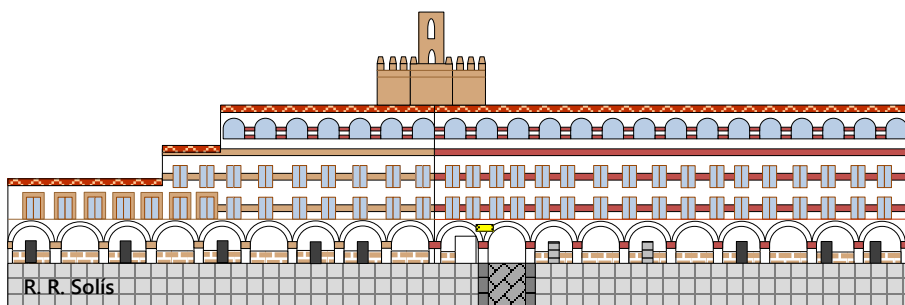
Phytotoxicity germination assays of *Lactuca Sativa* denoted no inhibition after 180 min of photocatalytic treatment. Solid properties of Co/Ti=0.1:1 ratio catalyst were studied by means of SEM (LaCoO₃ aggregates linked to a variety of shapes and sizes of TiO₂), XRF (6.1% of LaCoO₃), XPS (superficial Co³⁺, La³⁺ and Ti⁴⁺ oxidation states), XRD (anatase, rutile and rhombohedral LaCoO₃) and DRS-UV-vis reflectance (visible range absorption and bandgap of 2.88 eV for TiO₂).

Finally, photocatalytic processes combined with MPS were studied for the depuration of biologically treated Winery Wastewater (WW). Hence, a combined biological + chemical process was applied in order to achieve the degradation of biodegradable and recalcitrant organic content present in this kind of effluent. In this sense, biological oxidation by diluting WW with simulated urban wastewater was carried out by using aerobic activated sludge. Acclimation of sludge to Diluted Winery Wastewater (DWW) was first applied, and afterwards some aspects of paramount importance concerning biological oxidation were evaluated. Moreover, parameters of sedimentation design were also studied. After DWW was biologically oxidized (40-50% of COD removal in 8 hours), chemical processes based on UVA-LEDs radiation, monoperoxysulfate (MPS) and photocatalysts were applied in order to complete oxidation of the remaining Chemical Oxygen Demand (COD) and complete oxidation of the polyphenols, which were poorly degraded by means of activated sludge. From the all options tested, the combination of UVA, MPS and a novel LaCoO₃-TiO₂ composite, with double route of MPS decomposition through heterogeneous catalysis and photocatalysis, reached the best results (95% of polyphenol degradation, and additional 60% of COD removal). MPS concentration and pH effect in this process were also assessed.

CHAPTER ONE

INTRODUCTION & OBJECTIVES

The aim of this chapter is to present a brief summary about the state of the art of water treatment through photocatalysis involving ozone and monoperoxysulfate as chemical oxidation technologies. Thus, the problematic of water pollution is first described, emphasizing on water pollution based on emerging contaminants, specifically on pesticides; and, afterwards, a detailed description about chemical technologies based on advanced oxidation processes is presented. Last research advances focused on photocatalytic ozonation and oxidation with monoperoxysulfate, by direct reaction or as a Fenton-like system, applied for removing organic aqueous contaminants, are assessed. Finally, the main objectives in which this dissertation has been developed are summarized.



Plaza Alta, Badajoz

1.1. PRESENTATION

The work of this doctoral thesis has been developed within the activity of the *TRATAGUAS* research group in the Department of Chemical Engineering and Physical Chemistry of the University of Extremadura. *TRATAGUAS*, framed within the scope of environmental engineering, has been conducting extensive research in the field of drinking water purification as well as purification and reuse of wastewater since last decade. Specifically, research activity has lately been concentrated on the research of new technologies with beneficial effects in the elimination of new pollutants, named as emerging contaminants, whose existence is a consequence of current consumption habits. These pollutants require new procedures for their elimination in the purification processes of water using emerging technologies. In this sense, the group's efforts have been dedicated to photocatalytic processes, especially combined with ozone or other oxidant compounds presenting synergistic effects in the process. The project in which this thesis has mainly been framed was entitled '*Preparación de catalizadores y su aplicación en la eliminación de contaminantes refractarios de aguas residuales mediante ozonación fotocatalítica*', reference CTQ2012/35789/C02-01.

The experimental work has been carried out in the laboratory dependencies of the research group inside the Department of Chemical Engineering and Physical Chemistry of the University of Extremadura. In addition, research work has been enriched with two short-stays, in national and international centers. Concretely, a first stay in the '*Centro de Investigaciones de Energía Solar (CIESOL)*', mixed center of the '*Universidad de Almería y Plataforma Solar de Almería-CIEMAT*', in Almería (Spain), during the months of March and April of 2015; and a second stay in the '*Centro de Química-Vila Real (CQ-VR)*' of the '*Universidade de Trás-os-Montes e Alto Douro (UTAD)*', in Vila Real (Portugal), during the months of September, October and November of 2016.

1.2. GLOBAL WATER SITUATION. WATER CRISIS: SCARCITY AND POLLUTION

1.2.1. Importance of water in life

Water is a chemical compound with physical and chemical properties which are unique and irreplaceable. Talking about water is talking about life since the leading role it has had in the development of life in the Earth planet. Without water, life would be impossible to be understood. Actually, first organic molecules that were responsible of the present life forms emerged inside the water. Water is the main component of cells, and the medium in which much of the reactions and metabolic processes take place.

Water forms part of more than 70% of most living organisms, including humans. Specifically, the human body is composed of 55 to 78% of water, depending on the measurements and complexion of each individual. Some need to live inside the water, while others have developed complex mechanisms to survive in extreme conditions of scarcity. All organisms maintain a constant relationship with water in order to perform their vital functions satisfactorily. However, they all return part of consumed water, either in the form of vapor, through evapotranspiration processes, or in liquid form, through body excretions.

Water, under normal conditions of pressure and temperature, is a colorless, odorless and tasteless liquid. Its chemical formula, H_2O , indicates a proportion of two hydrogen atoms per one of oxygen. The oxygen atom, which is bonded to two hydrogens, has a certain negative charge due to its greater electronegativity. This makes the molecule present a defined electrical dipole moment, forming a bipolar structure responsible for some of its physical properties. For example, it can be electrically bonded to other water molecules, in particular four in tetrahedral arrangement, which is known as hydrogen bond. In the liquid state, each water molecule is considered to form hydrogen bonds with at least three molecules. But since molecules are in liquid state under constant motion, these hydrogen bonds are not fixed, they are constantly made and undone, resulting groups of water molecules of different sizes. This makes water not really a single molecule, but a set of molecules, more or less large, whose size depends, among other factors, on temperature.

1.2.2. Water as resource

Water is a resource in constant circulation, either composition or physical state. This continuous movement is known as hydrological cycle or water cycle. The water cycle describes the continuous movement of water on, above, and below the surface of the Earth. This cycle consists of two distinct phases: the terrestrial, which is related to the transport and storage of water on the Earth and at sea, mainly in its liquid and solid state; and the atmospheric phase, which is related to the transport of water in the atmosphere, mainly in the form of vapor. The energy needed to start the cycle, and maintain such an enormous amount of water in motion, comes from the Sun. Part of the solar radiation that reaches Earth's surface is absorbed by water, which allows it to warm up and evaporate. Water that evaporates on the surface of the sea and on the continents, and in lesser extent, appears in the processes of evapotranspiration of living beings and

soil, accumulates in the atmosphere. This water vapor ascends and forms clouds. Due to the gravitational force, the water falls again on the sea or on the continents in the form of rain, ice or snow. The fall in the continents is filtered by the ground, feeding subterranean aquifers that emerge to the surface forming rivers, returning the water to the sea. Sometimes transient accumulations of water appear in the form of lakes or glaciers.

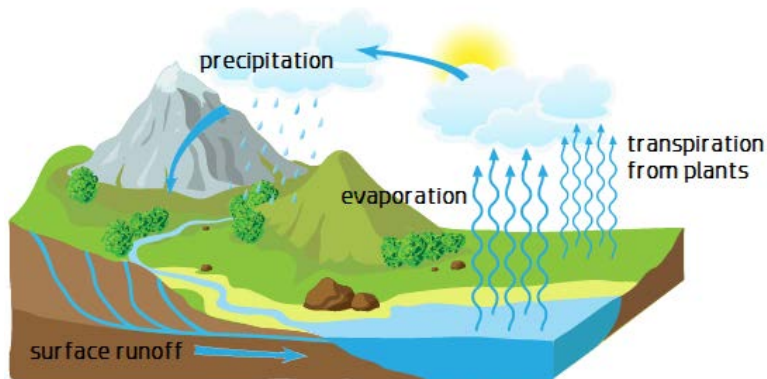


Figure 1.1 Scheme of water cycle

A molecule of water that evaporates and returns to the surface of the Earth in the form of rain, ice or snow, spends about 9 days on average [1]. The mean residence time in each natural reservoir exerts a relevant influence on the persistence of pollution in aquatic ecosystems. For example, a river needs a few days or weeks to be cleaned by the entrainment of pollutants to the sea, where they are diluted. Nevertheless, if an aquifer is polluted, the problem will expect to persist for dozens of years.

The main feature that differentiates the Earth planet from others is the huge amount of water it can accommodate, that is why it is known as Blue Planet. More than three-quarters of the Earth's surface is covered by water, which in more than 97% is presented as salty water [2]. It is estimated that there are about 1,400 millions of km^3 of water on Earth [2,3]; however, only a small portion is fresh water, of which the majority is in the form of ice, steam or located in inaccessible places. Figure 1.2 shows a schematic detail of the distribution of water on the planet.

Water is a resource distributed heterogeneously on the planet, mainly due to the differences between the distributions of precipitation. Also, in some cases the availability is also limited by the quality of water, since its level of pollution renders it unusable for certain uses. The availability of water is especially problematic in big areas of the world, and therefore, properly

exploiting and conserving water resources has become an issue of concern to governments around the world. The exponential growth of population and industrial expansion has created the need to supply and distribute water in greater quantities. World population is projected to peak at 11.21 billion in 2100 compared to 7.34 billion in 2015 [4]. The widespread application of modern technology to the provision of abundant water for municipal, industrial and agricultural uses, without restriction, without incentives to encourage reuse or conservation, has increased competition from readily accessible water sources. In addition to the technical problems involved in meeting water needs, there are increasing environmental concerns that need to be addressed. Concerns about the long-term effects of water use and water loss are in conflict with the objective of maintaining a cheap supply.

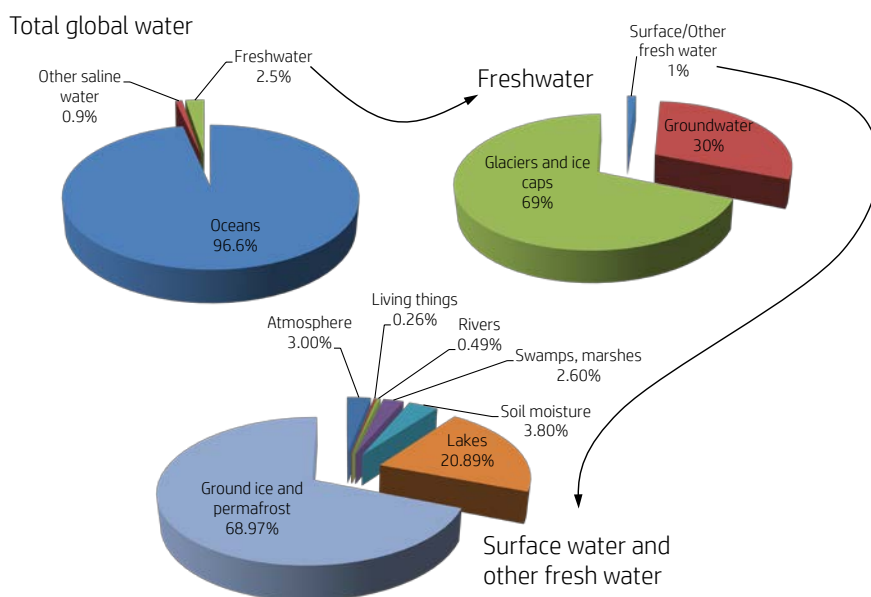


Figure 1.2 Water distribution in the Earth planet according to its origin [2]

Global freshwater reserves are rapidly depleting and a significant impact is expected in many densely populated areas of the world, such as India or China; and others where the resource is scarce, as it happens in regions of West Asia, North Africa or the Middle East. In this future forecast, developed countries, with high consumption rates of water per inhabitant, face the challenge of reducing it through the improvement of practices and techniques of saving and management. The underdeveloped and developing countries, even though with low consumption rates, face serious availability problems due to the scarcity of resources and the disproportionate growth of population, which requires efficient use for all.

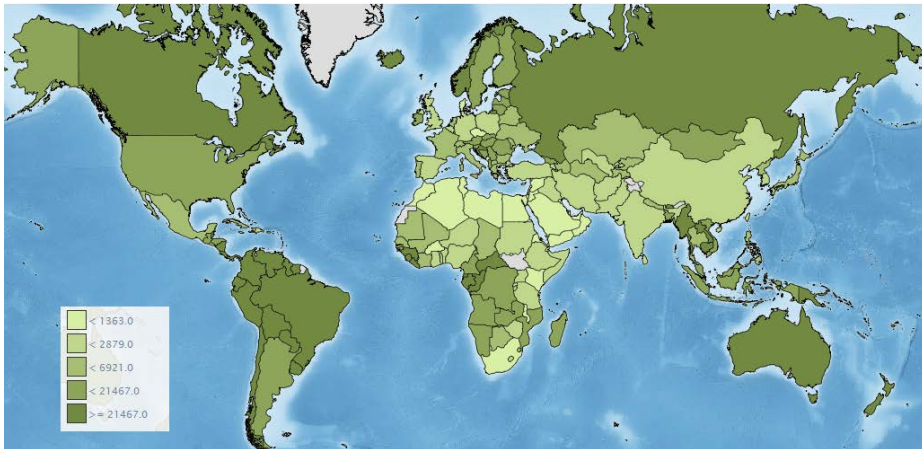


Figure 1.3 Mundial fresh water availability per inhabitant, in kL year⁻¹ person⁻¹ for 2015 (Source: FAO, 2015. AQUASTAT [5])

Irrigated crops consume much of the available fresh water, while domestic and industrial uses account for a small percentage of the resource exploitation. Even so, consumption varies according to the degree of urbanization and industrialization that entails an increase in the industrial and urban sectors, to the detriment of the agricultural. From a deep analysis of the water consumed by a society, great information can be extracted on its habits, degree of development and natural hydraulic availability. Thus, in Europe, with a great industrial and urban development, and a more humid climate, less water is needed for agricultural activity in irrigation. In Spain, domestic, public, commercial and tourist consumption stand out over the rest, which is explained by the great tourist demand in summer and recreational uses.

Domestic use

The amount of water required by a household increases proportionately with the standard of living of the population. However, once a certain threshold has been met, water consumption loses its relation with the quality of life and economic well-being, becoming part of uses not strictly necessary, lack of savings or inefficient distribution systems. Average, 50 L day⁻¹ is required per individual to satisfy their needs [2]. The main problem of water use in the city is its inefficient use. It is used more than is really necessary, and of a quality far superior to what it would really need.

As a consequence of domestic use on water resources, there is an increasing pollutant load after use. In the daily activities of a household, organic and inorganic substances are supplied to the aquatic environment, and they should be treated in order to minimize or eliminate environmental

impacts on the sources where they are discharged. The urban residual water is the most important to be treated, having considerable effects. It is characterized by the plurality and variable concentration of contaminants.

Industrial use

In the industry, large amounts of water are usually required, with extractive, manufacturing and food industries being the most demanding. Water is consumed as a raw material, as a refrigerant, as a source of energy, in cleaning tasks, which explains why the location of many industrial estates near natural water courses. The importance of water in industry lies not only in its physicochemical properties, such as its heat capacity or solvent power. Water is a fast, efficient and essential refrigerant in most industrial processes, and its solvent power is exploited in chemical reactions and cleaning processes.

The degree of industrialization leads to an increase in water consumption. In the world, a quarter of water is destined for industrial uses. In developed countries, water for industrial use can exceed 50% of total consumption (53% in Europe); while in the predominantly agricultural countries, it does not exceed 10% (Spain, 6.4%) [6].

Industrial wastewater consists of aqueous solutions of high concentration of products according to the nature of the industry of origin. The treatment of this type of effluents is essential due to the high polluting power that characterizes them, variable according to the concentration and nature of the pollutant.

Agricultural use

The modernization of traditional farming techniques has succeeded in increasing production and expanding the variety of cultivated species. In addition, thanks to the use of irrigation it is possible to improve the productivity, being possible to increase the number of harvests during the year and to allow the variety of cultures in the same zone. In this sense, the evolutionary process has been directed toward the industrialization of the process, without taking into account that water is a limited and forgotten resource, and in few cases, efforts have been made to reduce its consumption. One of the challenges of the current agriculture is to obtain more yield of each liter of inverted water.

Water available in traditional natural reservoirs has declined considerably due to increased consumption and infrastructure built to meet demand in agriculture, such as reservoirs, canals and distribution systems. The use of

biocides and fertilizers has favored the imbalance of natural systems, which has a significant impact on biodiversity.

Water scarcity is a challenge for today's agriculture, and may affect production. In 2050 an increase in population will require 60% more food. Therefore, water irrigation and food production constitutes one of the greatest pressures on freshwater resources. Agriculture accounts for roughly 70% of global freshwater withdrawals, up to 90% in some fast-growing economies [7]. Overexploitation of fresh water resources leads to numerous problems for agriculture itself. Therefore, in many cases it has been chosen to reconvert the crops to others with less water consumption, or to increase the efficiency of the irrigation process with more efficient techniques.

On the other hand, irrigation has transformed many of the most fertile land on the planet. In regions with a dry climate, the evaporation of water can cause, depending on the characteristics of soil, an ascent of salts towards the surface, compromising the absorption of water by vegetables, accelerating dehydration.

The indiscriminate application of chemical fertilizers and pesticides, in quantities greater than the really necessary, causes that much of these products are not absorbed in the cultures and accumulate in the soil. Excessive watering and rain drags them to rivers and aquifers, where they accumulate in concentrations usually higher than the self-purification capacity of the natural reservoir. At present, the use of pesticides is increasingly restrictive due to the development of demanding legislation on the use of agrochemicals, which evolves to natural and biodegradable substances, more respectful to the environment. Even so, its use still poses a threat.

1.3. PESTICIDES AS EMERGING CONTAMINANTS. THE MODEL COMPOUNDS USED IN THIS THESIS

1.3.1. Emerging organic microcontaminants

Recently there has been a growing interest in what has been named as Emerging Contaminants (ECs) in aquatic ecosystems. This diverse group of organic micropollutants emerges as a consequence of the vast increase of anthropogenic organic compounds synthesized for many purposes, such as preservation and production of food, industrial and manufacturing processes, human and animal healthcare, etc. The presence of this large amount of new compounds in the environment generates alarming concern due to their potential toxicity and environmental fate [8,9]. They are labelled as micropollutants since the reported concentrations of their presence in aquatic

ecosystems are considered too low to cause acute effects, i.e. typically inferior to 100 ng L^{-1} . However, it is unclear and understood the toxic effects due to the long-term exposure to a combination of low concentrations of a vast range of ECs. In last decades, the pollution of ground water resources by ECs has contributed to an increase of research in the ECs area since groundwater provides the most reliable perennial source of freshwater on the Earth [10].

ECs is a term that covers either newly developed compounds or compounds newly discovered in the environment, due to the refinement of analytical techniques allowing detection at extremely low levels [11]. ECs cover a large range of different compounds, as well as their metabolites and transformation products, including pharmaceutical compounds, hormones, drugs, endocrine disruptors, personal care products, pesticides, veterinary products, perfluorinated compounds, flame retardants, food additives, platificizers, engineered nano-materials, etc.

Surface and wastewater seem to be the main sources of ECs in the environment, being the situation of the aquifers unknown due to the lack of enough studies [12]. ECs enter the environment from diverse number of sources and pathways: discharged wastewater effluent from municipal treatment plants [13], septic tanks [14], hospital effluents [15], livestock activities [16], and agriculture [12].

Biological treatment technologies are by far the most widely used for water treatment in general, mainly including aerobic activated sludge. It has been reported that some non-biodegradable and refractory ECs micropollutants cannot be sufficiently removed using biological treatment processes [17-19]. As a consequence, the presence of a large list of ECs in concentrations ranging from low nanograms to milligrams per liter are being reported in the last years at the exit of wastewater treatment plants [20-22], drinking water [23-25], ground water [10, 26, 27], and surface water like rivers and lakes [12, 28-29]. Not only might ECs be poorly degraded, but also adsorbed to the sludge particles. At the end of the process, the sludge is removed and, as it is high in nutrients, in many regions is then applied to agricultural land as a fertilizer. Adsorbed ECs can therefore enter the environment [30,31].

1.3.2. Pesticides as pollutants in agriculture

Pesticides are a broad group of chemical substances of anthropogenic origin, widely used in agriculture to control pests of different origin. Thus, there are herbicides, insecticides, fungicides, nematicides and rodenticides, depending on the nature of the plague to be combated. The continuing need

for food production for a rapidly growing population has forced the development of compounds that ensure the protection and quality of agricultural crops [32]. Thanks to the use of these substances, agricultural production has been able to increase in volume and quality since the 1950s. Unfortunately, this development has not been accompanied by benefits, representing in many cases a threat to the long-term survival of important ecosystems, loss of biodiversity and consequences to human health. During the last decades there have been changes in the protection of crops, focused on the use of less toxic and more selective compounds [33].

The first generation of pesticides encompassed primarily organochlorine compounds, which were gradually replaced in the 1960s and 1970s by a second generation: organophosphates and carbamates. The family of pyrethroids subsequently burst into the market, requiring smaller doses of application. Thus, organophosphates, along with carbamates and pyrethroids, replaced other highly toxic ones such as DDT and dieldrin [34].

Organochlorines are the most widely used pesticides. They are derived from chlorinated hydrocarbons, which give them a high physical and chemical stability, being practically insoluble in water and low volatile. These properties favor their persistence in the medium and slow biodegradation. Their average life, although variable according to the product, is situated in an average value of 5 years [35], and some of them were still detectable in surface waters 20 years after their use had been banned [36]. Either the compounds or its metabolites are contaminants of various tissues in humans and mammals in general. Due to their high lipophilicity, they tend to accumulate mainly in the subcutaneous cellular tissue, in the fatty component of the breast milk or in the blood. Some examples of organochlorine pesticides are DDT, aldrin, dieldrin, endrin, endosulfan and lindane.

Organophosphates are esters, amides or thiols derived from phosphoric acids. They are more easily decomposed and degraded by oxidation and hydrolysis, producing water-soluble, less preservative and less accumulative products in the human body. Examples of this group are malathion, diazinon, chlorpyrifos and dichlorvos.

Carbamates are subdivided into three main groups: carbamate esters, commonly applied as insecticides; thiocarbamic acid derivatives, applied as fungicides; and carbamates themselves, used as herbicides. All of them are unstable; they are attributed a low time of environmental persistence and have certain selectivity. Their degradation includes the oxidation and their final metabolites are water soluble, being able to be eliminated by the urine or

feces. Among the most common can be mentioned alicarb, carbaryl and carbofuran.

Finally, pyrethroids are obtained by drying, milling and spraying the flower of the chrysanthemum, which powder contains from 1 to 3% of the active principle. Of medium selectivity, they present low toxicity. Allethrin, permethrin, fluralinate and tetramethrin are some examples.

Pesticides can reach aquatic ecosystems by different routes; some are schemed in Figure 1.4. Once pesticides are used in agriculture, move through the ground surface by penetrating the soil, washed away by water and wind. Thus they end up in subterranean waters, rivers, lakes, and finally in oceans in the form of sediments transported by rivers. Water that flows on the surface, whether in the form of rain, irrigation or other sources, dissolves adsorbed pesticides. Additionally, herbicides promote pollution from nearby aquatic sources. Once in water, the pesticide dissolves and moves in it. Water flows on the surface, in the form of rain, irrigation or other sources, promoting the dissolution of adsorbed pesticides [37]. Additionally, improper cleaning of containers used in the application of herbicides promotes runoff and contamination of nearby aquatic resources [38]. If it is associated with particles, it moves and disperses mechanically [33, 37].

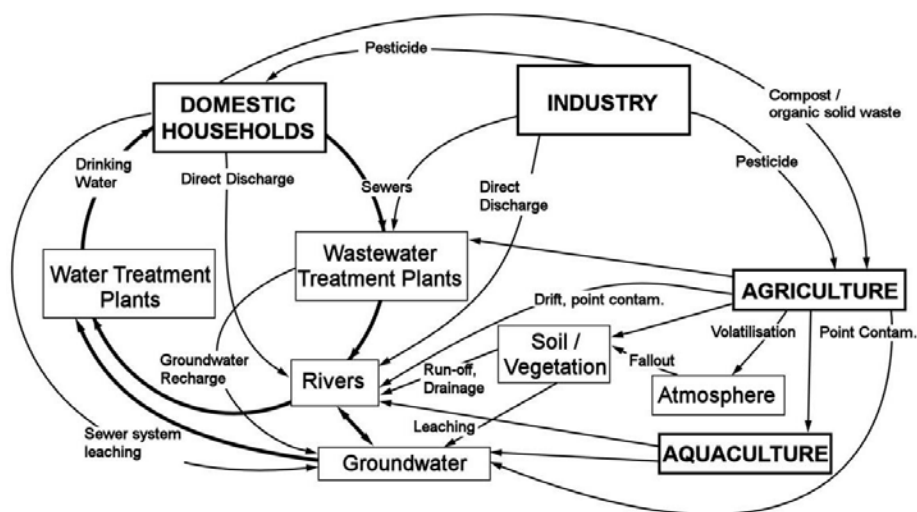


Figure 1.4 Pathways of pesticide insertion into water cycle

The ecological effects of pesticides on water depend on their toxicity, persistence in the environment, degradation products and environmental fate. The toxicological response or effect may be acute or chronic, that is, it can go from direct death to an effect that may not cause death but that does affect the organism for the rest of its life. Much research has been performed on the

toxicity of pesticides. Examples of these effects are cancers and tumors [39-43], reproductive deficiencies [44, 45], growth inhibition [46, 47], teratogenic effects [48-52], neuronal diseases [53-56], etc. Perhaps the greatest threat posed by pesticides; however, is their endocrine disrupting potential [57, 58]. These effects are not necessarily exclusively caused by exposure to pesticides and other organic pollutants; but may be associated to combinations of environmental pressures. Many of them, which are chronic and non-lethal, go unnoticed by the surface observer.

The active ingredient used in each pesticide can have a very variable half-life or persistence that is determined by the biotic and abiotic processes of degradation. While the first involves biodegradation and metabolism by living organisms, the second refers to degradation by physicochemical processes, such as hydrolysis, photolysis and oxidation. Having been taken place the degradation process, transformation products, whose toxicity may be higher, equal to or less than the parent compound, are generated. Finally, the environmental fate where the compound ends is also diverse in the case of pesticides, depending on the physicochemical affinity of the substance with respect to solid (organic and mineral matter), liquid via solubility in water, gaseous form (volatilization) and biotic (biodegradability). This behavior comprises the determination of the soil absorption coefficient, solubility, Henry constant, and n-octanol-water repartition coefficient. The solubility in water is essential to elucidate the behavior of the pesticide in the aquatic environment, as it influences the bioconcentration and the adsorption in the sediment [37].

1.3.3. The herbicides studied in this thesis

MCPA: aryloxyalkanoic acid derivative

MCPA, 2-methyl-4-chlorophenoxyacetic acid, is a synthetic auxin herbicide derived from aryloxyalkanoic acids. These herbicides were introduced after the Second World War and they still keep being the most used around the world. Although they are mainly applied to foliage, they can be also absorbed by roots, where they keep immobilised. Then, the active ingredient disrupts vegetable's growth by means of apoplast and symplast. Its real mechanism of action is still unknown; however, it is highly accepted that they act as being real auxins that disrupt the natural auxin level of indoleacetic acid, needed for organized growing [59]. The vegetable detects acid excess, which is quickly degraded by the plant, but the synthetic regulator, the active ingredient, is not. As a consequence, the plant growth is disrupted. The structure of the organic plays an important role during the process, especially in terms of selectivity.

The external symptoms or effects in sensitive plants are abnormal production of roots and buds, destroying vessels, burns, epinasty, sprawl development, gradual yellowing, twisting of the plant and finally, its death. Physiologically they increase breathing, reducing the photosynthesis process as nutrient reserves are depleted.

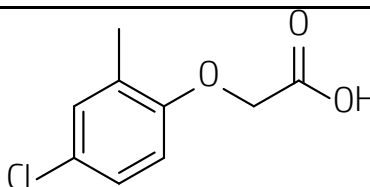
Aryloxyalkanoic acids are selective in monocotyledon crops, or narrow-leaved plants, as well as numerous dicotyledons. They are also used to control broadleaf woody plants in cultivated and non-cultivated areas, and aquatic plants in some situations. Some examples of broadleaf weed sensitive to this family are: corn, sorghum, wheat, barley, oats, rye, rice, sugarcane and pasture. They are applied in post-emergency situations, and they may damage other susceptible crops (cotton, tomato, grapevine, etc.).

The oxidation of these compounds is, according to some authors, by means of hydroxylation of aromatic ring or microorganisms. They have a relatively low persistence in the soil due to their high solubility in water.

The most popular herbicides of this family are 2,4-D, the first organic synthesized herbicide; MCPA, other pioneering synthesized in England; 2,4,5-T, a well-known carcinogenic similar to 2,4-D but more effective; 2,4-DP; MCPB; MCPP; and 2,4,5-TP.

Table 1.1 Physicochemical properties of MCPA [61]

Name	MCPA		
IUPAC Name	4-chloro-2-methylphenoxyacetic acid		
Formula	$C_9H_9ClO_3$		
CAS number	94-74-6		
Family	Aryloxyalkanoic acid		
Action mode	Selective, systemic with translocation. Synthetic auxin.		
Molar weight, g mol⁻¹	200.62	Octanol-water partition coefficient (logK_{ow}), at pH=7 and 20°C	-0.81
Water solubility, mg L⁻¹	29,390	Dissociation constant (pK_a) at 25°C	3.73
Toxicity	<i>Daphnia Magna</i> : EC ₅₀ (48 h) > 190 mg L ⁻¹		



MCPA has been popularly formulated and sold throughout the world under numerous trade names for the various amine, ester, and inorganic salt forms. It was one of the first hormone-type herbicide discovered in England. MCPA is used as a post-emergency herbicide to control broadleaf weeds, including thistle and dock, in cereal crops and pasture; with characteristics similar to those of 2,4-D. Nevertheless, MCPA is more selective than 2,4-D at equal

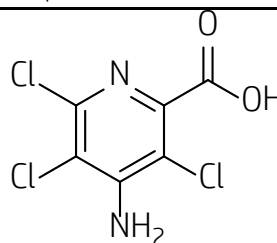
doses in wheat crops, legumes and linen; and highly selective in some crops such as barley, corn and sorghum [60].

Clopyralid (CLO), picloram (PIC) and triclopyr (TRI): pyridine herbicides

Pyridine herbicides, whose chemical structures all contain the pyridine aromatic ring, regulate vegetable's growth. Their action is the same as aryloxyalkain acids. Although pyridine herbicides are foliar and root absorbed, contact action is the most remarkable. They can be sprayed on foliage, injected into plants, applied to cut surfaces, or placed at the base of the plant where it will leach to the roots. Once absorbed by the foliage, stem, or roots, active ingredient is transported through vegetable cells and accumulated in young shoots [35]. The mechanism inhibits auxins, acts enlarging leaf and stalks by means of cellular respiration. Heat is needed in order to reach their effect.

Table 1.2 Physicochemical properties of picloram [61]

Name	Picloram		
IUPAC name	4-amino-3,5,6-trichloropyridine-2-carboxylic acid		
Formula	$C_6H_3Cl_3N_2O_2$		
CAS number	1918-02-1		
Family	Pyridine compound		
Action mode	Selective, systemic absorbed by roots and leaves and translocated. Synthetic auxin.		
Molar weight, g mol⁻¹	241.46	Octanol-water partition coefficient (logK_{ow}), at pH=7 and 20°C	-1.93
Water solubility, mg L⁻¹	560	Dissociation constant (pK_a) at 25°C	2.30
Toxicity	<i>Daphnia Magna</i> : EC ₅₀ (48h) = 44.2 mg L ⁻¹		



Picloram gives excellent control of woody plants and many annual and perennial broadleaved species. It is used to control broadleaf weeds on rangeland and permanent grass pastures, fallow cropland, small grains, flax on grain-land and non-croplands. Picloram is very persistent and lasts for up to one year, or longer, to affect succeeding crops [35]. It is water soluble, not highly adsorbed, and therefore susceptible to leaching. These characteristics are undesirable, although its high activity is convenient for control of perennial weeds. Picloram is very persistent in soil, which is other of the reasons why it is a restricted-use herbicide. Microorganisms slowly degrade it. Some

conditions that favour microbial growth, such as warm, moist soil and organic matter, may reduce its period of resistance.

Clopyralid is less persistent and less leachable than picloram, but effective for broadleaf weeds, especially thistles and clovers. Sugar beet, field corn, small grains (wheat, oats and barley), fallow cropland, rangeland and permanent grass pastures, and non-crop areas are some examples where clopyralid is used to control broadleaf weeds and woody brush species. Clopyralid is not strongly adsorbed by soil. It exists in the soil primarily in the salt form and is therefore subject to leaching. It is degraded by microorganisms at a medium to fast rate in a wide range of soils [35].

Table 1.3 Physicochemical properties of clopyralid [61]

Name	Clopyralid		
IUPAC name	3,6-dichloropyridine-2-carboxylic acid		
Formula	C ₆ H ₃ Cl ₂ NO ₂		
CAS number	1702-17-6		
Family	Pyridine compound		
Action mode	Selective, systemic, absorbed through leaves and roots. Synthetic auxin.		
Molar weight, g mol ⁻¹	192.0	Octanol-water partition coefficient (logK _{ow}), at pH=7 and 20°C	-2.63
Water solubility, mg L ⁻¹	143,000	Dissociation constant (pK _a) at 25°C	2.01
Toxicity	<i>Daphnia Magna</i> : EC ₅₀ (48h) > 99 mg L ⁻¹		

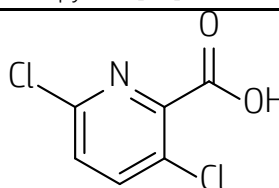
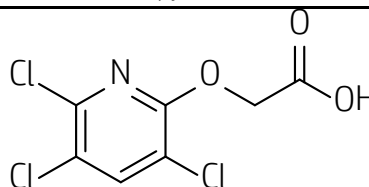


Table 1.4 Physicochemical properties of triclopyr [61]

Name	Triclopyr		
IUPAC name	3,5,6-trichloro-2-pyridyloxyacetic acid		
Formula	C ₇ H ₄ Cl ₃ NO ₃		
CAS number	55335-06-3		
Family	Pyridine compound		
Action mode	Selective, systemic, absorbed through roots and foliage. Synthetic auxin.		
Molar weight, g mol ⁻¹	256.5	Octanol-water partition coefficient (logK _{ow}), at pH=7 and 20°C	4.62
Water solubility, mg L ⁻¹	8,100	Dissociation constant (pK _a) at 25°C	3.97
Toxicity	<i>Daphnia Magna</i> : EC ₅₀ (48h) > 131 mg L ⁻¹		



Triclopyr is effective on woody plants and is used for brush control in natural tracks and defoliation of wooded areas leaving grasses and conifers

unaffected. Some uses are weed controlling in non-crop areas, rangelands, pastures and as basal treatments to stumps for woody plant control. Most grasses are tolerant and, while it is not used in many crops, with the exception of rice, it is used as a turf herbicide. Organic matter content and pH highly influence triclopyr adsorption, even so this herbicide is not considered to be strongly adsorbed on soil colloids. Some leaching may occur in lighted soils under high rainfall conditions. Triclopyr is degraded in soils by microorganisms at a rate that is considered to be relatively high [35].

Diuron (DIU): phenylurea

Phenylureas came from uric acid and are frequently halogenated. Their intervention mechanism involves inhibition of photosynthesis process, in particular blocking Hill's reaction whose purpose is the formation of carbohydrates [62]. As a consequence of their effect, necrosis of the plant takes place, finishing with death. They are supposed to be absorbed by the root system, blocking cellular division and nitrate formation. If phenylureas penetrate through leaves; local necrosis, which expands on all the plant, is generated.

Their solubility in water and adsorption to colloid depend on the number of halogen atoms, chloride usually, in the molecule. Thus, fenuron, which has not chloride atoms, is soluble in water and easily leachable in soil; while diuron, with two chloride atoms, is strongly fixed to colloids. The selectivity range based on metabolism is wide, as happens to chlortoluron and isoproturon in crops like wheat and barley, diuron and fluometuron in cotton, and linuron in potato. Anyway, as they have no high selectivity, most of them may be used for general purposes in weed control.

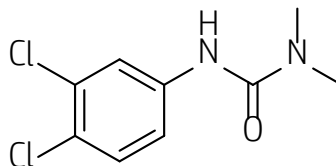
These herbicides are degraded in soil by the action of some microorganisms, which are able to consume them as carbohydrate reserve. Moreover, they can be oxidized by means of solar light, especially ultraviolet radiation [35].

Diuron is capable to be adsorbed in soil and resists to leaching. For that reason, it is registered as a preplant incorporated, preemergence, postemergence, and postemergence-directed application in a wide variety of crops, including alfalfa, artichokes, asparagus, corn, winter wheat and barley, oats, red clover, sorghum, cotton, sugarcane, tree fruit, bush fruits, citrus, vining fruits, olives, nuts, grapes, pineapple, bananas, plantains, papaws, mint, grass seed crops, and tree plantings in non-crop land, for control of a variety

of annual and perennial weeds, depending on the use. In general, diuron is widely used, at high doses, for controlling all kind of weeds.

Table 1.5 Physicochemical properties of diuron [61]

Name	Diuron		
IUPAC name	3-(3,4-dichlorophenyl)-1,1-dimethylurea		
Formula	C ₉ H ₁₀ Cl ₂ N ₂ O		
CAS number	330-54-1		
Family	Phenylurea		
Action mode	Systemic, absorbed via roots, acts by strongly inhibiting photosynthesis		
Molar weight, g mol⁻¹	233.09	Octanol-water partition coefficient (logK_{ow}), at pH=7 and 20°C	2.87
Water solubility, mg L⁻¹	35.6	Dissociation constant (pK_a) at 25°C	No dissociation
Toxicity	<i>Daphnia Magna</i> : EC ₅₀ (48h) = 5.7 mg L ⁻¹		



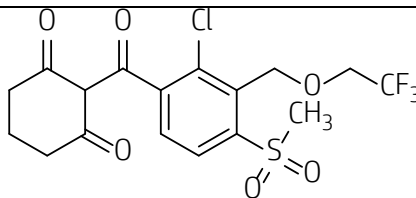
Temboatrione (TEMB): triketone

Commercial synthetic β -triketones derivatives were designed after the discovery of the herbicidal properties of leptospermon, the primary component of Manuka essential oils. These compounds have β -triketones backbones that inhibit the *p*-hydroxyphenylpyruvate dioxygenase enzyme [63], by complexing with Fe²⁺ within the catalytic domain. So, triketone herbicides are 4-hydroxyphenylpyruvate dioxygenase (HPPD) inhibitors, which act blocking the HPPD indispensable enzyme in plant growth. Thus, the plant develops leaf bleaching followed by necrosis and death [64]. HPPD inhibitors were brought to North American and European markets as newest class herbicides in late 1990s and 2000s considering that weeds had been developed resistance to traditional herbicides, such as glyphosate, and as pesticide legislation had become more restrictive to classical herbicides.

Temboatrione was launched in 2007 for different types of grass and broadleaf weeds control during the early to mid-post-emergence step of field corn [65]. Although it is mostly used in popcorn crop, sweet corn and seed corn fields; other applications, like in sorghum and soybeans, are still under research.

Table 1.6 Physicochemical properties of tembotrione [61]

Name	Tembotrione		
IUPAC name	2-[2-chloro-4-mesy]-3-[(2,2,2trifluoroethoxy)methyl]benzoyl] cyclohexane-1,3-dione		
Formula	C ₁₇ H ₁₆ ClF ₃ O ₆ S		
CAS number	335104-84-2		
Family	Triketone		
Action mode	Broad spectrum		
Molar weight, g mol⁻¹	440.82	Octanol-water partition coefficient (logK_{ow}), at pH=7 and 20°C	-1.09
Water solubility, mg L⁻¹	71,000	Dissociation constant (pK_a) at 25°C	3.18
Toxicity	<i>Daphnia Magna</i> : EC ₅₀ (48h) = 5.0 mg L ⁻¹		



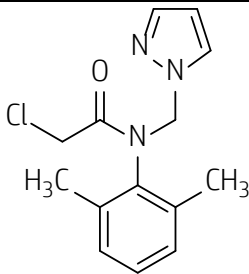
Metazachlor (METAZ): chloroacetamide

Most of chloroacetamides are applied as pre-emergence, while others have a post-activity. When they are used as pre-emergence, produce abnormal seedlings into susceptible grass and broadleaf weeds that may not emerge from the soil. The susceptible monocots that do emerge appear twisted and malformed with leaves tightly rolled in the leaf whorl and unable to roll normally. Leaves do not emerge properly from the coleoptile, but may do so underground. Broadleaf weed seedling may have slightly cupped or crinkled leaves and shortened midribs producing a drawstring effect on the leaf tip, especially under cold conditions. The primary site of action is presently regarded as inhibition of synthesis of very long chain fatty acids and functionally relates structures [35].

Chloroacetamides herbicides control germinating annual grasses and some broadleaf weeds in a wide range of crops. In germinating seedlings they are easily absorbed by the aerial part and root; however, their mobility within the plant is limited.

Metazachlor formulations are selective herbicides, absorbed by the hypocotyls and roots, and inhibiting germination. The products are used in pre-emergence and early post-emergence control of winter and annual grasses and broad-leaved weeds in artichokes, broccoli, asparagus, Brussels sprouts, cabbages, cauliflowers, sweetcorn, garlic, horseradish, kale, leeks, maize, white mustard, onions, peanuts, pome fruits, potatoes, radish, rape, soya beans, stone fruits, strawberries, sugar cane, sunflowers, tobacco and turnips.

Table 1.7 Physicochemical properties of metazachlor [61]

Name	Metazachlor		
IUPAC name	2-chloro- <i>N</i> -(pyrazol-1-ylmethyl)acet-2',6'-xylylidide		
Formula	C ₁₄ H ₁₆ ClN ₃ O		
CAS number	67129-08-2		
Family	Chloroacetamide		
Action mode	Ergosterol inhibitor. Inhibition of cell division		
Molar weight, g mol⁻¹	277.75	Octanol-water partition coefficient (logK_{ow}), at pH=7 and 20°C	2.49
Water solubility, mg L⁻¹	450	Dissociation constant (pK_a) at 25°C	No dissociation
Toxicity	<i>Daphnia Magna</i> : EC ₅₀ (48h) = 33 mg L ⁻¹		

Tritosulfuron (TRITO): sulphonylurea

Sulphonylureas were introduced in the 1980s, when they represented a major advance in global crop protection because of its unique mode of action. The core structure for the sulphonylureas combines the photosynthetic inhibition of phenylureas and triazines, but the primary mechanism of action is inhibition of amino acid synthesis, not photosynthesis. Secondary, they inhibit photosynthesis, respiration, and protein synthesis [66]. Plant symptoms include chlorosis, necrosis, terminal bud death, and vein discoloration. The site of action for the sulphonylureas catalyzes the first step in the biosynthesis of the three branched chain aliphatic amino acids valine, leucine, and isoleucine. A secondary effect is cessation of plant growth due to inhibition of cell division and slow plant death. Tolerance is related to a plant's ability to detoxify the herbicide.

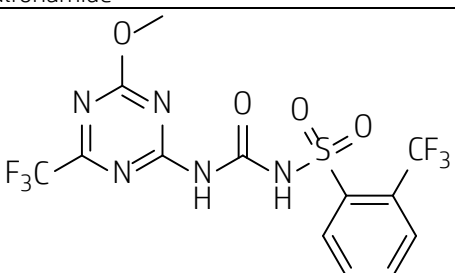
Moreover, other advantage introduced consists on their compatibility with other pests. Sulphonylureas replaced herbicides less safe and effective, which were used in larger quantities. Combined with the low application rates, selectivity for a variety of crops, and short half-life, sulphonylureas herbicides were a revolutionary advance in agrochemicals in the 1980s.

Sulphonylureas work on a broad range of grasses and broadleaf weeds, but not on crops that they are designed to protect. Some crops like rice, wheat, barley, soybean, maize and many others are able to metabolize sulphonylureas safely. They are supposed to have very low toxicity to mammals, low environmental risk due to their high solubility, which means

high probability to move around, and easiness to be microbiologically degraded. They are weak acids which are hydrolyzed at high pH, increasing their solubility in water [35].

Tritosulfuron is a systemic herbicide for the post-emergence control of a wide range of dicotyledonous weeds both winter or spring cereals and maize. Upon uptake by the leaves of the targeted weeds, tritosulfuron is acropetally and basipetally translocated in the plant resulting in a blockage of the enzyme acetohydroxy acid synthase. The inhibition of this enzyme activity acts directly on growth and cell development of the weeds. Tritosulfuron is a post-emergence herbicide of broad spectrum, mainly for use in cereals, rice, maize, and turf [67].

Table 1.8 Physicochemical properties of tritosulfuron [61]

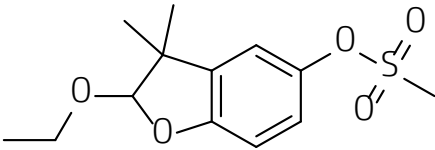
Name	Tritosulfuron		
IUPAC name	N-[[4-methoxy-6-(trifluoromethyl)-1,3,5-triazin-2-yl]carbonyl]-2-(trifluoromethyl)benzene-1-sulfonamide		
Formula	C ₁₃ H ₉ F ₆ N ₅ O ₄ S		
CAS number	142469-14-5		
Family	Sulfonylurea		
Action mode	Inhibits plant amino acid synthesis-acetohydroxy acid synthase		
Molar weight, g mol⁻¹	445.30	Octanol-water partition coefficient (logK_{ow}), at pH=7 and 20°C	2.93
Water solubility, mg L⁻¹	78.3	Dissociation constant (pK_a) at 25°C	4.69
Toxicity	<i>Daphnia Magna</i> : EC ₅₀ (48h) > 100 mg L ⁻¹		

Ethofumesate (ETHO): benzofuran

Ethofumesate is a selective systemic herbicide, absorbed by the emerging shoots (grasses) or roots (broad-leaved plants), with translocation to the foliage. Chemically, ethofumesate is a benzofuranyl that is readily absorbed by leaves after the plant has generated a mature cuticle [66]. Ethofumesate inhibits the growth of meristems, retards cellular division, and limits formation of waxy cuticles [68]. It is used pre and post-emergence in sugar beet and other beet crops, turf, ryegrass and the other pasture grasses against a wide range of grass and broad-leaved weeds, with persistence of activity in the soil. It is primarily a soil-applied herbicide, but it has some post-emergence activity on young weeds. Post-emergence activity may be increased when it is used in combination with certain other herbicides in sugar beets [69]. Some crops are

highly tolerant towards ethofumesate, including strawberries, sunflowers, common beans and tobacco, depending on the time of application. Ethofumesate appears to be adsorbed to organic matter in soil and is biologically degraded in soils [35].

Table 1.9 Physicochemical properties of ethofumesate [61]

Name	Ethofumesate		
IUPAC name	<i>(RS)</i> -2-ethoxy-2,3-dihydro-3,3-dimethylbenzofuran-5-yl methanesulfonate		
Formula	C ₁₃ H ₁₈ O ₅ S		
CAS number	26225-79-6		
Family	Benzofurane		
Action mode	Selective, systemic, absorbed through emerging shoots and roots. Inhibition of lipid synthesis.		
Molar weight, g mol⁻¹	286.34	Octanol-water partition coefficient (logK_{ow}), at pH=7 and 20°C	2.7
Water solubility, mg L⁻¹	50	Dissociation constant (pK_a) at 25°C	No dissociation
Toxicity	<i>Daphnia Magna</i> : EC ₅₀ (48h) = 13.52 mg L ⁻¹		

1.4. ADVANCED OXIDATION PROCESSES (AOPs) AS EMERGING TECHNOLOGY FOR OXIDATION OF AQUEOUS EMERGING CONTAMINANTS

Advanced Oxidation Processes were defined by Glaze and Kang (1987) as those ‘involving the generation of hydroxyl radicals in sufficient quantity to produce a purification effect on water’ [70]. Thus, the development of AOPs arises with the objective of producing hydroxyl radicals in greater concentration, enough to oxidize contaminants. They consist of a family of methods that make use of the high oxidative capacity of the hydroxyl radical (2.85 V [71]), and which only differ in the way of generating them. The hydroxyl radical, characterized by its high oxidation potential, is an extremely reactive radical that is able to attack and non-selectively oxidize most organic molecules, with reaction kinetic constants of the order of 10⁸-10¹⁰ M⁻¹ s⁻¹ [72-73], leading even towards complete mineralization. AOPs are also enhanced by the fact that they offer different possible ways for hydroxyl radical production, allowing a better compliance with the specific treatment requirements [74]. AOPs are usually classified as photochemical and non-photochemical, depending on whether or not they use radiation in the generation of radical species, as shown in Table 1.10.

Table 1.10 AOPs classification

HOMOGENEOUS PROCESSES	References
1) Without radiation	
Ozonation in alkaline medium (O_3/OH^-)	[75]
Catalytic homogeneous ozonation (O_3/CAT)	[76]
Ozonation with hydrogen peroxide, peroxone (O_3/H_2O_2)	[77]
Fenton (Fe^{2+}/H_2O_2)	[78, 79]
Fenton-Like (Fe^{3+}/H_2O_2)	[73]
Water Air Oxidation (WAO)	[80]
Supercritical Water Oxidation (SCWO)	[81]
2) With radiation	
Ozonation with UV radiation (O_3/UV)	[82]
Hydrogen peroxide with UV radiation (H_2O_2/UV)	[83]
Ozone, hydrogen peroxide and UV radiation ($O_3/H_2O_2/UV$)	[84]
Foto-Fenton (Fe^{2+} or $Fe^{3+}/H_2O_2/UV$)	[85]
Sonolysis (US)	[86]
HETEROGENEOUS PROCESSES	
Catalytic Wet Air Oxidation (CWAO)	[81]
Catalytic ozonation (O_3/CAT)	[87]
Heterogeneous photocatalytic oxidation ($O_2/UV-vis/CAT$)	[88]
Heterogeneous photocatalytic ozonation ($O_3/UV-vis/CAT$)	[89, 90]

Unfortunately, AOPs fail to degrade complex compounds completely, especially in the case of real wastewaters. Moreover, cannot be used for processing large volumes of water [91]. Only wastes with relatively small Chemical Oxygen Demand content, i.e. inferior to 5.0 g L^{-1} , can be suitably treated by hydroxyl radical based techniques since higher COD contents would require large amounts of expensive reactants [74]. In this sense, AOPs seem to be more suitable for depuration of water with low organic load, such as drinking water [92]. However, they have successfully been combined with biological processes for diverse purposes at pilot plant scale. Organic pollutants not treatable by conventional techniques due to their high chemical stability or low biodegradability can be oxidized through AOPs previously coupled to biological oxidation [93]. In addition to the use as pre-treatment, AOPs also can be considered in a post-biological step in order to reach high depuration rates or the degradation of those organic compounds that, being not toxic for biological metabolism, present biorecalcitrance [93].

1.4.1. Photocatalytic oxidation

Photocatalytic oxidation or heterogeneous photocatalysis is based on the excitation of a solid semiconductor by absorption of electromagnetic radiation, generally from the near UV zone. The radiation absorbed by the photocatalyst causes on the surface therefore the excitation of electrons, migrating from the conduction band to the valence band, generating in the first hollows, or deficit areas of electronic charge, characterized by very high oxidation potentials [94].



In the absence of suitable electron and hole scavengers, the stored energy is dissipated within a few nanoseconds by recombination. This quick recombination of electron-hole pair supposes an undesirable reaction for the process to be developed.



Nowadays, various semiconductor materials are used, such as TiO_2 , ZnO , CdS , iron oxides, WO_3 , SnO_2 , etc. These materials are economically affordable and most of them can be excited by non-high energy radiation, UVA and even visible light, absorbing part of the solar spectrum radiation incident on the Earth's surface (radiation >310 nm), which increases the interest for a possible use of sunlight. Nevertheless, some of them like the CdS and ZnO suffer from photocorrosion after several cycles of use. Figure 1.5 shows an outline of the position of the valence and conduction bands that define the band gap energy of some photocatalysts [95].

The main photocatalyst used is titanium dioxide, TiO_2 , due to its low toxicity, high stability and low cost [96]. Titanium dioxide has a band gap energy of 3.2 eV, that is, only radiation with a wavelength lower than 387 nm has an energy equal to or greater than this value [97], and therefore able to excite electrons from its valence band.

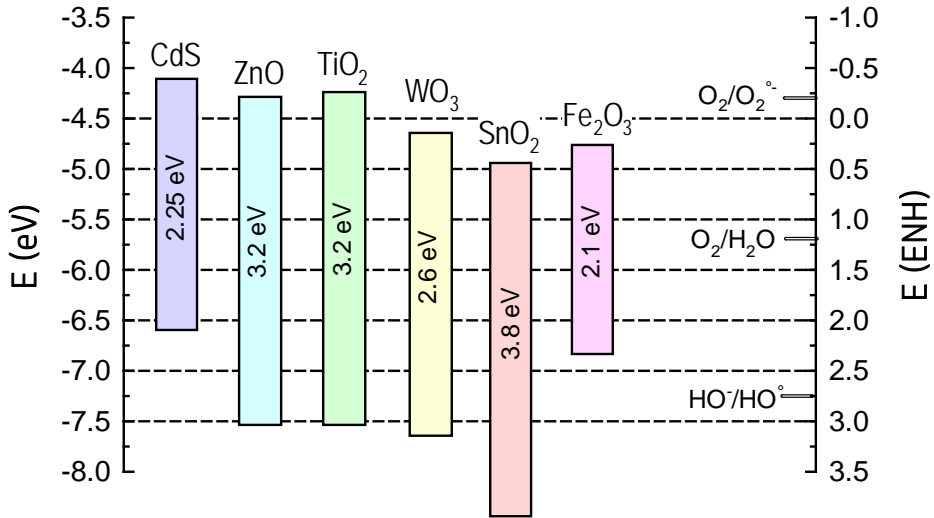


Figure 1.5 Relative positions of valence and conduction bands for some common photocatalysts [95]

The holes generated in the valence band can produce the oxidation of adsorbed organic compounds or decompose adsorbed water molecules. In this latter case, hydroxyl radicals are generated. Excited electrons of the conduction layer are able to reduce oxygen molecules. In aqueous phase and with the addition of oxygen as an oxidizing element, the equations representing the process are as shown below [94]:



If the medium is alkaline enough, the holes oxidize hydroxyl anions instead of water molecules, also forming hydroxyl radicals.



Figure 1.6 shows the schematic process of radical formation mechanism, considering the presence of oxygen for the reduction reaction of an organic molecule (R).

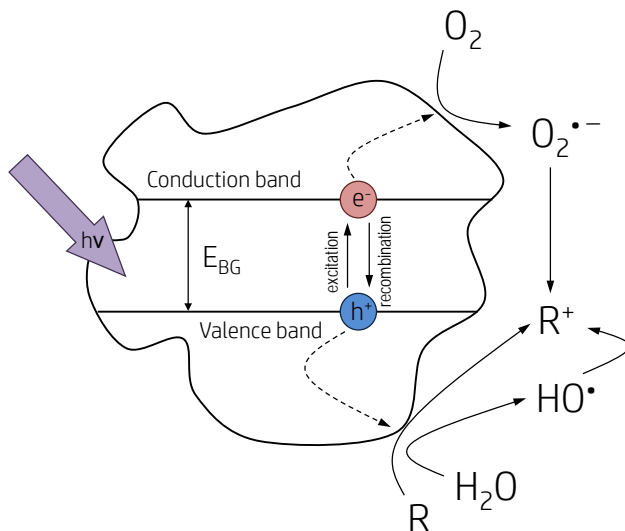


Figure 1.6 Photocatalytic radical formation mechanism in the presence of oxygen

Electron-hole recombination is avoided if electrons are withdrawn through pre-adsorbed oxygen, giving rise to the superoxide radical. Therefore, superoxide radicals can produce hydrogen peroxide, which reacts with additional electrons and/or more superoxide radicals, forming free hydroxyl radicals through the following reactions:



The undesirable phenomenon of recombination can also be resolved by doping of photocatalysts [98]. Doping of the semiconductor causes the generation of irregularities in the crystal lattice that favors the capture of holes and electrons, preventing them from being recombined [99, 100]. Moreover doping of titanium dioxide improves photocatalysis under visible spectrum by narrowing the band gap [101]. Thus, doping is based on the introduction of foreign elements into the TiO₂ structure in relatively low proportions so as not to produce changes in its crystalline structure. Substitution of both Ti⁴⁺ and O²⁻ positions by p block elements such as B, C, N, F, S, and P is what appears to provide better results [102].

Among all the anions, nitrogen seems to demonstrate greater benefits in the process of modifying the solid because the nitrogen has the closest atomic size to oxygen; smaller ionization energy; metastable center formation and stability [102]. In 1986 the first study related to the photoactivity of TiO₂

doped with nitrogen is published [103]. The presence of NO_x groups, formed from ammonium hydroxide used in the synthesis process was postulated as responsible for the effect. Asahi et al. (2001) applied a TiO_2 sputtering process and concluded that N-doping was the main cause of the photocatalytic effect observed under visible light [101]. Since then, a high number of works related to the issue have appeared.

To achieve a suitable N-doping, there are several protocols still in use such as physicochemical techniques like sputtering [101, 104, 105] and ion implantation [106-109], chemical treatment of pure oxides [110, 111], high temperature TiO_2 sintering under nitrogen atmosphere [112], sol-gel processes [113-117], titanium nitride oxidation [118-122], processes with plasma [122-127] and atomic deposition [128, 129]. In sputtering and implantation techniques, TiO_2 sheets are directly coated with nitrogen ions. In the sintering process, TiO_2 powder or film is calcined in the presence of nitrogen precursors such as ammonia or urea. However, the sol-gel method is the most popular because it does not require sophisticated equipment and is relatively easy to carry out. It also allows for controlling nanostructure, morphology and porosity of the material. In the sol-gel process the synthesis of TiO_2 and doping takes place together by means of hydrolysis of titanium precursors, generally alkoxides such as titanium isopropoxide or tertbutoxide, and different sources of nitrogen. NH_4Cl , N_2H_4 , NH_4NO_3 , HNO_3 , ammonia, urea and amines are the most common. In this way, size and proportion of doping agent can be easily controlled according to the synthesis conditions used such as pH, temperature, hydrolysis rate, etc. However, the hydrolysis process is complex and involves several steps and variables to be controlled.

1.4.2. Ozonation and photocatalytic ozonation

Currently, ozonation is one oxidation process that more land is gaining to the traditional oxidant, chlorine, in water treatment. Ozone bursted into drinking water treatment as a solution to trihalomethanes formation during the conventional process of chlorination, due to the presence of natural organic compounds in raw water [130]. On account of its high redox potential, although inferior to that of the hydroxyl radical (2.07 versus 2.85 V), ozone is a very powerful chemical oxidizer, a property that can be used for diverse purposes. The main use of ozone is concentrated on the disinfection [131], oxidation of iron and manganese ions, elimination of algae, odors, flavors and volatile organic compounds, removal of substances considered as priority pollutants, as well as improvement of certain stages of water treatment (flocculation, active carbon adsorption, biological oxidation, etc.) [132, 133]. In

addition, ozone is an effective oxidant in the elimination of organic compounds resistant to traditional biological treatments, such as pharmaceutical compounds, hormones, personal care products, surfactants, pesticides, etc.; either alone or in combination with other agents such as UV radiation, catalysts or photocatalysts, hydrogen peroxide, etc. [134].

Regardless of the purpose to be achieved, the application of ozone in water treatment involves action through four consecutive stages: in situ generation, transfer from the gas where it is generated to water, the chemical reaction and the destruction of residual ozone [132]. Once the ozone is transferred to the aqueous medium, it can react with diverse substrates by two well differentiated pathways. Firstly, the direct reaction between molecular ozone and the substrate; and secondly, the indirect reaction through radical species that come from the decomposition of ozone in water. In this way, during the process of ozonation part of dissolved ozone reacts directly with the organic matter in solution, in some cases with quite low reaction constants.

Molecular reactions are selective processes where molecular ozone can act primarily as a dipole, such as it happens in the cycloaddition of Criegee on unsaturated species; or as an electrophilic agent, in electronically high density sites, especially in aromatic rings. These reactions commonly follow second order kinetics and the main substrates that react with the ozone according to this route are unsaturated hydrocarbons and aromatic hydrocarbons activated with electron donating groups, such as the hydroxyl or amino group.

Simultaneously, another fraction of ozone is decomposed before reacting with the solutes and being desorbed. Such decomposition is catalyzed by hydroxyl anions and therefore takes place more rapidly and extensively as pH increases. All this leads to the formation of species with marked reactivity and oxidant character, among which the hydroxyl and hydroperoxide free radicals. In addition, this decomposition may be further accelerated by a typically radical chain reaction in which the free radicals produced act as propagators of the reaction chain. The complete mechanism proposed by Staehelin, Hoigné and Bühler [135, 136] is shown in Table 1.11, although there are other proposals such as the mechanism of Tomiyasu, Fukutomi and Gordon [137] where the alkaline water conditions are considered.

From all the intermediate species formed, the hydroxyl radical plays a primordial role. Its presence in ozonated water was first identified by Weiss in 1935 [138], and is among the most reactive oxidants in water since it can easily oxidize saturated hydrocarbons and halogenated derivatives, aliphatic acids, aldehydes, ketones, alcohols, deactivated aromatic hydrocarbons, etc.

Table 1.11 Mechanism of ozone decomposition in water [135, 136]

REACTIONS OF INITIATION	
$O_3 + OH^- \xrightarrow{k=40M^{-1}s^{-1}} HO_2^- + O_2$	(1.8)
$O_3 + HO_2^- \xrightarrow{k=2.2 \cdot 10^6 M^{-1}s^{-1}} HO_2^\bullet + O_3^{\bullet-}$	(1.9)
$H_2O_2 \xrightleftharpoons[5 \cdot 10^{10} M^{-1}s^{-1}]{0.25 s^{-1}} HO_2^- + H^+ \quad pK_a = 11.3$	(1.10)
REACTIONS OF PROPAGATION	
$HO_2^\bullet \xrightarrow{k=7.9 \cdot 10^5 M^{-1}s^{-1}} O_2^{\bullet-} + H^+$	(1.11)
$O_2^{\bullet-} + H^+ \xrightarrow{k=5 \cdot 10^{10} M^{-1}s^{-1}} HO_2^\bullet$	(1.12)
$O_3 + O_2^{\bullet-} \xrightarrow{k=1.6 \cdot 10^9 M^{-1}s^{-1}} O_3^{\bullet-} + O_2$	(1.13)
$O_3^{\bullet-} + H^+ \xrightarrow{k=5.2 \cdot 10^{10} M^{-1}s^{-1}} HO_3^\bullet$	(1.14)
$HO_3^\bullet \xrightarrow{k=3.3 \cdot 10^2 M^{-1}s^{-1}} O_3^{\bullet-} + H^+$	(1.15)
$HO_3^\bullet \xrightarrow{k=1.1 \cdot 10^5 M^{-1}s^{-1}} HO^\bullet + O_2$	(1.16)
$O_3 + HO^\bullet \xrightarrow{k=2 \cdot 10^9 M^{-1}s^{-1}} HO_4^\bullet$	(1.17)
$HO_4^\bullet \xrightarrow{k=2.8 \cdot 10^4 M^{-1}s^{-1}} HO_2^\bullet + O_2$	(1.18)
REACTIONS OF TERMINATION	
$HO_4^\bullet + HO_4^\bullet \xrightarrow{k=5 \cdot 10^9 M^{-1}s^{-1}} H_2O_2 + 2O_3$	(1.19)
$HO_4^\bullet + HO_3^\bullet \xrightarrow{k=5 \cdot 10^9 M^{-1}s^{-1}} H_2O_2 + O_2 + O_3$	(1.20)
$HO^\bullet + HO_2^\bullet \xrightarrow{k=3.7 \cdot 10^{10} M^{-1}s^{-1}} O_2 + H_2O$	(1.21)

If ozone is irradiated with UV radiation of enough energy, it can be decomposed into atomic oxygen in the excited state, $O(^1D)$, according to reaction 1.22, producing hydrogen peroxide when it reacts with water. The photolysis of the generated hydrogen peroxide could lead to the formation of hydroxyl radicals through equation 1.24 [139]:



The combination of ozone and photocatalysis, known as photocatalytic ozonation, establishes, in addition to the reaction mechanisms for simple

ozonation, reactions for the photocatalytic process and other mechanisms of radical generation by interaction between the different systems. The simultaneous application of the processes of ozonation and photocatalysis significantly improves the formation of free radicals, leading to a synergistic effect [89, 140, 141] and higher mineralization rates [142]. This improvement in the generation of free radicals comes from complementary and synergistic reactions of both processes. Figure 1.7 schemes the radical formation mechanism in this process.

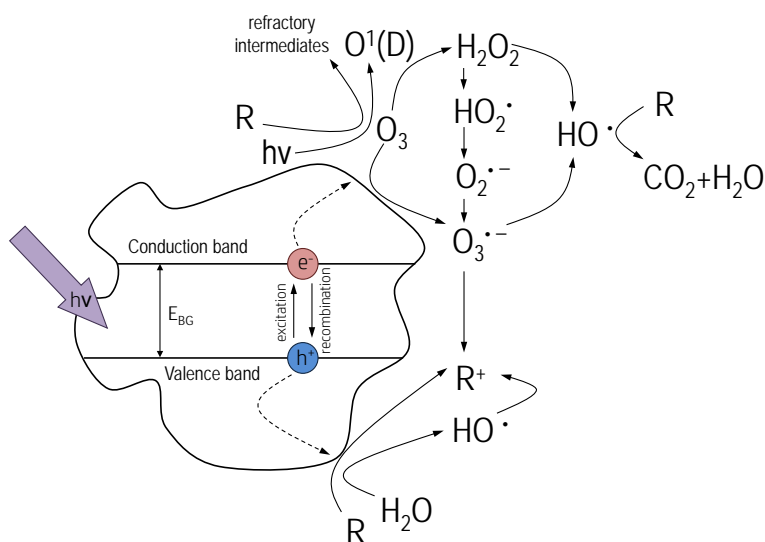


Figure 1.7 Mechanism of free radicals formation in photocatalytic ozonation process

Mainly six possible routes can be distinguished in the generation of hydroxyl radicals [141]:

1. Electron transfer from the surface of the photocatalyst to the ozone molecule in order to generate hydroxyl radicals through the formation of the ozonide radical. Ozone can interact with the surface of the photocatalyst by means of physisorption, hydrogen bonding with hydroxyl groups on the surface of the solid, or adsorption in Lewis acid groups [143]. If the present radiation is also considered, the adsorbed ozone can generate the ozone radical, which triggers the formation of the hydroxyl radical under acidic conditions prior to formation of the HO_3^\cdot radical through equations 1.14 and 1.16, already described.



2. Transfer of electrons from photocatalyst surface to the oxygen molecule, forming the superoxide radical, which reacts with the ozone present in the medium to form the ozone radical that triggers the generation of hydroxyl radicals. Taking into account that the process takes place with a mixture of oxygen-ozone, oxygen molecules that form superoxide radical promote the decomposition of ozone into hydroxyl radicals [144-146]. This reaction, already described in the simple ozonation process in equation 1.13, takes place additionally on the surface of the photocatalyst.
3. Generated holes that oxidize adsorbed H_2O molecules to generate hydroxyl radicals.
4. Photolytic decomposition of ozone to produce hydroxyl radicals in systems with radiation of wavelength below 300 nm, especially at 254 nm where the coefficient of ozone absorption is higher than that of hydrogen peroxide, 3300 versus $18.6 M^{-1} cm^{-1}$ [141].
5. Production of hydrogen peroxide as an intermediate in ozonation reactions.
6. Inhibition of recombination of the electron-hole pair due to the reaction of ozone and photogenerated electrons on the surface of the solid, which promotes the formation of radicals.

As a difference between the process of photocatalytic ozonation and catalytic ozonation, it is worth mentioning the process of initiation of the chain reaction. Thus, while the photocatalytic process starts with the transfer of an electron from the surface of the photocatalyst, the catalytic mechanism usually starts with the reaction between the hydroxyl radical and the ozone molecule [87]. In both processes the superoxide radical triggers the formation of ozone radical, which leads to the generation of more hydroxyl radicals. Superoxide radical is also supposed to react directly with organic molecules, albeit to a lesser extent, towards the complete mineralization [146].

1.4.3. Monoperoxysulfate and photocatalytic oxidation in the presence monoperoxysulfate

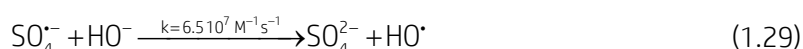
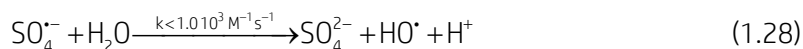
Oxidation with monoperoxysulfate and monoperoxysulfate decomposition into sulfate radicals

Monoperoxysulfate (MPS, HSO_5^-) is a versatile and environmentally-friendly oxidizing agent widely used in bleaching, cleaning and disinfection. It is commonly used in swimming pool disinfection, avoiding the formation of chloramines which commonly appear in chlorine oxidation. MPS is commercially available as triple salt ($2KHSO_5 \cdot KHSO_4 \cdot K_2SO_4$) under the names of Carat[®] and Oxone[®] and is able to oxidize diverse functional groups of

organic molecules [147]. Although MPS can directly react with organic molecules with a redox potential comparable to hydrogen peroxide (1.82 V versus 1.76 V, for MPS and H₂O₂ respectively), MPS can theoretically liberate a free radical reaction mechanism involving hydroxyl and sulfate ion radicals [148] in the presence of UV radiation or heat [149]:



Moreover, hydroxyl radicals are generated from the reaction between H₂O or hydroxyl anion and sulfate radicals:

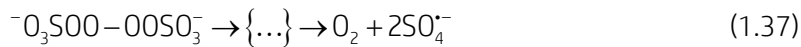
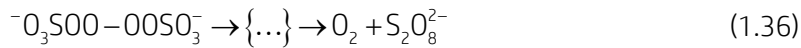
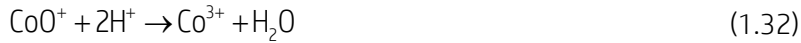
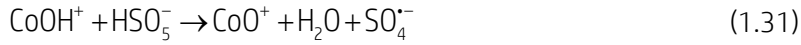


At pH below 9 sulfate radical is the dominant radical specie while at pH > 9, hydroxyl radical becomes the dominant reactive radical [150].

Many applications in MPS decomposition into radicals have been recently explored, such as oxidation of emerging contaminants and their metabolites, disintegration of activated sludge, disinfection or decontamination of pool water [151]. Sulfate-based AOPs are increasingly gaining attention in the research field of aqueous pollutants oxidation [151] due to some advantages if compared to hydroxyl radical [152]. Sulfate radical has a redox potential comparable or even higher than hydroxyl radical (2.5-3.1 V versus 1.90-2.70 V [153]); reacts selectively and efficiently via electron transfer with organic compounds with unsaturated bonds or aromatic electrons, while hydroxyl radical does it by hydrogen abstraction or electrophilic addition at high reaction rates [151]; it has not pH limitations in contrast to Fenton system being possible to work in a wider pH range (2-8); and it presents a higher half-life period which enables to have more stable mass transfer and better contact with target compounds [152].

MPS can also be chemically decomposed into radicals by means of transition metals such as Co(II), Ru(III) and Mn(II) [154, 155], in which Co(II) overwhelmingly outlines. Cobalt decomposition of MPS starts with the formation of CoOH⁺ which seems to be the most effective cobalt specie in its activation [156]. The regeneration of Co²⁺ by reducing from Co³⁺ closes the catalytic homogeneous cycle. Peroxydisulfate is a reported termination product [157].

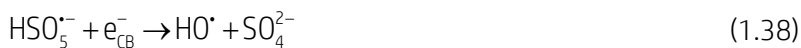




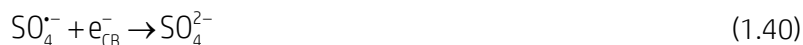
Homogeneous catalysis requires the further removal of the catalyst, especially in those cases where the active substance, i.e. cobalt, presents toxic properties. Although very small amounts of cobalt provide beneficial catalytic decomposition of MPS, toxicity of this metal causes health problems at very low concentrations, which results a clear disadvantage for the process to be extrapolated for a real application. Cobalt is a recognized toxic and carcinogenic metal in animals [158] and it leads to the development of dermatitis, asthma, pneumonia and cardiomyopathy in humans [159]. Consequently, heterogeneous catalysis emerges as a solution for both problems and the development of catalysts for the heterogeneous activation of MPS has raised interest in research community [151, 152]. Nevertheless, as acid conditions promote the dissolution of cobalt, the stability and leaching of cobalt in these materials must be taken into account in real applications.

Photocatalytic oxidation in presence of monoperoxsulfate

As indicated previously, a strategy to inhibit the electron-hole recombination step of photocatalytic process is the addition of electron acceptors to the reaction media. Inorganic peroxides can trap the photogenerated electrons more efficiently than oxygen [160]. Upon accepting an electron from the conduction band, MPS would participate in two different pathways [161]:



In addition, sulfate radicals can trap the photogenerated electrons which result prejudicial for the process:



Titanium dioxide is once again the most investigated photocatalyst in MPS photodecomposition [162]. However, alternative new photocatalysts are under research [163, 164]. Figure 1.8 shows the schematic formation of radicals in the MPS photocatalytic decomposition.

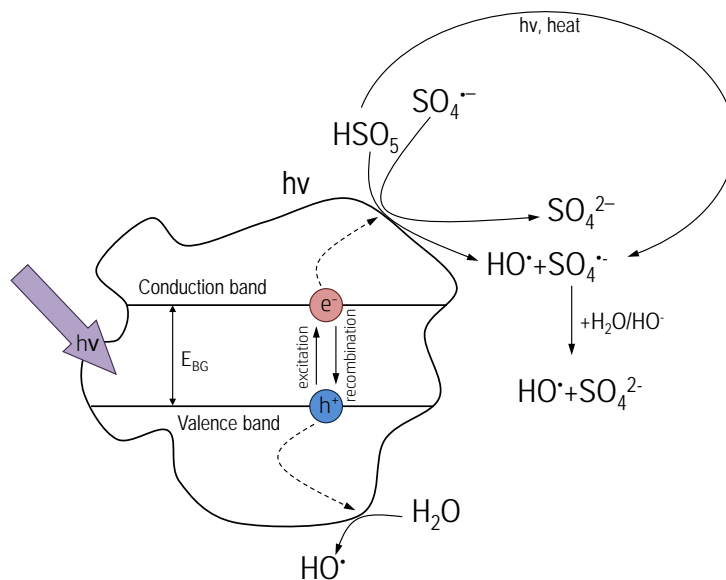


Figure 1.8 Photocatalytic radical formation mechanism in presence of MPS

Recently, the option of coupling cobalt oxides to photocatalysts like TiO_2 is gaining attention since electrons generated in photocatalytic process contribute to regenerate the original oxidation state of cobalt, minimizing therefore the electron-hole recombination [165, 166]:



Thus, a powerful reaction-chained mechanism is triggered, generating sulfate and hydroxyl radicals from photocatalytic reaction and Fenton-like heterogeneous reactions. To date, only cobalt oxides have been coupled to titania in order to produce this oxidation process [165-170].

1.5. SPECIFIC OBJECTIVES

The main goal of this dissertation research has been focused on the study of photocatalysis using radiation of low energy, i.e. UVA radiation, combined with ozone or peroxidic promoters like monoperoxysulfate, as emerging technology for the removal of aqueous organic compounds of environmental concern, such as herbicides. The specific objectives pursued can be summarized in the followings:

- Synthesis and characterization of nitrogen doped and bare titania and the study of their photocatalytic activity under UVA radiation. Comparison with commercial titania Degussa P25.
- Study of photocatalytic ozonation and comparison with single photocatalysis and single ozonation in the degradation of refractory organic pollutants. Importance of main parameters affecting the process and toxicological aspects of treated samples.
- Determination of second-order rate constant between molecular ozone and organic compounds.
- Determination of rate constant between the model compounds and hydroxyl radical, in case they are not available in literature.
- Identification of transformation products of photocatalytic techniques by means of LC-HPLC-MS-QTOF.
- Study of direct monoperoxysulfate oxidation kinetics of contaminants with high affinity towards this reaction.
- Application of photocatalysis promoted with monoperoxysulfate using commercial titania Degussa P25. Comparison in the absence of peroxidic promoter. Variables of special importance in the process.
- Synthesis and characterization of cobalt-based perovskite oxide in the heterogeneous activation of peroxidic promoters. Research of variables affecting the process and stability of the synthesized catalyst, paying attention to leaching.
- Combination of cobalt-based perovskites and titania in photocatalytic oxidation using monoperoxysulfate as promoter. Synthesis of the composite. Study of the main variables of the process and toxicological aspects.

REFERENCES

- [1] Echarri L. *Ciencias de la tierra y el medio ambiente*. Ed Teide, **1998**
- [2] Gleick PH. *Water resources* in *Encyclopedia of climate and weather*. Oxford University Press. New York, **1966**
- [3] Margalef R. *Limnología*. Ediciones Omega SL, primera edición, **1983**
- [4] United Nations, Department of Economic and Social Affairs, Population Division (**2015**). *World Population Prospects: The 2015 Revision, World Population 2015 Wallchart*. ST/ESA/SER.A/378.
- [5] FAO, **2015**. <http://www.fao.org> (last accessed january 2017)
- [6] Eurostat, **2014**. <http://ec.europa.eu/eurostat> (last accessed january 2017)
- [7] The Water Proyect, **2017**. <https://thewaterproject.org/> (last accessed January 2017)
- [8] Schwarzenbach RP, Escher BI, Fenner K, Hofstetter TB, Johnson CA, V-Guten U, Wehrli B. *The challenge of micropollutants in aquatic systems*. Sci 313 (**2006**) 1072-1077
- [9] Kümmerer K. *The presence of pharmaceuticals in the environment due to human use-present knowledge and future challenges*. J Environ Manag 90 (**2009**) 2354-2366
- [10] Lapworth DJ, Baran N, Stuart ME, Ward RS. *Emerging organic contaminants in groundwater: A review of sources, fate and occurrence*. Environ Pollut 163 (**2012**) 287-303
- [11] Richardson SD, Ternes TA. *Water analysis: emerging contaminants and current issues*. Anal Chem 83 (**2011**) 4614-4648
- [12] Pal A, Gin KYH, Lin AYC, Reinhard M. *Impacts of emerging organic contaminants on freshwater resources: review of recent occurrences, sources, fate and effects*. Sci Total Environ 408 (**2010**) 6062-6069
- [13] Kolpin DW, Furlong ET, Meyer MT, Thurman EM, Zaugg SD, Barber LB, Buxton HT. *Pharmaceuticals, hormones, and other organic wastewater contaminants in US streams, 1999-2000: a national reconnaissance*. Environ Sci Technol 36 (**2002**) 1202-1211
- [14] Swartz WCH, Reddy S, Benotti MJ, Yin HF, Barber LB, Brownawell BJ, Rudel RA. *Steroid estrogens, nonylphenol ethoxylate metabolites, and other wastewater contaminants in groundwater affected by a residential*

- septic system on Cape Cod, MA. Environ Sci Technol 40 (2006) 4894-4902*
- [15] Kümmerer K. *Drugs in the environment: emission of drugs, diagnostic aids and disinfectants into wastewater by hospitals in relation to other sources—a review. Chemosphere 45 (2001) 957-969*
- [16] Watanabe N, Bergamaschi BA, Loftin KA, Meyer MT, Harter T. *Use and environmental occurrence of antibiotics in freestall dairy farms with manure forage fields. Environ Sci Technol 44 (2010) 6591-6600*
- [17] Bolong N, Ismail AF, Salim MR, Matsuura T. *A review of the effects of emerging contaminants in wastewater and options for their removal. Desalination 239 (2009) 229-246*
- [18] Rivera-Utrilla J, Sánchez-Polo M, Ferro-García MA, Prados-Joya G, Ocampo-Pérez R. *Pharmaceuticals as emerging contaminants and their removal from water. A review. Chemosphere 93 (2013) 1268-1287*
- [19] Ahmed MB, Zhou JL, Ngo HH, Guo W, Thomaidis NS, Xu J. *Progress in the biological and chemical treatment technologies for emerging contaminant removal from wastewater: a critical review. J Hazard Mater 323 (2017) 274-298*
- [20] Gómez MJ, Martínez-Bueno MJ, Lacorte S, Fernández-Alba AR, Agüera A. *Pilot survey monitoring pharmaceuticals and related compounds in a sewage treatment plant located on the Mediterranean coast. Chemosphere 66 (2007) 993-1002*
- [21] Martínez-Bueno MJ, Gomez MJ, Herrera S, Hernando MD, A. Agüera A, Fernández-Alba AR. *Occurrence and persistence of organic emerging contaminants and priority pollutants in five sewage treatment plants of Spain: two years pilot survey monitoring. Environ Pollut 164 (2012) 267-273*
- [22] Loos R, Carvalho R, António DC, Comero S, Locoro G, Tavazzi S, Paracchini B, Ghiani M, Lettieri T, Blaha L, Jarosova B, Voorspoels S, Servaes K, Haglund P, Fick J, Lindberg RH, Schwesig D, Gawlik BM. *EU-wide monitoring survey on emerging polar organic contaminants in wastewater treatment plant effluents. Water Res 47 (2013) 6475-6487*
- [23] Petrović M, González S, Barceló D. *Analysis and removal of emerging contaminants in wastewater and drinking water. Trends Anal Chem 22 (2003) 685-696*

- [24] Rodríguez-Mozaz S, López De Alda MJ, Barceló D. *Monitoring of estrogens, pesticides and bisphenol A in natural waters and drinking water treatment plants by solid-phase extraction-liquid chromatography-mass spectrometry*. J Chromatogr A 1045 (2004) 85-92
- [25] Schriks M, Heringa MB, van der Kooi MME, de Voogt P, van Wezel AP. *Toxicological relevance of emerging contaminants for drinking water quality*. Water Res 44 (2010) 461-476
- [26] Focazio MJ, Kolpin DW, Barnes KK, Furlong ET, Meyer MT, Zaugg SD, Barber LB, Thurman ME. *A national reconnaissance for pharmaceuticals and other organic wastewater contaminants in the United States - II) Untreated drinking water sources*. Sci Total Environ 402 (2008) 201-216
- [27] Loos R, Locoro G, Comero S, Contini S, Schwesig D, Werres F, Balsaa P, Gans O, Weiss S, Blaha L, Bolchi M, Gawlik BM. *Pan-European survey on the occurrence of selected polar organic persistent pollutants in ground water*. Water Res 44 (2010) 4115-4126
- [28] Konstantinou IK, Hela DG, Albanis TA. *The status of pesticide pollution in surface waters (rivers and lakes) of Greece. Part I. Review on occurrence and levels*. Environ Pollut 141 (2006) 555-570
- [29] Kuster M, López de Alda MJ, Hernando MD, Petrovic M, Martín-Alonso J, Barceló D. *Analysis and occurrence of pharmaceuticals, estrogens, progestogens and polar pesticides in sewage treatment plant effluents, river water and drinking water in the Llobregat river basin (Barcelona, Spain)*. J Hydrol 358 (2008) 112-123
- [30] Kinney CA, Furlong ET, Zaugg SD, Burkhardt MR, Werner SL, Cahill JD, Jorgensen. *Survey of organic wastewater contaminants in biosolids destined for land application*. Environ Sci Technol 40 (2006) 7207-7215
- [31] Topp E, Monteiro SC, Beck A, Ball Coehlo B, Boxall AB, Duenk PW, Kleywegt S, Lapen DR, Payne M, Sabourin L, Li H, Metcalfe CD. *Runoff of pharmaceuticals and personal care products following application of biosolids to an agricultural field*. Sci Total Environ 396 (2008) 52-59
- [32] Carvalho FP, Nhan DD, Zhong C, Tarares T, Klaine S. *Tracking Pesticides in the Tropics*. Bulletin IAEA 40 (1998) 24-30
- [33] Dierksmeier G. *Plaguicidas, residuos, efectos y presencia en el medio*. Ed. Científico-Técnica, La Habana, 2001

- [34] Sulecki CJ. *Argentina, rapidly modernizing agriculture sector. Power house in grain and oilseed export is developing a giant appetite for agrochemicals, fertilizers, biotech seeds and new equipment.* Farm Chem Int 12 (1998)
- [35] Monaco TJ, Stephen CW, Floyd MA. *Weed science: principles & practices.* Fourth edition. John Wiley & sons, INC. USA, 2001
- [36] Larson SJ, Capel PD, Majewski MS. *Pesticides in surface waters-distribution, trends, and governing factors.* Series of Pesticides in Hydrologic System, vol. 3. Ann Arbor Press, Chelsea, Michigan, 1997
- [37] Arias-Estévez M, López-Periago E, Martínez-Carballo E, Simal-Gándara J, Mejuto JC, García-Río L. *The mobility and degradation of pesticides in soils and the pollution of groundwater resources.* Agric Ecosyst Environ 123 (2008) 247-260
- [38] Criswell J. *Pesticides and Water.* Water Quality Handbook for Nurseries, Division of Agricultural Sciences and Nature Resources, Oklahoma, State University, 1998
- [39] Wolff MS, Toniolo PG, Lee EW, Rivera M, Dubin N. *Blood levels of organochlorine residues and risk of breast cancer.* J Natl Cancer Inst 85 (1993) 648-652
- [40] Alavanja MCR, Sandler DP, McMaster SB, Zahm SH, McDonnell CJ, Lynch CF, Pennybacker M, Rothman N, Dosemeci M, Bond AE, Blair A. *The agricultural health study.* Environ Health Perspect 104 (1996) 362-369
- [41] Dich J, Zahm SH, Hanberg A, Adami HO. *Pesticides and cancer.* Cancer Causes Control 8 (1997) 420-443
- [42] Cantor KP. *Drinking water and cancer.* Cancer Causes Control 8 (1997) 292-308
- [43] Alavanja MCR, Hoppin JA, Kamel F. *Health effects of chronic pesticide exposure: Cancer and neurotoxicity.* Annu Rev Public Health 25 (2004) 155-197
- [44] Whorton D, Krauss, RM, Marshall S, Milby TH. *Infertility in male pesticide workers.* The Lancet 310 (1977) 1259-1261
- [45] Lyons G. *Pesticides posing hazards to wildlife reproduction.* Middle East Fertil Soc J 3 (1998) 30-39

- [46] Peterson HG, Boutin C, Martin PA, Freemark KE, Ruecker NJ, Moody MJ. *Aquatic phyto-toxicity of 23 pesticides applied at expected environmental concentrations*. *Aquat Toxicol* 28 (1994) 275-292
- [47] Relyea RA. *Growth and survival of five amphibian species exposed to combinations of pesticides*. *Environ Toxicol Chem* 23 (2004) 1737-1742
- [48] Robens JF. *Teratologic studies of carbaryl, diazinon, norea, disulfiram, and thiram in small laboratory animals*. *Toxicol Appl Pharmacol* 15 (1969) 152-163
- [49] Hoffman DJ, Albers PH. *Evaluation of potential embryotoxicity and teratogenicity of 42 herbicides, insecticides, and petroleum contaminants to mallard eggs*. *Arch Environ Contam and Toxicol* 13 (1984) 15-27
- [50] Dolk H, Vrijheid M. *The impact of environmental pollution on congenital anomalies*. *Br Med Bull* 68 (2003) 25-45
- [51] Thulstrup AM, Bonde JP. *Maternal occupational exposure and risk of specific birth defects*. *Occup Med* 56 (2006) 532-543
- [52] Demicco A, Cooper KR, Richardson JR, White LA. *Developmental neurotoxicity of pyrethroid insecticides in zebrafish embryos*. *Toxicol Sci* 113 (2009) 177-186
- [53] Sherer TB, Betarbet R, Testa CM, Seo BB, Richardson JR, Kim JH, Miller GW, Yagi T, Matsuno-Yagi A, Greenamyre JT. *Mechanism of Toxicity in Rotenone Models of Parkinson's Disease*. *J Neurosci* 23 (2003) 10756-10764
- [54] Liu B, Gao HM, Hong JS. *Parkinson's disease and exposure to infectious agents and pesticides and the occurrence of brain injuries: Role of neuroinflammation*. *Environ Health Perspect* 111 (2003) 1065-1073
- [55] Cannon JR, Greenamyre JT. *The role of environmental exposures in neurodegeneration and neurodegenerative diseases*. *Toxicol Sci* 124 (2011) 225-250
- [56] Franco R, Li S, Rodriguez-Rocha H, Burns M, Panayiotidis MI. *Molecular mechanisms of pesticide-induced neurotoxicity: Relevance to Parkinson's disease*. *Chem Bio Interact* 188 (2010) 289-300
- [57] Diamanti-Kandarakis E, Bourguignon JP, Giudice LC, Hauser R, Prins GS, Soto AM, Zoeller RT, Gore AC. *Endocrine-disrupting chemicals: An Endocrine Society scientific statement*. *Endocr Rev* 30 (2009) 293-342

- [58] Schug TT, Janesick A, Blumberg B, Heindel JJ. *Endocrine disrupting chemicals and disease susceptibility*. J Steroid Biochem Mol Biol 127 (2011) 204-215
- [59] Grossmann K. *Auxin herbicides: current status of mechanism and mode of action*. Pest Manag Sci 66 (2010) 113-120
- [60] Labrada R, Caseley JC, Parker C. *Weed management for developing countries*. FAO plant production and protection paper 120. FAO, Rome, 1994
- [61] PPDB, Pesticide Properties DataBase, 2017. University of Hertfordshire. <http://sitem.herts.ac.uk/aeru/footprint/es/> (last accessed January 2017)
- [62] Good NE. *Inhibitors of the Hill reaction*. Plant Physiol, 36 (1961) 788-803
- [63] Meazza G, Scheffler BE, Tellez MR, Rimando AM, Romagni JG, Duke SO, Nanayakkara D, Khan IA, Abourashed EA, Dayan FE. *The inhibitory activity of natural products on plant p-hydroxyphenylpyruvate dioxygenase*. Phytochem 60 (2002) 281-288
- [64] Sutton P, Richards CL, Buren L, Glasgow L. *Activity of mesotrione on resistant weeds in maize*. Pest Manag Sci 58 (2002) 981-984
- [65] Tarara G, Fliege R, Desmarteau D, Kley C, Peters B. *Environmental fate of tembotrione*. Bayer Crop Sci J 62 (2009) 63-78
- [66] Zimdahl RL. *Fundamentals of weed science*. Academic Press, 2007
- [67] European Food Safety Authority. *Reasoned opinion on the review of the existing maximum residue levels (MRLs) for tritosulfuron according to Article 12 of Regulation (EC) No 396/2005*. EFSA Journal 13 (2015) 3964
- [68] Trenkamp S, Martin W, Tietjen K. *Specific and differential inhibition of very-long-chain fatty acid elongases from Arabidopsis thaliana by different herbicides*. Proc Natl Acad Sci 101 (2004) 11903-11908
- [69] Duncan DN, WF Meggett WF, Penner D. *The basis for selectivity of root-applied ethofumate in sugarbeet and three weed species*. Weed Sci 30 (1982) 191-194
- [70] Glaze WH, Kang JW. *The chemistry of water treatment process involving ozone, hydrogen peroxide and ultraviolet radiation*. Ozone Sci Eng 9 (1987) 335-352

- [71] Dorfman LM, Adams GE. *Reactivity of the Hydroxyl Radical*. National Bureau of Standards, Report No. NSRDS-NBS-46, **1973**
- [72] Hoigné J, Bader H. *Rate constants of reaction of ozone with organic and inorganic compounds in water. Part II. Dissociating organic compounds*. Water Res 17 (**1983**) 185-194
- [73] Buxton GV, Greenstock CL, Helman WP, Ross AB. *Critical review of rate constant for reactions of hydrated electrons, hydrogen atoms and hydroxyl radicals ($HO^{\bullet}/O^{\bullet-}$) in aqueous solutions*. J Phys Chem Ref Data 17 (**1988**) 513-886
- [74] Andreozzi R, Caprio V, Insola A, Marotta R. *Advanced oxidation processes (AOP) for water purification and recovery*. Catal Today 53 (**1999**) 51-59
- [75] Rizzuti L, Augugliaro V, Marucci G. *Ozone absorption in alkaline solutions*. Chem Eng Sci 31(**1976**) 877-880
- [76] Legube B, Karpel Vel Leitner N. *Catalytic ozonation: a promising advanced oxidation technology for water treatment*. Catal Today 53(**1999**) 61-72
- [77] McGuire MJ, Davis MK. *Treating water with peroxone: a revolution in the making*. Water Eng Manag 135 (**1988**) 42-46
- [78] Fenton HJH. *Oxidation of tartaric acid in the presence of iron*. J Chem Soc 65 (**1894**) 899-910
- [79] Haber F, Weiss J. *The catalytic decomposition of hydrogen peroxide by iron salts*. Proc R Soc Series A 147 (**1934**) 332-351
- [80] Pruden BB, Le H. *Wet air oxidation of soluble components in waste water*. Can J Chem Eng 54 (**1976**) 319-325
- [81] Luck F. *Wet air oxidation: past, present and future*. Catal Today 53 (**1999**) 81-91
- [82] Peyton GR, Glaze WH. *Destruction of pollutants in water by ozone in combination with ultraviolet radiation. 3. Photolysis of aqueous ozone*. Environ Sci Technol 22 (**1988**) 761-767
- [83] Baxendale JH, Wilson JA. *The photolysis of hydrogen peroxide at high light intensities*. Trans Faraday Soc 53 (**1957**) 344-356
- [84] Lucas MS, Peres JA, Li Puma G. *Treatment of winery wastewater by ozone-based advanced oxidation processes (O_3 , O_3/UV and $O_3/UV/H_2O_2$)*

- in a pilot-scale bubble column reactor and process economics.* Sep Purif Technol 72 (2010) 235-241
- [85] Kiwi J, Pulgarin C, Peringer P, Gratzel M. *Beneficial effect of homogeneous photo-Fenton pretreatment upon the biodegradation of anthraquinone sulfonate in wastewater treatment.* Appl Catal B Environ 3 (1993) 85-99
- [86] Berberidou C, Poullos I, Xekoukoulotakis NP, Mantzavinos D. *Sonolytic, photocatalytic and sonophotocatalytic degradation of malachite green in aqueous solutions.* Appl Catal B Environ 74 (2007) 63-72
- [87] Nawrocki J, Kasprzyk-Hordern B. *The efficiency and mechanisms of catalytic ozonation.* Appl Catal B Environ 99 (2010) 27-42
- [88] Ollis D, Al-Ekabi H. *Photocatalytic Purification of Water and Air.* Elsevier, New York, 1993
- [89] Agustina TE, Ang HM, Vareek VK. *A review of synergistic effect of photocatalysis and ozonation on wastewater treatment.* J Photochem Photobiol C Photochem Rev 6 (2005) 264-273
- [90] Augugliaro V, Litter M, Palmisano L, Soria J. *The combination of heterogeneous photocatalysis with chemical and physical operations: A tool for improving the photoprocess performance.* J Photochem Photobiol C Photochem Rev 7 (2006) 127-144
- [91] Gogate PR, Pandit AB. *A review of imperative technologies for wastewater treatment I: oxidation technologies at ambient conditions.* Adv Environ Res 8 (2004) 501-551
- [92] Matilainen A, Sillanpää M. *Removal of natural organic matter from drinking water by advanced oxidation processes.* Chemosphere 80 (2010) 351-365
- [93] Oller I, Malato S, Sánchez-Pérez JA. *Combination of Advanced Oxidation Processes and biological treatments for wastewater decontamination-a review.* Sci Total Environ 409 (2010) 4141-4166
- [94] Hoffmann MR, Martin ST, Choi W, Bahnemann DW. *Environmental applications of semiconductor photocatalysis.* Chem Rev 95 (1995) 69-96
- [95] Carp O, Huisman CL, Reller A. *Photoinduced reactivity of titanium dioxide.* Prog Solid State Chem 32 (2004) 33-177

- [96] Fujishima A, Rao TN, Tryk DA. *Titanium dioxide photocatalysis*. J Photochem Photobiol C Photochem Rev 1 (2000) 1-21
- [97] Blanco J, Malato S. *Tecnología de la fotocátalisis solar: utilización de la radiación solar para el tratamiento de contaminantes industriales*. Instituto de Estudios Almerienses. El Ejido (Almería), 1996
- [98] Malato S, Fernández-Ibáñez P, Maldonado MI, Blanco J, Gernjak W. *Decontamination and disinfection of water by solar photocatalysis: Recent overview and trends*. Catal Today 147 (2009) 1-59
- [99] Choi W, Termin A, Hoffmann MR. *The role of metal ion dopants in quantum-sized TiO_2 : Correlation between photoreactivity and charge carrier recombination dynamics*. J Phys Chem 98 (1994) 13669-13679
- [100] Cong Y, Zhang J, Chen F, Anpo M. *Synthesis and characterization of nitrogen-doped TiO_2 nanophotocatalyst with high visible light activity*. J Phys Chem C 111 (2007) 6976-6982
- [101] Asahi R, Morikawa T, Ohwaki T, Aoki K, Taga Y. *Visible-light photocatalysis in nitrogen-doped titanium dioxides*. Sci 293 (2001) 269-271
- [102] Devi LG, Kavitha R. *A review on non metal ion doped titania for the photocatalytic degradation of organic pollutants under UV/solar light: Role of photogenerated charge carrier dynamics in enhancing the activity*. Appl Catal B Environ 140-141 (2013) 559-587
- [103] Sato S. *Photocatalytic activity of NO_x -doped TiO_2 in the visible light region*. Chem Phys Lett 123 (1986) 126-128
- [104] Nakano Y, Morikawa T, Ohwaki T, Yasunori T. *Deep-level optical spectroscopy investigation of N-doped TiO_2 films*. Appl Phys Chem B 108 (2004) 10617-10620
- [105] Mwabora JM, Lindgren T, Avendaño E, Jaramillo TF, Lu j, Lindquist SE, Granqvist CG. *Structure, composition, and morphology of photoelectrochemically active $TiO_{2-x}N_x$ thin films deposited by reactive DC magnetron sputtering*. J Phys Chem 108 (2004) 20193-20198
- [106] Premkumar J. *Development of super-hydrophilicity on nitrogen-doped TiO_2 thin film surface by photoelectrochemical method under visible light*. Chem Mater 16 (2004) 3980-3981

- [107] Diwald O, Thompson TL, Goralski EG, Walck SD, Yates JT. *The effect of nitrogen ion implantation on the photoactivity of TiO₂ rutile single crystals*. J Chem B 108 (2004) 52-57
- [108] Glicov A, Macak JM, Tsuchiya H, Kunze J, Haeublein V, Frey L, Schmuki P. *Ion implantation and annealing for an efficient N-doping of TiO₂ nanotubes*. Nano Lett 6 (2006) 1080-1082
- [109] Batzill M, Morales EH, Diebold U. *Surface studies of nitrogen implanted TiO₂*. Chem Phys 339 (2007) 36-43
- [110] Irie H, Watabe Y, Hashimoto K. *Nitrogen-concentration dependence on photocatalytic activity TiO_{2-x}N_x powders*. J Phys Chem B 107 (2003) 5483-5486
- [111] Nosaka Y, Matsushita M, Nishino J, Nosaka AY. *Nitrogen-doped titanium dioxide photocatalysts for visible response prepared by using organic compounds*. Sci Technol Adv Mater 6 (2005) 143-148
- [112] Nakamura R, Tanaka T, Nakato Y. *Mechanism for visible light response in anodic photocurrents at N-doped TiO₂ films electrodes*. J Phys Chem B 108 (2004) 10617-10620
- [113] Satish M, Viswanathan B, Viswanath RP, Gopinath CS. *Synthesis, characterization, electronic structure and photocatalytic activity of nitrogen-doped TiO₂ nanocatalyst*. Chem Mater 17 (2005) 6349-6353
- [114] Prokes S, Gole JL, Chen X, Burda C, Carlos WE. *Defect-related optical behavior in surface modified TiO₂ nanostructures*. Adv Funct Mater 15 (2005) 161-167
- [115] Qiu X, Zhao Y, Burda C. *Synthesis and characterization of nitrogen-doped group IV B visible-light-photoactive metal oxide nanoparticles*. Adv Mater 19 (2007) 3995-3999
- [116] Jagadale TC, Takale SP, Sonawane S, Joshi HM, Patil SI, Kale BB, Ogale SB. *N-doped TiO₂ nanoparticle based light photocatalyst by modified peroxide sol-gel-method*. J Phys Chem C 112 (2008) 14595-14602
- [117] Mitoraj D, Kisch H. *On the mechanism of urea-induced titania modification*. Chem A Eur J 16 (2010) 261-269
- [118] Morikawa T, Asahi R, Ohwaki T, Aoki K, Taga Y. *Band-gap narrowing of titanium dioxide by nitrogen doping*. Jpn J Appl Phys 40 (2001) L561

- [119] Wu Z, Dong F, Zhao W, Guo S. *Visible light induced electron transfer process over nitrogen doped TiO₂ nanocrystals prepared by oxidation of titanium nitride*. J Hazard Mater 157 (2008) 57-63
- [120] Liu G, Yang HG, Wang X, Cheng L, Pan J, Lu GQ, Cheng HM. *Visible light responsive nitrogen doped anatase TiO₂ sheets with dominant {001} facets derived from TiN*. J Am Chem Soc 131 (2009) 12868-12869
- [121] Iwase M, Yamada K, Kurisaki T, Wakita H. *Characterization and photocatalytic activity of nitrogen-doped titanium (IV) oxide prepared by doping titania with TiN powder*. Appl Catal A Gen 445 (2013) 86-91
- [122] Huang JG, Zhao XG, Zheng MY, Li S, Wang Y. *Preparation of N-doped TiO₂ by oxidizing TiN and its application on phenol degradation*. Water Sci Technol 68 (2013) 934-939
- [123] Suda Y, Kawasaki H, Ueda T, Ohshima T. *Preparation of high quality nitrogen doped TiO₂ thin film as a photocatalyst using a pulsed laser deposition method*. Thin Solid Films 453-454 (2004) 162-166
- [124] Hong YC, Bang CU, Shin DH, Uhm HS. *Band gap narrowing of TiO₂ by nitrogen doping in atmospheric microwave plasma*. Chem Phys Lett 413 (2005) 454-457
- [125] Maeda M, Yamada T, Watanabe T. *Photocatalytic properties of plasma-nitrided TiO₂ films*. J Electrochem Soc 154 (2007) 29-31
- [126] Liu X, Liu Z, Zheng J, Yan X, Li D, Chen S, Chu W. *Characteristics of N-doped TiO₂ nanotube arrays by N₂-plasma for visible light-driven photocatalysis*. J Alloys Compd 509 (2011) 9970-9976
- [127] Dhar JC, Mondal A, Bhattacharya S, Singh NK, Ngangbam C, Chattopadhyay, KK. *Band gap tailoring of TiO₂ nanowires by nitrogen doping under N₂/Ar plasma environment*. J Nanosci Nanotechnol 15 (2015) 3951-3955
- [128] Pore V, Heikkilä M, Ritala M, Leskelä M, Areva S. *Atomic layer deposition of TiO_{2-x}N_x films for photocatalytic applications*. J Photochem Photobiol A Chem 177 (2006) 68-75
- [129] Cheng HE, Chen YR, Wu WT, Hsu CM. *Effect of nitrogen doping concentration on the properties of TiO₂ films grown by atomic layer deposition*. Mater Sci Eng B Solid State Mater Adv Technol 176 (2011) 596-599

- [130] Gallard H, Von Gunten U. *Chlorination of natural organic matter: Kinetics of chlorination and of THM formation*. Water Res 36 (2002) 65-74
- [131] Von Gunten U. *Ozonation of drinking water: Part II. Disinfection and by-product formation in presence of bromide, iodide or chlorine*. Water Res 37 (2003) 1469-1487
- [132] Beltrán FJ. *Ozone reaction kinetics for water and wastewater systems*. Lewis Publishers, CRC Press, Boca Ratón 2004
- [133] Von Sonntag C, von Gunten U. *Chemistry of ozone in water and wastewater treatment. From basic principles to applications*. IWA Publishing, London, 2012
- [134] Ibáñez M, Gracia-Lor E, Bijlsma L, Morales E, Pastor L, Hernández F. *Removal of emerging contaminants in sewage water subjected to advanced oxidation with ozone*. J Hazard Mater 260 (2013) 389-398
- [135] Bühler RE, Staehelin J, Hoigné J. *Ozone decomposition in water studied by pulse radiolysis. 1. HO₂/O₂ and HO₃/O₃ as intermediates*. J Phys Chem 88 (1984) 2560-2564
- [136] Staehelin J, Bühler RE, Hoigné J. *Ozone decomposition in water studied by pulse radiolysis. 2. OH and HO₄ as chain intermediates*. J Phys Chem 88 (1984) 5999-6004
- [137] Tomiyasu H, Fukutomi H, Gordon G. *Kinetics and mechanism of ozone decomposition in basic aqueous solution*. Inorg Chem 24 (1985) 2962-2966
- [138] Weiss J. *Investigations of the radical HO₂ in solution*. Trans Far Soc 31 (1935) 668-681
- [139] Peyton GR, Glaze WH. *Destruction of pollutants in water with ozone in combination with ultraviolet radiation. Photolysis of aqueous ozone*. Environ Sci Technol 22 (1988) 761-767
- [140] Mehrjouei M, Müller S, Möller D. *A review on photocatalytic ozonation used for the treatment of water and wastewater*. Chem Eng J 263 (2005) 209-219
- [141] Xiao J, Xie Y, Cao H. *Organic pollutants removal in wastewater by heterogeneous photocatalytic ozonation*. Chemosphere 121 (2015) 1-17
- [142] Farré MJ, Franch MI, Malato S, Ayllón JA, Peral J, Doménech X. *Degradation of some biorecalcitrant pesticides by homogeneous and*

- heterogeneous photocatalytic ozonation*. Chemosphere 58 (2005) 1127-1133
- [143] Bulanin KM, Lavalley JC, Tsyganenko AA. *Infrared study of ozone adsorption on TiO₂ (anatase)*. J Phys Chem 99 (1995) 10294-10298
- [144] Naydenov A, Mehandjiev D. *Complete oxidation of benzene on manganese dioxide by ozone*. Appl Catal A Gen 97 (1993) 17-22
- [145] Beltrán FJ, Rivas FJ, Montero-de-Espinosa R. *Catalytic ozonation of oxalic acid in an aqueous TiO₂ slurry reactor*. Appl Catal B Environ 39 (2002) 221-231
- [146] Jing Y, Li LS, Zhang QY, Lu P, Liu PH, Lü XH. *Photocatalytic ozonation of dimethyl phthalate with TiO₂ prepared by hydrothermal method*. J Hazard Mater 189 (2011) 40-47
- [147] Hussain H, Green IR, Ahmed I. *Journey describing applications of oxone in synthetic chemistry*. Chem Rev 113 (2013) 3329-3371
- [148] Kennedy RJ, Stock AM. *The oxidation of organic substances by potassium peroxymonosulfate*. J Org Chem 25 (1960) 1901-1906
- [149] Yang S, Wang P, Yang X, Shan L, Zhang W, Shao X, Niu R. *Degradation efficiencies of azo dye Acid Orange 7 by the interaction of heat, UV and anions with common oxidants: persulfate, peroxymonosulfate and hydrogen peroxide*. J Hazard Mater 179 (2010) 552-558
- [150] Guan YH, Ma J, Li XC, Fang JY, Chen LW. *Influence of pH on the formation of sulfate and hydroxyl radicals in the UV/Peroxymonosulfate system*. Environ Sci Technol 45 (2011) 9308-9314
- [151] Oh WD, Dong Z, Lim TT. *Generation of sulfate radical through heterogeneous catalysis for organic contaminants removal: Current development, challenges and prospects*. Appl Catal B Environ 194 (2016) 169-201
- [152] Hu P, Long M. *Cobalt-catalyzed sulfate radical-based advanced oxidation: a review on heterogeneous catalysts and applications*. Appl Catal B Environ 181 (2016) 103-117
- [153] Neta P, Huie RE, Ross AB. *Rate constants for reactions of inorganic radicals in aqueous solution*. Phys Chem Ref Data 17 (1988) 1027-1284.

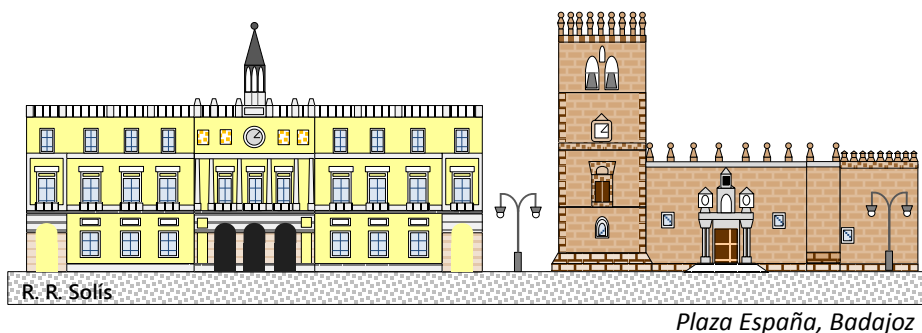
- [154] Anipsitakis GP, Dionysiou DD. *Radical generation by the interaction of transition metals with common oxidants*. Environ Sci Technol 38 (2004) 3705-3712
- [155] Rodríguez-Chueca J, Amor C, Silva T, Dionysiou DD, Li Puma G, Lucas MS, Peres JA. *Treatment of winery wastewater by sulphate radicals: HSO_5^- /transition metal/UV-A LEDs*. Chem Eng J 310 (2017) 473-483
- [156] Kim J, Edwards JO. *A study of cobalt catalysis and copper modification in the coupled decompositions of hydrogen peroxide and peroxymonosulfate ion*. Inorg Chim Acta 235 (1995) 9-13
- [157] Anipsitakis GP, Dionysiou DD. *Degradation of organic contaminants in water with sulfate radicals generated by the conjunction of peroxymonosulfate with cobalt*. Environ Sci Technol 37 (2003) 4790-4797
- [158] Behl M, Stout MD, Herbert RA, Dill JA, Baker GL, Hayden BK, Roycroft JH, Bucher JR, Hooth MJ. *Comparative toxicity and carcinogenicity of soluble and insoluble cobalt compounds*. Toxicol 333 (2015) 195-205
- [159] Barceloux DG. *Cobalt*. J Toxicol-Clin Toxicol 37 (1999) 201-216
- [160] Pelizzetti E, Carlin V, Minero C, Gratzel M. *Enhancement of the rate of photocatalytic degradation of organic pollutants on TiO_2 by inorganic oxidizing species*. New J Chem 15 (1991) 351-359
- [161] Malato S, Blanco J, Richter C, Braun B, Maldonado MI. *Enhancement of the rate of solar photocatalytic mineralization of organic pollutants by inorganic oxidizing species*. Appl Catal B Environ 17 (1998) 347-356
- [162] Chen X, Wang W, Xiao H, Hong C, Zhu F, Yao Y, Xue Z. *Accelerated TiO_2 photocatalytic degradation of Acid Orange 7 under visible light mediated by peroxymonosulfate*. Chem Eng J 193-194 (2012) 290-295
- [163] Chi FL, Zhou GD, Song B, Yang B, Lv YH, Ran SL, Li CG. *CoTiO_3 nanoparticles as a highly active heterogeneous catalyst of peroxymonosulfate for the degradation of organic pollutants under visible-light illumination*. J Nano Res 42 (2016) 73-79
- [164] Liu Y, Guo H, Zhang Y, Tang W, Cheng X, Liu H. *Activation of peroxymonosulfate by BiVO_4 under visible light for degradation of Rhodamine B*. Chem Phys Lett 653 (2016) 101-107

- [165] Chen Q, Ji F, Liu T, Yan P, Guan W, Xu X. *Synergistic effect of bifunctional Co-TiO₂ catalyst on degradation of Rhodamine B: Fenton-photo hybrid process*. Chem Eng J 229 (2013) 57-65
- [166] Chen Q, Ji F, Guo J, Fan J, Xu X. *Combination of heterogeneous Fenton-like reaction and photocatalysis using Co-TiO₂ nanocatalyst for activation of KHSO₅ with visible light irradiation at ambient conditions*. J Environ Sci 26 (2014) 2440-2450
- [167] Yang Q, Choi H, Dionysiou DD. *Nanocrystalline cobalt oxide immobilized on titanium dioxide nanoparticles for the heterogeneous activation of peroxymonosulfate*. Appl Catal B Environ 74 (2007) 170-178
- [168] Yang Q, Choi Y, Chen Y, Dionysiou DD. *Heterogeneous activation of peroxymonosulfate by supported cobalt for the degradation of 2,4-dichlorophenol in water: the effect of support, cobalt precursors, and UV radiation*. Appl Catal B Environ 77 (2008) 300-307.
- [169] Chan KH, Chu W. *Degradation of atrazine by cobalt-mediated activation of peroxymonosulfate: different cobalt counteranions in homogeneous process and cobalt oxide catalysts in photolytic heterogeneous process*. Water Res 43 (2009) 2513-2521
- [170] Sathiskumar P, Mangalaraja RV, Anandana S, Ashokkumar M. *CoFe₂O₄/TiO₂ nanocatalysts for the photocatalytic degradation of reactive red 120 in aqueous solutions in the presence and absence of electron acceptors*. Chem Eng J 220 (2013) 302-310

CHAPTER TWO

EXPERIMENTAL SECTION

This chapter summarizes the experimental content related to the work developed in this dissertation research. Thus, experimental installations, either for oxidation processes or kinetic studies, are described as well as material used and the typical procedure followed. Afterwards, the chapter follows with the description of the main parameters analyzed in aqueous samples. Finally, catalysts' synthesis is detailed and the techniques used for the analyses of its characterization.



2.1. MATERIALS & CHEMICALS

Reagents and chemical substances used along the research here presented were generally analytical or pure grade, and were used as received. Below, Table 2.1 summarizes, alphabetically listed, their name, chemical formula, CAS code, commercial manufacturer and purity.

Table 2.1 Chemicals substances used in this research alphabetically ordered

Name	Formula	CAS	Manufacturer	Purity (%)
<i>Herbicides and model pollutants</i>				
Acetaminophen	C ₈ H ₉ NO ₂	103-90-2	Sigma-Aldrich	99.0
Clopyralid (2-hydroxyethyl) Ammonium	C ₈ H ₁₀ Cl ₂ N ₂ O ₃	57754-85-5	Sigma-Aldrich	99.2
4-chloro-2-methylphenol	C ₇ H ₇ ClO	1570-64-5	Sigma-Aldrich	99.4
Cliophar 425	-	-	Agriphar	42.5
Diuron	C ₉ H ₁₀ Cl ₂ N ₂ O	330-54-1	Sigma-Aldrich	98
Ethofumesate	C ₁₃ H ₁₈ O ₅ S	26225-79-6	Sigma-Aldrich	99.6
MCPA	C ₉ H ₉ ClO ₃	94-74-6	Sigma-Aldrich	98.1
MCPA60%	-	-	Kenogard	60
Metazachlor	C ₁₄ H ₁₆ ClN ₃ O	67129-08-2	Sigma-Aldrich	99.6
Picloram	C ₆ H ₃ Cl ₃ N ₂ O ₂	1918-02-1	Sigma-Aldrich	99.6
Tembotrione	C ₁₇ H ₁₆ ClF ₃ O ₆ S	335104-84-2	Sigma-Aldrich	99.4
Triclopyr	C ₇ H ₄ Cl ₃ NO ₃	55335-06-3	Sigma-Aldrich	99.5
Tritosulfuron	C ₁₃ H ₉ F ₆ N ₅ O ₄ S	142469-14-5	Sigma-Aldrich	99.9
<i>Catalysts & chemicals for catalyst synthesis</i>				
Aeroxide Degussa-P25	TiO ₂	-	Evonik industries	99.6
Ammonium fluoride	NH ₄ F	12125-01-8	Sigma-Aldrich	98
Citric acid	C ₆ H ₈ O ₇	77-92-9	Aldrich	99
Cobalt(II) acetate tetrahydrate	CoC ₄ H ₆ O ₄ · 4H ₂ O	6147-53-1	Sigma-Aldrich	98
Ethanol	C ₂ H ₆ O	64-17-5	Panreac	99.5
Hydrochloric acid (37%)	HCl	7647-01-0	Fisher	36.71
Lanthanum(III) nitrate hexahydrate	La(NO ₃) ₃ · 6H ₂ O	10277-43-7	Sigma-Aldrich	99.99
2-propanol	C ₃ H ₈ O	67-63-0	Panreac	99.5
Titanium (IV) isopropoxide	C ₁₂ H ₂₈ O ₄ Ti	546-68-9	Sigma-Aldrich	97
Urea	CH ₄ N ₂ O	57-13-6	Panreac	99.0
Triethylamine	C ₆ H ₁₅ N	121-44-8	Panreac	99.5
<i>Chemicals for analysis & solution preparation</i>				
Acetic acid	C ₂ H ₄ O	64-19-7	Fisher	99
Acetonitrile HPLC grade	C ₂ H ₃ N	75-05-8	Fisher	99.99
Ammonium chloride	NH ₄ Cl	12125-02-9	Panreac	99
Ammonium fluoride	NH ₄ F	12125-01-8	Sigma-Aldrich	98
Ammonium sulfate	(NH ₄) ₂ SO ₄	7783-20-2	Merck	99.5
Arabic acid	C ₅ H ₁₀ O ₆	32609-14-6	Sigma-Aldrich	-
Beef extract powder	-	68990-09-0	Sigma-Aldrich	-
1,4-benzoquinone	C ₆ H ₄ O ₂	106-51-4	Merck	98
Boric acid	H ₃ BO ₃	10043-35-3	Panreac	99.5
Calcium chloride	CaCl ₂	10043-52-4	Panreac	95

Cobalt (II) chloride 6-hydrate	CoCl ₂ · 6 H ₂ O	7791-13-1	Panreac	99.0
N,N-Diethyl-p-phenylenediamine Sulfate	C ₁₀ H ₁₆ N ₂ ·H ₂ SO ₄	6283-63-2	Alfa Aesar	97
Folin & Ciocalteu's reagent	-	-	Merck	-
Formic acid	CH ₂ O ₂	64-18-6	Fisher	98
Glucose	C ₆ H ₆ O ₆	50-99-7	Panreac	99
Glutamic acid	C ₅ HNO ₄	56-86-0	Merck	99
Gum arabic (from acacia tree)	-	9000-01-5	Sigma-Aldrich	-
Humic acid	-	1415-93-6	Sigma-Aldrich	-
Hydrochloric acid (37%)	HCl	7647-01-0	Fisher	36.71
Hydrogen peroxide (33%)	H ₂ O ₂	7722-84-1	Panreac	33
Iron (III) perchlorate hydrate	Fe(ClO ₄) ₃ · xH ₂ O	15201-61-3	Sigma-Aldrich	99.9
Iron (II) sulfate heptahydrate	FeSO ₄ ·7H ₂ O	7782-63-0	Panreac	99.5
Lignosulfonic acid sodium salt	-	8061-51-6	Sigma-Aldrich	-
Manganese (II) sulfate monohydrate	MnSO ₄ ·H ₂ O	10034-96-5	Panreac	99
Magnesium sulfate 7-hydrate	MgSO ₄ ·7H ₂ O	10034-99-8	Panreac	99.0
Meat peptone	-	91079-38-8	Panreac	-
Mercury (II) sulfate	HgSO ₄	7783-35-9		
Methanol	CH ₄ O	67-56-1	Panreac	99.99
2-methyl-2-propanol	C ₄ H ₁₀ O	75-65-0	Panreac	99
Nitric acid (65%)	HNO ₃	7697-37-2	Fisher	65
Orthophosphoric acid (85%)	H ₃ PO ₄	7664-38-2	Scharlau	85
Oxalic acid	C ₂ H ₂ O ₄	6153-56-6	Sigma-Aldrich	99.5
Oxone®, monoperoxy sulfate compound	2KHSO ₅ ·KHSO ₄ ·K ₂ SO ₄	70693-62-8	Sigma-Aldrich	47 KHSO ₅ basis
			Alfa Aesar	4.5-5 active oxygen
Perchloric acid	HClO ₄	7601-90-3	Panreac	70
1,10-phenanthroline monohydrate	C ₁₂ H ₈ N ₂ · H ₂ O	5144-89-8	Sigma-Aldrich	99
Dipotassium hydrogen phosphate	K ₂ HPO ₄	7758-11-4	Panreac	98
Potassium di-hydrogen phosphate	KH ₂ PO ₄	7778-77-0	Panreac	98
Potassium hydrogen phtalate	C ₆ H ₄	877-24-7	Nacalai Tesque	99
Potassium indigo-trisulfonate	C ₁₆ H ₇ K ₃ N ₂ O ₁₁ S ₃	67627-18-3	Sigma-Aldrich	98
Potassium iodide	KI	7681-11-0	Panreac	99
Potassium dichromate	K ₂ Cr ₂ O ₇	7778-50-9	Panreac	99.5
2-propanol	C ₃ H ₈ O	67-63-0	Panreac	99.5
Propionic acid	C ₃ H ₆ O ₂	70-09-4	Panreac	99.5
Silver sulfate	Ag ₂ SO ₄	10294-26-5	AnalaR Normapur	98.5
Sodium carbonate	Na ₂ CO ₃	497-19-8	Nacalai Tesque	99.8
Sodium carbonate	Na ₂ CO ₃	497-19-8	Panreac	99.8
Sodium chloride	NaCl	7647-14-5	Panreac	99.0
Sodium dodecyl sulfate	C ₁₂ H ₂₅ NaO ₄ S	151-21-3	Sigma-Aldrich	98.5
Sodium nitrate	NaNO ₃	7631-99-4	Panreac	99
Sodium hydrogen carbonate	NaHCO ₃	144-55-8	Nacalai Tesque	99.5
Sodium hydrogen carbonate	NaHCO ₃	144-55-8	Panreac	99.7
Sodium hydroxide	NaOH	1310-73-2	Panreac	98
Sodium polymetaphosphate	(NaPO ₃) _n	50813-16-6	Panreac	99.8
Sodium thiosulfate pentahydrate	Na ₂ S ₂ O ₃ · 5H ₂ O	10102-17-7	Cosela	99.5
Sulfuric acid	H ₂ SO ₄	7664-93-9	Panreac	98

Tannic acid	$C_{76}H_{52}O_{46}$	1401-55-4	Sigma-Aldrich	-
Tiron	$C_6H_4Na_2O_8 \cdot H_2O$	270573-71-2	Sigma-Aldrich	99
Titanium (IV) oxysulfate-sulfuric acid solution	$TiO_5S \cdot x H_2SO_4$	123334-00-9	Sigma-Aldrich	27-31 H_2SO_4 Basis
Tungstosilicic acid hydrate	$H_4[Si(W_3O_{10})_4] \cdot xH_2O$	12027-43-9	Sigma-Aldrich	99.9
Zinc sulfate heptahydrate	$ZnSO_4 \cdot 7H_2O$	7446-20-0	Panreac	99
Zincon monosodium salt	$C_{20}H_{15}N_4NaO_6S$	62625-22-3	Sigma-Aldrich	98

Solutions were prepared with MilliQ® ultrapure water from a MilliQ® Academic device connected to a RiOs-DI® water purification apparatus, both from Millipore.

2.2. EXPERIMENTALS SETUPS AND PROCEDURES

This section describes in detail the experimental setups used and the procedure in their use.

2.2.1. General photocatalytic processes setup with UVA lamps

Figure 2.1 illustrates the experimental setup used in photocatalytic ozonation, photocatalytic oxidation and ozonation tests. The installation consists of an ozone generator, an ozone analyzer and a borosilicate glass reactor of one liter capacity, provided with a glass cover. This cover has five mouths to connect diverse accessories such as thermometer, sampling, as well as outlet and inlet of gaseous currents, this latter equipped with a stainless steel diffuser. Finally, in photocatalysis tests, the installation was completed with a cylindrical tube whose walls were covered with reflective paper and in which four black light lamps (LAMP15TBL HQPOWER™ of Velleman®) were equidistantly arranged. These lamps, with nominal power of 15 W, emit radiation in the range 350-400 nm, with a maximum located at 365 nm.

Ozone, if used, was generated from industrial grade oxygen by electrical discharges in a Sander Labor Ozonisorator 301.7. This equipment, refrigerated with water, is capable of producing ozone at maximum mass flow rates up to 12 g L^{-1} . In case of using oxygen, the gaseous flow passes through the disconnected equipment lines.

The inlet gas flow rate, oxygen or oxygen-ozone mixture, depending on the case, was regulated with a rotameter located at the exit of the ozone generator. By properly positioning two three-way switches at the output of the rotameter, the gas current can be sent either to the reactor or to an Anseros Ozomat GM 6000 analyzer. This analyzer measures the concentration

of ozone in the gas stream, by the spectrophotometric measurement at 254 nm, wavelength at which ozone presents a maximum absorbance.

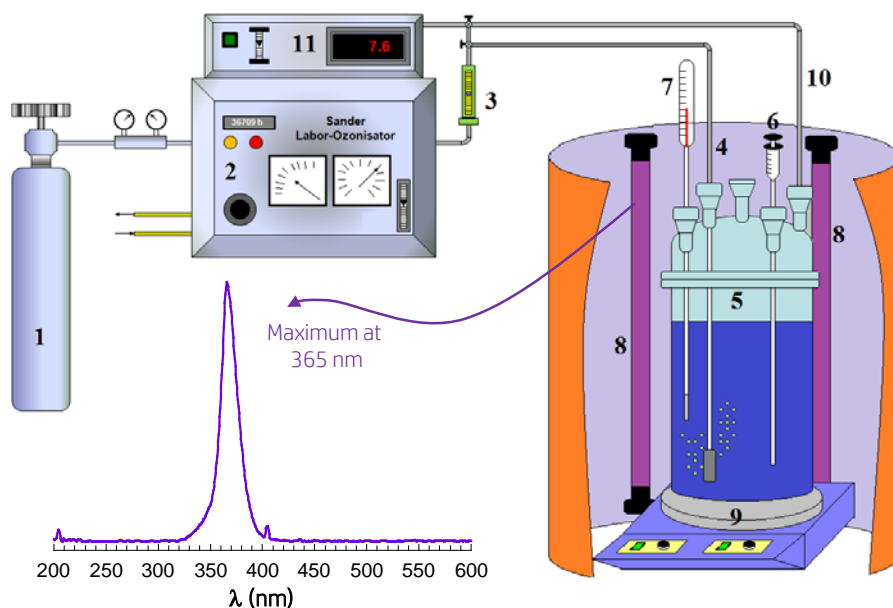


Figure 2.1 Experimental setup for ozonation and photocatalytic processes & emission spectrum of UVA lamp. (1: oxygen tank; 2: ozone generator; 3: rotameter; 4: gas inlet; 5: gas outlet; 6: sampling; 7: thermometer; 8: black light lamp; 9: magnetic stirrer; 10: gas outlet; 11: ozone analyzer)

In those cases where oxygen was fed into the reactor, the ozone generator and analyzer apparatus remained switched off. The flow of oxygen was regulated with the rotameter, and the moment when the three-way switches were arranged for the gas to enter the reactor, was considered as the initial time of the assay.

In those cases where ozone was used, oxygen was first fed to the system, and the desired gas flow rate regulated with the rotameter. The switches were then positioned at the output of the rotameter, making possible that the gaseous stream was sent directly to the analyzer without passing through the reactor. Then, waiting is necessary until obtaining stable reading of $0 \text{ mg L}^{-1} \text{ O}_3$ in the analyzer. Thereafter, the ozone generator was switched on to produce ozone at the desired concentration. Once it was on, the reading of the analyzer will increase until reaching a stable desired value. At this point, the assay can be started. The position of the three-way switches is changed, so that the generator output stream is passed through the reactor and the

reactor output stream to the analyzer. Working in this way, the concentration of ozone gas in the outlet stream would be measured during the development of the reaction. The purpose of these two switches was to use a single analyzer to measure the initial concentration of ozone gas at the inlet and the outlet concentration during the test. At the end of the reaction, the position of the switches was changed again, passing the outlet gas stream directly to the analyzer, without going through the reactor. In this way, the ozone gas inlet was again read at the end of the process.

Installation depicted in Figure 2.1 was also applied in photocatalytic assays without feeding a gas stream. Trials carried out in the presence of peroxidic promoters, i.e. monoperoxysulfate, were developed without considering the gaseous part of the installation. The required amount of monoperoxysulfate was previously dissolved in 10 mL of ultrapure water, and then put into the aqueous reaction system.

At different reaction times, samples were extracted with a syringe and filtered with Millex-HA filters (Millipore®, 0.45 μm) in order to remove the catalyst loaded, if necessary. Dissolved ozone was removed by bubbling air, and when monoperoxysulfate was used, thiosulfate 0.1 M was added as quencher (10 μL per 10 mL of extracted sample, approximately).

2.2.2. Photocatalytic processes setup with UVA LEDs

Figure 2.2 depicts the experimental installation in photocatalytic processes with UVA radiation coming from Light Emitting Diodes (LEDs), used during the stay in the *Universidade de Trás-os-montes e Alto Douro (UTAD)*. The setup was equipped with a magnetic stirrer, a glass reactor of 500 mL, and a photosource of 12 InGaN LEDs lamps (Roithner APG2C1-36E LEDs, nominal consumption of 1.4 W each), emitting within the range of 360–380 (maximum located at 368 nm). The resultant UVA irradiance of the system was estimated to be 85 W m^{-2} . LEDs system was located in the top of the glass reactor, perfectly mixed through magnetic stirring, which was externally covered with aluminum foil in order to increase photon absorption by reflection.

This setup was used to assay photocatalytic oxidation processes in presence of monoperoxysulfate (MPS). The photocatalytic assays carried out in this setup started by loading the 500 mL of the aqueous sample to be treated, the catalyst and the amount of MPS required. It was added by dissolving MPS in a small volume of reaction, i.e. 10–15 mL. pH was adjusted when it was necessary by immersing the pH electrode into the aqueous solution. UVA LEDs, previously stabilized during 30 min, were placed in the top of the reactor, and time started to be counted.

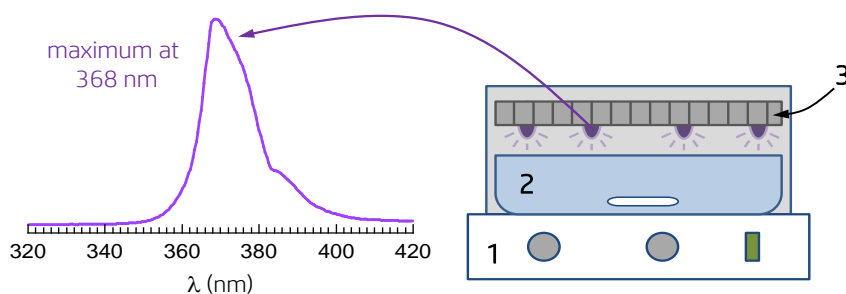
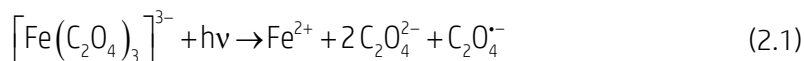


Figure 2.2 Experimental setup for photocatalytic processes & emission spectrum of UVA LEDs. (1: magnetic stirrer; 2: glass reactor; 3: LEDs photosource)

Samples were extracted and filtered at different times with Millex-HA filters (Millipore®, 0.45 μm) in order to remove the catalyst.

2.2.3. Photocharacterization of the radiation source. Chemical actinometry

The radiation intensity of the black light lamps reaching the solution was quantified by chemical actinometry based on the photochemical reduction of the ferrioxalate complex, $[\text{Fe}(\text{C}_2\text{O}_4)_3]^{3-}$, in acid medium. The iron (III) of the ferrioxalate complex is reduced to iron (II) by the action of radiation, being the main reaction of the process the following [1]:



The rate of iron (II) formation can be described with the equation:

$$\frac{dC_{\text{Fe(II)}}}{dt} = I_0 \phi_{\text{Fe(II)}} \left[1 - \exp\left(-2.303 L \epsilon_{[\text{Fe}(\text{C}_2\text{O}_4)_3]^{3-}} C_{\text{Fe(III)}}\right) \right] \quad (2.2)$$

where I_0 represents the incident radiation intensity, $\phi_{\text{Fe(II)}}$ the quantum yield of the reaction at the wavelength of the radiation source ($1.2 \text{ mol Einstein}^{-1}$ at 365 nm [1]), L stands the effective path of the radiation through the reactor, $\epsilon_{[\text{Fe}(\text{C}_2\text{O}_4)_3]^{3-}}$ is the molar attenuation coefficient of ferrioxalate complex ($500 \text{ M}^{-1} \text{ cm}^{-1}$ at 365 nm) and $C_{\text{Fe(III)}}$ the concentration of iron (III).

If the concentration of iron (III) is high enough, the exponential term of equation 2.2 can be neglected, resulting:

$$C_{\text{Fe(II)}} = I_0 \phi_{\text{Fe(II)}} t \quad (2.3)$$

From this equation, by means of experimental adjustment of the evolution of iron (II) concentration versus time, a straight line is obtained. From its slope can be extracted the value of incident radiation intensity.

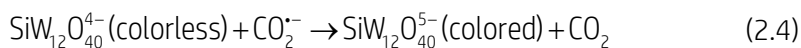
The actinometries assays were performed with oxalic acid 0.15 M and iron perchlorate (III) 5 mM in perchloric acid 0.03 M at pH=2. To avoid the interference of oxygen in the medium, nitrogen gas was bubbled.

The actinometric tests were carried out with one, two, three and four lamps working in the presence of a reflecting surface on the inner wall of the cylinder. Moreover, in the case of the four lamps also the reflective surface was covered with black cardboards, to study the contribution of this factor. From the results of Table 2.2 it can be concluded that the intensity increases almost proportionally with the number of lamps on, and that the contribution of the reflecting surface accounts for about 50% of the total.

Table 2.2 Incident radiation intensity in actinometric assays of UVA lamps installation

Number of lamps	Kind of surface	$I_0 \cdot 10^5$ (Einstein L ⁻¹ min ⁻¹)	R ²
1	Reflective	1.77	0.9967
2	Reflective	3.26	0.9965
3	Reflective	5.13	0.9995
4	Reflective	6.86	0.9966
	Black	3.60	0.9977

Alternatively, and just for LEDs setup characterization, a modification of ferrioxalate actinometry was applied. Ferrioxalate was combined with a polyoxometalate, SiW₁₂O₄₀⁴⁻. CO₂ radical anions formed in ferrioxalate actinometry react with SiW₁₂O₄₀⁴⁻, leading to the production of blue colored SiW₁₂O₄₀⁵⁻, whose concentration can be easily determined spectrophotometrically by measuring the absorbance at 730 nm [2]:



Analogously to equation 2.3, the kinetics of the formation of blue colored SiW₁₂O₄₀⁵⁻ follows the expression:

$$C_{\text{SiW}_{12}\text{O}_{40}^{5-}} = I_0 \phi_{\text{SiW}_{12}\text{O}_{40}^{5-}} t \quad (2.5)$$

From this equation can be deduced the incident radiation intensity by adjusting concentration of blue polyoxometalate ($C_{\text{SiW}_{12}\text{O}_{40}^{5-}}$) through time to a linear curve. From its slope can be obtained the value of incident intensity radiation (I_0) by considering a value of quantum yield at 365, $\phi_{\text{SiW}_{12}\text{O}_{40}^{5-}} = 0.18 \text{ mol Einstein}^{-1}$ [2]. It must be highlighted that this method

underestimates the light intensity when it is lower than $7 \cdot 10^{-5} \text{ Einstein min}^{-1} \text{ L}^{-1}$, reason why it was not considered in the characterization of black light lamps.

As recommended in literature [2], this modified actinometry was carried out using oxalic acid 60 mM, $\text{Fe}(\text{ClO}_4)_3$ 5 mM, and $\text{SiW}_{12}\text{O}_{40}^{4-}$ 1 mM. pH was adjusted to 4.8 with HClO_4 and NaOH in order to avoid self decomposition of $\text{SiW}_{12}\text{O}_{40}^{4-}$. Under this conditions a value of $1.46 \cdot 10^{-4} \text{ Einstein L}^{-1} \text{ min}^{-1}$ was obtained.

2.2.4. Kinetic determinations

Determination of the direct rate constant with molecular ozone by homogeneous competitive experiments in semicontinuous or discontinuous mode

In order to determine the rate constant of the reaction between ozone and organic compounds, homogeneous competitive assays were performed in the installation shown in Figure 2.3. The setup is a modification of the single ozonation installation in which a second reactor is added.

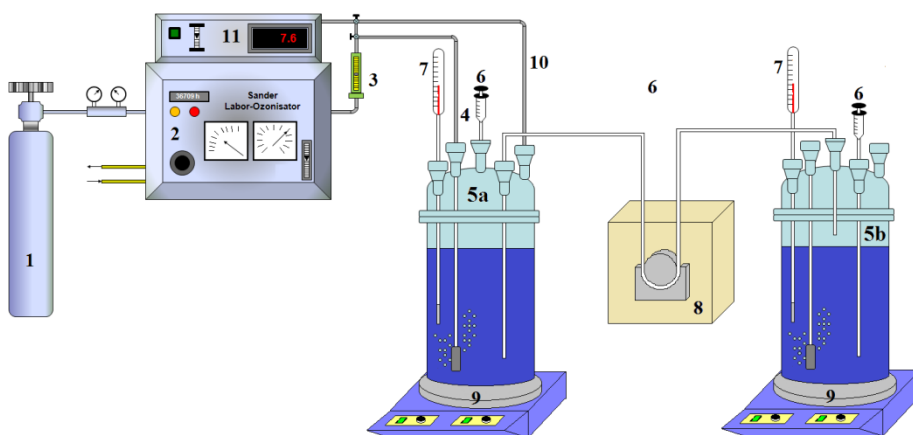


Figure 2.3 Experimental setup for determination of the direct rate constant with molecular ozone by competitive homogeneous in semicontinuous or discontinuous mode (1: oxygen tank; 2: ozone generator; 3: rotameter; 4: gas inlet; 5a: reactor for saturating ultrapure water with ozone; 5b: reactor with target and reference compounds; 6: sampling; 7: thermometer; 8: peristaltic pump; 9: magnetic stirrer; 10: gas outlet; 11: ozone analyzer)

The first mode of operation was semicontinuous. The method consists in the continuous pumping of an ozone saturated solution to a tank containing the target and a reference compound whose ozonation rate constant is

previously known. The mass balance describing for the system responds to [3]:

$$\left. \begin{aligned} V \frac{dC_T}{dt} + C_T \frac{dV}{dt} &= -z_T V k_{O_3-C_T} C_{O_3} C_T \\ V \frac{dC_R}{dt} + C_R \frac{dV}{dt} &= -z_R V k_{O_3-C_R} C_{O_3} C_R \\ \frac{dV}{dt} &= Q \end{aligned} \right\} \quad (2.6)$$

balances in which Q stands for the ozone saturated solution flow rate, V is the reaction volume, C is the concentration, z the stoichiometric coefficient, and the subscripts T and R refer to target and reference compounds, respectively. To eliminate the unknown C_{O_3} concentration, if the reference and target compound mass balances are divided, after integration it follows:

$$\ln \frac{VC_T}{VC_T|_{t=0}} = \frac{z_T k_{O_3-C_T}}{z_R k_{O_3-C_R}} \ln \frac{VC_R}{VC_R|_{t=0}} \quad (2.7)$$

Basically, the installation for these assays consists of a simple ozonation reactor in which a second reactor is added. In the first reactor, ultrapure water is ozonized to completely saturate it in ozone, which is verified by analyzing dissolved ozone with the colorimetric method of indigo, or by measuring aqueous absorbance at 254 nm, where the ozone has a maximum. In the second reactor, the dissolution is arranged with the problem compound and another one (the reference) whose kinetic constant is known at a controlled pH, in the presence of *tert*-butanol 10^{-2} M. Both compounds must exhibit similar ozone reactivity. Initially, the second reactor was charged with 500 mL, and ozone-saturated ultrapure water was added from the first reactor using a peristaltic pump at a rate of 10 mL min^{-1} . Simultaneous ozonation of both compounds takes place. This procedure was carried out for the determination of the rate constant with molecular ozone of 4-chloro-2-methylphenol, using acetaminophen as reference compound.

Rate constant of those compounds that react with ozone developing slow kinetic regime was determined in the same installation without using the second reactor and the peristaltic pump. The first reactor was loaded with a mixture of target and reference compound, and was directly ozonized in the presence of *tert*-butanol (10^{-2} M) at controlled pH. Since reaction volume in this case is constant, the following expression describes the process:

$$\ln \frac{C_T}{C_T|_{t=0}} = \frac{z_T k_{O_3-C_T}}{z_R k_{O_3-C_R}} \ln \frac{C_R}{C_R|_{t=0}} \quad (2.8)$$

A plot of the left term of equation 2.8 versus the logarithmic term of the right side, adjusted to a straight line, let obtain the rate constant of reference compound from the slope.

Determination of the direct rate constant with hydroxyl radical through H₂O₂ decomposition with UVC radiation

The determination of the reaction constants of the studied compounds with the hydroxyl radical was completed by the photolytic decomposition of hydrogen peroxide with UVC radiation. In this case, the installation consists of a UVC lamp (low-pressure mercury vapour lamp Heraeus Model TNN 15/32, maximum emission at 254 nm), a quartz sleeve, a borosilicate glass reactor of 1 L volume and a magnetic stirrer. The lamp, with a maximum emission at 254 nm, is put inside the quartz sleeve, equipped with a cooling jacket, and inserted through the top of the reactor for this purpose. A complete installation diagram is depicted in Figure 2.4.

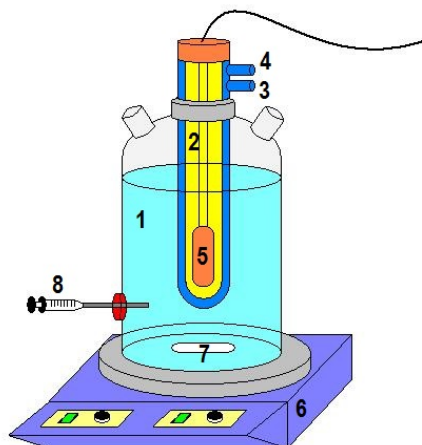


Figure 2.4 Experimental setup for determination of the direct rate constant with hydroxyl radicals through H₂O₂ decomposition with UVC radiation. (1: glass reactor; 2: quartz sleeve; 3: refrigeration inlet; 4: refrigeration outlet; 5: UVC lamp; 6: magnetic stirrer; 7: stir bar; 8: sampling)

In this system, the photolytic decomposition of H₂O₂ leads to the formation of hydroxyl radicals:



2.3. METHODS FOR AQUEOUS ANALYSES

This section details the different methods of analysis applied in aqueous samples. Table 2.3 summarizes the analytical methods and the equipment employed in the diverse parameters analyzed.

Table 2.3 Methods and equipment applied in aqueous analyses of aqueous

Parameter	Method of analysis	Equipment
Aqueous herbicides concentration	High Performance Liquid Chromatography with UV detection (LC-HPLC-UV)	Agilent 1100 HPLC
Transformation products of oxidation	Liquid Chromatography coupled to a Quadrupole Time-of-Flight Mass Spectrometry (LC-QTOF-MS)	Agilent 1260 HPLC + Agilent 6520 QTOF Agilent 1260 HPLC + ABSciex TRIPLE TOF® 5600+
Total Organic Carbon (TOC)	Oxidation + Infrared spectroscopy	Shimadzu TOC-V _{CSH} and Shimadzu TOC-L _{CSH}
Inorganic and organic anions	Ionic Chromatography with conductivity detection	Methrom® 881 Compact IC pro
Dissolved O ₃ concentration	Oxidation + UV-vis spectrophotometry	
H ₂ O ₂ concentration	Oxidation/complex formation + UV-vis spectrophotometry	Spectrophotometer ThermoSpectronic HeLios α
Monoperoxy sulfate concentration	Oxidation + UV-vis spectrophotometry	
Iron (II) concentration	Complex formation + UV-vis spectrophotometry	
Aqueous cobalt concentration	Atomic absorption spectroscopy Complex formation + UV-vis spectrophotometry	Varian SpectrAA Series 140 Spectrophotometer ThermoSpectronic HeLios α
Chemical Oxygen demand (COD)	Chemical oxidation + spectrophotometry	Hach® COD block heater + DR/2400 Hach®
Biological Oxygen Demand (BOD)	Biological oxidation + pressure fall measure	Oxitop® respirometers
Toxicity	Acute toxicity to <i>Daphnia Parvula</i> and <i>Culex Pipiens</i>	-
	Bioluminescence inhibition	Microtox® M500 photometer
	Root growth inhibition in the germination of <i>Lactuca Sativa</i> or <i>Solanum Lycopersicum</i> seeds	-
Turbidimetry	Nephelometry	2100N IS Hach® turbidimeter GLP 21+ CRISON®
pH & temperature	Potenciometry	PH & REDOX 26 CRISON® Jenway 3510
Conductivity	Conductimetry	Conductimeter CRISON® 524

2.3.1. Aqueous herbicides concentration by High Performance Liquid Chromatography with UV detection (LC-HPLC-UV)

Concentration of herbicides in water, used as model compounds, was analyzed by HPLC. The apparatus used was an Agilent 1100 HPLC, equipped with four modules: vacuum degasser, quaternary pump, system of autosampler and monochromatic wavelength UV detector. The software 'ChemStation for LC System' was used for analysis of acquired data.

The stationary phase consisted of a Kromasil 100 5C18 (150 x 21 mm), packed with octadecyl silane particles (C18) of 5 μm of size and porous of 100Å. In all cases a mixture of acetonitrile (A) and 0.1% (v/v) of H_3PO_4 (B) was applied as mobile phase. Thus, different methods were applied by varying A:B proportion to quantify different herbicides, or mixtures of them, either under isocratic or gradient conditions.

The quality of each analytical method was validated by obtaining its linearity, Relative Standard Deviation (RSD) and Limit of Detection (LOD) [4]. The linearity between the obtained signal, i.e. peak area, and the concentration of the analyte was determined by obtaining the regression coefficient (R^2) of the calibration curve of different standards. Precision, described as the closeness to the true value of a single measurement, was quantified by repeating the measurement of the same sample and expressing the result as RSD. Finally, the LOD is usually described as the smallest quantity of analyte that can be detected with a given degree of confidence. Although there is still no full agreement, there is an increasing trend to define LOD as the analyte concentration giving a signal equal to the blank signal, y_B , plus three standard deviations of the blank, s_B [4]:

$$f(\text{LOD}) = y_B + 3s_B \quad (2.10)$$

Table 2.4 shows operational conditions of each method and the parameters for the validation of the calibration curve.

Table 2.4 Methods used for analysis of herbicides by HPLC and results of calibration

Method & Analytes Analyzed	Method. Mobile phase (A:B) and UV detection	Retention time (min)	R^2	RSD (%)	LOD ($\mu\text{g L}^{-1}$)
1	MCPA	6.8	0.9998	0.85	137
	CMP	7.7	1.0000	0.12	14
2	TRI	3.3	0.9999	0.86	57
3	PIC	4.9	0.9999	0.13	34

4	CLO	Isocratic method with 1 mL min ⁻¹ of 25:75 elution and 220 nm	5.1	0.9996	0.23	134
	CLO	Gradient with 1 mL min ⁻¹ , increasing A from 10 to 50% in 12 min and kept at 50% for 6 min. 230 nm	7.6	0.9987	0.74	70
5	PIC	Isocratic method with 1 mL min ⁻¹ of 50:50 elution and 250 nm	9.5	0.9988	0.42	85
	TRI	Gradient with 1 mL min ⁻¹ , increasing A from 50 to 65% in 6 min. 243 nm	16.9	0.9953	0.38	166
6	DIU	Isocratic method with 1 mL min ⁻¹ of 50:50 elution and 250 nm	4.0	0.9999	0.27	62
7	TEMB	Isocratic method with 1 mL min ⁻¹ of 55:45 elution and 220 nm	6.6	1.0000	0.46	54
	METAZ	Isocratic method with 1 mL min ⁻¹ of 55:45 elution and 220 nm	6.4	0.9999	0.23	29
8	TEMB	Isocratic method with 1 mL min ⁻¹ of 55:45 elution and 220 nm	11.2	0.9999	0.20	33
	TRITO	Isocratic method with 1 mL min ⁻¹ of 55:45 elution and 220 nm	12.5	0.9999	0.24	41
	ETHO	Isocratic method with 1 mL min ⁻¹ of 55:45 elution and 220 nm	14.9	0.9999	0.15	80

2.3.2. Transformation Products by Liquid Chromatography coupled to a Quadrupole Time-of-Flight Mass Spectrometer (LC-QTOF-MS)

Transformation products during oxidation processes were tentatively identified by liquid chromatography through HPLC apparatus coupled to Quadrupole Time-of-Flight Mass Spectrometer (QTOF-MS). Two different systems were used for that purpose.

The first system was composed by an Agilent 1260 HPLC coupled to an Agilent 6520 Accurate-Mass QTOF-LC-MS equipped with a dual ESI electrospray interface. The chromatographic separation was conducted in a Zorbax SB-C18 column (3.5 μm , 4.6 x 150 mm). Pure MilliQ[®] water and acetonitrile were used as mobile phase. Elution gradient at 0.2 mL min⁻¹ flow rate initially was increased from 10% of acetonitrile to 100% in 40 min, and kept thereafter for 15 min before equilibration. The analytical operating conditions of the electrospray unit were as follows: capillary 3500 V; nebulizer, 30 psi; gas flow, 5 L min⁻¹; gas temperature 300°C; skimmer voltage, 65 V; octapole RF, 750 V; fragmentor, 100 V. The mass spectra were processed by means of the Agilent Mass Hunter Qualitative Analysis B.04.00 software. Analyses in this apparatus were carried out by the '*Servicio de Análisis Elemental y Molecular (SAEM)*' of '*Servicios de Apoyo a la Investigación de la Universidad de Extremadura (SAIUEx)*'.

The second system consisted of an Agilent 1260 Infinity system connected to a hybrid quadrupole time-of-flight mass spectrometer TRIPLE TOF 5600+ system (AB Sciex) with an electrospray interface (ESI). HPLC was equipped with a Poroshell 120 EC-C18 (2.7 μm , 4.6 x 50 mm) column. Pure MilliQ[®] water or

acidified water with 0.1% formic acid (for negative and positive ionization modes, respectively), and acetonitrile were used as mobile phases. Elution gradient at 0.4 mL min⁻¹ flow rate went from 10% of acetonitrile to 100% in 10 min, and kept thereafter for 5 min before returning to initial conditions. Injection was completed with 10 µL. Both ESI(+) and ESI(-) modes were considered for unknown transformations products identification. The equipment worked via TOF MS survey scan followed by four IDA (Information Dependent Acquisition) TOF MS/MS scans. Alternatively to IDA mode, other tools like 'mass defect filters' and 'include list' for potential candidates were used in order to focus and shorten TPs identification during the acquisition process. Scanned mass range was from m/z = 50 to 800 Da, either in TOF or MS/MS experiments. An accumulation time of 100 ms was used in each scan. IDA criteria considered dynamic background subtraction. Collision energy of 30 eV with a ±10 eV spread was used in MS/MS fragmentation. Diverse AB SCIEX software (Analyst TF 1.5, PeakView™ 2.2 and MasterView 1.1) was used to record and process LC-QTOF-MS data. Analyses developed in this second system were performed during a short stay in the '*Centro de Investigación en Energía Solar (CIESOL), Instituto mixto UAL-PSA CIEMAT*' located in the University of Almería.

2.3.3. Total Organic Carbon (TOC) and Inorganic Carbon (IC)

Total Organic Carbon (TOC), as well as Inorganic Carbon (IC), were determined by means of a Shimadzu® TOC-V_{CSH} analyzer coupled to an ASI-V automatic sample injector. The analysis is based on the catalytic oxidation of the carbon content and the determination of the CO₂ released by means of Non-Dispersive InfraRed detection (NDIR). During the stay in UTAD was used a Shimadzu® TOC-L_{CSH} analyzer coupled to ASI-L sample injector.

Total Carbon (TC) was first determined in an oxidation tube filled in a combustion catalyst (platinum supported onto alumina spheres). Purified air was passed at 150 mL min⁻¹ through the combustion tube, heated at 680°C. Thus, as the sample was injected, carbon content was oxidized or decomposed to generate CO₂. Carrier gas, i.e. purified air, carrying the products generated was cooled and dehumidified before passing into the sample cell of the NDIR detector. The NDIR signal forms a peak, and the data processor (software TOC-Control V) calculated the peak area. The relationship between TC concentration and the peak area was obtained by means of a calibration curve using a TC standard solution (reagent grade potassium phthalate).

As TC comprises TOC and IC, is necessary to distinguish between the organic and inorganic (carbonate and bicarbonate) content by means of a second determination. IC can be quantified by an automatic internal acidification of the sample (with H_3PO_4 at 25%) and sparging it with the carrier gas in order to convert only the IC in the sample into carbon dioxide. The CO_2 is detected in the NDIR detector. IC concentration was correlated with NDIR signal in the same way as TC. The IC calibration curve was built using a mixture of sodium hydrogen carbonate and sodium carbonate as standards.

Subtracting IC concentration from the TC concentration makes possible the determination of TOC concentration.

2.3.4. Inorganic and organic anions by Ionic Chromatography

Inorganic and short-chain organic anions were analyzed by ion chromatography coupled to a conductivity detector. This technique develops the analysis of ions and polar molecules by chromatographic separation in an ion-exchange column.

The Ionic Chromatographic system was a Methrom® 881 Compact IC pro equipped with chemical suppression, autosampler (863 Compact autosampler) and conductivity detector. The stationary phase was an anionic-exchange column (MetroSep A Supp 5, 250x4.0 mm, particles of 5 μm of polyvinyl alcohol with quaternary ammonium groups) thermally controlled at 45°C. Data acquisition and processing was carried out with the software MagIC NET™.

The used mobile phase program consisted of a gradient of 0.7 mL min^{-1} of an aqueous solution of Na_2CO_3 from 0.6 mM to 14.6 mM in 50 min, followed by 10 min of reequilibration. For that purpose, an 800 Dosino dispenses a concentrated Na_2CO_3 solution (35.6 mM) to the eluent system. Calibration curves were built in a range of 0.1-10 mg L^{-1} for the detected inorganic and short-chained organic anions.

2.3.5. Dissolved ozone concentration

The concentration of ozone dissolved in aqueous solution was analyzed following the colorimetric method proposed by Bader and Hoigné [5]. This method involves the determination of aqueous ozone concentration by the decolorization of indigo trisulfonate (potassium 5,5',7-indigo trisulfonate) as ozone rapidly oxidizes it in acidic solution. Solutions of potassium 5,5',7-indigo trisulfonate present blue color with a maximum in absorbance at 600 nm with a molar attenuation coefficient of 20,000 $\text{M}^{-1} \text{cm}^{-1}$ [5]. Thus, ozone concentration can be determined based on the difference in absorbance

between the test sample and a blank. Blank sample is prepared under identical conditions replacing the test sample by the non ozonized sample. The method presents a LOD of 0.1 μM of dissolved ozone and an error inferior to 2% [5].

The stock indigo trisulfonate solution was prepared with 900 mL of buffer solution $\text{H}_3\text{PO}_4/\text{KH}_2\text{PO}_4$ (28 and 35 g L^{-1} of KH_2PO_4 and H_3PO_4 , respectively) and 100 mL of a concentrated indigo trisulfonate solution (0.6 and 2.3 g L^{-1} of indigo trisulfonate and H_3PO_4 , respectively). After mixing, pH was adjusted to 2 by adding a concentrated NaOH solution.

In a typical test, 4 mL of the above stock indigo solution were mixed with 2 mL of the test sample. At the same time, a blank sample was prepared by adding 4 mL of the indigo solution to 2 mL of the water sample before being ozonized. The volumes of stock indigo solution and sample can be modified depending on the expected concentration of dissolved ozone in the sample.

According to Lambert-Beer law, there is a linear relationship between the grade of decoloration and dissolved ozone concentration, $C_{\text{O}_3,\text{d}}$, as shown in the following equation:

$$C_{\text{O}_3,\text{d}} = \frac{A_{600}^{\text{blank}} - A_{600}^{\text{sample}}}{\epsilon_{600} c} f_D \quad (2.11)$$

where A_{600}^{blank} stands for absorbance of the blank sample at 600 nm, A_{600}^{sample} the same for the test sample, ϵ_{600} is the molar attenuation coefficient at 600 nm of indigo trisulfonate, c the cell path length, and f_D the dilution factor after sample alteration by adding indigo solution.

2.3.6. Hydrogen peroxide concentration

Hydrogen peroxide at low concentrations (<5 10^{-5} M)

Hydrogen peroxide generated during photocatalytic processes was analyzed by means of the colorimetric method proposed by Masschelein and co-workers [6]. This determination is based on the oxidation of Co (II) to Co (III) by hydrogen peroxide in solution, taking place a reaction between Co (III) and bicarbonate to produce a complex whose maximum of absorbance is located at 260 nm with a molar attenuation coefficient of 26,645 $\text{M}^{-1} \text{cm}^{-1}$. The limit of detection of the method was estimated to be 3 10^{-7} M [6].

The analytical procedure started by mixing 0.5 mL of cobalt (II) solution (16.1 g L^{-1} of cobalt (II) chloride hexahydrate), 0.5 mL of sodium

hexametaphosphate solution (10 g L⁻¹), 10 mL of saturated sodium bicarbonate, and 1 mL of sample test. Since at 260 nm the organic content in the sample can interfere in the determination, it is also necessary to prepare a second mixture by replacing cobalt (II) solution with ultrapure water. Additionally, two blanks using ultrapure water as test sample must also be prepared. Samples were transferred to a quartz cell of 1 cm of path length and absorbance at 260 nm was measured.

According to Lambert-Beer law, the aqueous concentration of H₂O₂, C_{H₂O₂}, is related to the absorbance of the mentioned mixtures by the expression:

$$C_{\text{H}_2\text{O}_2} = \frac{(A_{\text{cobalt}}^{\text{sample}} - A_{\text{without cobalt}}^{\text{sample}}) - (A_{\text{cobalt}}^{\text{blank}} - A_{\text{without cobalt}}^{\text{blank}})}{\epsilon_{260} \cdot c} f_D \quad (2.12)$$

where $A_{\text{cobalt}}^{\text{sample}}$ and $A_{\text{without cobalt}}^{\text{sample}}$ are the absorbances of the sample tests at 260 nm with and without cobalt (II), respectively; $A_{\text{cobalt}}^{\text{blank}}$ and $A_{\text{without cobalt}}^{\text{blank}}$ the absorbances of blank tests with and without adding cobalt (II), respectively; ϵ_{260} stands for the molar attenuation coefficient of the complex at 260 nm; c the cell path length; and, f_D is the dilution factor.

Hydrogen peroxide at high concentrations (5 10⁻⁵-10⁻³ M)

Rate constant or reaction between hydroxyl radical and organic compounds was obtained through the UVC photolytic decomposition of H₂O₂. In these experiments the concentration of H₂O₂ was analyzed by the colorimetric method reported by Eisenberg [7]. This method quantifies the aqueous H₂O₂ concentration by allowing it to react with titanium (IV) oxysulfate reagent to produce the yellowish pertitanic acid, generated with the selective reaction of Ti (IV) ions. The reaction is effectively instantaneous and the yellow-colored pertitanic acid stable for at least 6 hours, presenting a maximum in absorbance at 405 nm with a molar attenuation coefficient of 720 M cm⁻¹ [7].

The procedure of analysis consisted of mixing 0.5 mL of commercial solution of titanium (IV) oxysulfate in sulfuric acid, and 4.5 mL of test sample. However, depending on the expected concentration of H₂O₂, test samples were diluted in order to obtain a H₂O₂ concentration within the range 5 10⁻⁵-10⁻³ M. Samples were measured at 405 nm in a quartz cell of 1cm of path length.

Once again, Lambert-Beer law is followed and the yellow color intensity is proportional to the H₂O₂ concentration (C_{H₂O₂}), giving a linear relationship:

$$C_{\text{H}_2\text{O}_2} = \frac{(A_{405}^{\text{sample}} - A_{405}^{\text{blank}})}{\epsilon_{405} c} f_D \quad (2.13)$$

where A_{405}^{sample} and A_{405}^{blank} represent the absorbance of sample and blank measured at 405 nm; ϵ_{405} is the molar attenuation coefficient at 405 nm of the yellow pertitanic acid generated; c the cell path length; and, f_D is the dilution factor that undergoes the sample in the process.

2.3.7. Monoperoxysulfate concentration

Concentration of monoperoxysulfate (MPS) was determined spectrophotometrically by a colorimetric method based on N,N-diethyl-phenylenediamine (DPD) oxidation [8].

The oxidation of DPD amine is commonly used in the determination of aqueous chlorine. In this way, DPD amine is oxidized by chlorine giving two oxidation products. At neutral pH, a semi-quinoid cationic compound known as Würster dye is the primary oxidation product. Würster dye shows magenta color, with a maximum of absorbance at 551 nm. When DPD reacts with low concentrations of chlorine at neutral pH, the Würster dye is the main oxidation product. However, at higher oxidant levels, the formation of an unstable colorless imine takes importance, which interferes in Würster dye determination. This DPD method for chlorine was considered in MPS quantification.

In a typical assay, 9 mL of 0.05 M phosphate buffer at pH=6 was pipetted into a glass vial and then mixed with 1 mL of test sample. Immediately, 100 μ L of DPD solution (DPD at 1% with H₂SO₄ 0.1 M) was added and the mixture vigorously mixed. After 30 min, the magenta-colored mixture was transferred to a 1 cm quartz cuvette, and absorbance at 551 nm was measured. A blank test, replacing the test sample with ultrapure water, was required in order to subtract the possible contribution of the stock solutions at 551 nm. For quantification purposes, a linear calibration curve in the range of 0-20 mm of MPS was obtained ($R^2 > 0.99$, LOD=11.7 μ M).

2.3.8. Aqueous iron (II) concentration

Concentration of iron (II), photo-reduced from iron (III) in ferrioxalate actinometry, was colorimetrically analyzed by the reaction of complexation between iron (II) and 1,10-phenanthroline at acidic pH. The red-colored

complex formed presents a maximum in absorbance at 510 nm whose molar attenuation coefficient is $11,040 \text{ M}^{-1} \text{ cm}^{-1}$ [9].

The analysis started by mixing 1.5 mL of 0.1 M acetic/acetate buffer at pH=3-4, 1.0 mL of 1,10-phenanthroline solution (0.02%), 5.0 mL of sample, and 1 mL of 2.0 M ammonium fluoride solution. After stirring and waiting 20 min to complete the formation of the complex, absorbance at 510 nm was measured. A blank test was required; replacing test sample by ultrapure water.

Having in mind the law of Lambert-Beer, and supposing absence of substances which might absorb radiation at 510 nm in the sample, iron (II) concentration is obtained from:

$$C_{\text{Fe(II)}} = \frac{(A_{510}^{\text{sample}} - A_{510}^{\text{blank}})}{\epsilon_{510} c} f_D \quad (2.14)$$

Where $C_{\text{Fe(II)}}$ refers to iron (II) concentration, A_{510}^{sample} and A_{510}^{blank} represent the absorbance of sample and blank measured at 510 nm, respectively; ϵ_{510} is the molar attenuation coefficient of the 1,10-phenanthroline-iron(II) complex at 510 nm; c the cell path length; and, f_D is the dilution factor in the process of measurement.

2.3.9. Aqueous cobalt concentration

Cobalt leaching into aqueous solution by cobalt-based catalysts was analyzed by two different analytical methodologies.

Determination of aqueous cobalt by atomic absorption spectroscopy

Atomic Absorption Spectroscopy (AAS) is a spectroanalytical technique for the quantitative determination of chemical elements using the absorption of optical radiation by free atoms in gaseous state. In AAS, the sample is atomized and a beam of electromagnetic radiation emitted from a radiation source is passed through the vaporized sample. Some of the radiation is absorbed by the cobalt atoms in the sample. The amount of radiation absorbed is proportional to the number of cobalt atoms. The amount a standard absorbs is compared with the sample in a previous calibration curve. This enables the quantification of cobalt in the unknown sample.

The apparatus used was a Varian SpectrAA Series 140, controlled by Varian's AA worksheet software. Aqueous cobalt sample was nebulized and mixed with the flame with acetylene as fuel and air as carrier. A hollow

cathode multielement lamp (Part Number 56-101076-00) was used as light source operating at a wavelength of 240.7 nm and 0.2 nm of slit.

A second-order polynomial calibration curve was obtained in the range 1-30 mg L⁻¹ of cobalt (R²=0.9992). The limit of detection was estimated to be 0.49 mg L⁻¹ and the relative standard deviation of 0.62%.

Spectrophotometric determination of aqueous cobalt (II)

Additionally, aqueous cobalt was spectrophotometrically determined using a metallochromic indicator, zincon monosodium salt [10]. Zincon is a blood-red complexometric indicator (maximum in absorbance at 620 nm) that undergoes a color change in the presence of some metals, such as Co (II). pH in the process must be controlled since the complex generated is sensitive to pH changes.

Following this method, Co (II) was analyzed by mixing 1.0 mL of zincon solution (100 mg of zincon in 100 mL of a mixture methanol: ultrapure water 50:50), 1.5 mL of buffer at pH=9 (8.4 and 31 g L⁻¹ of NaOH and H₃BO₃, respectively) and 10 mL of sample. After 30 min of complexation, absorbance was measured in a quartz cell of 1 cm of path at 620 nm. Additionally, a blank replacing the sample with ultrapure water was considered to be subtracted.

A calibration curve, adjusted to a second-order polynomial fit (R²=0.996), was built in the range 0-5 mg L⁻¹ of Co (II). Relative standard deviation was estimated to be inferior to 1%, and the limit of detection was calculated to be 0.36 mg L⁻¹.

2.3.10. Total polyphenol content

Total polyphenol content was determined by the Folin-Ciocalteu method [11]. Folin-Ciocalteu reagent [12] is a mixture of phosphotungstic (H₃PW₁₂O₄₀) and phosphomolibdic (H₃PMo₁₂O₄₀) acids used for the colorimetric assay of phenolic compounds. In presence of polyphenolic substances, this reagent is reduced in alkaline conditions leading the formation of a blue mixture of tungsten (W₈O₂₃) and molybdenum oxides (Mo₈O₂₃), whose absorbance presents a maximum located at 740 nm [11].

In a typical assay, 0.5 mL of commercial Folin-Ciocalteu reagent, 0.5 mL of test sample and 6.5 mL of ultrapure water were placed in a glass vial. After mixing and standing for 5 min, 4.5 mL of Na₂CO₃ (7%) was increased. Reaction is considered to be completed after 60 min [11], when absorbance at 740 nm can be measured.

Polyphenol total content was determined using phenol as base of calculation to express the results in terms of concentration. A lineal calibration curve in the range of 0-200 mg L⁻¹ of phenol was obtained ($R^2 > 0.998$ and LOD = 0.98 mg L⁻¹).

2.3.11. Chemical Oxygen Demand (COD)

Chemical Oxygen Demand (COD) represents the amount of oxygen required to oxidize either organic or inorganic aqueous matter. COD is measured in a standardized close-reflux assay in which the test sample is oxidized by a strong chemical oxidant, potassium dichromate, in acidic conditions under specific conditions of temperature and period of time. AgSO₄ is added since silver cation catalyzes the oxidation reaction. Moreover, chloride anions, which represent an important interference, can be precipitated as HgCl₂ in presence of HgSO₄.

COD test were carried out in cylindrical glass tubes of 15 mL, in which were placed 4 mL of digestion solution (20.432 g L⁻¹ of K₂Cr₂O₇, 334 mL L⁻¹ of concentrated H₂SO₄ and 66.6 g L⁻¹ of HgSO₄) and 4 mL of acid solution (solution of AgSO₄ in concentrated H₂SO₄ in a proportion of 5.5 g kg⁻¹) and 2 mL of test sample. Cylindrical tubes were then placed into a preheated Hach® COD block heater (COD reactor, model 45600) where oxidation process took place at 148°C during 2 hours. After that, absorbance at 600 nm coming from the reduced Cr³⁺ was measured in a DR/2400 Hach® spectrophotometer, adapted to insert cylindrical vials.

Calibration curve was previously built by using a potassium phthalate standard of 850 mg L⁻¹ (COD of 1000 mg O₂ L⁻¹) in the range 0-1000 mg O₂ L⁻¹ ($R^2 > 0.99$ and LOD estimated to be 55 mg L⁻¹).

2.3.12. Biological Oxygen Demand (BOD)

Biological Oxygen Demand (BOD) was conducted in respirometer systems where microorganisms in the sample consume oxygen and generate CO₂ as consequence of the metabolism of organic content. The CO₂ produced is absorbed by NaOH, creating a vacuum which is measured, expressing the BOD value as consumed O₂ in mg L⁻¹.

BOD at five days of incubation (BOD₅) was assessed in Oxitop® respirometers of 500 mL of volume, in which a certain amount of sample was placed depending on the expected value of BOD₅ (432 mL for values in a range of 0-40 mg L⁻¹ of O₂). pH of sample must firstly be adjusted to 6.5-7.5. As inoculum, 1 mL of activated sludge from the municipal wastewater treatment plant of Badajoz was added. Then, 2-3 pellets of NaOH were placed

in the rubber cap that the device has for that purpose. After putting the measuring head in the glass bottle, incubation was developed in a temperature controlled chamber ($22\pm 2^{\circ}\text{C}$) and the automatic saving registered the values during the first five days.

2.3.13. Toxicity tests

Toxicity of aqueous samples was evaluated with different methods according to the capacity of response to the organism considered.

Acute toxicity to Daphnia parvula and Culex pipiens larvae

The acute toxicity tests using *Daphnia parvula* were conducted adapting US EPA standard operating procedures [13]. This procedure was extrapolated to carry out similar trials with mosquito *Culex pipiens*. Acute toxicity tests are usually designed to provide dose-response expressed as the percent of effluent concentration that is lethal to 50% of the test organisms (LC_{50}), within the prescribed period of time (24-96 h). Nevertheless, toxicity evolution through the time of the oxidation treatment applied was assessed by measuring survival rate in samples taken from the reactor at different times. LC_{50} was just analyzed before applying any oxidation technology.

In a typical trial, 100 mL of test sample were placed in sterile plastic pots and pH was adjusted to 7 ± 0.1 . After that, 20 young *D. parvula* or 15 second-instar *C. pipiens* larvae were transferred using a sterile plastic container. Cultures of *D. parvula* and *C. pipiens* larvae were received from installations of Extremadura's University, where organisms were naturally cultured in artificial ponds. After adding test organisms, samples were subjected to natural 16:8 light: dark photoperiods at room temperature. Survival rate was monitored at 6, 24 and 48 h for *D. parvula*; and at 24, 46, 72 and 96 h for *C. pipiens*, without any feeding during the experiments. Simultaneously, a triplicated blank test, using the same aqueous matrix free of herbicide content, was carried out. For the test results to be acceptable, control survival must be superior to 90%.

Vibrio Fischeri toxicity assay

Toxicity of reaction samples was also studied by the inhibition of the bioluminescent bacterium *Vibrio Fischeri*. Since the bacterium emits light within the visible range (490-505 nm) as a natural part of its metabolism, the exposure to a toxic substance causes disruption of the respiratory process which consequently develops an inhibition of bioluminescence. A Microtox® M500 photometer was applied for that purpose.

In a typical assay, a stock bottle of lyophilized and specially selected strain of the marine bacterium *Vibrio Fischeri* (formerly known as *Photobacterium Phosphoreum*, Microtox Acute Toxicity Test Reagent, NRRL-11177, stored in between -15 and -25°C) was rehydrated with 1 mL of Reconstitution Solution at 4°C, which consists of specially prepared and nontoxic ultrapure water. This process provides a ready-to-use suspension of microorganisms. Next, 2.5 mL of test sample was added in a glass cuvette (vial A) as well as 250 µL of Microtox Osmotic Adjustment Solution (MOAS, 22% of NaCl and ultrapure water solution), in order to adjust the osmotic pressure of the test sample to approximately 2% of NaCl. In a second cuvette (vial B), 0.5 mL of Diluent (nontoxic solution that is made of 2% NaCl in ultrapure water) was pipetted and 10 µL of suspension of microorganisms was added. During the process, the cuvettes were inserted in specific holes that Microtox® Model 500 device provides in order to keep bacteria to the adequate temperature. After 15 min, bioluminescence in vial B is measured (named as SET), and 0.5 mL of vial A is transferred to vial B. At this point, time is controlled and vial B is newly measured after 5, 15 and 30 min. Microtox® calculates the percentage of inhibition as the fall of bioluminescence in vial B before and after adding test sample from vial A.

Phytotoxicity assays with Lactuca Sativa and Solanum Lycopersicum

Phytotoxicity tests were used to examine the evolution of toxicity of aqueous samples through the reaction time. The bioassay applied was an acute seed germination-root elongation toxicity test, based on US EPA procedures [14]. Lettuce (*Lactuca Sativa*) is commonly used as target specie due to its short period of germination and its sensitiveness to phytochemicals. Tomato seeds (*Solanum Lycopersicum*) were also tested as target species.

Fifteen seeds of *Lactuca Sativa* (Vilmorin®, *Batavia Blonde of Paris* or *Romana Bionda Degli Ortolani*) or *Solanum Lycopersicum* (Vilmorin®, *cherry tomato*) were equally placed in a Petri dish (90 mm of diameter) equipped with paper discs. 4 mL of aqueous test sample were transferred, moistening the paper disc. Dishes were covered with parafilm plastic in order to avoid liquid evaporation, and afterwards incubated in a germination chamber isolated from light at 22±2°C. After 5 days of incubation, the root length, as the sum of hypocotyl and radicle, was measured in those seeds whose germination had taken place.

Additionally, a negative control or blank (ultrapure water) and a positive control of H₂O₂ 300 mM were carried out. The validity criteria for the test were an upper 90% of germination, and a variation coefficient for the root growth

below 30% in blank control experiments, done in triplicate. Positive control led to germination of none of the seeds. The percentage root growth of test sample was calculated by comparing the radicle lengths of each sample with those observed in the control.

2.3.14. Turbidity

Turbidity of an aqueous sample is defined as the propensity of particles to scatter a light beam focused on them. Suspended particulates are quantified by employing a source beam and a light detector set to one side, usually 90°, of the source beam. Particle density is then a function of the light reflected into the detector from the particles in the sample. The extent of this process depends upon properties of the particles like their shape, color, and reflectivity. The units of turbidity from a calibrated nephelometer are called Nephelometric Turbidity Units (NTU).

The device used for turbidity measures, during the stay in UTAD, was a 2100N IS Hach® turbidimeter. The apparatus was calibrated with a commercial turbidimetry standards (kit stablcal®) of stabilized formazin (<0.1, 20, 200, 1000 and 4000 NTU).

2.3.15. pH and temperature

pH was measured in a GLP 21+ CRISON® pH-meter equipped with an 50 21T electrode and automatic temperature correction. pH calibration curves were carried out dialy with CRISON® buffers.

Moreover, for those cases in which pH and temperature in the solution were monitored continuously, a CRISON® multimeter (PH & REDOX 26) was used. This device is equipped with pH, redox and temperature electrodes in a single body. Calibration was performed daily with CRISON® buffers.

pH during the stay in UTAD was analyzed in a Jenway 3510 pH meter. It was used for monitoring pH during the reaction by inserting the electrode into the aqueous solution. Calibration was carried out with commercial buffers.

2.3.16. Conductivity

Conductivity was measured in a Crison® 524 conductimeter equipped with graphite cell and automatic compensation of temperature, being the results expressed at 20°C. The device was calibrated with standard of 1413 $\mu\text{S cm}^{-1}$ (or a standard of 12.88 mS cm^{-1} for measurements higher to 5 mS cm^{-1}).

2.4. CATALYSTS' SYNTHESIS AND CHARACTERIZATION

In this section, the methodology to synthesize the lab-made catalysts and the techniques used for its characterization are presented.

2.4.1. Catalysts' synthesis

Bare & nitrogen-doped titanium dioxide (TiO_2 & N- TiO_2)

Bare or nitrogen-doped titanium dioxide was manufactured and used in photocatalytic processes. Firstly, research presented in chapter 3 is focused on the use of bare or nitrogen-doped titania (doping either urea or triethylamine) for the conventional photocatalytic oxidation process, i.e. feeding oxygen as oxidant. Secondly, chapter 5 concentrates in the use of photocatalytic ozonation with bare or nitrogen-doped titania, using triethylamine as doping agent in the process of synthesis. Whatever the case may be, the process of synthesis followed was the same.

The manufactured photocatalysts were synthesized adapting the methodology described by Senthilnathan and Philip [14]. Basically, the process for bare titania (TiO_2) starts with the hydrolysis of titanium (IV) isopropoxide (0.01 mol) dissolved in ethyl alcohol (20 mL) by adding drop by drop a 0.1 M solution of HCl (20 mL). Precipitation is completed after thermal treatment at 80°C for 12 hours. Afterwards, the resultant suspension is centrifuged at 3500 rpm and washed with ethyl alcohol and water. Then, the solid is dried at 100-110°C in an oven. Finally, the dried solid is grinded and calcined at a specified temperature for 4 hours. Nitrogen-doped titania was made following the same steps, adding a fixed amount of urea previous to the hydrolysis step, or triethylamine, to meet a required N:Ti ratio.

Lanthanum-cobalt perovskites ($LaCoO_3$)

Lanthanum-cobalt perovskite oxide ($LaCoO_3$) was considered as an active Fenton-like catalyst for the heterogeneous decomposition of monoperoxysulfate, as reported in chapter 9. It was prepared by a specific mild sol-gel method, known as the citrate route.

$LaCoO_3$ oxide was synthesized by the citrate method [16]. Citrate method is the most widespread and effective route to create high-surface area perovskites [17]. The process starts preparing an aqueous solution of metal precursors, $La(NO_3)_3 \cdot 6H_2O$ and $Co(CH_3COO)_2 \cdot 4H_2O$. Thus, 0.01 mol of each metallic salt is dissolved in 400 mL of ultrapure water. After 1 hour mixing under magnetic stirring, 100 mL of citric acid in excess, i.e. twice the stoichiometrically needed for each metal, is slowly added. Citric acid acts as an

organic complexing agent and the methal-citrate complex is formed. The resultant solution is heated at 100°C to remove water excess, drying thereafter the obtained pinkish gel. During the drying step, the decomposition of amorphous citrate precursors leads to solid solution of high homogeneity. The solid is grinded and calcined at 700°C for 7 hours, considering an initial ramp of 10°C min⁻¹ from room temperature.

Lanthanum-cobalt perovskites coupled to titanium dioxide (LaCoO₃-TiO₂)

Chapter 10 reports the investigation of the heterojunction of the previous perovskite oxide and titanium dioxide (LaCoO₃-TiO₂). This catalyst is prepared in two different steps.

Firstly, LaCoO₃ perovskite is synthesized in the presence of citric acid as complexing organic agent as described in previous section. Secondly, LaCoO₃-TiO₂ heterojunction was prepared by hydrothermal precipitation of a titanium organic precursor in the presence of the previous synthesized perovskite. 0.0405 mol of titanium (IV) isopropoxide was dissolved in 100 mL of 2-propanol and a fixed amount of the previously LaCoO₃ was added under stirring to meet a specific LaCoO₃:TiO₂ molar ratio (0:1, 0.05:1, 0.1:1, 0.25:1, 0.5:1, 0.75:1 and 1:0). Afterwards, 100 mL of ultrapure water was gradually dropped into the above suspension. The precipitation of titanium dioxide was thermally completed by autoclaving the mixture at 80°C for 12 h. The resultant suspension was centrifuged at 3500 rpm and the solid washed with water and 2-propanol. Finally, the solid dried overnight at 100°C was calcined at 500°C for 4 hours under air atmosphere (initial ramp, 10°C min⁻¹).

2.4.2. Techniques for analysis and characterization of catalysts

Synthesized catalysts properties and surface characteristics were analyzed by the ‘Servicio de Análisis y Caracterización de Sólidos y Superficies (SACSS)’ of ‘Servicios de Apoyo a la Investigación de la Universidad de Extremadura (SAIUEX)’, with the exception of diffuse-reflectance UV-vis spectroscopy which was carried out by the analysis service of the ‘Instituto de Catálisis y Petroleoquímica (ICP) del CSIC’, in Madrid. Table 2.5 summarizes the parameters studied and the techniques used for that purpose.

Table 2.5 Methods and equipments applied in analyses of catalysts

Parameter	Method of analysis	Equipment
Superficial morphology & semiquantitative superficial composition	Scanning Electron Microscopy (SEM) with Energy Dispersive X-ray (EDX) detection	Hitachi S-4800
		FEI ESEM-FIB QUANTATM 3D FEG

Cristal morphology at nanoscale range	Transmission Electron Microscopy (TEM)	FEI TECNAI G2 20 Twin
Cristallyne composition	X-Ray Difraccction (XRD)	Bruker® D8 ADVANCE
Superficial composition & oxidation state	X-Ray Photoelectron Spectroscopy (XPS)	ThermoFisher Scientific XPS K-Alpha
UV-vis absorption spectra. Band gap determination	Difusse Reflectance Spectroscopy UV-vis (DRS-UV-vis)	Varian Cary 5000
Elemental composition	Wavelength Dispersive X-Ray Fluorescence (WDXRF)	Bruker® S8 Tiger 4K
Specific surface area	Nitrogen adsorption isotherm. BET area	Quantachrome QUADRASORB evo™ Quantachrome Autosorb iQ2-C
Variation of mass, released heat and gases with temperature treatment	TermoGravimetry-Diffraction Thermal Analysis coupled to Mass Spectrometry (TG-DTA-MS)	Setaram SETSIS Evolution-16 + Prisma™ QMS200
pH of point of zero charge (pH _{pzc})	Mass titration	-

Scanning Electron Microscopy (SEM)

The scanning electron microscopy (SEM) is a microscopy technique that produces images scanning it with a focused beam of high-energy electrons. Accelerated electrons carry significant amounts of kinetic energy, and this energy is dissipated as a variety of signals produced by electron-sample interactions when the incident electrons are decelerated in the solid sample. As a result, a variety of signals at the surface of solid specimens is generated. These derived signals reveal information about the sample, including external morphology and texture, chemical composition, crystalline structure and orientation of materials. Thus, a 2-dimensional generated image displays spatial variations in these properties. Secondary electrons, backscattered electrons (BSE), diffracted backscattered electrons, characteristic X-rays that are used for elemental analysis, visible light, and heat are the most commonly signals derived from interaction of accelerated electron with the solid surface. From them, secondary electrons and BSE are commonly used for depicting samples. Secondary electrons are useful for showing morphology; while BSE are valuable for illustrating contrasts in composition in multiphase samples. Furthermore, characteristic X-rays that are produced by the interaction of electrons with the sample can also be detected in an SEM device equipped for

Energy-Dispersive X-ray (EDX) spectroscopy, allowing semiquantitative analyses of elements abundance in the sample.

SEM images, either built with secondary electrons or BSE, were obtained from two different SEM microscopes. Both devices were equipped with EDX analysis technique for microanalysis. The first microscope was a Hitachi S-4800 working at 0.5-30 kV with amplification of 30x-800kx. The second one was an ESEM-FIB QUANTA™ 3D FEG of FEI Company working at 0.2-30 kV with amplification of 30x-1280kx.

Transmission Electron Microscopy (TEM)

Transmission electron microscopy (TEM) is another microscopy technique working with a high-energy beam of electrons which are transmitted through an ultra-thin sample, interacting with it as result of its penetration. The interaction between the electrons and the atoms is used to depict detailed micro-structural examination through high-resolution and high magnification imaging, allowing the investigation of crystal structures, specimen orientations and chemical compositions of phases. Range of visualisation and analysis of specimens covers the realms of microspace to nanospace.

The TEM microcope used was a TEM TECNAI G2 20 Twin of FEI Company fitted with electron source from LaB₆ emitter, working at high tension between 20 and 200 kV. It also had a combination of 3 opening condensers from 30 to 200 μm and 8 target apertures from 10 to 100 μm for Low Magnification, Normal and High Magnification applications in Microprobe and Nanoprobe. The device is complete with a CCD FEI Eagle 4k camera. The maximum magnification available was 1.05Mx.

X-Ray Diffraction (XRD)

X-ray diffraction relies on the phenomenon of radiation dispersion by a crystalline sample. The dominant effect that occurs when an incident beam of monochromatic X-rays interacts with a target material is scattering of those X-rays from atoms within the target material. The incident scattered monochromatic X-rays that are in phase, produce constructive interference at certain angles, giving rise to the diffracted rays. This process of diffraction of X-rays by crystals is described by Bragg's Law, which says that the difference of paths traveled by the scattered rays must be equal to an interger number of wavelengths:

$$n\lambda = 2d \sin \theta \quad (2.15)$$

where n is a positive integer, λ is the wavelength of incident wave, d is the interplanar distance, and θ is the scattering angle. The intensities of the diffracted waves depend on the kind and arrangement of atoms in the crystal structure. However, most materials are not single crystals, but are composed of many tiny crystallites in all possible orientations called a polycrystalline aggregate or powder. When a powder with randomly oriented crystallites is placed in an X-ray beam, the beam will see all possible interatomic planes. If the experimental angle is systematically changed, all possible diffraction peaks from the powder will be detected.

XRD spectra were produced in a microcrystalline powder diffractometer Bruker® D8 ADVANCE. This device has Bragg-Brentano geometry, operating in both reflection and transmission. It allows measuring polycrystalline and sintered samples, as well as samples in capillaries. It is equipped with a Vårio-1 primary monochromator (Ge-111) that allows the use of monochromatic Cu $K\alpha_1$ radiation ($\lambda=1.5406 \text{ \AA}$). It also has a point detector and a Våntec-1 position sensitive detector with aperture up to 12° . Furthermore, it offers the possibility of swapping the sample holder, by either a temperature chamber or the capillary support.

X-Ray Photoelectron Spectroscopy (XPS)

X-Ray Photoelectron Spectroscopy (XPS) is a surface quantitative spectroscopic technique that measures the elemental composition, chemical state and electronic state of the elements that exist within a solid sample. The interaction of a beam of X-ray onto the atoms of a solid sample provides them with enough energy to remove electrons of different elements of the first layers of the surface (effective penetration of 2-10 nm). These electrons come out of atoms with a characteristic kinetic energy that gives information about what type of atom they belong to, and what kind of atoms they may be interacting with. Thus, as the energy of the X-ray source is known, and since the kinetic energy of the emitted electrons are measured, the electron binding energy of each emitted electron can be determined by using the following expression:

$$E_{\text{binding}} = E_{\text{X-ray source}} - (E_{\text{kinetic}} + \phi) \quad (2.16)$$

where E_{binding} is the binding energy of the electron, $E_{\text{X-ray source}}$ the energy of the incident X-ray photons being used, E_{kinetic} is the kinetic energy of the electron as measured by the instrument, and ϕ is the work function dependent on both the spectrometer and the material.

The XPS device used was a ThermoFisher Scientific XPS K-Alpha model spectrometer working with a monochromatic radiation source $K\alpha$ of Al radiation (1486.68 eV). Working conditions undergo until a maximum voltage of 12 kV and current of 6 mA. Source was placed with an inclination of 30° respect to the horizontal of the sample. The spot size resolution of 30 to 400 μm in ellipsoidal arrangement. Spectral energy resolution: 0.9% of the values set in pass energy. It also includes a depth profile source of Ar^+ ion bombardment (energies 1, 2 or 3 KeV), placing the source at a 30° inclination with respect to the horizontal of the sample.

Post-acquired data were processed with XPSpeak 4.1 for background extraction (Shirley type) and peak fitting. Superficial atomic ratio determination was estimated from the peak areas using Wagner atomic sensitivity factors [18].

Diffuse Reflectance Spectroscopy UV-visible (DRS-UV-vis)

Diffuse reflectance spectroscopy relies upon the focused projection of a spectrometer beam into the sample where it is reflected, scattered and transmitted through the sample material. The back reflected, diffusely scattered light is then collected by the accessory and directed to the detector optics. Only the part of the beam that is scattered within a sample and returned to the surface is considered to be diffuse reflection. A diffuse reflectance accessory, i.e. an integration sphere, is capable of collecting the reflected flux. The integrating sphere is essentially a hollow sphere coated with a white material whose diffuse reflectance is close to 1.

DRS-UV-vis spectra were carried out in a UV-Vis-NIR Varian Cary 5000, equipped with double beam spectrophotometer and synchronized double shutter. The sources used were Deuterium (UV) and halogen quartz. The detectors consisted of a photomultiplier, and a refrigerated PbS detector for the NIR zone. Spectra can be registered in the range 200-2500 nm.

Band gap indicates the difference in energy between the top of the valence band filled with electrons and the bottom of the conduction band devoid of electrons. Tauc plot is a widespread method for the determination of band gap from a diffuse reflectance spectrum. Tauc, Davis and Mott proposed the following formula for computing the band gap [19, 20]:

$$(\alpha h\nu)^{1/n} = c(h\nu - E_{BG}) \quad (2.17)$$

where α is a coefficient of absorption, h refers to Plank's constant, ν means the frequency of inciden photons, c is a proportional constant, E_{BG} represents

the band gap energy of the semiconductor, and the value of the exponent n denotes the nature of the sample transition. This parameter takes the following values: direct allowed transitions, $n=1/2$; direct forbidden transitions, $n=3/2$; indirect allowed transition, $n=2$; indirect forbidden transition, $n=3$. Since the direct allowed transition is used in titania based semiconductors, a value of $n=1/2$ can be considered. The absorption coefficient of measured material can be provided by the following expression:

$$\alpha = \frac{\ln 10}{L} A \quad (2.18)$$

where L is the optical path length, and A means the absorbance measured at a specific frequency of incident photons.

Consequently, plotting $(\alpha h\nu)^2$ versus $h\nu$ and extrapolating the linear interval with a straight line makes possible to obtain in the intersection with the abscissa axis the value of E_{BG} .

Wavelength Dispersive X-Ray Fluorescence (WDXRF)

Wavelength Dispersive X-Ray Fluorescence (WDXRF) is one of two general types of X-Ray Fluorescence (XRF) techniques used for elemental analysis application. Thus, in a WDXRF spectrometer, the analysis is based on the detection of secondary X-ray that comes from the simultaneously excitation from a primary X-ray source. All of the elements in the sample are excited simultaneously. The different energies of the characteristic radiation emitted from the elements in the sample are diffracted into different directions and are characteristic of each element.

The device used was a Bruker[®] S8 Tiger 4K WDXRF spectrometer. It was equipped with an excitation X-ray source of rhodium (4kW) operating at maximum voltage of 60 kV and at maximum current of 170 mA. The mask sizes were 32, 24 and 8 mm; the analyzer crystals available were XS-55, PET, LiF(200), XS-Ge-C, LiF(220), XS-B, XS-C and XS-N; being the apparatus fitted with proportional and scintillation counter detectors (for light and heavy elements, respectively). Spectra^{plus} (version 3) analytical software package supported the acquisition and evaluation of measured data.

Nitrogen adsorption isotherms. BET area determination

Physical adsorption of gases and vapors in solids is a commonly applied technique for the analysis of porous texture of a solid surface. Not only surface is analyzed, but also information of volume and distribution of different sized pores are also provided. This surface phenomenon consists in

the adsorption of a gaseous adsorbate (commonly N₂ or CO₂) on a solid adsorbent at a constant temperature, creating a film of adsorbate adhered molecules onto the surface of the adsorbate. The exact nature of the adhesion depends on the details of the species involved; nevertheless, the process is generally classified as physisorption, characteristic of weak Van der Waals forces; or chemisorption, which involves covalent bonding.

Isotherms were determined in two different devices. Samples were previously outgassed under high vacuum conditions at 120-150°C during 4-12 hours. The first device was a Quantachrome QUADRASORB evo™ gas sorption surface area and pore size apparatus working with N₂ as adsorbent (minimum surface area and p/p₀, 0.01 m² g⁻¹ and 4 · 10⁻⁵, respectively). The second one was an Autosorb iQ2-C series of Quantachrome, using N₂ as adsorbent (minimum area detectable, 0.01 m² g⁻¹; and minimum relative pressure, 3 · 10⁻⁷).

The specific surface area was determined from the amount of gas needed to form a statistical monolayer of molecules adsorbed onto the surface of a solid sample using the model proposed by Brunauer, Emmett and Teller, which provides the known as BET area [21]:

$$\frac{1}{V[(p_0/p)-1]} = \frac{C-1}{V_m C} \frac{p}{p_0} + \frac{1}{V_m C} \quad (2.19)$$

where p and p₀ mean the equilibrium and the saturation pressure of adsorbates at the temperature of adsorption (77 K), respectively; V displays the specific adsorbed gas quantity and V_m represents the specific monolayer adsorbed gas quantity. The BET constant C is related to the strength and interaction of the solid with the adsorbate, and therefore, to the heat of the process. The representation of the left term of BET equation versus p/p₀ (typically linear in the interval between p/p₀=0.05-0.3) makes possible to obtain the specific BET area (S_{BET}) from the following expression:

$$S_{BET} = \frac{N_A A_{molec} V_m}{M_V} \quad (2.20)$$

where N_A is Avogadro number, A_{molec} refers to the projected area of a N₂ molecule (0.162 nm²) and M_V the molar volume at normal conditions (22.414 L mol⁻¹).

ThermoGravimetry and Differential Thermal Analysis coupled to Mass Spectrometry (TG-DTA-MS)

The thermogravimetric analysis determines, by controlled heat, the variations of weight that a solid experiences with the temperature due to the compounds that are being adsorbed, desorbed, decomposed or reacted. The technique submits a sample of known weight to a controlled temperature program under a known atmosphere, usually air or oxygen, recording the evolution of the weight with the temperature. Thermogravimetry measures the variation in mass of the sample through a temperature program. It is possible to couple a mass spectrometer to the thermobalance, permitting to analyze the gases involved in the thermal process. Moreover, a measure of temperature changes gives information about heat flow in Differential Thermal Analysis (DTA).

Thermal Gravimetry, Differential Temperature Analysis and released gases Mass Spectrometry (TG-DTA-MS) was performed in a Setaram SETSYS Evolution-16 equipment connected to a Prisma™ QMS200 quadrupole mass spectrometer. The operation conditions were: air flow rate 50 mL min⁻¹ and heating rate of 10°C min⁻¹ from room temperature.

pH of point zero charge (pH_{pzc})

Point of zero charge is commonly described as the pH value at which a solid submerged in an electrolyte exhibits zero net electrical charge on the surface. pH of point zero charge (pH_{pzc}) is a tool to describe zero net charge only for systems in which H⁺/OH⁻ are the determining ions, i.e. aqueous environments. Therefore, when pH is inferior to pH_{pzc}, the acidic solution donates more H⁺ than OH⁻ and so the adsorbent surface is positively charged, being capable of attracting anions. Conversely, at pHs up to pH_{pzc} surface is negatively charged, attracting cations.

pH of point of zero charge (pH_{pzc}) was obtained by mass titration method [22]. Briefly, a solution of HNO₃ 0.1 M was prepared and pH adjusted until value of 3 with NaOH 0.1 M. Different containers with increasing amounts of solid (0.05, 0.1, 0.5, 1, 5, 10 and 20%) were filled with 15 mL of solution. Solutions were kept under stirring and pH was measured after 48 h of equilibria. A plot of pH versus solid fraction (%) gives a curve which tends asymptotically to pH_{pzc} value.

REFERENCES

- [1] Goldstein S, Rabani J. *The ferrioxalate and iodide-iodate actinometers in the UV region*. J Photochem Photobiol A Chem 193 (2008) 50-55
- [2] Lee J, Kim J, Choi W. *Ferrioxalate-polyoxometalate system as a new chemical actinometer*. Environ Sci Technol 41 (2007) 5433-5438
- [3] Rivas FJ, Sagasti J, Encinas A, Gimeno O. *Contaminants abatement by ozone in secondary effluents. Evaluation of second-order rate constants*. J Chem Technol Biotechnol 86 (2011) 1058-66
- [4] Miller JN, Miller JC. *Statistics and Chemometrics for Analytical Chemistry*. Pearson Education. 6th edition, Harlow (England), 2010
- [5] Bader H, Hoigné J, *Determination of ozone in water by the indigo method*. Water Res 15 (1981) 449-456
- [6] Masschelein W, Denis M, Ledent R. *Spectrophotometric determination of residual hydrogen peroxide*. Water Sew Works (1977) 69-72
- [7] Eisenberg GM. *Colorimetric determination of hydrogen peroxide*. Ind Eng Chem 15 (1943) 327-328
- [8] Fukushima M, Tatsumi, K. *Effect of Hydroxypropyl- β -cyclodextrin on the degradation of pentachlorophenol by potassium monoperoxysulfate catalyzed with iron (III)-porphyrin complex*. Environmental Science & Technology 39 (2005) 9337-9342
- [9] Rodríguez E, Mimbbrero M, Masa FJ, Beltrán FJ. *Homogeneous iron-catalyzed photochemical degradation of muconic acid in water*. Water Res 41 (2007) 1325-1333
- [10] Ghasemi J, Ahmadi Sh, Torkestani K. *Simultaneous determination of copper, nickel, cobalt and zinc using zincon as a metallochromic indicator with partial least squares*. Analytica Chimica Acta 487 (2003) 181-188
- [11] Box JD. *Investigation of the Folin-Ciocalteau phenol reagent for the determination of polyphenolic substances in natural waters*. Water Res 17 (1983) 511-525
- [12] Folin O, Ciocalteau V. *On tyrosine and tryptophane determinations in proteins*. J Biol Chem 73 (1927) 627-650
- [13] EPA. *Methods for measuring the acute toxicity of effluents and receiving water to freshwater and marine organisms*. 5th ed. Washington DC, 2002

- [14] EPA. *Ecological effects test guidelines. Seed germination/root elongation toxicity test OPPTS 850.4200*, **1966**
- [15] Senthilnathan J, Philip L. *Photocatalytic degradation of lindane under UV and visible light using N-doped TiO₂*. Chem Eng J 161 (**2010**) 83-92
- [16] Sotelo JL, Ovejero G, Martínez F, Melero JA, Milieni A. *Catalytic wet peroxide oxidation of phenolic solutions over a LaTi_{1-x}Cu_xO₃ perovskite catalyst*. Appl Catal B: Environ 47 (**2004**) 281-294
- [17] Granger P, Parvulescu VI, Kaliaguine S, Prellier W. *Perovskites and Related Mixed Oxides: Concepts and Applications, Volume 1*. John Wiley & Sons. **2016**
- [18] Wagner CD, Davis LE, Zeller MV, Taylor JA, Raymong RH, Gale LH. *Empirical atomic sensitivity factor for quantitative analysis by electron spectroscopy for chemical analysis*. Surf Interf Anal 3 (**1981**) 211-225
- [19] Tauc J, Grigorovici R, Vancu A. *Optical properties and electronic structure of amorphous Germanium*. Phys Stat Sol 15 (**1966**) 627-637
- [20] Davis EA, Mott NF. *Conduction in non-crystalline systems V. Conductivity, optical absorption and photoconductivity in amorphous semiconductors*. Philos Mag 22 (**1970**) 903-922
- [21] Brunauer S, Emmett PH, Teller E. *Adsorption of Gases in Multimolecular Layers*. J Am Chem Soc 60 (**1938**) 309-319
- [22] Noh JS, Schwarz JA. *Effect of HNO₃ treatment on the surface acidity of activated carbons*. Carbon 28 (**1995**) 675-682

CHAPTER THREE

PAPER ONE

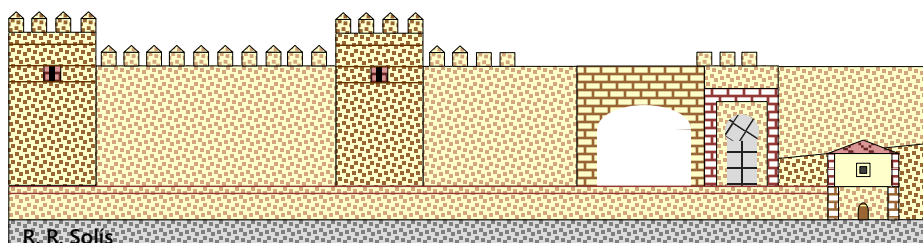
Photocatalytic elimination of aqueous 2-methyl-4-chlorophenoxyacetic acid in the presence of commercial and nitrogen-doped TiO₂

Int J Environ Sci Technol 12 (2015) 513-526

J. Rivas, R. R. Solís, O. Gimeno, J. Sagasti

ABSTRACT. An attempt to synthesize an active photocatalyst for 2-methyl-4-chlorophenoxyacetic acid removal has been accomplished. Black light (main emission wavelength at 365 nm) photocatalytic experiments with bare and N-doped titania have been carried out, and the results compared to those obtained in the presence of titania Degussa P25. Doping percentage and calcination temperature influences have been investigated in photocatalytic runs using pure and commercial 2-methyl-4-chlorophenoxyacetic acid. In no case, the results obtained with synthesized titania improved the activity of P25. Some kinetic tests allowed for the proposal of a pseudoempirical reaction mechanism capable of acceptably simulating the process in the presence of P25. From the proposed mechanism, the roles played by hydroxyl, peroxy and organic radicals have been suggested.

KEYWORDS: Black light, photocatalysis, reaction mechanism, titania



Alcazaba, Badajoz

3.1. INTRODUCTION

2-Methyl-4-chlorophenoxyacetic acid (MCPA) is an herbicide belonging to the phenoxy or phenoxyacetic acid family. MCPA is used as a post-emergence herbicide for the selective control of broadleaf weeds. Phenoxy herbicides act by simulating the action of natural hormones, producing uncoordinated plant growth. MCPA disrupts both seedling emergence and vegetative vigor, and can be used to control both dicots and monocots. In USA, approximately 4.6 million pounds of MCPA active ingredient is annually applied [1].

Surface water contamination by MCPA may directly result from spray drift or indirectly from runoff and/or leaching. Extreme contamination is generated from spills, deliberate dumping of tank residues, or equipment-washing operations. Groundwater contamination may occur through improper handling procedures or through normal use in areas with shallow aquifers. Contamination of water with MCPA is common due to its extensive application, high water solubility, and low affinity for most soils. Thus, MCPA is frequently found in rivers and wastewater treatment plants effluents [2,3]. Phenoxyacid herbicides are only moderately toxic compared to other family herbicides; however, they can affect the nervous system irreversibly after adsorption through the skin. Additionally, their prolonged inhalation can cause dizziness, burning in the chest, and coughing [4].

Development of inexpensive and suitable technologies to remove trace contaminants in waters is in continuous growth. Hence, since solar radiation is an incessant source of energy in Mediterranean countries, water treatments developed under the idea of using solar radiation constitute an interesting research field from the economic point of view [5]. Also, the use of low-cost black light lamps (if compared to UV-C lamps) can be considered as a parallel alternative in those regions where solar radiation is limited by weather conditions.

In this context, illumination of photocatalysts with photons of energy equal to or greater than their band gap leads to the formation of electron/hole pairs with free electrons moving to the empty conduction band (e_{CB}^-), leaving behind an electron vacancy or "hole" in the valence band (h_{VB}^+). Under appropriate conditions, these charged species can react with adsorbed electron donors or electron acceptors to generate a free radical mechanism.

Having in mind all the previous statements, in this work, an attempt has been conducted to manufacture a TiO₂-based photocatalysts to efficiently remove MCPA from water while showing acceptable settling properties. Due to the influence of the presence of substances other than the parent compound

in photocatalytic process, runs have been conducted in the presence of MCPA of high purity degree and also by using marketable MCPA (60%) commonly used in agriculture. Additionally, some tests have also been conducted to clarify the species involved in the photocatalytic degradation of MCPA. From the previous results, a pseudoempirical mechanism has been proposed and tested. All the experiments have been carried out at the University of Extremadura (Badajoz, Spain) during the second half of 2012 and first half of 2013.

3.2. MATERIALS AND METHODS

3.2.1. Photoreactor and procedure

A 1.0 L capacity perfectly mixed borosilicate glass photoreactor was used in all the experiments (see Figure 3.1). The reactor was placed in the middle of a 31 cm external diameter pipe (54 cm height). The internal wall of the pipe was covered by aluminium foil to increase the photons reflection towards the reaction media. Four black light lamps (41 cm length) were evenly distributed and attached to the pipe. The lamps (LAMP15TBL HQPOWER™ manufactured by Velleman®) had a nominal power of 15 W mainly emitting within the range 350-400 nm, the maximum being located at 365 nm. Actinometry experiments in the presence of ferrioxalate led to values of 1.77, 3.26, 5.13 and $6.86 \cdot 10^{-5}$ Einstein $L^{-1} \text{ min}^{-1}$ when 1, 2, 3 and 4 lamps were used. Additionally, when the aluminium foil covering the internal walls of the installation was substituted by a black surface, the intensity (4 lamps switched on) decreased to $3.60 \cdot 10^{-5}$ Einstein $L^{-1} \text{ min}^{-1}$.

Previously to the photodegradation experiments, the mixture water-photocatalyst was stirred for 60 min in the dark to achieve the MCPA adsorption equilibrium on the photocatalyst surface. With the exception of the run conducted at low oxygen concentration (nitrogen bubbling), oxygen was continuously bubbled into the water bulk by means of a diffuser placed at the reactor bottom.

The gas flow rate was kept constant at 30 L h^{-1} in all the experiments. Photocatalysts were maintained in suspension by magnetic stirring. Prior to the analysis, the solid was removed from samples by filtration through Millex-HA filters (Millipore, $0.45 \mu\text{m}$).

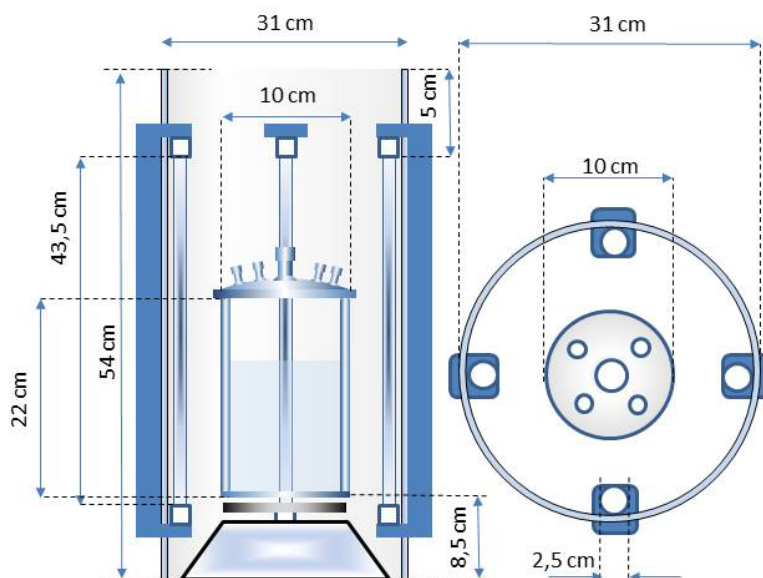


Figure 3.1 Experimental setup. *Front and top views*

3.2.2. Materials

Commercially available MCPA (60%) and pure MCPA from Aldrich (>99%) were used in different experiments, and the rest of chemicals were purchased from Sigma-Aldrich and used as received. Organic solvents were HPLC grade obtained from Panreac. For comparison purposes, a commercial TiO₂ Degussa P25 photocatalyst (70% anatase and 30% rutile) was used with an average particle size of 30 nm and BET surface area of 50 m² g⁻¹. Water purified by a Milli-Q water system (Millipore) was used in the preparation of solutions and suspensions.

Different manufactured photocatalysts abbreviated as TiO₂ (U or E 1:x_T°C) were used. In this nomenclature, the first letter indicates the nitrogen source (urea -U- or ethylenediamine -E-), 1:x is the ratio of N atoms to Ti atoms in the synthesis process and T°C is the calcination temperature in Celsius. The photocatalysts were synthesized following the methodology described by Senthilnathan and Philip [6]. Basically, the steps were the mixing of titanium isopropoxide in ethyl alcohol and addition of predetermined amounts of the nitrogen source to meet the N:Ti ratio. When required, NH₄F was added to get a ratio Ti:F 5:1 [nitrogen from NH₄F is not accounted for in the general formula TiO₂ (U or E 1:x_T°C)]. HCl was added to the previous mixture to get a clear liquid. Precipitation was accomplished after autoclaving

at 80 °C for 12 h. The suspension was centrifuged and the solid dried at 100 °C. Calcination was carried out for 4 h.

3.2.3. Analysis

MCPA was analysed by high-performance liquid chromatography (Agilent 1100). The column used was a Kromasil 100 5C18. The mobile phase acetonitrile (40)/water (60) was acidified with 0.1% of phosphoric acid and pumped at a flow rate of 1 mL min⁻¹. Detection was conducted at 230 nm. Reaction intermediates were tentatively identified by direct comparison of retention times and pure standards in the HPLC analysis. Some intermediates were also confirmed by LC-MS.

In order to assess the degree of mineralization, total organic carbon (TOC) was determined by a Shimadzu TOC 5000A analyzer by directly injecting the aqueous solution.

The pH of the reaction media was measured by means of a Radiometer Copenhagen pH-meter (HPM82).

3.2.4. Catalyst characterization

XPS spectrum was obtained by means of a XPS K-alpha Thermo Scientific apparatus with a $K\alpha$ monochromatic source of Al (1,486.68 eV). Peak energies corresponding to Ti2p, N1s were calibrated based on the response of the C1s peak at 284.8 eV.

TEM analysis was carried out by a TEM Tecnai G2 20 Twin-FEI Company apparatus (filament LaB₆, voltage hasta 200 kV, magnification up to 1.05 10⁶) while SEM was conducted in a Quanta 3D FEG-FEI Company device.

3.3. RESULTS AND DISCUSSION

3.3.1. Experiments carried out with pure MCPA: influence of TiO₂ doping

The positive effect of titania doping with different anions has previously been reported [7]. This positive effect is normally associated with a decrease in the energy band gap of the photocatalyst; however, some controversy has been raised in relation to this positive influence. Moreover, in some cases, titania doping can lead to an increase in the undesirable recombination rate of holes and electrons. In order to assess the effect of nitrogen doping, some experiments were carried out with pure MCPA in the presence of N-doped titania. For comparison purposes, control runs were also completed by using bare titania and the well-known Degussa P25. Figure 3.2 shows the results obtained.

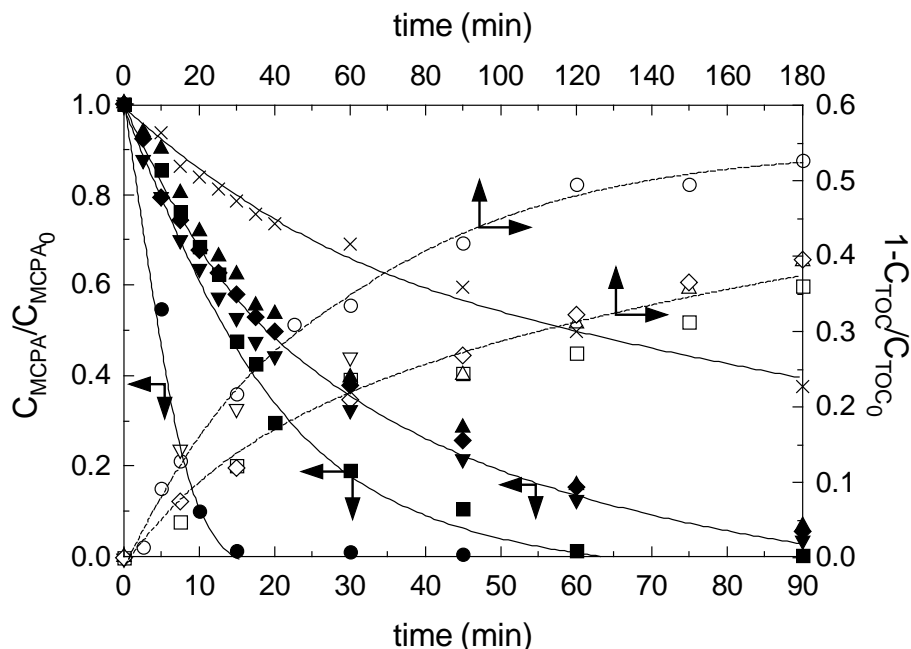


Figure 3.2 Photocatalysis of pure MCPA (0.025 mM) in the presence of different photocatalysts (0.5 g L⁻¹). ●, Degussa P-25; TiO₂ (U 0:1.0_550); ■, TiO₂ (U 1:0.4_550); ▲ TiO₂ (U 1:0.8_550); ▼, TiO₂ (U1:1.2_550); ◆, TiO₂ (U 1:1.6_550). Open symbols stand for TOC conversion

From Figure 3.2, it can be observed that in no case, the manufactured photocatalyst did show a better activity than the commercial P25. Thus, in the presence of 0.5 g L⁻¹ of P25, MCPA was degraded in just 15 min compared to 60–90 min when doped titania was used. Similar trends were experienced when analysing the mineralization degree in terms of TOC conversion. The photocatalyst Degussa P25 was capable of removing approximately the 50 % of the initial TOC in 180 min, and slightly lower values around 40 % of mineralization were obtained when N-TiO₂ was used. The reason for these differences in reactivity may rely, amongst others, in the different particle size observed for the two types of catalysts. Hence, particle size of synthesized photocatalysts was higher than P25 grain size suggesting that some external diffusion limitations may occur in the adsorption process previous to the photocatalytic reaction.

The influence of the ratio N:Ti adopted in the synthesis process is also depicted in Figure 3.2. In this study, bare titania showed a lower activity than N-doped titania, indicating the beneficial effect of the doping stage. Additionally, the photocatalyst manufactured with the lowest urea dose (lowest N:Ti ratio) showed a better performance in terms of MCPA removal. No appreciable variances between the rest of experiments were experienced.

When monitoring TOC conversion, no significant differences were experienced regardless of the N:Ti ratio used. The role played by N in doped titania is controversial. Hence, even if N-doped TiO₂ materials may absorb visible light, some authors claimed that they are frequently inactive in photooxidation reactions under visible light irradiation [8]. Similarly to the results found in this work, under visible light irradiation, the quantum yield of isopropanol decreased with increasing the dopant N content, a fact that was attributed to the parallel increased formation of oxygen vacancies, acting as recombination centers for photoproduced electron-hole couples [9]. Fu et al. [10] claimed that many examples of visible light photo-decomposition of organics on N-doped TiO₂ actually proceeded via electron-mediated reactions involving O₂⁻ and not through holes generated at N dopant sites.

In spite of the fact of a poorer performance of the TiO₂ (U 1:0.4_550) photocatalyst, its settling properties were significantly better than Degussa P25. Hence, contrarily to Degussa P25, almost 90-100% of the manufactured photocatalyst could be recovered from solution by the action of gravity with no need of centrifugation. However, this behavior can just be attributed to the higher particle size.

The TiO₂ (U 1:0.4_550) catalysts were characterized by TEM, SEM and XPS. Figure 3.3 shows the results obtained. TEM image (up right) depicts the normal anatase bipyramidal shape with a large percentage of {101} facets although some truncated octahedral shapes largely dominated with {101} and {001} facets are also envisaged. SEM analysis shows a broad range of particle sizes. It has to be highlighted the rugosity of particle surfaces (bottom right).

The N1s peak showed a bonding energy of 400.2 eV, typical of interstitial positions in the environment O-Ti-N [11]. Formation of N-Ti-N structures is ruled out due to the lower binding energy (397.2 eV) of TiN [12]. The substitution of oxygen atoms by N atoms involves the decrease in the electronic density around N if compared to TiN crystals. Accordingly, the binding energy of N1s in O-Ti-N is higher than in N-Ti-N. Ti2p peak appears at 458.8 eV, also indicating the presence of structures O-Ti-N [6]. Nitrogen shifts the binding energy of Ti2p in pure anatase (459.1 eV). The presence of nitrogen atoms provokes the increase in the titanium atoms electronic density. The Shirley method led to a N:Ti ratio of roughly 1%.

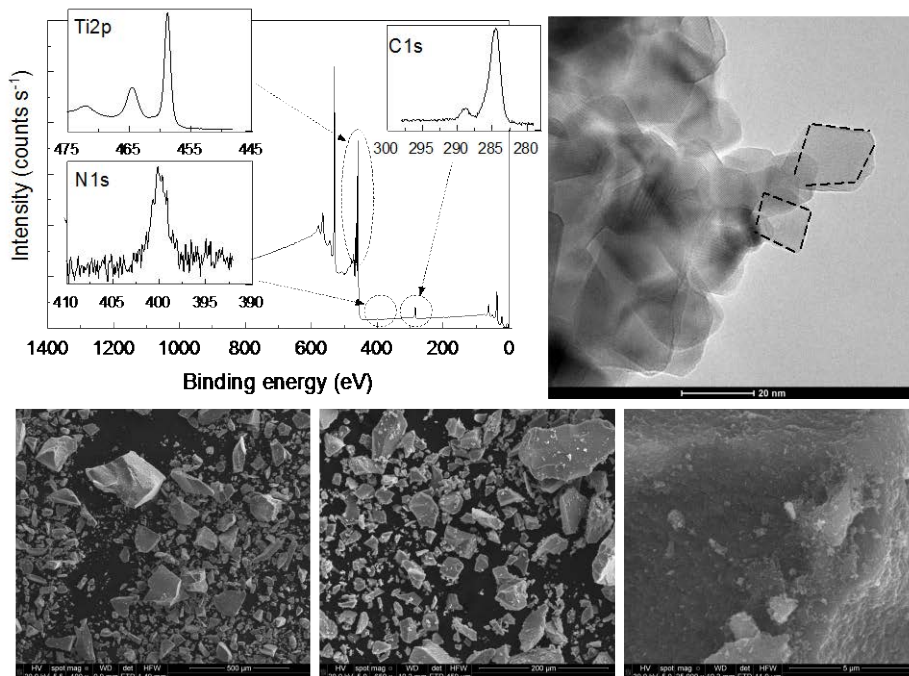


Figure 3.3 XPS, TEM and SEM of catalyst TiO₂ (U 1:0.4_550)

3.3.2. Experiments carried out with commercial MCPA: influence of calcination temperature

Following the results obtained previously, it was decided to assess the influence of the photocatalyst calcination temperature. Hence, the ratio N:Ti of 1:0.4 was thereafter used to photodegrade an aqueous solution of the commercial MCPA.

Calcination temperature plays a crucial role in the activity of synthesized titania. Accordingly, temperature governs the elimination rate of organics used in the synthesis process and the distribution of the rutile and anatase phases. At macroscopic scale, the transformation of anatase to rutile reaches a measurable speed for bulk TiO₂ at T>600 °C.

Figure 3.4 shows the results obtained. As seen in this figure, once again none of the photocatalysts manufactured at different calcination temperatures could enhance the results obtained with P25. Low temperatures (i.e. 200 °C) seem to be insufficient to remove the organic template used in the synthesis process while high temperatures (i.e. 700 °C) seem to favor the formation of the less active rutile phase in contraposition to the anatase phase. In any case, according to the literature, the presence of both phases (anatase and rutile) shows a better photocatalytic activity than the use of

single anatase [13]. Also, the sintering process into larger particles may be favored at high temperatures decreasing the photocatalyst activity.

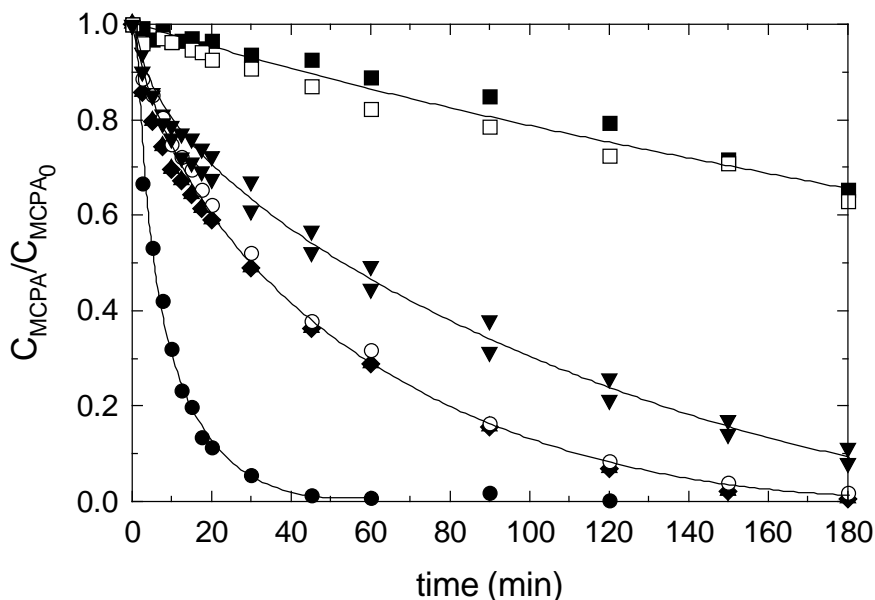


Figure 3.4 Photocatalysis of commercial MCPA (0.025 mM) in the presence of different photocatalysts (0.5 g L⁻¹). ●, Degussa P-25; ■, TiO₂ (U 1:0.4_200); ▲, TiO₂ (U 1:0.4_300); ▼ TiO₂ (U 1:0.4_400); ◆, TiO₂ (U 1:0.4_500); ○, TiO₂ (U 1:0.4_600); □, TiO₂ (U 1:0.4_700)

3.3.3. Experiments carried out with commercial MCPA: influence of the ratio N:Ti in the synthesis process

Based on previous results, a new attempt to synthesize a photocatalyst with similar activity than P25 was completed. Accordingly, a series of photocatalytic experiments was carried out with different catalysts calcinated at 300 °C (lowest temperature with maximum activity) and using different N:Ti ratios in the synthesis process. Figure 3.5 illustrates the results obtained. From this figure, it is inferred that an excess of urea in the synthesis process leads to the deactivation of the photocatalyst. It seems that an excessive doping of the titania crystals increases the sites of electron hole recombination, reducing therefore the beneficial effects of band gap narrowing. It can be hypothesized that there exists an optimum in nitrogen doping, assuming a balance between the positive narrowing of the band gap and the negative effect of increasing electron hole recombination.

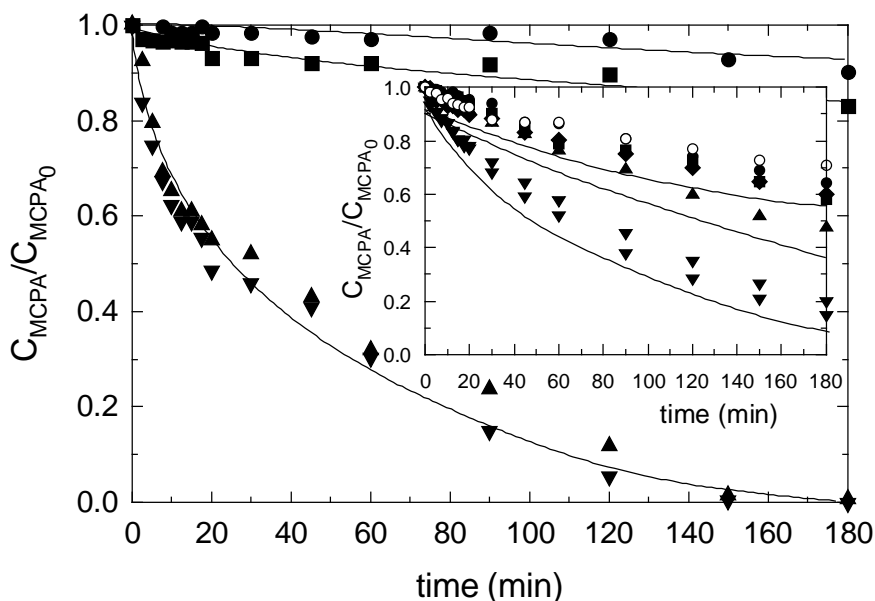


Figure 3.5 Photocatalysis of commercial MCPA (0.025 mM) in the presence of different photocatalysts (0.5 g L⁻¹). ●, TiO₂ (U 1:0.2_300); ■, TiO₂ (U 1:0.3_300); ▲, TiO₂ (U 1:0.4_300); ▼, TiO₂ (U 1:0.5_300). **Inset figure:** ●, TiO₂ (U 1:0.4_300) + NH₄F; ■, TiO₂ (U 1:0.4_500) + NH₄F; ▲, TiO₂ (E 1:0.4_500) + NH₄F; ▼, TiO₂ (E 1:0.4_500); ◆, TiO₂ (E 1:0.4_700); ○, TiO₂ (E 1:0.4_300)

Stabilization of the {001} faces of anatase was also tried by adding NH₄F [14] in the synthesis process; however, no positive results were obtained (see Figure 3.5 inset). Similarly, based on the work of Senthilnathan and Philip [6], the nature of the nitrogen source was changed from urea to ethylenediamine leading to disappointing results if compared to the performance of the P25 photocatalyst (see Figure 3.5 inset).

3.3.4. Preliminary kinetic tests

In an attempt to assess the species involved in the photocatalysis of MCPA, some experiments with pure MCPA and Degussa P-25 were completed in the presence of different specific scavengers of the common reactive species in photocatalytic processes.

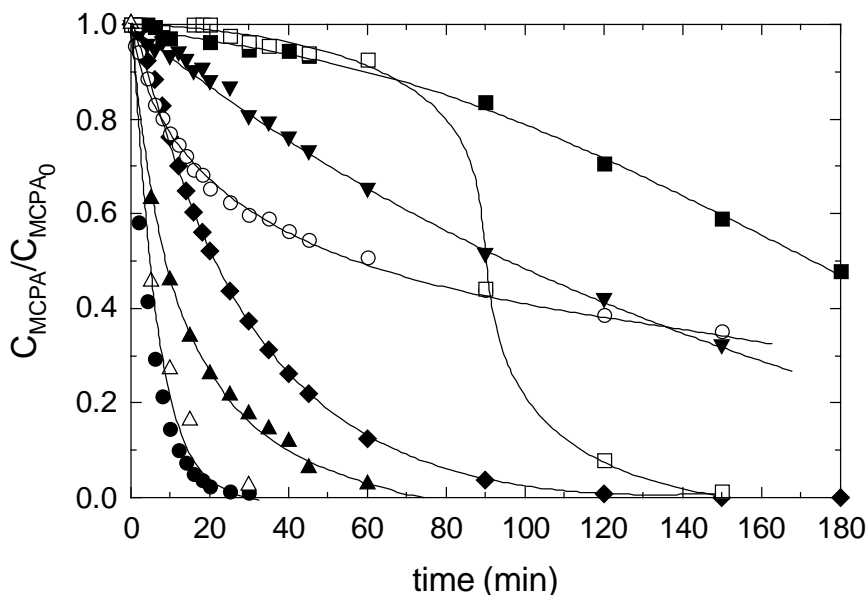
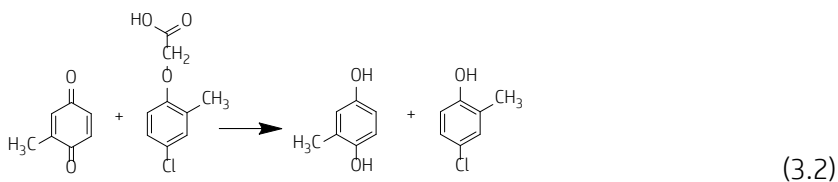
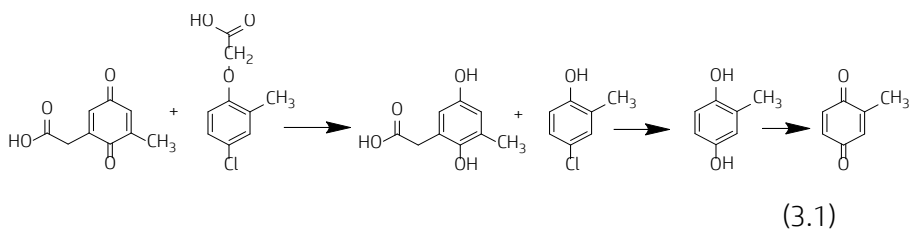


Figure 3.6 Photocatalysis of pure MCPA in the presence of Degussa P-25 (0.5 g L^{-1}). Influence of scavengers: ●, No scavenger; ■, 0.25 M TBA; ▲, 0.25 M 2-propanol; ▼, $3 \cdot 10^{-4}$ M KI; ◆, 10^{-3} M Oxalate; ○, 10^{-3} M p-benzoquinone; □, $2.5 \cdot 10^{-5}$ M Tiron, △, N₂ bubbling

Influence of free hydroxyl radicals scavengers

Tert-butyl alcohol (TBA) was chosen as a molecule capable of scavenging free radicals in solution with a low tendency to be absorbed onto titania particles [15]. The rate constant of free hydroxyl radicals and TBA is in the proximity of $6 \cdot 10^8 \text{ M}^{-1} \text{ s}^{-1}$. Accordingly, an experiment in the presence of 0.25 M in TBA was conducted. The results are plotted in Figure 3.6. From this figure, it can be inferred that free hydroxyl radicals in solution play an important role; however, even in the case of using an extremely high TBA concentration, MCPA removal was not totally prevented. As the reaction time increased, some MCPA conversion was experienced. Hence, it is hypothesized that MCPA can be degraded by other routes different from free HO[•] attack, leading to the formation of reactive intermediates (i.e. organic radicals or peroxyradicals, quinones, etc.), which can act as promoters of the chain reaction. In this way, Zertal et al. [16] report the significant role played by quinonic derivatives in MCPA photodegradation. These authors claim the occurrence of an auto-photocatalytic mechanism according to:



Similarly to TBA, the influence of 2-propanol was also tested in photocatalytic experiments. This alcohol can react with free and adsorbed HO[•] radicals and also with generated holes. As observed in Figure 3.6, the curve of MCPA degradation was altered in the presence of 0.25 M of 2-propanol. In this case, however, the influence was less pronounced than in the case of TBA. The rate constant between 2-propanol and HO[•] radicals is $2 \cdot 10^9 \text{ M}^{-1}\text{s}^{-1}$. These results are somehow contradictory. According to the rate constants between hydroxyl radicals and the two alcohols used, 2-propanol should deactivate MCPA degradation to a higher extent than TBA. Hence, 2-propanol could not quench the reaction to the same extent than TBA due to the formation of peroxy radicals (see reactions 3.3-3.5), suggesting the participation of the pair O₂^{•-}/HO₂[•] in MCPA degradation [17].



Additionally, the radicals C₃H₆OH[•] and C₃H₆OOOH[•] might also attack the MCPA molecule initiating an alternative route of MCPA degradation. In this sense, the reaction between C₃H₆OH[•] and 2-propanol has been given a value of $53 \text{ M}^{-1} \text{ s}^{-1}$ [18].

Influence of electron donors (hole reacting substances)

The effect of $3 \cdot 10^{-4} \text{ M}$ of KI was investigated in the photodegradation of MCPA. As inferred from Figure 3.6, potassium iodide significantly reduced the conversion rate of MCPA if compared to the control run. It has to be highlighted that the amount of KI used was sensibly lower than the

concentration of TBA, leading to comparable results. Iodide can react with holes; however, it can also be oxidized by free HO• radicals (rate constant $1.3 \cdot 10^{10} \text{ M}^{-1} \text{ s}^{-1}$), so the negative effect experienced cannot be associated with a unique scavenging effect.

Oxalate has been claimed to mainly react with photogenerated holes [19]. However, oxalate ions can also scavenge hydroxyl radicals with a lower rate constant ($7 \cdot 10^6 \text{ M}^{-1} \text{ s}^{-1}$) than KI. Accordingly, an experiment was carried out in the presence of 10^{-3} M in oxalate. The curve obtained suggests that MCPA is partially photodegraded by holes. The influence experienced is less pronounced than in the case of KI. According to these results, it can be hypothesized that HO• radicals play a more important role than holes in MCPA photocatalytic degradation.

Alternatively, hydroperoxyl radicals generated in oxalate photodegradation (Equations 3.6-3.7) might also contribute to MCPA conversion.



The possible reactivity of $\text{CO}_2^{\bullet-}$ with MCPA could also be considered. Hence, the reaction between the radical COOHCOO^{\bullet} and oxalate has been given a value of $2 \cdot 10^5 \text{ M}^{-1} \text{ s}^{-1}$ [20].

Influence of $^1\text{O}_2$ reacting substances

The addition of 0.01 M of NaN_3 to the reaction media completely deactivated the MCPA photodegradation process. NaN_3 is known to steadily react with singlet oxygen [21]; however, this compound can also react with hydroxyl radicals and holes. The azide ion reacts with HO• with a high rate constant value, $8 \cdot 10^{10} \text{ M}^{-1} \text{ s}^{-1}$ [22]. Accordingly, from the results obtained, no fundamental conclusions can be derived.

Influence of quinonic substances

To ascertain the occurrence of reactions similar to those presented in Equations 3.1-3.2, an additional reaction was carried out in the presence of 10^{-3} M in p-benzoquinone. The results indicate the deactivating nature of this species, capable of reacting with HO• radicals, peroxy and hydroperoxy radicals. According to the MCPA profile obtained, it seems that reactions of the type 3.1-3.2 do not occur.

Influence of HO₂[•]/O₂^{•-} scavengers

The potential role played by the pair HO₂[•]/O₂^{•-} has been postulated in previous sections. To assess the participation of these species, one experiment in the presence of a substance capable of scavenging the HO₂[•]/O₂^{•-} radicals has been conducted. Hence, when MCPA photocatalysis was carried out in the presence of 2.5 · 10⁻⁵ M in 1,3-benzenedisulfonic acid, 4,5-dihydroxy-disodium salt (Tiron), the process experienced an induction period of roughly 60 min. Thereafter, MCPA disappeared with a rate similar to the control run. Likely, after 60 min, Tiron has been removed from the media and afterwards MCPA is photodegraded. Unfortunately, this substance can also react with HO[•] radicals so the participation of the pair HO₂[•]/O₂^{•-} cannot be confirmed but only suggested.

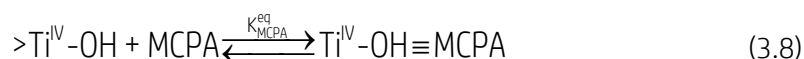
Influence of oxygen concentration

One more experiment was carried out by firstly purging the system with nitrogen and bubbling this gas throughout the experiment. Amazingly, it can be seen that oxygen had no influence at all. This fact was mechanistically confirmed in next section

3.3.5. The proposed mechanism

From the previous results and identification of some intermediates by direct comparison of retention time and standards, the following considerations can be assumed to tentatively propose a pseudoempirical model mechanism (see Figure 3.7).

The adsorption of contaminants onto the TiO₂ surface is normally a crucial stage in photocatalytic processes; however, in this study, adsorption of MCPA has not been detected to an appreciable extent in dark experiments (or, alternatively, adsorption is under the detection limit used in the analytical procedure). Some authors have reported the partial adsorption of MCPA onto Degussa P25. Hence, Zertal et al. [23] claim 20% of MCPA (5.6 · 10⁻⁴ M initial concentration) removal in dark experiments in the presence of 1 g L⁻¹ of P25. Considering a concentration of adsorption sites in the proximity of 4 · 10⁻⁵ M [24] and the initial concentration of MCPA used in this study (2.5 · 10⁻⁵ M), by using 0.5 g L⁻¹ of TiO₂ (6.25 · 10⁻³ M), only 2.5 · 10⁻⁷ M in MCPA could have been adsorbed, below the detection limit of the analytical procedure. In any case, an adsorption stage has been added to the model:



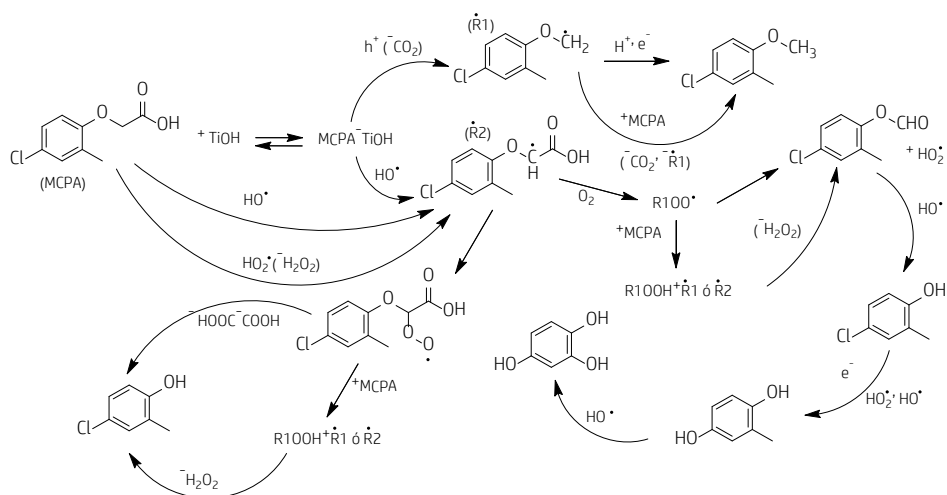


Figure 3.7 Proposed mechanism scheme

The value of the equilibrium constant is normally high and does not affect the kinetics of the process [25]. This is particularly applicable to molecules mainly degraded in the water bulk (as in this case). Noncompetitive oxygen adsorption was also considered. It is assumed that reduction sites ($>TiO_2^{RED}$) are different from oxidation sites ($>Ti^{IV}-OH$) [26]. The adsorption of O_2 ($\log K_{eq} O_2 = 4$) has been taken from the work of Feitz and Waite [27]. The number of oxygen molecules adsorbed ($TiO_2^{RED}=O_2$) at any time is constant, provided that oxygen is continuously fed.



The simultaneous presence of radiation and TiO_2 involves a series of well-assumed reactions in photochemistry. For instance, the initiation stage is the formation of holes and electrons:

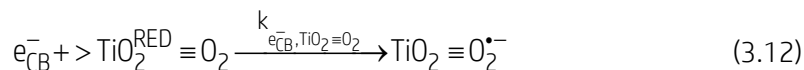


Generation of holes and electrons mainly depends on the lamps characteristics, catalyst nature and concentration. Theoretical calculations about the rate of holes/electrons generation and recombination can be conducted by computing the Local Volumetric Rate of Photon Absorption (LVRPA); however, this is out of the scope of this study and the formation rate of holes and electrons has been considered to be proportional to TiO_2 concentration and optimized according to experimental data:

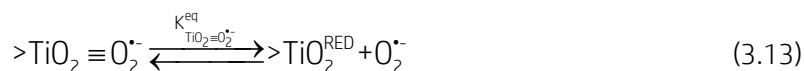
$$\frac{dC_{e_{CB}^-}}{dt} = \frac{dC_{h_{VB}^+}}{dt} = k'_{e_{CB}^-, h_{VB}^+} C_{TiO_2} \quad (3.11)$$

The parameter $k'_{e_{CB}^-, h_{VB}^+}$ is not a true constant and depends on the radiation intensity and catalyst loading [25].

Trapping of electrons by adsorbed oxygen has been considered with a rate constant of $7.6 \cdot 10^7 \text{ M}^{-1} \text{ s}^{-1}$ [28]:



The adsorbed peroxy radical can be desorbed according to the equilibrium with $\log \left(K_{TiO_2 \equiv O_2^{\bullet -}}^{eq} \right) = 4$ [27].



$O_2^{\bullet -}$ is in equilibrium with the hydroperoxyl radical $\log K_{HO_2^{\bullet -}}^{eq} = 4.8$:

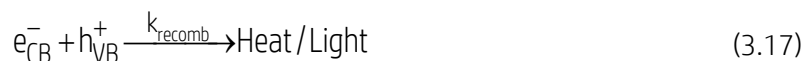


Radical-radical recombination can lead to hydrogen peroxide formation,

$k_{HO_2^{\bullet -}, O_2^{\bullet -}} = 9.7 \cdot 10^7 \text{ M}^{-1} \text{ s}^{-1}$ and $\log K_{H_2O_2}^{eq} = 11.7$:



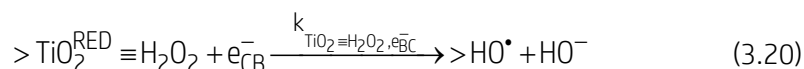
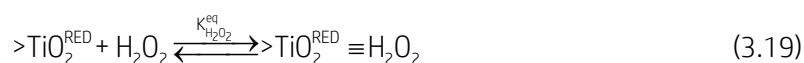
Hole-electron recombination ($k_{recomb} = 4.6 \cdot 10^{23} \text{ M}^{-1} \text{ s}^{-1}$) can proceed lowering the efficiency of the photocatalytic process:



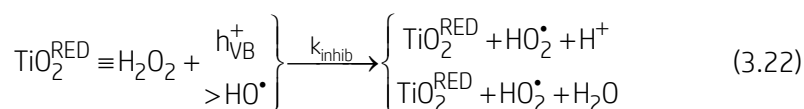
Holes can react with adsorbed water or hydroxide groups to generate hydroxyl radicals [29].



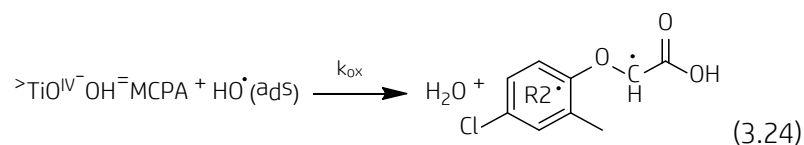
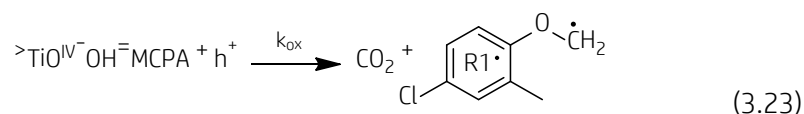
In equation 3.18, k_{HO^\bullet} is a lumped rate constant involving the invariability of the concentration of adsorbed water/ OH^- molecules. Davis and Huang [30] used a value of $2.0 \cdot 10^{12} \text{ M}^{-1}\text{s}^{-1}$ for this constant. When hydrogen peroxide is generated, trapping of e_{CB}^- by this species might occur [25]:



where $K_{H_2O_2}^{eq}$ has been given a value similar to $K_{O_2}^{eq}$ and $k_{TiO_2 \equiv H_2O_2, e_{CB}^-} = 1.1 \cdot 10^{10} \text{ M}^{-1}\text{s}^{-1}$ has been assumed to be similar to the reaction of aqueous electrons and hydrogen peroxide [31]. The scavenging effect of H_2O_2 is represented by:



The negative effect of TBA (this alcohol does not adsorb onto titania) in MCPA degradation suggests that the removal process of the parent compound mainly takes place in solution. Accordingly, once the initiating stages proceed, MCPA degradation can progress through the following steps. A small fraction of MCPA adsorbed onto TiO_2 can react with adsorbed HO^\bullet radicals or/alternatively directly oxidized by holes [23]:



The main oxidation pathway seems to be the oxidation with free HO^\bullet in solution:

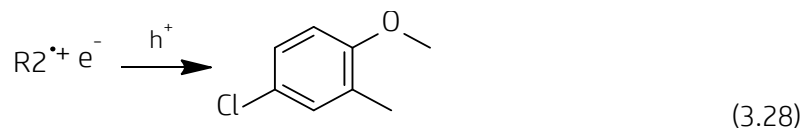


The value of $k_{\text{oxidation}} = 8.5 \cdot 10^9 \text{ M}^{-1} \text{ s}^{-1}$ [32] has been assumed to be similar for reactions 3.23-3.25. Radical species R1[•] and R2[•] can trap dissolved oxygen leading to:



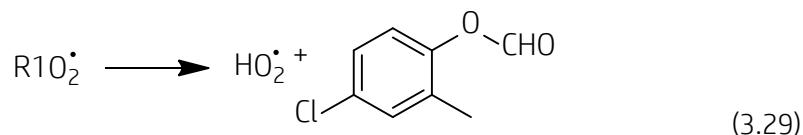
Rate constants corresponding to oxygen addition to organic radicals are in the order of $10^9 \text{ M}^{-1} \text{ s}^{-1}$ [33].

R2[•] can be reduced to generate 4-chloro-2-methylanisole:



Rate constant in equation 3.28 has been assumed to be of similar order than the reaction between hydrated electrons and anisole, $3 \cdot 10^5 \text{ M}^{-1} \text{ s}^{-1}$ [31].

The organic peroxyradical R1O₂[•] decomposes into 4-chloro-2-methylphenylformate, releasing one hydroperoxyl radical:

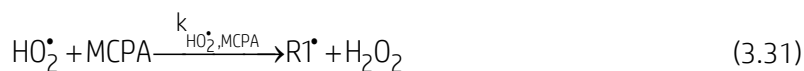


First-order decomposition of organic peroxy radicals varies in a wide range of values from some hundreds (or even lower figures) to values in the interval 10^5 - $10^6 \text{ M}^{-1} \text{ s}^{-1}$ [33]. An intermediate value of $10^3 \text{ M}^{-1} \text{ s}^{-1}$ has been used in this work. 4-chloro-2-methylphenylformate can be further oxidized by HO[•] radicals (or holes) to 4-chloro-2-methylphenol (main intermediate detected in the process). This stage has been given a generic rate constant of $5 \cdot 10^9 \text{ M}^{-1} \text{ s}^{-1}$.

As stated previously, the fact that TBA at high concentrations (0.25 M) cannot completely deactivate the MCPA degradation process suggests the existence of parallel routes of MCPA removal other than the direct attack of hydroxyl radicals. The autocatalytic behaviour observed has been attributed to reactions of organic peroxyradicals and MCPA:



No data are available for k_{Peroxyl} . Reactions of substituted alkylperoxyl radicals with several organic substrates were compiled by Neta et al. [33]. A generic value of $10^5 \text{ M}^{-1} \text{ s}^{-1}$ has been assumed. Also, MCPA is assumed to react with hydroperoxyl radicals to generate hydrogen peroxide ($k_{\text{Hydroperoxyl}} = 1 \cdot 10^5 \text{ M}^{-1} \text{ s}^{-1}$, assumed value). Pichat et al. [34] state the role played by $O_2^{\bullet -}/HO_2^{\bullet -}$ in photocatalytic processes.



Other routes of H_2O_2 generation include the first-order decomposition of organic peroxides:



Decomposition rates in equations 3.32-3.33 have been optimized to fit experimental and calculated results. 4-Chloro-2-methylphenol can further be oxidized by means of hydroxyl ($k_{\text{CMP-HO}^{\bullet}}$) and/or perhydroxyl ($k_{\text{CMP-HO}_2^{\bullet}}$) radicals leading to methylhydroquinone. The later can also be oxidized to 1,2,4-trihydroxybenzene. Finally, 4-chloro-2-methylanisole can also be oxidized to 4-chloro-2-methylphenol by hydroxyl radicals.

The set of differential equation derived from the previous reactions applied to a discontinuous batch reactor was numerically solved by the fourth-order Runge-Kutta method. Figure 3.8 (top) shows the results obtained after modelling the MCPA photocatalytic degradation in the presence of 0.5 g L^{-1} of Degussa P25. As observed, the model does an adequate job when simulating the evolution profile of the parent compound. Additionally, given the complexity of the system and the excessive number of unknown rate constants, the trends observed in H_2O_2 accumulation and 4-chloro-2-methylphenol generation are also acceptably calculated. It is obvious that the model is not complete and additional reactions leading to ring opening and low molecular weight compounds formation should be considered.

In spite of the system complexity, the proposed mechanism is also capable of simulating the effect of different scavengers. As observed in Figure 3.8

(bottom), the model adequately predicts the MCPA profiles after addition of 0.25 M of TBA or $3 \cdot 10^{-4}$ M of I⁻ by just considering their reactions with free hydroxyl radicals (rate constants $6 \cdot 10^8$ and $1.3 \cdot 10^{10} \text{ M}^{-1} \text{ s}^{-1}$, respectively).

When the addition of 2-propanol was modelled, reactions 3.3-3.5 led to a lineal MCPA degradation, different from the curved profile experimentally observed. However, if MCPA removal by organic radicals generated after HO[•] attack to 2-propanol is considered, the MCPA conversion acquires the observed curvature. A value of $20 \text{ M}^{-1} \text{ s}^{-1}$ given to this constant allows for obtaining the theoretical profile observed in Figure 3.8 (bottom). It should be noticed the similar magnitude of the adopted value and the rate constant corresponding to the reaction between C₃H₆OH[•] and 2-propanol.

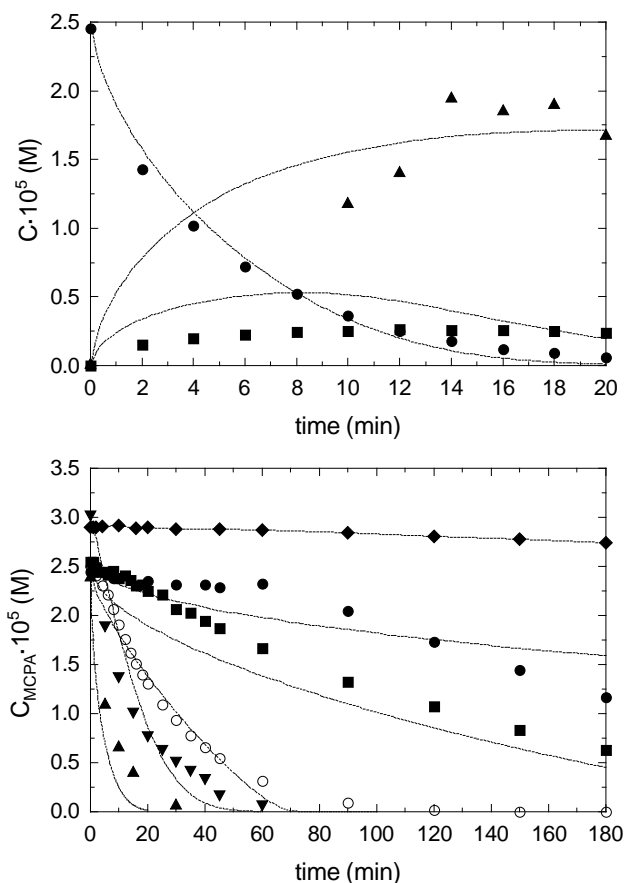


Figure 3.8 Modelling the photocatalysis of pure MCPA in the presence of Degussa P25 (0.5 g L^{-1}). **Top figure:** ●, MCPA evolution; ■, 4-chloro-2-methylphenol generation; ▲, H₂O₂ formation. **Bottom figure:** Experiment in the presence of: ●, 0.25 M TBA; ■, $3 \cdot 10^{-4}$ M KI; ▲, $2.5 \cdot 10^{-6}$ M O₂; ▼, 0.25 M 2-propanol; ◆, 0.01 M NaN₃; ○, 10^{-3} M Oxalate (Dashed lines = model calculations)

The total deactivation of the process in the presence of 0.01 M in sodium azide was theoretically obtained by just considering the reaction of this species with hydroxyl radicals.

The effect of oxalate was also adequately simulated by considering its degradation by direct attack of holes and further generation of hydroperoxyl radicals. Similar results could be obtained by taking into account the direct attack of $\text{CO}_2^{\cdot-}$ to MCPA.

Finally, theoretical calculations conducted at low oxygen concentration ($2.5 \cdot 10^{-6}$ M) could also acceptably simulate the results obtained in the experiment carried out by bubbling nitrogen (the reactor was open to the atmosphere, so oxygen concentration was not considered zero).

As stated previously, the mechanism here presented is not complete and probably lacks of some reactions. Accordingly, the optimized rate constants used should be taken with caution. Nevertheless, the reaction mechanism reveals the importance of HO^{\cdot} in MCPA photodegradation and also the presumably important role played by organic radicals and hydroperoxyl radicals. A sensitivity analysis of different parameters is shown in Figure 3.9.

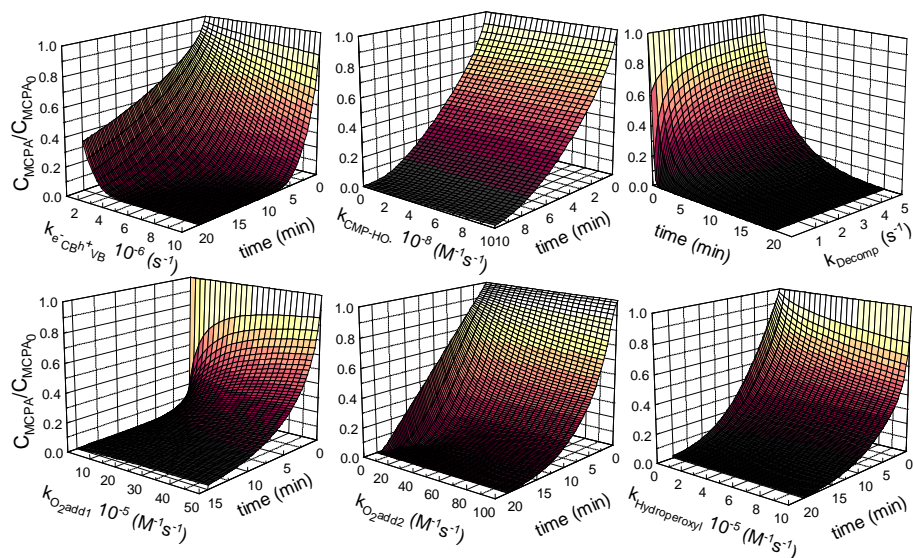


Figure 3.9 Sensitivity analyses of some of the rate constants in the proposed reaction mechanism

From Figure 3.9, it has to be highlighted the obvious influence of the holes/electrons generation rate. Oxygen addition to radicals R1^{\cdot} and R2^{\cdot} affects MCPA conversion profiles only for rate constant values well below the normal ones (10^8 - 10^9 $\text{M}^{-1}\text{s}^{-1}$). In a similar way, the rate constant in equation

3.29 only influences MCPA degradation when low values are used. The effect of $k_{\text{Hydroperoxyl}}$ confirms the hypothesis previously suggested of the role played by the pair $\text{HO}_2^*/\text{O}_2^{\cdot-}$.

3.4. CONCLUSIONS

From the experiments completed in this investigation, the following conclusions can be withdrawn:

- MCPA can be photocatalytically degraded in the presence of powdered titania.
- Doping of bare titania with nitrogen enhances the MCPA removal rate. An optimum in doping percentage can be foreseen.
- Calcination temperature at the time of catalyst preparation is a crucial variable.
- In spite of the high number of attempts, in no case the results obtained improve those obtained by using the commercial P25.
- A mechanistic approach to the process reveals the importance of free radicals in MCPA photocatalytic oxidation.
- Other minor degradation routes include the role played by organic and hydroperoxyl radicals.

Acknowledgments

This work has been supported by the *CICYT* of Spain (Project CTQ2012-35789-C02-01). Rafael Rodriguez Solis thanks the *Gobierno de Extremadura* and *FSE* Funds for the granted financial support.

REFERENCES

- [1] Environmental Protection Agency (2013) http://www.epa.gov/oppsrrd1/REDs/mcpa_red.pdf. Last accessed May 2013
- [2] Kuster M, López de Alda MJ, Barata C, Raldúa D, Barceló D, *Analysis of 17 polar to semi-polar pesticides in the Ebro river delta during the main growing season of rice by automated online solid-phase extraction-liquid chromatography-tandem mass spectrometry*. *Talanta* 75 (2008) 390-401
- [3] Kuster M, López de Alda MJ, Hernando MD, Petrovic M, Martín-Alonso J, Barceló D, *Analysis and occurrence of pharmaceuticals, estrogens,*

- progestogens and polar pesticides in sewage treatment plant effluents, river water and drinking water in the Llobregat river basin (Barcelona, Spain)*. J Hydrol 358 (2008) 112-123
- [4] Crespín MA, Gallego M, Valcárcel M, *Study of the degradation of the herbicides 2-4 D and MCPA at different depths in contaminated agricultural soil*. Environ Sci Technol 35 (2001) 4265-4270
- [5] Muñoz I, Rieradevall J, Torrades F, Peral J, Doménech X, *Environmental assessment of different solar driven advanced oxidation processes*. Sol Energy 79 (2005) 369-375
- [6] Senthilnathan J, Philip L, *Photocatalytic degradation of lindane under UV and visible light using N-doped TiO₂*. Chem Eng J 161 (2010) 83-92
- [7] Veréb G, Manczinger L, Bozsó G, Sienkiewicz A, Forró L, Mogyorósi K, Hernádi K, Dombi A, *Comparison of the photocatalytic efficiencies of bare and doped rutile and anatase TiO₂ photocatalysts under visible light for phenol degradation and E coli inactivation*. App Catal B: Environ 129 (2013) 566-574
- [8] Dozzi MV, Selli E, *Doping TiO₂ with p-block elements: effects on photocatalytic activity*. J Photochem Photobiol C Photochem Rev 14 (2013) 13-28
- [9] Irie H, Watanabe Y, Hashimoto K, *Nitrogen concentration dependence on photocatalytic activity of TiO_{2-x}N_x powders*. J Phys Chem B 107 (2003) 5483-5486
- [10] Fu HB, Zhang LW, Zhang SC, Zhu YF, Zhao JC, *Electron spin resonance spin-trapping detection of radical intermediates in N-doped TiO₂-assisted photodegradation of 4-chlorophenol*. J Phys Chem B 110 (2006) 3061-3065
- [11] Chen X, Burda C, *Photoelectron spectroscopic investigation of nitrogen-doped titania nanoparticles*. J Phys Chem B 108 (2004) 15446-15449
- [12] Saha NC, Tomkins HC, *Titanium nitride oxidation chemistry: an X-ray photoelectron spectroscopy study*. J Appl Phys 72 (1992) 3072-3079
- [13] Sun Q, Xu Y, *Evaluating intrinsic photocatalytic activities of anatase and rutile TiO₂ for organic degradation in water*. J Phys Chem C 114 (2010) 18911-18918
- [14] Gong XQ, Selloni A, *Reactivity of anatase TiO₂ nanoparticles: the role of the minority (001) surface*. J Phys Chem B 109 (2005) 19560-19562

- [15] Klauson D, Portjanskaja E, Preis S, *Visible light-assisted photocatalytic oxidation of organic pollutants using nitrogendoped titania*. Environ Chem Lett 6 (2008) 35-39
- [16] Zertal A, Sehili T, Boule P, *Photochemical behaviour of 4-chloro-2-methylphenoxyacetic acid: influence of pH and irradiation wavelength*. J Photochem Photobiol A Chem 146 (2001) 37-48
- [17] Bielski BHJ, Cabelli DE, Arudi RL, Ross AB, *Reactivity of HO₂/O₂[•] radicals in aqueous solutions*. J Phys Chem Ref Data 14 (1985) 1041-1100
- [18] Burchill CE, Ginns IS, *Radiation induced oxidation of 2-propanol by hydrogen peroxide in aqueous solution*. Can J Chem 48 (1970) 1232-1238
- [19] Waldner G, Gómez R, Neumann-Spallart M, *Using photoelectrochemical measurements for distinguishing between direct and indirect hole transfer processes on anatase: case of oxalic acid*. Electrochim Acta 52 (2007) 2634-2639
- [20] Ershov BG, Janata E, Alam MS, Gordeev AV, *Studies of the reaction of the hydroxyl radical with the oxalate ion in an acidic aqueous solution by pulse radiolysis*. Russ Chem Bull Int Ed 57 (2008) 1187-1189
- [21] Xu Z, Jing C, Li F, Meng X, *Mechanisms of photocatalytical degradation of monomethylarsenic and dimethylarsenic acids using nanocrystalline titanium dioxide*. Environ Sci Technol 42 (2008) 2349-2354
- [22] Shinohara K, Shida T, Saito N, *Radiation decomposition of aqueous azide solution*. J Chem Phys 37 (1962) 173-178
- [23] Zertal A, Molnár-Gábor D, Malouki MA, Sehili T, Boule P, *Photocatalytic transformation of 4-chloro-2-methylphenoxyacetic acid (MCPA) on several kinds of TiO₂*. App Catal B: Environ 49 (2004) 83-89
- [24] Feitz AJ, Waite TD, Jones GJ, Boyden BH, Orr PT, *Photocatalytic degradation of the blue green algal toxin microcystin-Lr in a natural organic-aqueous matrix*. Environ Sci Technol 33 (1999) 243-249
- [25] Gimeno O, Carbajo M, López MJ, Melero JA, Beltrán F, Rivas FJ *Photocatalytic promoted oxidation of phenolic mixtures: an insight into the operating and mechanistic aspects*. Water Res 41 (2007) 4672-4684
- [26] Minero C, *A rigorous kinetic approach to model primary oxidative steps of photocatalytic degradations*. Sol Energ Mat Sol C 38 (1995) 421-430
- [27] Feitz AJ, Waite TD, *Kinetic modelling of TiO₂ catalyzed photodegradation of trace levels of microcystin-LR*. Environ Sci Technol 37 (2003) 561-568

- [28] Bahnemann DW (1999), Photocatalytic detoxification of polluted waters. In: Boule P (ed) Environmental photochemistry, Springer, Berlin
- [29] Almquist CB, Biswas P, *A mechanistic approach to modeling the effect of dissolved oxygen in photo-oxidation reactions on titanium dioxide in aqueous system*. Chem Eng Sci 56 (2001) 3421-3430
- [30] Davis AP, Huang CP, *A kinetic model describing photocatalytic oxidation using illuminated semiconductors*. Chemosphere 26 (1993) 1119-1135
- [31] Buxton GV, Greenstock CL, Helman WP, Ross AB, *Critical review of rate constants for reactions of hydrated electrons, hydrogen atoms and hydroxyl radicals in aqueous solution*. J Phys Chem Ref Data 17 (1988) 513-886
- [32] Zona R, Solar S, Sehested K, *OH-radical induced degradation of 2,4,5-trichlorophenoxyacetic acid (2,4,5-T) and 4-chloro-2-methylphenoxyacetic acid (MCPA): a pulse radiolysis and gamma-radiolysis study*. Rad Phys Chem 81 (2012) 152-159
- [33] Neta P, Huie R, Ross AB, *Rate constants for reactions of peroxy radicals in fluid solutions*. J Phys Chem Ref Data 19 (1990) 413-513
- [34] Pichat P, Guillard Ch, Amalric L, Renard A, Plaidy O, *Assessment of the importance of the role of H_2O_2 and $O_2^{\bullet-}$ in the photocatalytic degradation of 1,2 dimethoxybenzene*. Sol Energ Mat Sol C 38 (1995) 391-399

CHAPTER FOUR

PAPER TWO

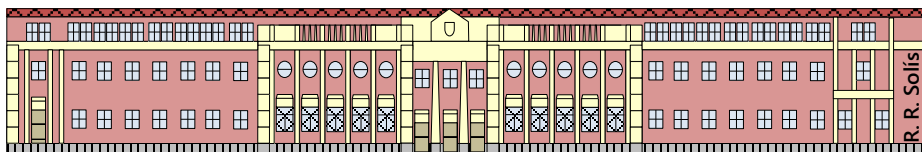
Photocatalytic ozonation of 4-chloro-2-methylphenoxyacetic acid and its reaction intermediate 4-chloro-2-methyl phenol

J Taiwan Inst Chem Eng 46 (2015) 125-131

R. R. Solís, F.J. Rivas, J.L. Pérez-Bote, O. Gimeno

ABSTRACT. Aqueous 4-chloro-2-methylphenoxyacetic acid (MCPA) has been treated by the systems UVA/TiO₂/N₂, O₃, TiO₂/O₃, UVA/O₃, UVA/TiO₂/O₂, and UVA/TiO₂/O₃. Under the conditions investigated (T=20°C, pH=4.5, Q_{gas}=30 L h⁻¹, V=1 L, C_{O₃}=5 mg L⁻¹, C_{MCPA}=5 mg L⁻¹, C_{TiO₂}=0.5 g L⁻¹), MCPA is removed in less than 30 min. Photocatalytic ozonation is the most efficient process both in terms of MCPA removal rate (100% conversion in less than 15 min) and mineralization extent (60% after 3 h and 25°C). 4-chloro-2-methyl phenol (CMP) is detected in those systems combining TiO₂ and UVA radiation. The presence of ozone involves the complete depletion of CMP following its generation. The direct rate constant between CMP and ozone corroborates the high reactivity observed (7.2±0.3 10⁴ M⁻¹s⁻¹, 4.4±0.2 10⁵ M⁻¹s⁻¹, and 2.9±0.7 10⁶ M⁻¹s⁻¹ at pHs 4, 7 and 10, respectively). Identified intermediates detected in the UVA/TiO₂/O₃ applied to MCPA correspond to oxygenated species derived from the parent compound after loss of some substitution groups. No significant toxicity of intermediates is observed in BOD₅, *Daphnia parvula*, and *Culex pipiens larvae* tests.

KEYWORDS: MCPA, photocatalytic ozonation, 4-chloro-2-methyl phenol, kinetics, herbicides



I.E.S. Zurbarán, Badajoz

4.1. INTRODUCTION

4-Chloro-2-methylphenoxyacetic acid (MCPA) is a widely used herbicide of the chlorophenoxy type family. Phenoxy herbicides act by simulating the action of natural hormones to produce uncoordinated plant growth. Their action is selective as they are toxic to dicotyledonous plants. The acid is the parent compound, but a number of formulations in use contain the more water soluble amine salts or the ester derivatives, which are readily dissolved in an organic solvent. Regulatory agencies in their evaluations of these two constituents have found MCPA unlikely to be human carcinogen; however, a number of epidemiologic studies have found positive associations between exposure to chlorophenoxy compounds and an increased risk of some lymphohematopoietic cancers, primarily non-Hodgkins lymphoma, but also Hodgkin's disease, soft tissue sarcoma, and to a lesser extent, leukemia [1].

MCPA can be easily degraded in aqueous solution by means of TiO_2 mediated photocatalysis in the presence of UVA or visible light [2,3]. MCPA photocatalysis leads to the complete removal of the parent compound in a relatively short period of time; however, the herbicide is not completely mineralized and some inter-mediate accumulate in the reaction media [4]. 4-Chloro-2-methyl phenol (CMP) is the main intermediate that accumulates in the MCPA photocatalytic process. CMP is generated from MCPA by direct photolysis and $\cdot\text{OH}/h^+$ reaction (higher CMP yield). CMP is more toxic than the parent compound [5]. Accordingly, water treatment technologies dealing with MCPA removal should take into consideration the evolution of this byproduct. The accumulation of CMP in the Degussa P25 mediated photocatalysis has been previously experienced [6].

In the present study, the photocatalytic ozonation of MCPA is investigated and compared to other systems such as single ozonation, photolytic ozonation, catalytic ozonation and photocatalysis. Use of ozone in photocatalytic processes shows some advantages if compared to the system in the absence of ozone, namely the presence of an additional oxidant (O_3) reacting with organic molecules by direct or indirect ($\cdot\text{OH}$) pathways, additional generation of free radicals by ozone photolytic scission, potential catalytic ozone decomposition by the TiO_2 surface, etc. [7].

Photocatalytic ozonation has normally been applied by using UV-C radiation, few works have applied cheap black light lamps (UVA radiation), [8,9]. Additionally, the number of studies focused on the photocatalytic ozonation of pesticides is also limited. Some works can be listed. Rajeswari and Kanmani [10] combined UVA radiation and ozone in the presence of

titanium dioxide and carbaryl as model pollutant. Under their experimental conditions, 76.5% of total organic carbon (TOC) removal and increase of the five day biological oxygen demand-chemical oxygen demand ratio (BOD_5/COD) were reported. Farré and co-workers [11,12] conducted a preliminary chemical treatment of pentachlorophenol, isoproturon, diuron, alachlor and atrazine pesticides in aqueous solutions analyzing the toxicity of the effluent after the treatment. Beduk and collaborators [13] carried out the photocatalytic ozonation in the presence of UV-C radiation of the organophosphorus pesticides malathion and parathion. Cernigoj and co-workers [14,15] also studied the photocatalytic ozonation of thiacloprid and neonicotinoid insecticides.

In this work the influence of pH, photocatalyst and MCPA initial concentration has been assessed in the UVA/ TiO_2/O_3 system. Additionally, the response of CMP toward the studied technologies has also been investigated. Toxicity tests have completed the work.

4.2. EXPERIMENTAL

4.2.1. Photoreactor and procedure

A 1 L capacity perfectly mixed borosilicate glass photoreactor was used in all the experiments. The reactor was placed in the middle of a 31 cm external diameter pipe (54 cm height). The internal wall of the pipe was covered by aluminum foil to increase the photons reflection toward the reaction media. Four black light lamps (41 cm length) were evenly distributed and attached to the pipe. The lamps (LAMP15TBL HQPOWER™ manufactured by Velleman®) had a nominal power of 15 W mainly emitting within the range 350-400 nm, the maximum being located at 365 nm. Actinometry experiments in the presence of ferryoalate led to a value of $6.86 \cdot 10^{-5}$ Einstein $L^{-1} \text{ min}^{-1}$ when 4 lamps were used.

Previously to the photodegradation experiments, the mixture water + photocatalyst was stirred for 60 min in the dark to achieve the MCPA adsorption equilibrium on the photocatalyst surface. Oxygen or a mixture oxygen-ozone was continuously bubbled into the water bulk by means of a diffuser placed at the reactor bottom. The gas flow rate was kept constant at 30 L h^{-1} in all the experiments. Photocatalysts were maintained in suspension by magnetic stirring. Prior to the analysis, the solid was removed from samples by filtration through Millex-HA filters (Millipore, $0.45 \mu\text{m}$).

Ozone was produced from pure oxygen by using a Sander Laboratory Ozone Generator. Dissolved ozone in solution was determined by the indigo

method, the analysis is based on the decoloration of the 5,5,7-indigotrisulfonate [16]. Ozone in the gas phase was monitored by means of an Anseros Ozomat ozone analyser. The analysis was based on the absorbance at 254 nm. All experiments were conducted at the natural pH of the solutions, with no addition of buffering substances.

4.2.2. Materials

Pure MCPA from Aldrich (>99%) was used in different experiments, the rest of chemicals were purchased from Sigma-Aldrich and used as received (acetaminophen >99%, CMP 97%, phosphoric acid 85%). Organic solvents were HPLC grade obtained from Panreac. Commercial TiO_2 Degussa P25 photocatalyst (70% anatase and 30% rutile) was used with an average particle size of 30 nm and BET surface area of $50 \text{ m}^2 \text{ g}^{-1}$. Water purified by a Milli-Q water system (Millipore®) was used in the preparation of solutions and suspensions.

4.2.3. Analysis

MCPA and CMP were analyzed by high-performance liquid chromatography (Agilent 1100). The column used was a Kromasil 100 5C18. The mobile phase acetonitrile:water:phosphoric acid (40:54:6) was pumped at a flow rate of 1 mL min^{-1} . Detection was conducted at 230 nm. In the case of acetaminophen, the reference compound in rate constant determination experiments, the mobile phase was changed to acetonitrile:water:phosphoric acid (18:76.5:8.5), and detection was conducted at 244 nm. Byproducts were tentatively identified by HPLC coupled to mass spectrometry. The detector was a quadrupole-time-of-flight mass spectrometer (Agilent Technologies 6520, Accurate-Mass Q-TOF LC/MS) equipped with a dual ESI electrospray interface. The analytical operating conditions were as follows: capillary 3500 V; nebulizer, 30 psi; gas flow, 5 L min^{-1} ; gas temperature 300°C ; skimmer voltage, 65 V; octapole rf, 750 V; fragmentor, 100 V. The mass spectra were processed by means of the Agilent Mass Hunter Qualitative Analysis B.04.00 software.

In order to assess the degree of mineralization, total organic carbon was determined by a Shimadzu TOC 5000A analyzer by directly injecting the aqueous solution. The pH of the reaction media was measured by means of a Radiometer Copenhagen pH meter. pH adjustment was carried out by addition of NaOH or perchloric acid. Biological oxygen demand after five days determination was conducted by the respirometric method, based on the absorption of the CO_2 generated in the microbial metabolism by solid NaOH.

4.2.4. Ecotoxicity bioassays with *Daphnia parvula* and *Culex pipiens larvae*

The acute toxicity tests using *Daphnia parvula* were conducted using US EPA standard operating procedures [17]. This procedure was extrapolated to carry out similar trials with mosquito *Culex pipiens* larvae. A culture for *D. parvula* or *C. pipiens* larvae was received from installations of Extremadura's University, where organisms were naturally cultured in artificial ponds.

20 young *D. parvula* or 15 second instar *C. pipiens* larvae were placed in 100 mL of test solution using a disposable plastic transfer pipette, and were subjected to 16:8 light:dark photoperiods at room temperature. Survival numbers were recorded and monitored at 6, 24 and 48 h for *D. parvula*; 24, 46, 72 and 96 h for *C. pipiens*. Organisms were not fed during the experiments. In ecotoxicity tests, commercial MCPA (MCPA 60% from KENO-GARD®) or CMP solutions were prepared in mineral water (10.7 mg L⁻¹ HCO₃⁻, 5.3 mg L⁻¹ SO₄²⁻, 19.0 mg L⁻¹ Cl⁻, 2.7 mg L⁻¹ Ca²⁺, 2.7 mg L⁻¹ Mg²⁺, 14.7 mg L⁻¹ Na⁺, and 14.3 mg L⁻¹ SiO₂). pH was adjusted to 7±0.1. Three blank tests, without MCPA or CMP addition, were considered per each run.

Initially trials were carried out at various parent compound initial concentrations in order to determine the concentration which causes the 50% mortality (LC₅₀). Organisms were exposed to nine concentrations (1000, 500, 250, 125, 62.5, 31.2, 15.6, 7.8, and 3.9 mg L⁻¹ of MCPA; or 10, 5, 2.5, 1.25, 0.62, 0.31, 0.15, 0.08 and 0.04 mg L⁻¹ for CMP). After this preliminary study, samples from photocatalytic ozonation experiments at different stages of oxidation extent (0, 25, 50, 75, 100% of initial MCPA removal) were taken. An additional sample was also considered when TOC removal reached the steady state level.

4.3. RESULTS AND DISCUSSION

4.3.1. Preliminary experiments: Technologies comparison

4-Chloro-2-methylphenoxyacetic acid oxidation

Some preliminary experiments were initially carried out to compare the performance of individual systems derived from the UVA/TiO₂/O₃ technology. Figure 4.1 shows the results obtained in terms of MCPA normalized degradation and TOC conversion when an aqueous solution of the herbicide was treated by means of UVA/TiO₂/N₂, O₃, TiO₂/O₃, UVA/O₃, UVA/TiO₂/O₂, and UVA/TiO₂/O₃.

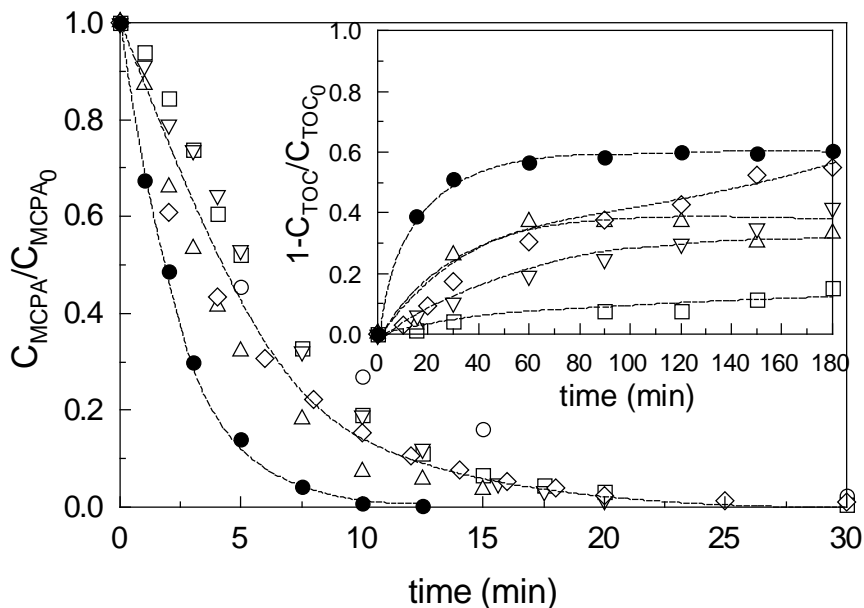


Figure 4.1 Removal of MCPA and TOC conversion by different systems. Experimental conditions: $T=298\text{ K}$, $\text{pH}=4.5$, $Q_{\text{gas}}=30\text{ L h}^{-1}$, $V=1\text{ L}$, $C_{\text{O}_3}=5\text{ mg L}^{-1}$, $C_{\text{MCPA}}=5\text{ mg L}^{-1}$, $C_{\text{TiO}_2}=0.5\text{ g L}^{-1}$. \circ , UVA/TiO₂/N₂; \square , O₃; \triangle , TiO₂/O₃; ∇ , UVA/O₃; \diamond , UVA/TiO₂/O₂; \bullet , UVA/TiO₂/O₃.

From Figure 4.1 it can be observed that, under the operating conditions investigated, MCPA (5 mg L^{-1}) quickly disappears in less than 20-25 min regardless of the oxidizing system used. Roughly, all the technologies used present a similar efficiency with the exception, perhaps, of the photocatalytic ozonation, capable of reducing the time to completely oxidize MCPA to 12-14 min. However, different patterns were experienced when TOC conversion was monitored. In this latter case, single MCPA ozonation only achieved a scarce 15% in TOC conversion after 180 min of treatment. The combination of ozone with either TiO₂ or UVA light increased the final TOC removal to values close to 30-35%. TiO₂ can act as a catalyst in ozonolysis reactions by accelerating the ozone decomposition into radical species. Alternatively, oxidation reactions can take place on the solid surface decreasing the activation energy of the ozonolysis [18-21]. The positive effect of the pair ozone-UVA may be attributed to the photoactivity of ozonation intermediates that would accumulate in the absence of the radiation.

The photocatalysis in the presence of ozone (UVA/TiO₂/O₃) or oxygen (UVA/TiO₂/O₂) led to a TOC conversion in the proximity of 60%, however this

high value was reached by the UVA/TiO₂/O₃ system in just 60 min, compared to >180 min required by the UVA/TiO₂/O₂ system. Roughly 40% of the initial TOC content remains in solution after 3 h of treatment. As occurring in most oxidation processes, accumulation of low weight oxygenated species (carboxylic acids, aldehydes, ketones, etc.) from the recalcitrant TOC remaining in solution.

The synergistic effect experienced when using the UVA/TiO₂/O₃ system is the result of a higher inhibition of electron-hole recombination, the catalytic effect of TiO₂ in the presence of ozone, and the high photoactivity of ozone intermediates.

CMP was only detected in those systems combining UVA radiation and titanium dioxide (no matter the presence or absence of ozone). As stated previously, CMP is generated from direct photolysis or •OH attack to MCPA, suggesting that the systems O₃ and/or O₃/TiO₂ proceed through a mechanism different from hydroxyl radical formation (i.e. direct ozone attack). In this sense, Benoit-Guyod and co-workers [22] report two distinct ozonolysis pathways in the presence and absence of UV radiation: ring-hydroxylation and cleavage by molecular ozone in the dark, and side-chain oxidation by hydroxyl radicals under irradiation. Alternatively, CMP could have been generated and instantaneously removed, as a consequence CMP presence could not be detected. Since CMP is the main intermediate detected in the MCPA photocatalytic ozonation (the most efficient system), the response of this compound to the oxidizing agents used in this work was also assessed.

4-Chloro-2-methyl phenol oxidation

Figure 4.2 shows the normalized CMP removal after application of different oxidizing systems. From this figure the fact that the UVA/TiO₂/O₂ process is the less effective technology is inferred, hence, the accumulation of this compound in the MCPA photocatalysis system is corroborated. However, when ozone is used, CMP is completely eliminated in less than 10 min regardless of the simultaneous application of UVA radiation or UVA+TiO₂. Similarly to MCPA degradation, in terms of TOC conversion, Degussa P25 did show some catalytic effect in the ozonation process if compared to the single ozone application.

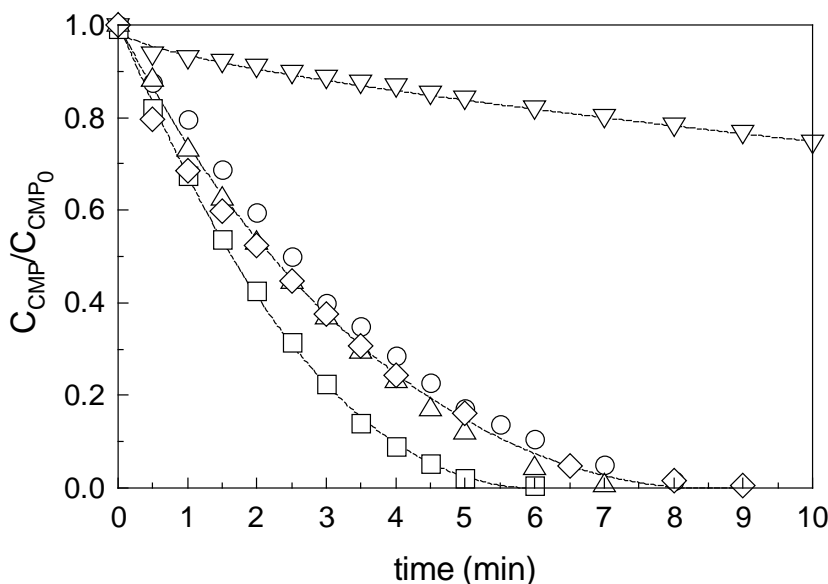


Figure 4.2 Removal of 4-chloro-2-methyl phenol by different systems. Experimental conditions: $T=298$ K, $pH=5.0$, $Q_{gas}=30$ L h^{-1} , $V=1$ L, $C_{O_3}=5$ mg L^{-1} , $C_{CMP}=5$ mg L^{-1} , $C_{TiO_2}=0.5$ g L^{-1} . \circ , O_3 ; \square , TiO_2/O_3 ; \triangle , UVA/O_3 ; ∇ , $UVA/TiO_2/O_3$; \diamond , $UVA/TiO_2/O_3$.

The potential of ozone to oxidize CMP was corroborated by calculating the second order rate constant corresponding to the direct reaction between molecular ozone and CMP. Accordingly, three series of ozonation experiments in a homogeneous and semicontinuous mode, in the presence of 0.01 M of *tert*-butanol (radical scavenger), were completed. The method consists in the continuous pumping of an ozone saturated solution to a tank containing CMP and a reference compound whose ozonation rate constant is previously known [21]. The mass balance equations describing the system are:

$$\left. \begin{aligned} V \frac{dC_T}{dt} + C_T \frac{dV}{dt} &= -z_T V k_{O_3, T} C_{O_3} C_T \\ V \frac{dC_R}{dt} + C_R \frac{dV}{dt} &= -z_R V k_{O_3, R} C_{O_3} C_R \\ \frac{dV}{dt} &= Q \end{aligned} \right\} \quad (4.1)$$

In the above equations, Q , is the ozone saturated solution flow-rate, V is the reaction volume, C is concentration, z , the stoichiometric coefficient, and the subscripts T and R refer to target and reference compounds, respectively.

To eliminate the unknown C_{O_3} concentration, if the reference and target compound mass balances are divided, after integration it follows:

$$\ln \frac{VC_T}{VC_T|_{t=0}} = \frac{z_T k_{O_3,T}}{z_R k_{O_3,R}} \ln \frac{VC_R}{VC_R|_{t=0}} \quad (4.2)$$

A plot of the left hand side of equation 4.2 versus $\ln (VC_R/VC_R|_{t=0})$ should lead to a straight line of slope $(z_T/z_R)(k_{O_3,T}/k_{O_3,R})$. By assuming a stoichiometric coefficient of one mol of ozone per mol of organic and acetaminophen as the reference compound [23], the rate constants of CMP-O₃ ($k_{O_3,CMP}$) at pHs 4, 7 and 10 were $7.2 \pm 0.3 \cdot 10^4 \text{ M}^{-1}\text{s}^{-1}$, $4.4 \pm 0.2 \cdot 10^5 \text{ M}^{-1}\text{s}^{-1}$, and $2.9 \pm 0.7 \cdot 10^6 \text{ M}^{-1}\text{s}^{-1}$, respectively (results not shown).

These values corroborate the high reactivity of ozone and CMP experimentally observed in this study. Also the variation of the rate constant with pH indicates the higher reactivity of the anionic form of CMP if compared to the neutral or protonated forms. The pK_a value from the neutral to the anionic form of CMP is 9.7 while no data is available on the pK_a value for the protonation, in any case protonation of phenols usually shows pK_a values in the proximity of 6.

In order to compare the direct ozonolysis of CMP versus the reaction with hydroxyl radicals, the second order rate constant of the latter was calculated by means of the hydrogen peroxide photolysis in the presence of CMP. Thus by using the method reported by Beltrán and co-workers [24], the calculated values of $k_{HO\cdot, MCPA}$ and $k_{HO\cdot, CMP}$ were $4.3 \cdot 10^9 \text{ M}^{-1}\text{s}^{-1}$ and $7.8 \cdot 10^9 \text{ M}^{-1}\text{s}^{-1}$. Typical $HO\cdot$ concentrations in advanced oxidation systems range in the interval 10^{-13} - 10^{-14} M suggesting that the following inequality applies ($k_{HO\cdot, CMP} C_{HO\cdot} \ll k_{O_3, CMP} C_{O_3}$).

4.3.2. The system UVA/TiO₂/O₃. Operating variables effect

Given the higher efficiency in TOC removal of the MCPA photocatalytic ozonation if compared to the rest of technologies studied, the former system was investigated in more detail. Accordingly, the influence of some operating variables was investigated, namely TiO₂ concentration, MCPA initial concentration and pH.

Catalyst concentration

TiO₂ concentration was tested in the range 0.01 to 1.5 g L⁻¹. Figure 4.3 shows the results obtained. As a rule of thumb, no significant differences were found in terms of MCPA degradation rate regardless of the amount of catalyst

used. The experiment conducted with 1.0 g L^{-1} of TiO_2 seems to proceed slightly faster than the rest, indicating the existence of an optimum in photocatalyst concentration, typical of photocatalytic processes, however differences are not statistically significant.

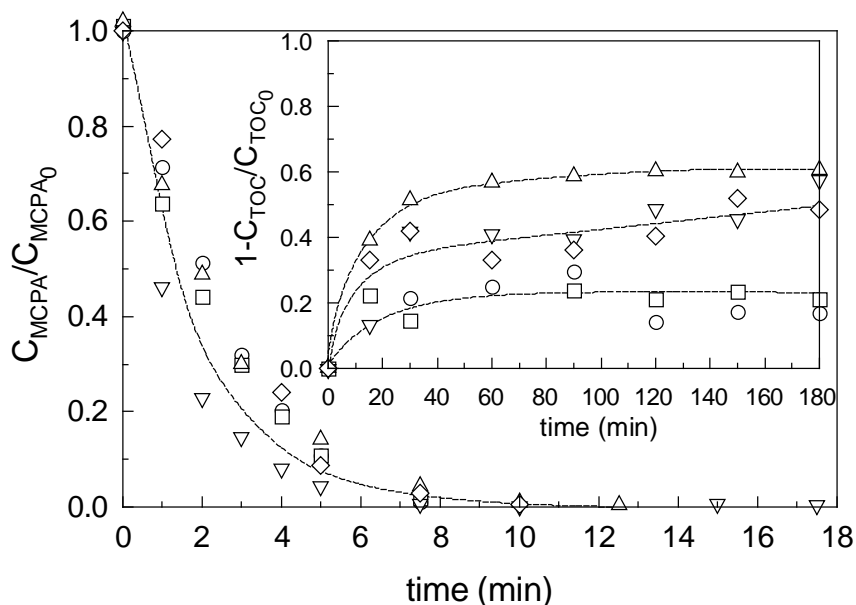


Figure 4.3 Removal of MCPA and TOC conversion in the UVA/ TiO_2 / O_3 system. Experimental conditions: $T=298 \text{ K}$, $\text{pH}=4.5$, $Q_{\text{gas}}=30 \text{ L h}^{-1}$, $V=1 \text{ L}$, $C_{\text{O}_3}=5 \text{ mg L}^{-1}$, $C_{\text{MCPA}}=5 \text{ mg L}^{-1}$, C_{TiO_2} (g L^{-1}): \circ , 0.01; \square , 0.1; \triangle , 0.5; ∇ , 1.0; \diamond , 1.5.

Differences in TOC conversion are more significant. Hence, TOC elimination is substantially lower in experiments conducted with the lowest TiO_2 amount, achieving removal degrees in the proximity of 20% when 0.01 and 0.1 g L^{-1} of catalyst were used. TOC elimination percentage increased to 50–60% in the rest of experiments. TiO_2 positive effect is undoubtedly related to its capacity to catalyze the ozonolysis process and its crucial role in the photocatalysis due to the formation of electron-hole pairs. The evolution of CMP is depicted in Figure 4.4. As inferred from this figure, the evolution of this intermediate is highly influenced by TiO_2 concentration. Broadly speaking, TiO_2 concentration exerts a positive influence in CMP generation. The presence of high amounts of TiO_2 promotes the photocatalytic process in detriment of the direct ozonation. This effect involves the formation of CMP which is apparently associated to the TiO_2 /UVA system. In all cases, the simultaneous application of ozone leads to a Gaussian profile of CMP concentration, being this compound removed from the reaction media in roughly 10 min.

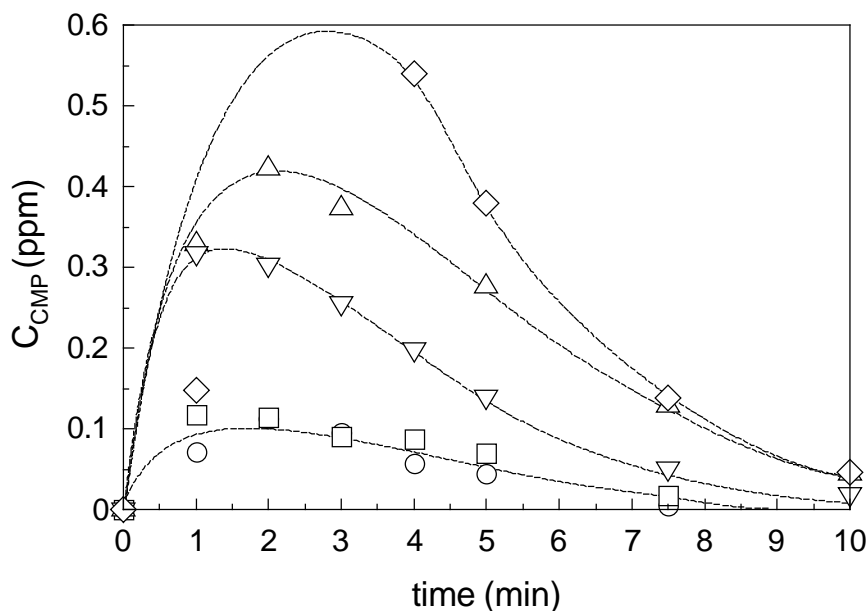


Figure 4.4 Evolution of 4-chloro-2-methyl phenol in the UVA/TiO₂/O₃ system applied to MCPA. Experimental conditions: T=298 K, pH=4.5, Q_{gas}=30 L h⁻¹, V=1 L, C_{O3}=5 mg L⁻¹, C_{MCPA}=5 mg L⁻¹, C_{TiO2} (g L⁻¹): ○, 0.01; □, 0.1; △, 0.5; ▽, 1.0; ◇, 1.5.

MCPA concentration

MCPA initial concentration was tested within the range 1.5–50 mg L⁻¹. Figure 4.5 shows the results obtained in terms of MCPA removal and TOC conversion. As expected, decay profiles are steep in those runs with low initial MCPA concentration. The slope is less pronounced in the run carried out with 50 mg L⁻¹ of MCPA. However, in terms of MCPA removal rate the trend is the opposite, thus, the higher the initial MCPA concentration the higher its elimination rate. An experiment was conducted at 35 °C showing the positive effect of this parameter, particularly in terms of mineralization extent after 180 min. Thus, TOC profiles indicate a lower conversion (35–40%) in the experiment completed with the lowest MCPA concentration than in the rest of runs. Conversion values of 50–60% are experienced when MCPA initial concentration is above 5 mg L⁻¹. This experimental fact suggests a partial autocatalytic behavior in terms of TOC removal. The maximum TOC conversion (90%) was achieved at the highest temperature tested. Temperature likely accelerates the reactions of organic radicals substantiating the hypothesis of the autocatalytic pathway in terms of mineralization.

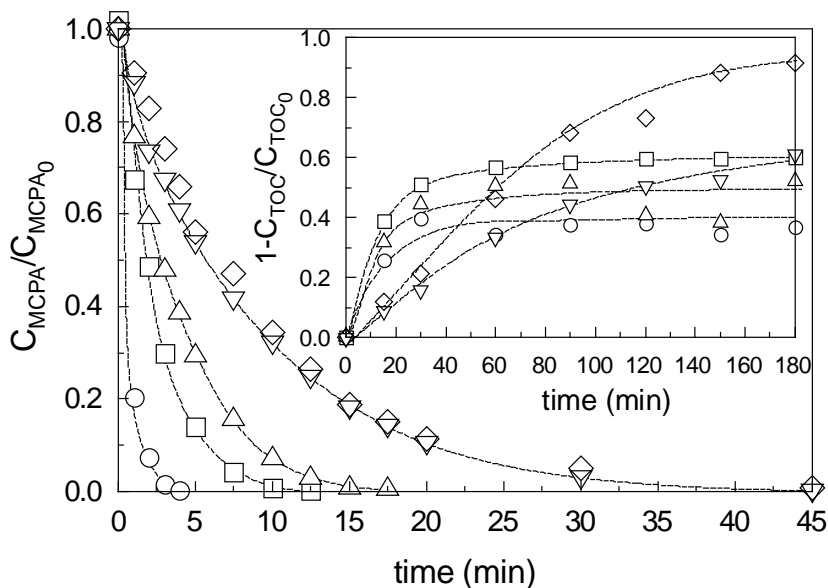


Figure 4.5 Removal of MCPA and TOC conversion in the UVA/TiO₂/O₃ system. Experimental conditions: T=298 K, pH=4.5 (average value), Q_{gas}=30 L h⁻¹, V=1 L, C_{O3}=5 mg L⁻¹, C_{TiO2}=0.5 g L⁻¹, C_{MCPA} (mg L⁻¹): ○, 1.5; □, 5; △, 11; ▽, 50; ◇, 50 (35 °C).

Figure 4.6 illustrates the evolution of CMP. As expected the higher the initial MCPA concentration, the higher the amount of CMP generated. Also, temperature exerted a significant effect in CMP generation.

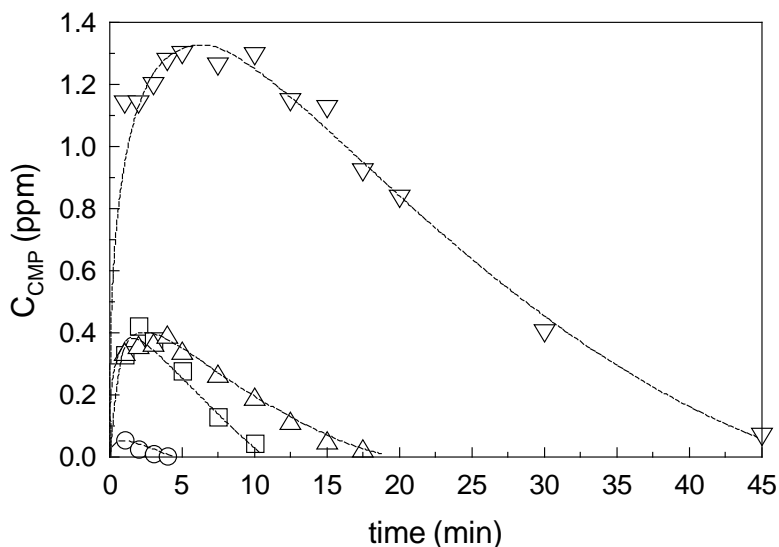


Figure 4.6 Evolution of 4-chloro-2-methyl phenol in the UVA/TiO₂/O₃ system applied to MCPA. Experimental conditions: T=293 K, pH=4.5, Q_{gas}=30 L h⁻¹, V=1 L, C_{O3}=5 mg L⁻¹, C_{TiO2}=0.5 g L⁻¹, C_{MCPA} (mg L⁻¹): ○, 1.5; □, 5; △, 11; ▽, 50; ◇, 50 (35 °C).

pH influence

Finally, pH was tested under acidic (pH=2), natural (pH=5), neutral (pH=7) and basic (pH=12) conditions (results not shown). pH did not appreciably affect MCPA removal rate, however CMP profiles were severely influenced by this parameter. Thus, when pH was initially varied by NaOH or HClO₄ addition, the amount of CMP generated was drastically reduced, with no significant CMP formation/detection at pHs 7 and 12. Similarly, variations in the initial pH also reduced the final TOC conversion after 180 min from 60% (no pH variation) to 20% (pHs 7 and 2). The worst results were obtained at pH 12 with no observable TOC reduction.

4.3.3. Detected intermediates and toxicity

Different samples of the MCPA photocatalytic ozonation were analyzed by mass spectrometry. Some positively identified intermediates are shown in Table 4.1.

Table 4.1 Transformation products tentatively identified in MCPA photocatalytic ozonation at low conversion values

Mass	Proposed formula	Ion m/z	Proposed structures
114	C ₄ H ₂ O ₄	112.9769	3-hydroxyl-2,5-furandione 2,3-dioxosuccinaldehyde
142	C ₇ H ₇ ClO	140.9989	4-chloro-2-methyl phenol (CMP)
200	C ₉ H ₉ ClO ₃	198.9978	MCPA
160	C ₇ H ₉ ClO ₂	158.9245	4-chloro-6-methyl-3,5-cyclohexadiene-1,2-diol 5-chloro-2-cyclohexene-1-carboxylic acid
196	C ₈ H ₄ O ₆	194.9704	2,5-dicarboxy-1,4-benzoquinone
158	C ₇ H ₇ ClO ₂	156.9920	4-chloro-2-(hydroxymethyl)phenol 5-chloro-3-methylbenzene-1,2-diol 3-chloro-2,5-cyclohexadiene-1-carboxylic acid
196	C ₆ H ₉ ClO ₅	195.0118	(2E)-2-chloro-2,3-dideoxyhex-2-enonic acid dimethyl 2-chloro-3-hydroxybutanedioate
126	C ₆ H ₆ O ₃	125.1081	4-hydroxycatechol
125	C ₇ H ₈ O ₂	123.9865	methyl hydroquinone

Identified intermediates are mainly oxygenated species derived from the parent compound after losing some of the substitution groups. In some cases the ring may have been opened leading to aliphatic oxygenated chains as it is the case of 2,3-dioxosuccinaldehyde. Not many works have dealt with subproducts in the photocatalytic ozonation of MCPA. Zertal and collaborators [4] report the formation of 4-chloro-2-methylphenol, methylhydro-quinone and 5-chloro-2-hydroxy-3-methylphenylacetic acid in photocatalytic

experiments in the presence of TiO_2 . The first two substances were also identified in this work. Topalov and co-workers [25] proposed the formation of 4-chloro-2-methylphenol in a similar process, further oxidation of this species would easily lead to the formation of 4-chloro-2-(hydroxymethyl)phenol or 5-chloro-3-methylbenzene-1,2-diol tentatively detected in this research. Benoit Guyod and co-authors [22] claim the formation of 4-chloro-2-methylphenyl formate, 4-chloro-salicylaldehyde, 4-chlorosalicylic acid and 5-chloro-3-methylbenzene-1,2-diol monomethyl ether in the photolytic ozonation of MCPA. None of them were found in the samples analyzed in this work.

Toxicity of the intermediates generated during the photocatalytic ozonation of MCPA was assessed by measuring the BOD_5 of the reacted solutions after 10 and 180 min of reaction. Nutrients were added to water samples according to the recipe given in the literature [26,28]. As seen in Figure 4.7, neither MCPA nor the intermediates showed any appreciable toxic effect toward the activated sludge used in the BOD analysis, even when a high MCPA initial concentration was applied.

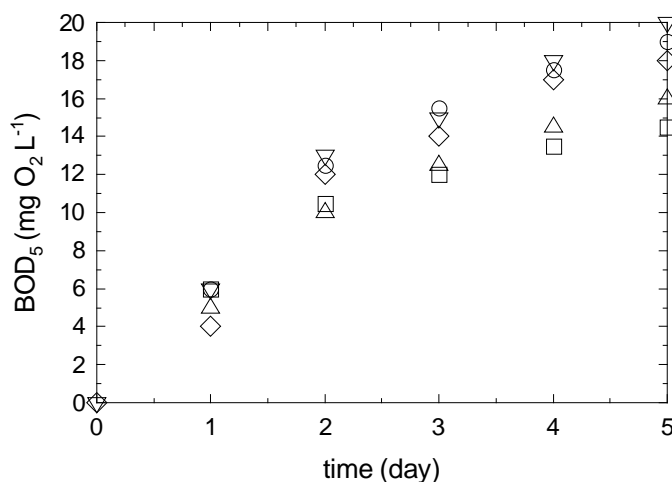


Figure 4.7 Evolution of BOD_5 after $\text{UVA}/\text{TiO}_2/\text{O}_3$ applied to MCPA. Experimental conditions: $T=293\text{ K}$, $\text{pH}=4.5$, $Q_{\text{gas}}=30\text{ L h}^{-1}$, $V=1\text{ L}$, $C_{\text{O}_3}=5\text{ mg L}^{-1}$, $C_{\text{TiO}_2}=0.5\text{ g L}^{-1}$. ○, Control run; □, 1.0 mg L^{-1} of initial MCPA, time reaction=0 min; △, 5.0 mg L^{-1} of initial MCPA, time reaction=0 min; ▽, 5.0 mg L^{-1} of initial MCPA, time reaction=10 min; ◇, 5.0 mg L^{-1} of initial MCPA, time reaction=180 min.

Additional toxicity tests were carried out by using two species, *D. parvula* and larvae of *C. pipiens* (common mosquito). For comparison purposes, some preliminary ecotoxicity assays were completed with the parent compounds

MCPA (commercial) and CMP at different concentrations. These tests are shown in Figure 4.8. Survival percentage was corrected to account for natural mortality in control runs by means of the expressions [29]:

$$\% \text{ corrected mortality} = \frac{\% \text{MWC} - \% \text{CM}}{100 - \% \text{CM}} 100 \quad (4.3)$$

$$\% \text{ corrected survival} = 100 - \% \text{ corrected mortality} \quad (4.4)$$

In equation 4.3, MWC and CM stand for mortality without correction and control mortality (mortality in blank runs), respectively. Figure 4.8 reveals that the intermediate CMP is more toxic than the parent compound MCPA. *D. parvula* LC₅₀ values corresponding to MCPA at 6, 24, and 48 h are approximately 717, 266 and 230 mg/L, in accordance with the data provided by the supplier (LC₅₀ to *D. magna* at 48 h >190 mg L⁻¹) while *D. parvula* LC₅₀ values corresponding to CMP at 6, 24, and 48 h are roughly 9.0, 6.5 and 1.5 mg L⁻¹. These differences in toxicity were also experienced when *C. pipiens* were used. In this latter case, MCPA and CMP showed values of 206 and 150 mg L⁻¹ (MCPA) and 1.5 and 0.5 mg L⁻¹ (CMP) after 72 and 96 h of larvae exposure, respectively.

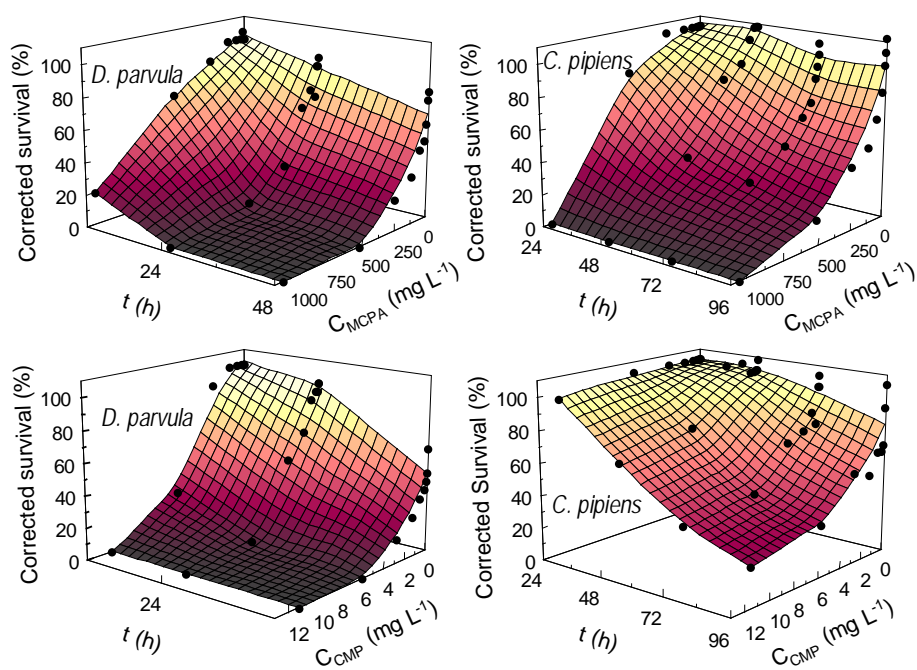


Figure 4.8 Percentage of survival of *D. parvula* and *C. pipiens* larvae as function of MCPA or CMP concentration and time of exposure.

The goal to be achieved is the application of the photocatalytic ozonation to remove MCPA without generating an effluent more toxic than the initial herbicide solution. Accordingly, a number of samples were withdrawn from the reactor at different oxidation times and the toxicity analyzed. Figure 4.9 illustrates the results obtained.

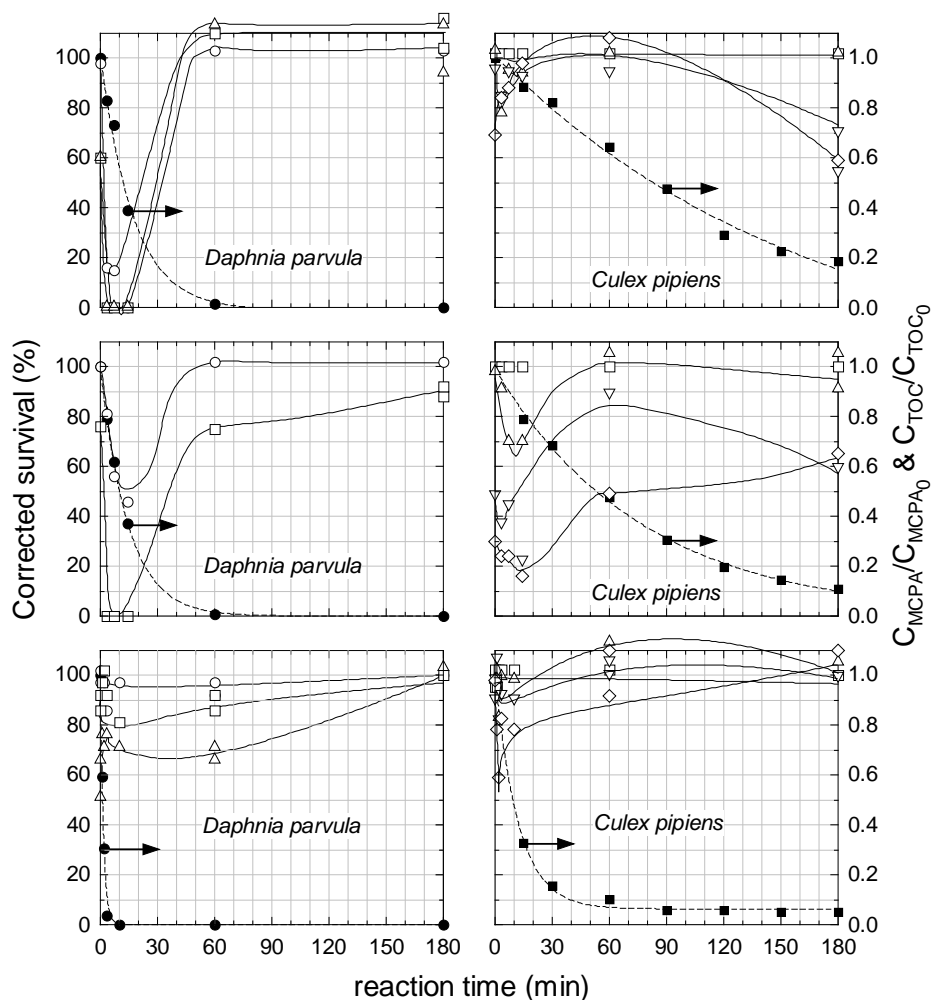


Figure 4.9 Percentage of survival of *D. parvula* and *C. pipiens* larvae in solutions of photocatalytic ozonated MCPA at different reaction periods. Initial MCPA concentration (mg L^{-1}): top figure=100; middle figure=50; bottom figure=5. Time of exposure (h): \circ , 6; \square , 24; \triangle , 48; ∇ , 72; \diamond , 96. (\bullet , MCPA removal; \blacksquare , TOC removal).

In the case of *D. parvula*, a clear relationship between toxicity and MCPA abatement is inferred. For instance, when analyzing the experiment completed with an initial MCPA of 100 mg L^{-1} , the oxidized solution goes through a period when mortality increases to values of 100% regardless of

the exposure time. Once MCPA is completely eliminated, the solution becomes non-toxic. Similar results were obtained when 50 mg L⁻¹ of MCPA were oxidized. The most diluted MCPA concentration barely showed a small increase in toxicity in the first 30 min of photocatalytic ozonation. Thereafter, *D. parvula* survival increased to values close to 100%.

In the case of *C. pipiens*, patterns are similar to those obtained when *D. parvula* was used. The experiment conducted with 5 mg L⁻¹ does not present appreciable toxicity after 5-10 min of treatment (100% MCPA conversion). When high MCPA concentrations were used, mortality significantly reduced to values close to zero when MCPA was removed from solution (60 min); however, 72 and 96 h samples slightly reduced the survival percentage when the ozonation process was extended to 180 min. Increasing the reaction period to 180 min involves the generation of low weight carboxylic acids and release of free chlorine. Likely the accumulation of these species affects the survival of the larvae.

In any case, as a rule of thumb, after the oxidation, all samples showed toxicity values lower than the initial nontreated MCPA solution.

4.4. CONCLUSIONS

- MCPA is easily degraded by single ozonation or any combination of light, ozone and TiO₂.
- The photocatalytic ozonation leads to a significant mineralization of the initial TOC content at acceptable rates.
- TOC removal in TiO₂/O₃/UVA is significantly increased when working at 35°C instead of 25°C.
- The main intermediate generated in the photocatalytic ozonation of MCPA is 4-chloro-2-methyl phenol which is steadily removed from the media due to its high reactivity with ozone.
- TiO₂ concentration does not affect MCPA removal rate. TOC conversion is dependent on the amount of solid used. An optimum at 0.5 g L⁻¹ was found under the experimental conditions investigated.
- End products accumulated after the photocatalytic ozonation present toxicity values toward *D. parvula* and *C. pipiens* larvae below the values obtained for the un-treated MCPA solutions.

Acknowledgments

This work has been supported by the *CICYT* of Spain (Project CTQ2012-35789-C02-01). Mr. Rafael Rodríguez Solís thanks the *Gobierno de Extremadura, Consejería de Empleo, Empresa e Innovación* and *FSE Funds* for his Ph.D. grant (PD12058).

REFERENCES

- [1] Von Stackelberg K. *A systematic review of carcinogenic outcomes and potential mechanisms from exposure to 2,4-D and MCPA in the environment.* J Toxicol (2013) art. no. 371610
- [2] Djebbar K, Zertal A, Sehili T, *Photocatalytic degradation of 2,4-dichlorophenoxyacetic acid and 4-chloro-2-methylphenoxyacetic acid in water by using TiO₂.* Environ Technol 27 (2006) 1192-1197
- [3] Šojić DV, Despotović VN, Abazović ND, Čomor MI, Abramović BF, *Photocatalytic degradation of selected herbicides in aqueous suspensions of doped titania under visible light irradiation.* J Hazard Mater 179 (2010) 49-56
- [4] Zertal A, Sehili T, Boule P. *Photochemical behavior of 4-chloro-2-methylphenoxyacetic acid: influence of pH and irradiation wavelength.* J Photochem Photobiol A: Chem 146 (2001) 37-48
- [5] De Laurentiis E, Minella M, Bodrato M, Maurino V, Minero C, Vione D, *Modelling the photochemical generation kinetics of 2-methyl-4-chlorophenol, an intermediate of the herbicide MCPA (2-methyl-4-chlorophenoxyacetic acid).* Surf Aquat Ecosyst Health Manage 16 (2013) 216-221
- [6] Rivas FJ, Solís RR, Gimeno O, Beltrán F. *MCPA photocatalytic degradation by bare and N doped titania.* In: Proceedings of the third European symposium on photocatalysis. Slovenia: University of Nova Gorica (2013)
- [7] Mena E, Rey A, Acedo B, Beltrán FJ, Malato S, *On ozone-photocatalysis synergism in black-light induced reactions: oxidizing species production in photo-catalytic ozonation versus heterogeneous photocatalysis.* Chem Eng J 204-206 (2012) 131-140
- [8] Encinas A, Rivas FJ, Beltrán FJ, Oropesa A, *Combination of black-light photo-catalysis and ozonation for emerging contaminants degradation in secondary effluents.* Chem Eng Technol 36 (2013) 492-499

- [9] Beltrán FJ, Aguinaco A, Rey A, García-Araya JF, *Kinetic studies on black light photocatalytic ozonation of diclofenac and sulfamethoxazole in water*. Ind Eng Chem Res 51 (2012) 4533-4544
- [10] Rajeswari R, Kanmani S, *A study on synergistic effect of photocatalytic ozonation for carbaryl degradation*. Desalination 242 (2009) 277-85
- [11] Farré MJ, Franch MI, Ayllón JA, Peral J, Domènech X, *Biodegradability of treated aqueous solutions of biorecalcitrant pesticides by means of photocatalytic ozonation*. Desalination 211 (2007) 22-33
- [12] Farré MJ, Franch MI, Malato S, Ayllón JA, Peral J, Domènech X, *Degradation of some biorecalcitrant pesticides by homogeneous and heterogeneous photo-catalytic ozonation*. Chemosphere 58 (2005) 1127-1133
- [13] Beduk F, Aydin ME, Ozcan S, *Degradation of malathion and parathion by ozonation, photolytic ozonation, and heterogeneous catalytic ozonation processes*. Clean Soil Air Water 40 (2012) 179-187
- [14] Cernigoj U, Lavrencic Stangar U, Jirkovsky J, *Effect of dissolved ozone or ferric ions on photodegradation of thiacloprid in presence of different TiO₂ catalysts*. J Hazard Mater 177 (2010) 399-406
- [15] Cernigoj U, Lavrencic Stangar U, Trebse P, *Degradation of neonicotinoid insecticides by different advanced oxidation processes and studying the effect of ozone on TiO₂ photocatalysis*. Appl Catal B: Environ 75 (2007) 229-238
- [16] Bader H, Hoigné J, *Determination of ozone in water by the indigo method*. Water Res 15 (1981) 449-456
- [17] EPA, *Methods for measuring the acute toxicity of effluents and receiving water to freshwater and marine organisms*. 5th ed. Washington DC, EPA (2002)
- [18] Hsu CF, Chen HW, Wu YY, Li YX, Huang WJ, *Enhanced oxidation of microcystins using TiO₂-O₃: kinetics and mutagenic assay*. Sep Purif Technol 103 (2013) 101-108
- [19] Rosal R, Gonzalo MS, Rodríguez A, García-Calvo E, *Ozonation of clofibric acid catalyzed by titanium dioxide*. J Hazard Mater 169 (2009) 411-418
- [20] Molnar JJ, Agbaba JR, Dalmacija BD, Klačnja MT, Dalmacija MB, Kragulj MM, *A comparative study of the effects of ozonation and TiO₂-catalyzed ozonation on the selected chlorine disinfection by-product precursor content and structure*. Sci Total Environ 425 (2012) 169-75

- [21] He Z, Cai Q, Hong F, Jiang Z, Chen J, Song S, *Effective enhancement of the degradation of oxalic acid by catalytic ozonation with TiO_2 by exposure of {001} facets and surface fluorination*. *Ind Eng Chem Res* 51 (2012) 5662-5668
- [22] Benoit-Guyod JL, Crosby DG, Bowers JB, *Degradation of MCPA by ozone and light*. *Water Res* 20 (1986) 67-72
- [23] Rivas FJ, Sagasti J, Encinas A, Gimeno O, *Contaminants abatement by ozone in secondary effluents. Evaluation of second-order rate constants*. *J Chem Technol Biotechnol* 86 (2011) 1058-1066
- [24] Beltrán FJ, Ovejero G, Rivas FJ, *Oxidation of polynuclear aromatic hydrocarbons in water. 3. UV radiation combined with hydrogen peroxide*. *Ind Eng Chem Res* 35 (1996) 883-890
- [25] Topalov A, Abramović B, Molnár-Gábor D, Csaná di J, Arcson O, *Photocatalytic oxidation of the herbicide (4-chloro-2-methylphenoxy)acetic acid (MCPA) over TiO_2* . *J Photochem Photobiol A: Chem* 140 (2001) 249-253
- [26] Seo GT, Suzuki T, Ohgaki S, *Biological powdered activated carbon (BPAC) microfiltration for wastewater reclamation and reuse*. *Desalination* 106 (1996) 39-45
- [27] Zhang R, Vigneswaran S, Ngo H, Nguyen H, *A submerged membrane hybrid system coupled with magnetic ion exchange (MIEX1) and flocculation in wastewater treatment*. *Desalination* 216 (2007) 325-333
- [28] Erdei L, Arecrachakul N, Vigneswaran S, *A combined photocatalytic slurry reactor-immersed membrane module system for advanced wastewater treatment*. *Sep Purif Technol* 62 (2008) 382-388
- [29] Abbott WS, *A method of computing the effectiveness of an insecticide*. *J Econ Entomol* 18 (1925) 265-267

CHAPTER FIVE

PAPER THREE

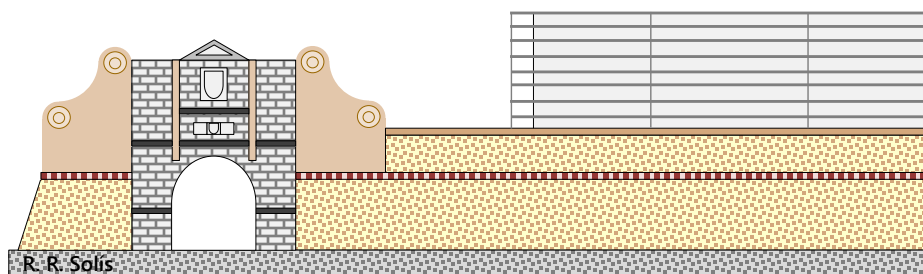
Photocatalytic ozonation of clopyralid, picloram and triclopyr. Kinetics, toxicity and influence of operational parameters

J Chem Technol & Biotechnol 91 (2016) 51-58

Rafael R. Solís, F. Javier Rivas, Olga Gimeno, José Luis Pérez-Bote

ABSTRACT. BACKGROUND. Photolysis, photocatalysis, ozonation and photocatalytic ozonation in the presence of titania have been applied to the elimination of three pyridine carboxylic acids herbicides (clopyralid, picloram and triclopyr) in water. RESULTS. Photocatalytic ozonation led to the best results in terms of herbicide elimination rate and mineralization. The herbicides were relatively recalcitrant to direct ozonation (rate constants: $20 \text{ M}^{-1} \text{ min}^{-1}$ for clopyralid and triclopyr, and $105 \text{ M}^{-1} \text{ min}^{-1}$ in the case of picloram). Herbicides degradation proceeds by hydroxyl radicals attack (rate constants: 0.73 , 3.80 and $1.73 \cdot 10^9 \text{ M}^{-1} \text{ s}^{-1}$ for clopyralid, picloram and triclopyr, respectively). Monitoring of chloride and nitrates suggests dechlorination as the primary stage in the process. Further ring opening led to the accumulation of nitrates and the appearance of some low weight carboxylic acids. Toxicity decreased at the end of the process. CONCLUSION. Tested herbicides slowly react with ozone. Photocatalytic ozonation shows different degrees of synergism; leading to 80% mineralization in less than 1 h. Small amounts of TiO_2 (i.e. 5 mg L^{-1}) maintain the efficiency of the photocatalytic ozonation. Quantitative free chloride and nitrates rapidly appear in the $\text{O}_3/\text{UVA}/\text{TiO}_2$ system. First intermediates in the photocatalytic ozonation of clopyralid show higher toxicity than the parent compound.

KEYWORDS: clopyralid, picloram, triclopyr, photocatalysis, photocatalytic ozonation, titania



Puerta del Pilar, Badajoz

5.1. INTRODUCTION

Picloram (4-amino-3,5,6-trichloro-2-pyridinecarboxylic acid), clopyralid (3,6-dichloro-2-pyridinecarboxylic acid) and triclopyr (3,5,6-trichloro-2-pyridinyloxyacetic acid) are three chlorinated pyridine selective herbicides used for control of broadleaf weeds.

The principal environmental risks of these herbicides relate to contamination of surface and ground water, and damage to non-target terrestrial plants including crops adjacent to areas of application via runoff or drift. Such damage to plants may also emanate from more distant areas where ground water is used for irrigation or is discharged into surface water. Non-target plants adjacent to areas of application may be exposed to concentrations many times the levels that have been associated with toxic effects. In addition, the US Environmental Protection Agency (EPA) has concerns related to endangered terrestrial mammals and endangered aquatic animals. These herbicides are highly soluble in water, resistant to biotic and abiotic degradation processes, and mobile under both laboratory and field conditions.

Clopyralid is an herbicide that has recently been reported to occur in drinking water at concentrations above the permitted concentration value (PCV) for an individual pesticide (EU directive 98/83/EC) [1]. Triclopyr acid is persistent, and is mobile. The predominant degradation pathway for triclopyr in water is photodegradation [2]. EPA is concerned about the potential chronic toxicity and persistence of the triclopyr degradate, 3,5,6-trichloro-2-pyridinol, in the aquatic environment and is requiring additional confirmatory data to better characterize the fate of this metabolite. Picloram is highly soluble in water, resistant to biotic and abiotic degradation processes, and mobile under both laboratory and field conditions. It is stable to hydrolysis and anaerobic degradation, and degrades very slowly with half-lives ranging from 167 to 513 days [3]. EPA is concerned about degradation of water quality in picloram use areas. Eventual contamination of ground water is virtually certain in areas where picloram residues persist in the overlying soil. Once in ground water, picloram is unlikely to degrade, even over a period of several years. Picloram also has a high potential to contaminate surface water by runoff from use areas.

Herbicides maximum concentration values for long-term runoff and peak runoff water contamination scenarios have been reported to be in the proximity of 0.11 and 1.2 mg L⁻¹, 2.3 and 13 µg L⁻¹, for clopyralid and triclopyr, respectively. Higher values have also been reported in accidental spillages [4].

In this work, several advanced oxidation systems have been applied to remove these pesticides from water. Among them, special emphasis has been paid to photocatalytic ozonation in the presence of TiO_2 . This powerful process is capable of combining the positive effect of three simpler processes (ozonation, photocatalysis and catalytic ozonation) leading to a global synergistic effect, especially significant when analyzing the mineralization extent.

Unreported data on ozone and hydroxyl radical reactions of tested herbicides are given in this work. Additionally, toxicity evolution is investigated when photocatalytic ozonation is applied.

5.2. EXPERIMENTAL

5.2.1. Photoreactor and procedure

A 1 L capacity perfectly mixed borosilicate glass photoreactor was used in all the experiments with the exception of those using UVC light. The reactor was placed in the middle of a 31 cm external diameter pipe (54 cm height). The internal wall of the pipe was covered by aluminium foil to increase photons reflection towards the reaction media. Four black light lamps (41 cm length) were evenly distributed and attached to the pipe. The lamps (LAMP15TBL HQPOWER™ manufactured by Velleman®) had a nominal power of 15 W mainly emitting within the range 350-400 nm, the maximum being located at 365 nm. Actinometry experiments in the presence of ferryoalate led to a value of $6.86 \cdot 10^{-5}$ Einstein $\text{L}^{-1} \text{min}^{-1}$ when four lamps were used.

Oxygen, nitrogen or a mixture of oxygen-ozone was continuously bubbled into the water by means of a diffuser placed at the reactor bottom. The gas flow rate was kept constant at 30 L h^{-1} in all the experiments. Photocatalysts were maintained in suspension by magnetic stirring. Previously to the photodegradation experiments, the mixture water-photocatalyst, was stirred for 30 min in the dark to achieve herbicide adsorption equilibrium on the photocatalyst surface. Before the analysis, the solid was removed from samples by filtration through Millex-HA filters (Millipore, $0.45 \mu\text{m}$). Thiosulfate was used to quench the reaction.

Ozone was produced from pure oxygen using a Sander Laboratory Ozone Generator. Ozone in the gas phase was monitored by means of an Anseros Ozomat ozone analyser, based on the absorbance at 254 nm.

Kinetic experiments carried out with the system UVC/ H_2O_2 were completed in a 1 L glass annular jacketed photochemical reactor. Water pumped from a thermostatic bath circulated through the reactor jacket to ensure a constant

temperature inside the reactor. The reactor walls were insulated to avoid release of radiation and/or heat outside. A 15 W HERAEUS low pressure mercury vapour lamp introduced in a quartz reactor was used for experiments carried out using UVC radiation (254 nm). Actinometry experiments led to the determination of the incident radiation flux ($q_0 = 2.5 \cdot 10^{-8}$ Einstein $\text{cm}^{-2} \text{s}^{-1}$) and radiant power ($E_0 = 3.3 \cdot 10^{-6}$ Einstein s^{-1}).

5.2.2. Materials

Herbicides were purchased from Sigma-Aldrich and were used as received. Cliophar 425 from AGRIPHAR® (42.5% in the amine salt of clopyralid) was considered for ecotoxicity bioassays. Organic solvents were HPLC grade obtained from VWR Chemicals. Commercial photocatalyst TiO_2 Aeroxide® P25 from Evonik Industries (70% anatase and 30% rutile) with an average particle size of 30 nm and BET surface area of $50 \text{ m}^2 \text{ g}^{-1}$ was used. Water purified by a Milli-Q® water system (Millipore) was used in the preparation of solutions and suspensions.

5.2.3. Analysis

Herbicides were analysed by high-performance liquid chromatography (Agilent 1100). The column used was a Kromasil 100 5C18. The mobile phase was pumped at a flow rate of 1 mL min^{-1} , and the acetonitrile: acidified water (0.1% phosphoric acid) volume percentages applied were 40:60, 20:80 and 25:75 for tryclopir, clopyralid and picloram, respectively. Detection was conducted at 230, 200 and 220 nm, respectively.

Ionic short chain organic and inorganic compounds were monitored by ionic chromatography (Metrohm 881 Compact Pro), whose performance is based on high selectivity conductivity measurements.

In order to assess the degree of mineralization, total organic carbon (TOC) was determined by a Shimadzu TOC 5000A analyzer by directly injecting the aqueous solution.

Dissolved ozone in solution was determined by the indigo method; the analysis is based on decolouration of the 5,5,7-indigotrisulfonate based on the Bader and Hoigné method [5]. The pH of the reaction media was measured by means of a GLP 21+ CRISON pH meter. This parameter remained uncontrolled in non-kinetic experiments, although it did not significantly change at the end of the process.

5.2.4. Ecotoxicity bioassays with *Daphnia parvula* and *Culex pipiens* larvae

Acute toxicity tests using *Daphnia parvula* were conducted using US EPA standard operating procedures [6]. This procedure was extrapolated to carry out similar trials with mosquito larvae *Culex pipiens*. A culture of *D. parvula* or *C. pipiens* larvae was received from installations of Extremadura's University, where organisms were naturally cultured in artificial ponds (experiments completed under the Spanish regulation on animal protections RD 50/2013).

20 young *D. parvula* or 15 second-instar *C. pipiens* larvae were placed in 100 mL of test solution using a disposable plastic transfer pipette, and were subjected to 16:8 light: dark photoperiods at room temperature. Survival numbers were recorded and monitored at 6, 24, and 48 h for *D. parvula*; 24, 46, 72, and 96 h for *C. pipiens*. Organisms were not fed during the experiments. In ecotoxicity tests, commercial clopyralid solutions were prepared in mineral water (10.7 mg L⁻¹ HCO₃⁻, 5.3 mg L⁻¹ SO₄²⁻, 19.0 mg L⁻¹ Cl⁻, 2.7 mg L⁻¹ Ca²⁺, 2.7 mg L⁻¹ Mg²⁺, 14.7 mg L⁻¹ Na⁺, and 14.3 mg L⁻¹ SiO₂). pH was adjusted to 7±0.1. Three blank tests, without commercial herbicide addition, were considered per each run.

Initially trials were carried out at various parent compound initial concentrations in order to determine the concentration causing the 50% mortality (LC₅₀). After this preliminary study, samples from photocatalytic ozonation experiments at different stages of oxidation extent were taken. An additional sample was also considered when TOC removal reached the steady state level.

Survival percentage was corrected to account for natural mortality in control runs by means of the expressions [7]:

$$\% \text{ corrected mortality} = \frac{\% \text{MWC} - \% \text{CM}}{100 - \% \text{CM}} 100 \quad (5.1)$$

$$\% \text{ corrected survival} = 100 - \% \text{ corrected mortality} \quad (5.2)$$

In Equation 5.1, MWC and CM stand for mortality without correction and control mortality (mortality in blank runs), respectively.

5.3. RESULTS AND DISCUSSION

5.3.1. Technologies comparison

In a preliminary experimental series, different systems were applied to individual herbicides to assess their potential to remove these substances from water. Accordingly, UVA (365 nm) photolysis, UVA (365 nm)

photocatalysis in the presence of titania, single ozonation and UVA (365 nm) photocatalytic ozonation in the presence of titania were investigated. Figure 5.1 shows the normalized remaining concentration of clopyralid, picloram and triclopyr with time and the corresponding mineralization degree in terms of total organic carbon conversion. From this figure a similar behavior is observed in all cases. Hence, none of the herbicides presents photolytic activity at the wavelength used (365 nm). Ozonation of clopyralid requires almost 180 min to reduce its concentration by 99% while in the case of picloram the reaction is slightly faster, showing conversions >99% in roughly 140 min. Triclopyr is the most recalcitrant compound when subjected to single ozonation. The presence of halogens in the molecules of the herbicides tested suggests their recalcitrant nature to ozonation. The electrophilic nature of halogens produces reactive molecular sites that are electron-deficient, inhibiting the ozonation process [8]. Also, due to the large size of the halogen atoms such as chlorine, bromine, etc. they create steric hindrance to attack by ozone on the herbicides. Single ozonation led to poor results in terms of mineralization reduction (20-30% TOC conversion after 180 min).

The low efficiency of the ozonation process could be corroborated by calculating the direct rate constant between the different herbicides and molecular ozone. Accordingly, some experiments were conducted in the presence of *tert*-butanol (t-BuOH), a well-known free hydroxyl radical scavenger. Under these conditions, the parent compound removal rate can be formulated as:

$$-\frac{dC_i}{dt} = k_{O_3,i} C_i C_{O_3} = k_{O_3,i} C_i [at + bt^2 + c \operatorname{atan}(t) + d \operatorname{tanh}(t)] \quad (5.3)$$

In equation 5.3, the experimental ozone concentration has been fitted to a mathematical expression with parameters a, b, c and d. In addition $k_{O_3,i}$ stands for the direct ozonation rate constant of compound i and C_i , C_{O_3} the concentration of parent compound and ozone in the bulk water, respectively. Equation 5.3 applies when slow kinetic regimes develop in the system, that is, when Hatta number values are below 0.02. This expression was numerically solved by using the 4th order Runge Kutta method. Unknown $k_{O_3,i}$ was optimized to minimize the squared differences between experimental and calculated herbicide concentrations. The SOLVER add-in included in the EXCEL spreadsheet was used in the optimization process.

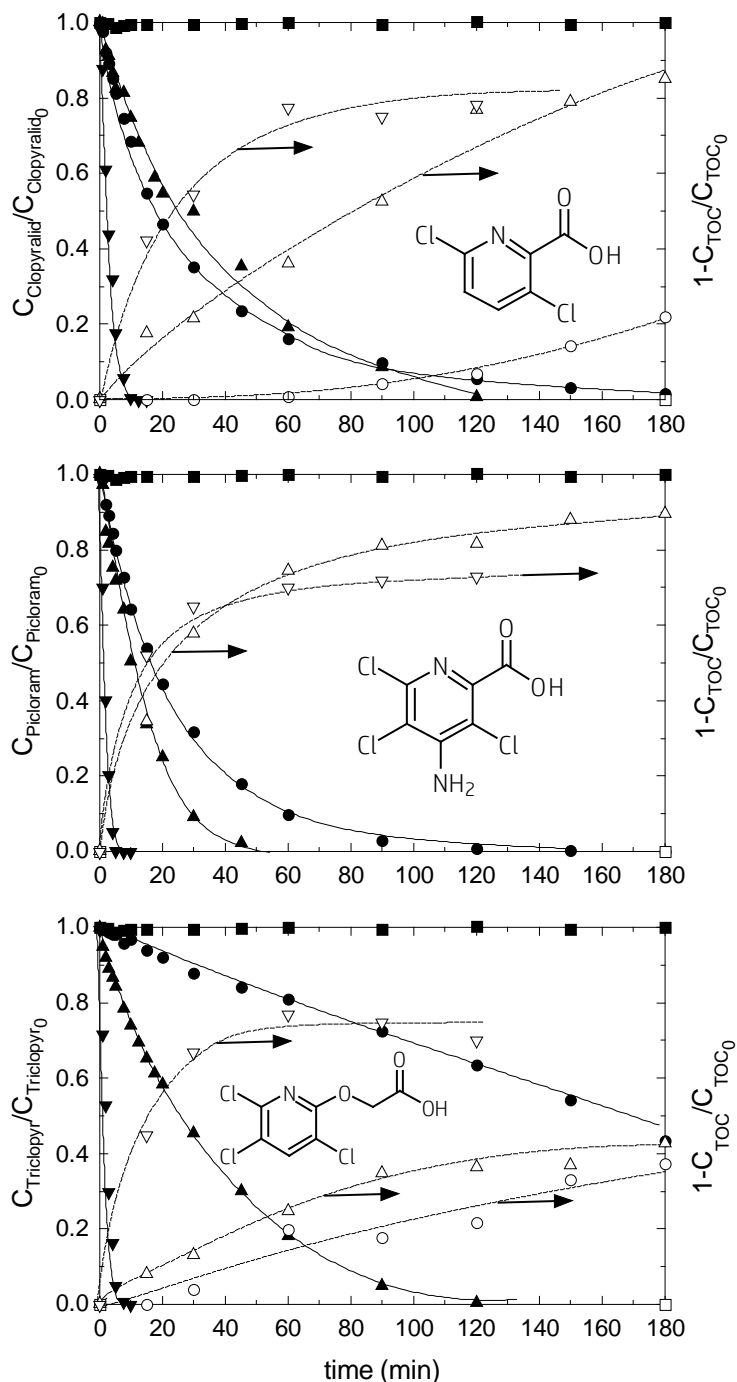


Figure 5.1 Removal of herbicides by different technologies. Experimental conditions: $V=1.0$ L, $C_{TiO_2}=0.5$ g L⁻¹; $Q_{Gas}=30$ L h⁻¹; $C_{O_3in}=10$ mg L⁻¹, pH=5.0; $C_{Herbicide}=5.0$ mg L⁻¹. Symbols: ●, O₃; ■, UVA; ▲, O₂/UVA/TiO₂; ▼, O₃/UVA/TiO₂

Figure 5.2 shows the experimental and calculated results obtained in ozonation experiments in the presence of t-BuOH. The optimization process led to $k_{03,i}$ values of $20.0 \pm 1.7 \text{ M}^{-1} \text{ min}^{-1}$ ($R^2=0.97$), $105 \pm 10.4 \text{ M}^{-1} \text{ min}^{-1}$ ($R^2=0.99$) and $20.0 \pm 3.1 \text{ M}^{-1} \text{ min}^{-1}$ ($R^2=0.96$) corresponding to the direct ozonation rate of clopyralid, picloram and triclopyr, respectively. The value obtained for picloram is below the interval $300\text{-}9000 \text{ M}^{-1} \text{ min}^{-1}$ proposed by Yao and Haag [9]. No available data were found for the other two compounds.

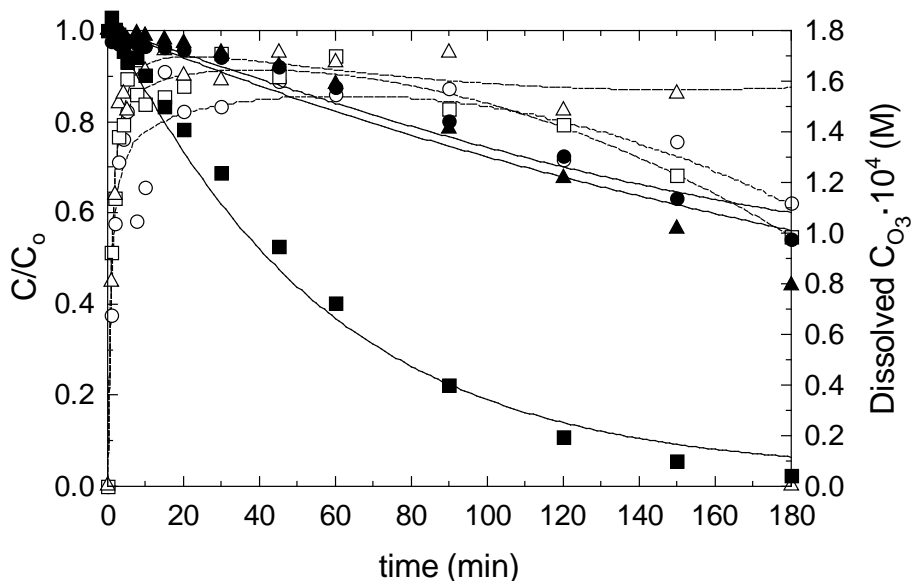


Figure 5.2 Removal of herbicides by ozonation in the presence of 10^{-2} M of t-BuOH. Experimental conditions: $V=1.0 \text{ L}$, $Q_{\text{Gas}}=30 \text{ L h}^{-1}$; $C_{\text{O}_3\text{in}}=50 \text{ mg L}^{-1}$; $\text{pH}=7.0$; $C_{\text{Herbicide}}=5.0 \text{ mg L}^{-1}$. Symbols: ●, clopyralid; ■, picloram; ▲, triclopyr. Open symbols correspond to dissolved ozone. Solid line=model calculations, dashed lines=mathematical fitting

The values of $k_{03,i}$ confirm the low reactivity of these herbicides towards ozone. Hatta number is below 0.02 in all cases, validating the use of Equation (5.3). In an attempt to corroborate the calculated $k_{03,i}$ values, a series of competitive experiments were carried out. Hence, when two herbicides (i and j) are simultaneously ozonated at pH 7 in the presence of *tert*-butanol, the following equation applies (slow regime):

$$\ln\left(\frac{C_i}{C_{i0}}\right) = \frac{k_{03,i}}{k_{03,j}} \ln\left(\frac{C_j}{C_{j0}}\right) \quad (5.4)$$

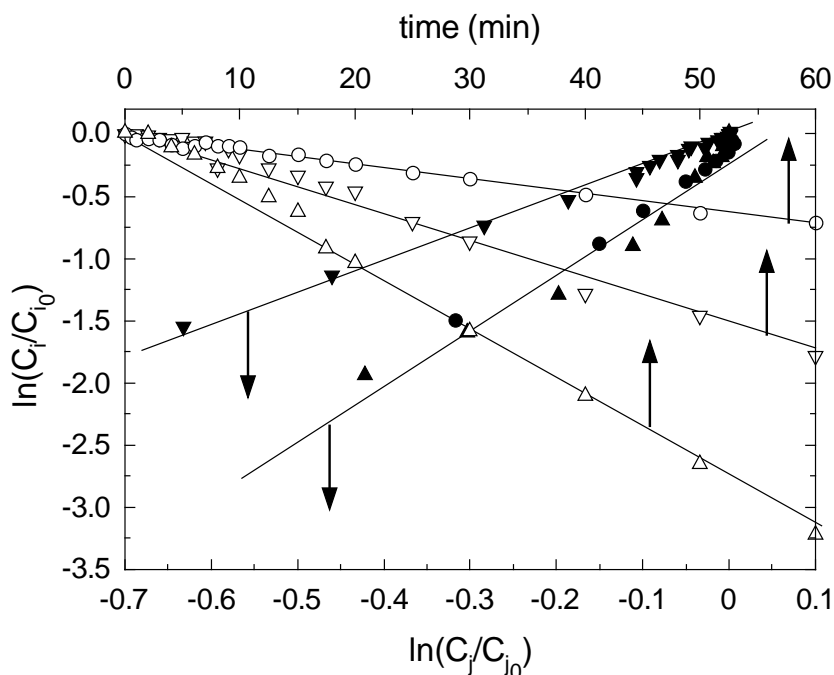


Figure 5.3 Competitive ozonation of herbicides in the presence of 10^{-2} M of t-BuOH. Experimental conditions: $V=1.0$ L; $pH=7.0$; $C_{\text{Herbicide}}=5.0$ mg L^{-1} . Symbols: ●, i=Triclopyr j=Picloram; ▼, i=Triclopyr j=Clopyralid; ▲, i=Picloram j=Clopyralid. UVC photolysis in the presence of H_2O_2 0.5 M ($V=1.0$ L; $pH=7.0$; $C_{\text{Herbicide}}=5.0$ mg L^{-1}). Symbols: ○, Clopyralid; △, Picloram; ▽, Triclopyr

Equation 5.4 is plotted in Figure 5.3. The slopes $k_{\text{O}_3, \text{Picloram}}/k_{\text{O}_3, \text{Triclopyr}}$ (4.1) and $k_{\text{O}_3, \text{Picloram}}/k_{\text{O}_3, \text{Clopyralid}}$ (4.7) were acceptably close to the expected value of 5.2, however the slope $k_{\text{O}_3, \text{Triclopyr}}/k_{\text{O}_3, \text{Clopyralid}}$ (2.5, $R^2=0.99$ in duplicated experiments) substantially differed from the expected value of roughly 1.0. By considering the evolution of the dissolved ozone concentration in the latter experiments the value of $k_{\text{O}_3, \text{Clopyralid}}$ was around $20 \text{ M}^{-1} \text{ min}^{-1}$; in other words, the presence of clopyralid increased the apparent value of $k_{\text{O}_3, \text{Triclopyr}}$ by a factor of 2.5. Given the experimental conditions used in the competitive experiments, any role played by hydroxyl radicals could be *a priori* neglected. The activity of organic peroxyradicals and other organic radicals formed upon ozonation of clopyralid might explain the observed results.

From Figure 5.1 it can be inferred that photocatalytic ozonation was the most efficient technology in terms of herbicide removal rate and mineralization degree achieved after 3 h of treatment. Photocatalysis also led

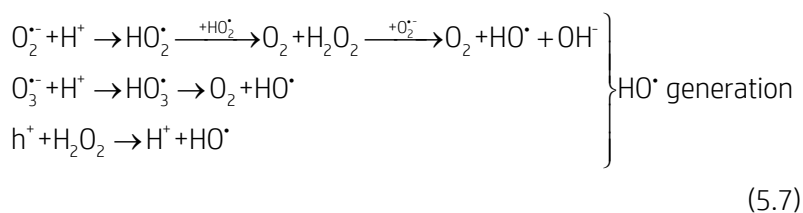
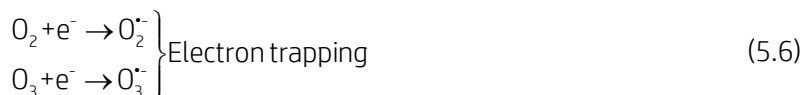
to acceptable results compared with the inefficient photolysis or even single ozonation of herbicides.

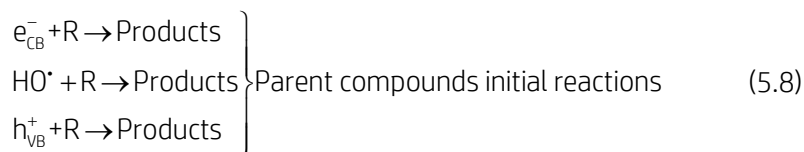
In order to assess the potential synergistic effect of the simultaneous application of ozone, UVA radiation and TiO₂, the apparent pseudo-first order rate constant was calculated for the system O₃/UVA/TiO₂ and compared with the sum of the corresponding k-values for O₃ and O₂/UVA/TiO₂. Obviously, the pseudo-first order rate constants calculated have no rigorous kinetic basis and they are just considered as a mere comparison tool. Table 5.1 shows the three constants obtained under the experimental conditions used, and the synergistic effect observed.

Table 5.1 Observed pseudo-first-order rate constant in different systems. Synergistic effect

Compound	Observed pseudo-k rate constant (10 ² , min ⁻¹)			Synergism (%)
	O ₃ (k ₁)	O ₂ /UVA/TiO ₂ (k ₂)	O ₃ /UVA/TiO ₂ (k ₃)	$\frac{k_3 - (k_1 + k_2)}{k_3} \cdot 100$
Clopyralid	2.3	3.9	22.6	72.6
Picloram	4.1	8.5	103.8	87.9
Triclopyr	0.42	3.1	67.4	94.8

As displayed in Table 5.1, the efficiency observed in photocatalytic ozonation cannot be explained by the simple summation of the single ozonation and photolysis processes. Thus, a higher generation of hydroxyl radicals is expected in the photocatalytic system when ozone is present in the media. Ozone is capable of trapping photocatalytic generated electrons more efficiently than oxygen, avoiding, therefore the recombination of electron-hole pairs according to the following mechanism [10].





In the above mechanism one molecule of ozone necessitates only one electron to produce one hydroxyl radical, compared with three electrons required by oxygen to get the same HO* yield.

Mineralization of the herbicides is much improved when TiO₂ is in the reaction media. The system O₃/UVA/TiO₂ leads to a final TOC conversion in the range 70-80% regardless of the oxidized herbicide. In addition, it should be highlighted that TOC elimination preferentially occurs in the first 40-50 min of photocatalytic ozonation, i.e. TOC concentration comes to a halt after the first hour of treatment. The photocatalytic oxidation by HO* radicals is hypothesized to be the main path to TOC abatement. Accordingly, the rate constants between this species and the used herbicides were calculated. The photolysis of each herbicide in the presence of a high concentration of H₂O₂ was completed by using UVC radiation. In this system, the following differential equations apply [11]:

$$-\frac{dC_i(t)}{dt} = \varphi_i \frac{\varepsilon_i C_i(t)}{A_{254nm}(t)} I_0 \left[1 - \exp(-2.303 L A_{254nm}(t)) \right] + k_{HO^*,i} C_i(t) C_{HO^*}(t) \quad (5.9)$$

$$-\frac{dC_{H_2O_2}(t)}{dt} = \varphi_{H_2O_2} \frac{\varepsilon_{H_2O_2} C_{H_2O_2}(t)}{A_{254nm}(t)} I_0 \left[1 - \exp(-2.303 L A_{254nm}(t)) \right] + k_{HO^*,H_2O_2} C_{H_2O_2}(t) C_{HO^*}(t) \quad (5.10)$$

$$\begin{aligned} \frac{dC_{HO^*}(t)}{dt} = & 2\varphi_{H_2O_2} \frac{\varepsilon_{H_2O_2} C_{H_2O_2}(t)}{A_{254nm}(t)} I_0 \left[1 - \exp(-2.303 L A_{254nm}(t)) \right] - k_{HO^*,i} C_i(t) C_{HO^*}(t) \\ & - k_{HO^*,H_2O_2} C_{H_2O_2}(t) C_{HO^*}(t) - k_{HO^*,Intermediates} C_{Intermediates}(t) C_{HO^*}(t) \end{aligned} \quad (5.11)$$

In the above mechanism, φ_i and ε_i are the quantum yield and molar absorptivity at 254 nm of compound i, respectively. $A_{254nm}(t)$ accounts for the absorption of UV light of all the species present in solution at time t, I_0 is the incident radiation intensity per volume ($1.73 \cdot 10^{-6}$ Einstein L⁻¹ s⁻¹) and L is the radiation pathlength in the reactor (3 cm).

Since H_2O_2 is in excess, complete adsorption of UVC radiation by H_2O_2 can be assumed. Generated hydroxyl radicals are mainly trapped by H_2O_2 and the parent compounds studied. Also, given the high hydrogen peroxide concentration used, its concentration does not appreciably vary with time. As a consequence, applying the steady state assumption to hydroxyl radical concentration, the herbicide removal rate simplifies to:

$$-\frac{dC_i(t)}{dt} = k_{HO^{\bullet},i} C_i(t) \frac{2\phi_{H_2O_2} I_0 \left[1 - \exp\left(-2.303 L \epsilon_{H_2O_2} C_{H_2O_2} \right) \right]}{k_{HO^{\bullet},i} C_i(t) + k_{HO^{\bullet},H_2O_2} C_{H_2O_2}} \quad (5.12)$$

after integration:

$$\ln\left(\frac{C_{i_0}}{C_i}\right) = k_{HO^{\bullet},i} \frac{2\phi_{H_2O_2} I_0 \left[1 - \exp\left(-2.303 L \epsilon_{H_2O_2} C_{H_2O_2} \right) \right]}{k_{HO^{\bullet},i} C_i(t) + k_{HO^{\bullet},H_2O_2} C_{H_2O_2}} t \quad (5.13)$$

From equation 5.13 (Figure 5.3), the following $k_{HO^{\bullet},i}$ values were obtained: 0.73 ± 0.05 , 3.8 ± 0.1 and $1.73 \pm 0.04 \cdot 10^9 \text{ M}^{-1}\text{s}^{-1}$ corresponding to clopyralid, picloram and triclopyr, respectively.

5.3.2. Photocatalytic ozonation. Influence of variables

Catalyst concentration

The effect of catalyst concentration was investigated in the range $0.5\text{-}0.005 \text{ g L}^{-1}$, in individual experiments. Figure 5.4 shows the results obtained. As observed from this figure, TiO_2 amounts as low as $5 \cdot 10^{-3} \text{ g L}^{-1}$ are able to degrade the target pesticides without significantly decreasing the oxidation rate if compared with experiments completed with higher titania concentrations. In the specific case of picloram, no significant differences were found between the experiment conducted with $5 \cdot 10^{-3} \text{ g L}^{-1} TiO_2$ and the experiment carried out with a concentration 100 times higher. In the case of triclopyr and clopyralid, a slight decrease in the efficiency can be envisaged, which is in agreement with the existence of an optimum concentration (m_{max}) in TiO_2 . This optimum concentration seems to be $m_{max} > 0.5 \text{ g L}^{-1}$ for clopyralid, $0.05 > m_{max} > 0.1 \text{ g L}^{-1}$ for triclopyr and $m_{max} < 0.005 \text{ g L}^{-1}$ for picloram. Similar results (not shown) were obtained when TOC evolution was analyzed. Differences in titania optimum concentrations may be attributed to the different adsorption properties of the herbicides on the TiO_2 surface, although this hypothesis has not been proven.

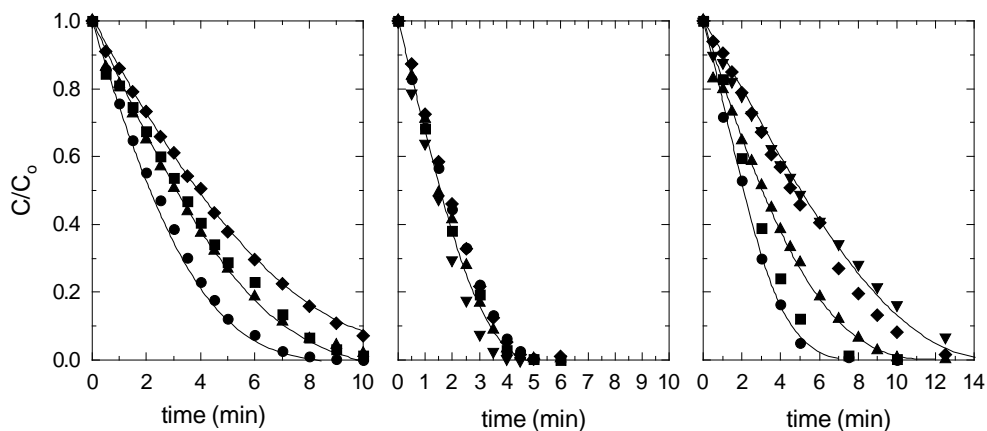


Figure 5.4 Photocatalytic ozonation of clopyralid (left), picloram (middle) and triclopyr (right). Influence of catalyst concentration. Experimental conditions: $V=1.0$ L; $pH=5.0$; $C_{\text{Herbicide}}=5.0$ mg L⁻¹, $Q_{\text{Gas}}=30$ L h⁻¹; $C_{O_3,in}=10$ mg L⁻¹. C_{TiO_2} (mg L⁻¹): ●, 500; ■, 100; ▲, 50; ▼, 10; ◆, 5

Catalyst reuse

One of the most important shortcomings in heterogeneous catalysis is the loss of activity of the solid after several cycles. In the particular case of titania at laboratory scale, this situation is aggravated by the difficulty to recover 100% of the catalyst amount used in each run. The latter drawback is minimized when experiments are carried out at pilot plant scale, where relative loss is minimized.

In this work an attempt was made to reuse TiO_2 in consecutive photocatalytic ozonation experiments by utilizing each time, the amount recovered after centrifugation. As a consequence, the amount of catalyst used in each consecutive run gradually diminishes. With this methodology, the potential deactivation of TiO_2 is not hindered by the addition of fresh catalyst that would be required to get the same initial solid concentration in all recycling experiments.

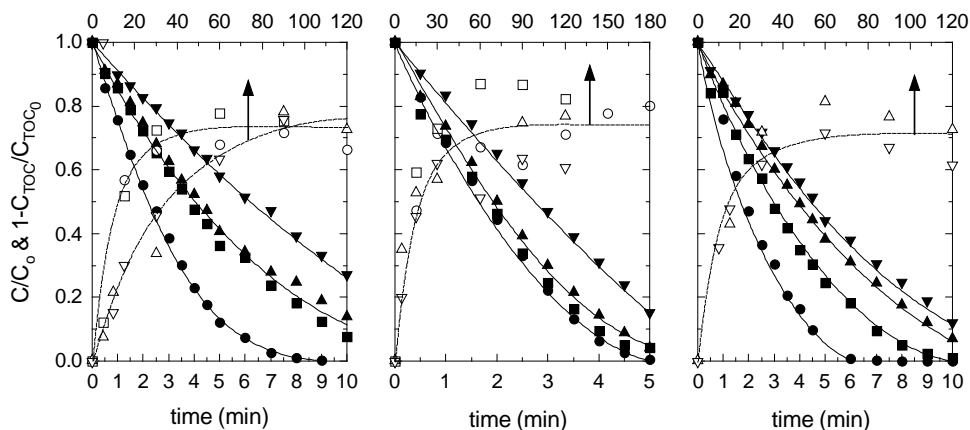


Figure 5.5 Photocatalytic ozonation of clopyralid (left), picloram (middle) and triclopyr (right). Influence of catalyst reuse. Experimental conditions: $V=1.0$ L; $pH=5.0$; $C_{\text{Herbicide}}=5.0$ mg L^{-1} , $Q_{\text{Gas}}=30$ L h^{-1} ; $C_{O_3,in}=10$ mg L^{-1} ; initial $C_{TiO_2}=0.5$ g L^{-1} . ●, fresh (0.5 g L^{-1}); ■, 1st reuse (0.32-0.35 g L^{-1}); ▲, 2nd reuse (0.22-0.25 g L^{-1}); ▼, 3rd reuse (0.12-0.13 g L^{-1})

Figure 5.5 shows the results obtained, indicating that the amount of catalyst used in each cycle decreases to 65%, 45%, and 25% of the initial TiO_2 added at the first, second and third reuses, respectively. From Figure 5.5 it is observed that catalyst deactivates in consecutive runs when the parent compound is monitored. The loss in TiO_2 concentration due to the inefficient recovery process does not explain the loss in herbicides removal efficiency. For instance, picloram is similarly degraded in the presence of 0.5 or 0.005 g L^{-1} of titania (Figure 5.4), however in Figure 5.5 it is observed how runs conducted with 0.5 g L^{-1} (fresh catalyst) and 0.12 g L^{-1} (3rd reuse) show a partial deactivation of the solid in terms of picloram removal. Similar reasoning can be applied to the other two herbicides.

The degree of mineralization did not follow the same pattern. Thus, besides some differences in the TOC abatement rate, at the end of the process TOC conversion is similar regardless of the reuse cycle of the catalyst. At this point it has to be highlighted that TOC final conversion is obtained after 180 min of treatment. After this time, all pesticides had disappeared so small changes in activity observed during the initial period of reaction are hindered when monitoring TOC evolution.

Initial herbicide concentration

Figure 5.6 shows the results of two experiments carried out with initial herbicide concentrations of 5, and 20 mg L⁻¹, respectively. As observed, increasing the initial herbicide load leads to the displacement of the curve to the right, so the time needed for complete herbicide removal is practically doubled. This curve shift discards the development of first-order kinetics, a complex reaction mechanism proceeds in this type of systems. Previous adsorption of the pesticides onto the catalyst likely occurs, so Langmuir type kinetics develops.

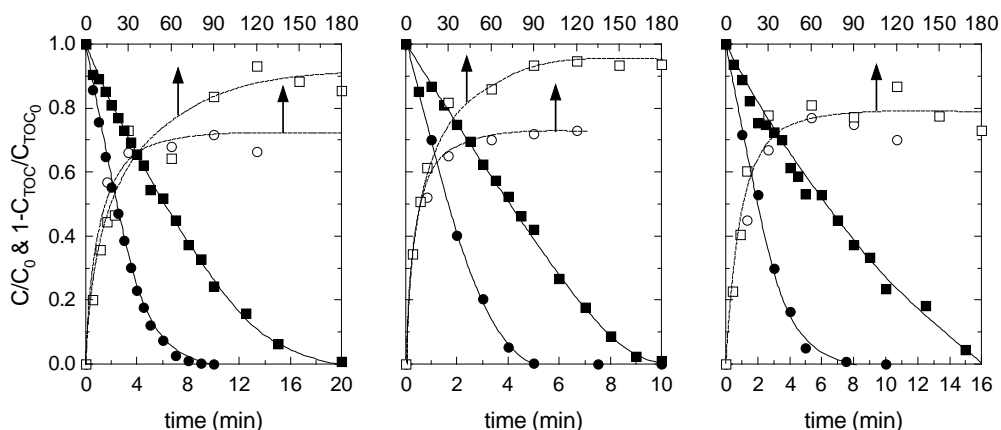


Figure 5.6 Photocatalytic ozonation of clopyralid (left), picloram (middle) and triclopyr (right). Influence of initial herbicide concentration. Experimental conditions: $V=1.0$ L; $pH=5.0$; $Q_{Gas}=30$ L h⁻¹; $C_{O_3,in}=10$ mg L⁻¹; $C_{TiO_2}=0.5$ g L⁻¹; $C_{Herbicide}$ (mg L⁻¹): ●, 5; ■, 20

In addition, TOC evolution should be highlighted. Hence, TOC conversion increases as the initial concentration of clopyralid or picloram is increased, while in the case of triclopyr no clear trend was experienced. These results suggest the development of autocatalytic mechanisms in TOC abatement, possibly due to the generation of reactive organic radicals. The TOC removal when 20 mg L⁻¹ of initial herbicide concentration was used was correlated with the evolution of some ionic species such as nitrate, chloride and some low weight organic acids (end-products). Figure 5.7 shows the evolution of the aforementioned species. As seen in Figure 5.7 some low weight organic acids such as acetic, formic, and oxalic acids were identified during the process. Particular importance is given to the evolution of chloride. This anion immediately reaches the maximum amount that can be released from the herbicide in just 10-15 min (represented by the dashed line Cl⁻_{MAX}), in agreement with the total abatement of the parent compound. These results suggest the primary attack is to the Cl-C bond in the herbicides. Some authors

have reported the generation of intermediates keeping the Cl moiety in their structures. Thus, Sojic et al. [12] claim the formation of 3,6-dichloropyridin-2-ol, 3,6-dichloro-4-hydroxypyridine-2-carboxylic acid and 3,6-dichloro-5-hydroxypyridine-2-carboxylic acid in the first stages of the photocatalysis of clopyralid. Also, 2,3,5-trichloropyridine-4-ylamine, 3,5,6-trichloropyridine-2-carboxylic acid, 4-amino-5,6-dichloro-3-hydroxypyridine-2-carboxylic acid and 5,6-dichloro-3-hydroxypyridine-2-carboxylic acid were detected in the degradation of picloram by the electro-Fenton process [13].

From chloride evolution in this work, dechlorination of herbicides seems to be the initial mechanism of parent compound abatement. These results are also substantiated in other work [14].

In addition, nitrate accumulation curves follow the same pattern as TOC conversion indicating that ring opening and pyridinic-nitrogen loss are the key stages in mineralization. Figure 5.7 shows the maximum nitrate concentration expected in solution from the pyridinic nitrogen. Nitrate final concentration reached 70-80% of the maximum amount in the case of clopyralid and triclopyr and 100% in the case of picloram. In the latter case formation of oxamic acid from the amine group is likely to occur [15].

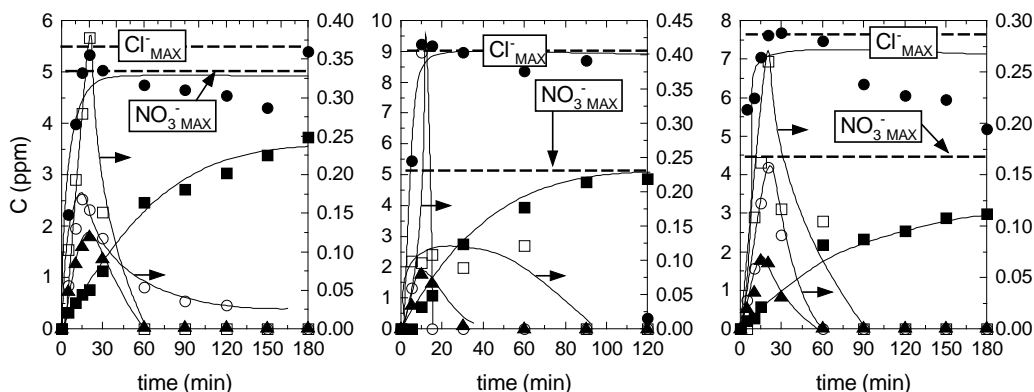


Figure 5.7 Photocatalytic ozonation of clopyralid (left), picloram (middle) and triclopyr (right). Ionic species evolution. Experimental conditions: $V=1.0$ L; $pH=5.0$; $Q_{Gas}=30$ L h^{-1} ; $k_{O_3,in}=10$ mg L^{-1} ; $C_{TiO_2}=0.5$ g L^{-1} ; $C_{Herbicide}=20$ mg L^{-1} . ●, chloride (left y-axis); ■, nitrates (left y-axis); ▲, formic acid (left y-axis); ○, acetic acid (right y axis); □, oxalic acid (right y-axis)

Among the identified low weight carboxylic acids, formic acid predominates over the rest, suggesting breakage of the COOH moiety in the herbicides.

5.3.3. Photocatalytic ozonation of commercial clopyralid. Toxicity evolution

Given the similarity between the structures of the herbicides used, it was decided to evaluate the toxicity of only one of them in its commercial form. Hence, branded clopyralid was oxidized and the toxicity of intermediates generated evaluated at different parent compound conversions. Previously, some preliminary tests were carried out to assess the potential toxicity of the non-treated herbicide. Several herbicide concentrations were used and the toxicity to *D. parvula* and *C. pipiens* larvae monitored at 6, 24, 48, 72, and 96 exposure hours.

Figure 5.8 shows a higher toxicity of clopyralid to *D. parvula*. In all cases, toxicity levels are relatively low for both the crustacean and the larvae. From Figure 5.8 the following LC_{50} values towards *D. parvula* can be calculated, 184 mg L^{-1} (24 h) and 70 mg L^{-1} (48 h). An EC_{50} (48 h) value of 225 mg L^{-1} can be found in the EPA database [16] when using *D. magna*. In the case of *C. pipiens* larvae, clopyralid concentrations tested are not sufficiently high to achieve the zero survival limit; however, assuming that 100% mortality can be achieved at high concentrations, calculated LC_{50} values are 3550 mg L^{-1} (72 h) and 3100 mg L^{-1} (96 h).

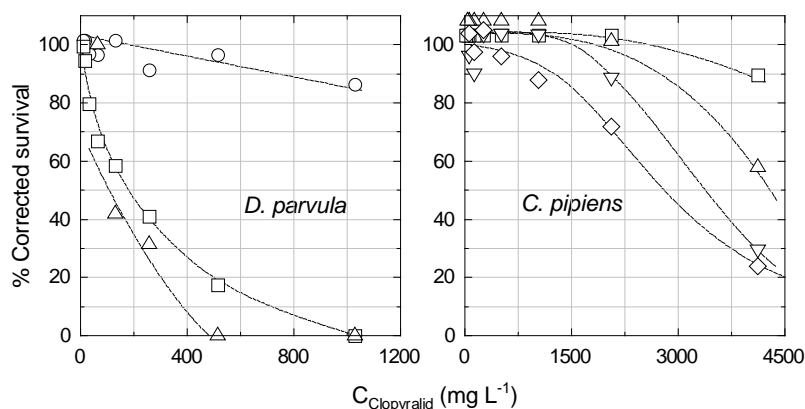


Figure 5.8 Survival percentages of *D. parvula* and *C. pipiens* larvae at increasing values of clopyralid concentration. Exposure time (h): \circ , 6.0; \square , 24; \triangle , 48; ∇ , 72; \diamond , 96

As stated previously, photocatalytic ozonation is a suitable process to eliminate the herbicides used in this study. Nevertheless, the toxicity of intermediates and accumulated end products in the reaction media requires attention. Subsequently, toxicity bioassays were completed by considering different stages in the oxidation process, i.e. considering several values of clopyralid conversion. In addition, different clopyralid initial concentrations were also used in these runs. Figure 5.9 shows a general trend in toxicity

profiles. Apparently, the first intermediates generated in clopyralid oxidation are more toxic than the parent herbicide. For instance, when 100 mg L⁻¹ of clopyralid was treated, *D. parvula* mortality at 24 and 48 h of exposure reached the top limit of 100% when the herbicide was present in solution. However, the survival percentage drastically increased once clopyralid was removed from solution. As expected, the experiment carried out with the lowest clopyralid concentration (5 mg L⁻¹) barely exhibited toxicity regardless of the time exposure.

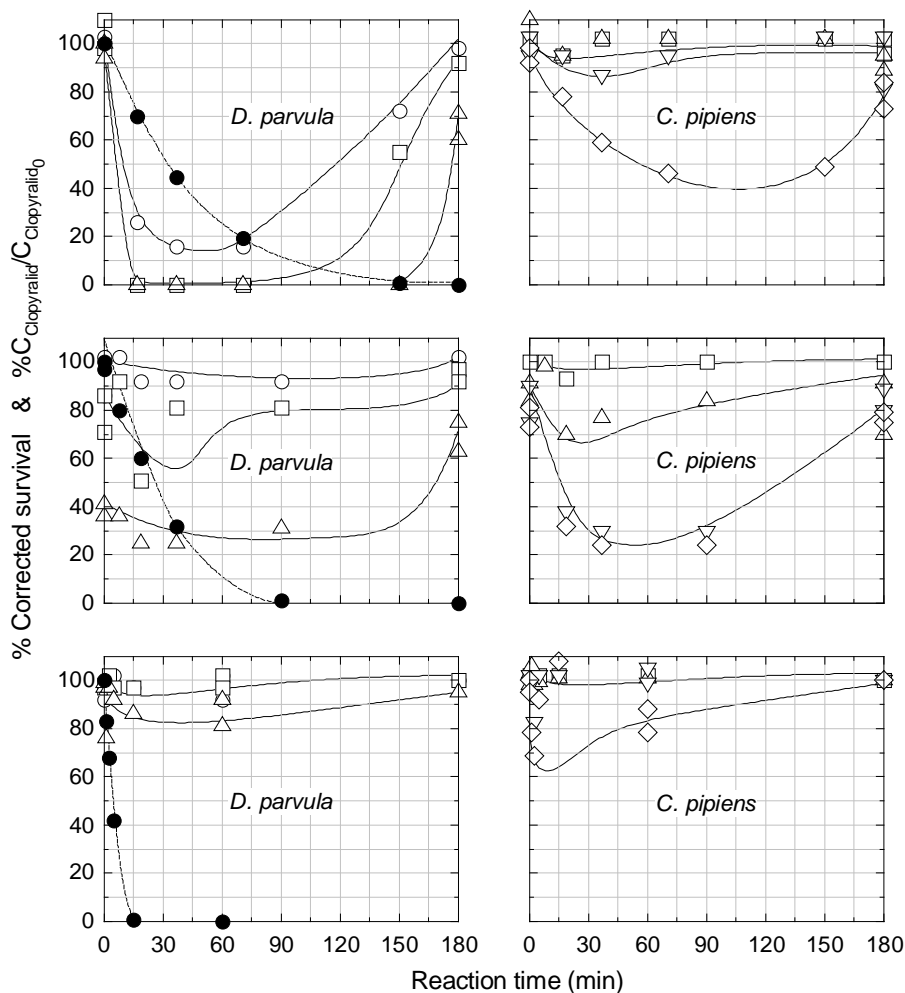


Figure 5.9 Survival percentages of *D. parvula* and *C. pipiens* larvae in solutions of photocatalytically ozonated clopyralid for different reaction periods. Initial MCPA concentration: top figure = 100 mg L⁻¹; middle figure = 75 mg L⁻¹; bottom figure = 5 mg L⁻¹. Time of exposure (h): ○, 6.0; □, 24; △, 48; ▽, 72; ◇, 96 (solid circles = remaining clopyralid percentage)

As stated previously, *C. pipiens* larvae are less sensitive to the herbicide than *Daphnia*. This can also be translated to intermediates, although again the 'U' type profiles in survival percentage (mainly after 72-96 h exposure) can be envisaged when high clopyralid concentration is used. Again, the lowest value of clopyralid initial concentration led to solutions of negligible toxicity towards the larvae.

5.4. CONCLUSIONS

The following conclusions can be listed:

- Clopyralid, picloram and triclopyr are relatively recalcitrant towards ozone. These species are better degraded in those systems capable of generating radical species.
- The combination of ozone and photocatalysis lead to the best results in terms of herbicide abatement rate and mineralization extent.
- In the photocatalytic ozonation process, TOC conversion is not negatively affected by an increase in the initial herbicide concentration, suggesting the development of autocatalytic reactions.
- The photocatalyst partially deteriorates after several reuses when the herbicide evolution was monitored; however, the solid kept its mineralization activity after the third reuse.
- Free chloride immediately accumulates in the reaction media, dechlorination is supposed to occur in the first stages of the photocatalytic ozonation process.
- In order to decrease the toxicity of treated effluents, special care must be considered to completely remove herbicides from water. In any case, intermediates generated in the photocatalytic ozonation of diluted herbicides do not present toxicity problems.

Acknowledgments

The authors acknowledge the economic support received from *Gobierno de Extremadura* and *CICYT* of Spain through Projects GRU10012 and CTQ2012-35789-C02-01, respectively. Mr. Rafael Rodríguez Solís thanks *Gobierno de Extremadura*, *Consejería de Empleo, Empresa e Innovación*, and *FSE* Funds for his PhD grant (PD12058).

REFERENCES

- [1] Tizaoui C, Mezughi K, Bickley R, *Heterogeneous photocatalytic removal of the herbicide clopyralid and its comparison with UV/H₂O₂ and ozone oxidation techniques*. Desalination 273 (2011) 197-204
- [2] Environmental Protection Agency (2014) <http://www.epa.gov/oppsrrd1/REDs/factsheets/2710fact.pdf> (Last accessed 3 August 2014)
- [3] Environmental Protection Agency (2014) <http://www.epa.gov/oppsrrd1/REDs/factsheets/0096fact.pdf> (Last accessed 3 August 2014)
- [4] Marin Municipal Water District (2014) <http://www.marinwater.org/documentcenter/> (Last accessed 3 August 2014)
- [5] Bader H, Hoigné J, *Determination of ozone in water by the indigo method*. Water Res 15 (1981) 449-456
- [6] EPA, Methods for measuring the acute toxicity of effluents and receiving water to freshwater and marine organisms. US Environmental Protection Agency Office of Water, Washington (2002).
- [7] Abbott WS, *A method of computing the effectiveness of an insecticide*. J Econom Entomol 18 (1925) 265-267
- [8] Lei H, Snyder SA, *3D QSPR models for the removal of trace organic contaminants by ozone and free chlorine*. Water Res 41 (2007) 4051-4060
- [9] Yao CCD, Haag WR, *Rate constants for direct reactions of ozone with several drinking water contaminants*. Water Res 25 (1991) 761-773
- [10] Agustina TE, Ang HM, Vareek VK, *A review of synergistic effect of photocatalysis and ozonation on wastewater treatment*. J Photochem Photobiol C 6 (2005) 264-273
- [11] Rivas J, Gimeno O, Borrallho T, Carbajo M, *UV-C photolysis of endocrine disruptors. The influence of inorganic peroxides*. J Hazard Mater 174 (2010) 393-397
- [12] Sojic DV, Anderluh VB, Orcic DZ, Abramovic BF, *Photodegradation of clopyralid in TiO₂ suspensions: identification of intermediates and reaction pathways*. J Hazard Mater 168 (2009) 94-101

- [13] Özcan A, Şahin Y, Koparal AS, OturanMA, *Degradation of picloram by the electro-Fenton process*. J Hazard Mater 153 (2008) 718-727
- [14] Westphal K, Saliger R, Jäger D, Teevs L and Prüße U, *Degradation of Clopyralid by the Fenton Reaction*. Ind Eng Chem Res 52 (2013) 13924-13929
- [15] Özcan A, Oturan N, Şahin Y, Oturan MA, *Electro-Fenton treatment of aqueous clopyralid solutions*. Int J Environ An Chem 90 (2010) 478-486
- [16] Environmental Protection Agency (2014), <http://cfpub.epa.gov/ecotox/> (Visited 9 August 2014)

CHAPTER SIX

PAPER FOUR

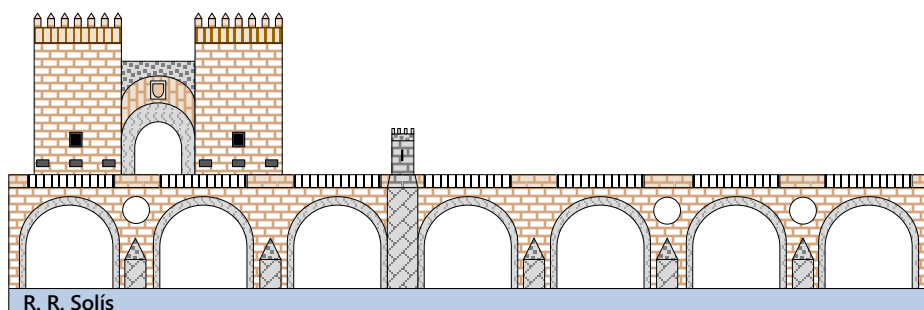
Photocatalytic ozonation of pyridine-based herbicides by N-doped titania

J Chem Technol & Biotechnol 91 (2016) 1998–2008

Rafael R. Solís, F. Javier Rivas, Olga Gimeno, José Luis Pérez-Bote

ABSTRACT. BACKGROUND: A mixture of three pyridine herbicides in water (clopyralid, triclopyr and picloram) has been treated with photocatalytic processes, involving oxygen or ozone. Nitrogen doped and undoped titania were used in the process. Toxicity evolution during photocatalytic ozonation was monitored considering BOD, *Daphnia parvula* and fitotoxicity trials. RESULTS: N doped titania with an optimized photoactivity was tested in photocatalytic ozonation, leading to nearly 95% mineralization in 180 min. This catalyst was characterized by SEM, TEM, XRD and XPS techniques (13.5 nm crystal size, anatase phase, 1% of nitrogen, and formation of O-Ti-N linkage). No loss of photocatalytic activity was observed after five consecutive runs. Although no toxicity from the parent compounds was observed, this parameter increased during the early stages of the oxidation process. When parent compounds were totally degraded and dechlorination was completed, toxicity decayed again to negligible values. CONCLUSION: N doping improves bare titania photoactivity through an optimum amount of N. Photocatalysis/ozone showed better behavior than photocatalysis/oxygen in herbicide removal and mineralization, and no significant loss of activity was observed after five runs. Toxicity initially increased due to toxic byproducts formation; however, it decreased after their abatement.

KEYWORDS: clopyralid, picloram, triclopyr, photocatalysis, photocatalytic ozonation, doped titania



Puerta y Puente de Palmas, Badajoz

6.1. INTRODUCTION

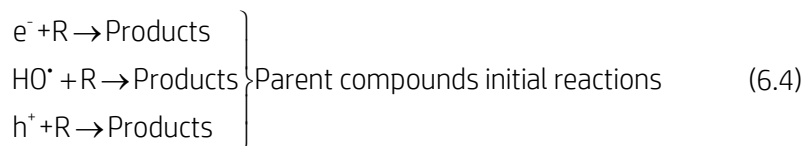
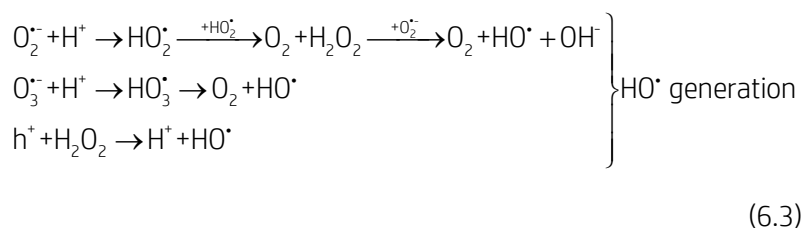
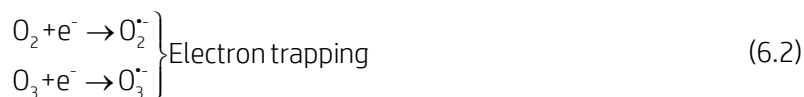
Picloram (4-amino-3,5,6-trichloro-2-pyridinecarboxylic acid), clopyralid (3,6-dichloro-2-pyridinecarboxylic acid) and triclopyr (3,5,6-trichloro-2-pyridinyloxyacetic acid) are selective herbicides included in the chlorinated pyridine derivatives family. Picloram and clopyralid belong to the picolinic acid family while triclopyr derives from pyridiniloxyacetic acid.

Picloram is used to kill unwanted broad-leaved plants on pastures and rangeland, in reforestation programs, in uncultivated areas, and along rights-of-way, the majority being used on pasture and rangeland [1]. In the case of clopyralid, it is used to kill unwanted annual and perennial broadleaf plants in turf and lawns, range, pasture, rights-of-way, and some agricultural crops [2]. Pastures, woodlands, and rights-of-way are the main scenarios of triclopyr uses, while rice is the major agricultural use [3].

The main concern related to the use and application of these herbicides is their relatively high solubility in water, persistence and mobility. Due to this, they are likely to leach into groundwater or surface water which is certain in those areas where residues may be persistent in the overlying solid [4-7]. Once in water, the herbicides are unlikely to degrade even after a long period of time. In addition, of special relevance is the potential carryover of picolinic herbicides in animal manure, compost, plant mulch, etc. These species may pose phytotoxic properties for non-target plants after their uncontrolled application. Some crops such as tomatoes, potatoes (picloram, clopyralid) or tobacco (picloram) are negatively affected by exposure to these herbicides.

Efficient methods of water treatment to remove microcontaminants involve physical processes such as adsorption on activated carbon, membrane technologies, or chemical stages such as oxidation/reduction processes. Among the latter, photocatalysis has emerged as one of the most attractive technologies, especially when solar radiation or low cost radiation sources are used. Black light lamps are economical devices characterized by their emission in the proximity of 365 nm. Furthermore, they may be a suitable alternative in areas where climate limits the use of solar radiation. The correct selection of an active and stable photocatalyst is of paramount importance. Titanium dioxide is an economical and suitable choice due to its nontoxic nature and photocatalytic activity. Generation of hole-electron pairs is produced for wavelengths lower than 387 nm. Doping of TiO_2 can lead to an increase of the maximum wavelength of excitation or, alternatively a higher quantum yield at a particular wavelength.

One of the reactions to be minimized during photocatalysis is the recombination of electron-hole leading to inefficient heat release. This step is partially prevented by the oxygen presence which is reduced while holes directly react with contaminants or with water to produce hydroxyl radicals. Trapping of electrons can also be accomplished by inorganic peroxides such as H_2O_2 , monoperoxy sulfate, persulfate, etc. [8]. A promising alternative is the simultaneous application of ozone and photocatalysis. This combination allows for the concurrent action of molecular ozone and photocatalysis with the synergistic effect of electron trapping by O_3 . Electron trapping by ozone leads to the development of a radical mechanism capable of generating more powerful hydroxyl radicals than the process in the presence of oxygen [9]:



In this work an attempt has been made to synthesize a TiO_2 based photocatalyst by improving its properties using nitrogen doping [10-14]. For that purpose, triethylamine was considered because of its high capacity for forming a stable organic titanium complex which plays an important role during the hydrolysis stage [15].

A mixture of picloram, clopyralid and triclopyr has been used to test the activity and stability of the catalyst. These herbicides have been eliminated from aqueous media by several technologies such as Fenton [16], electro-Fenton [17], photo-Fenton [18], O_3/H_2O_2 [19], photocatalysis [20-24], UV [25] and H_2O_2/UV [26], etc. However, to the best of the author's knowledge, the efficiency of photocatalytic ozonation has not been investigated for the removal of pyridine-based herbicides.

6.2. EXPERIMENTAL

6.2.1. Photoreactor and procedure

A schematic of the experimental setup is shown in Figure 6.1. It is composed of a 1.0 L reactor inside an external cylindrical pipe (54 cm of height and 31 cm of external diameter) with four black light lamps of 41 cm length attached to the inner wall. The lamps (LAMP15TBL HQPOWER™ manufactured by Velleman®, 41 cm length and 15W nominal power emitting in the range 350-400 nm) were equidistantly distributed at 90°. The inner wall was covered by aluminum foil to increase photons reflection. Actinometry experiments in the presence of ferryxalate led to quantification of the radiation at a value of $6.86 \cdot 10^5$ Einstein $L^{-1} \text{ min}^{-1}$ when the four lamps were in use.

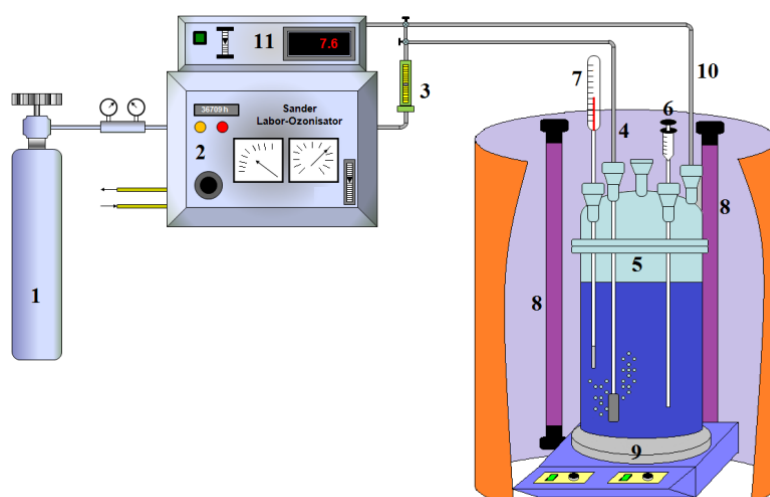


Figure 6.1 Experimental setup: 1, oxygen tank; 2, ozone generator; 3, flow rate controller; 4, gas inlet; 5, cylindrical reactor; 6, sampling port; 7, thermometer; 8, black-light lamps; 9, magnetic stirrer; 10, gas outlet; 11, ozone analyzer

The photoreactor was continuously fed with oxygen, nitrogen or a mixture of oxygen-ozone by means of a diffuser placed inside the reaction bulk. 30 L h^{-1} gas flow rate was used in all trials. The solid photocatalysts were added before the photoreaction to reach the herbicides adsorption equilibria onto their surface. When samples were extracted, the solid was removed by filtration through Millex-HA filters (Millipore, $0.45 \mu\text{m}$).

Ozone was produced by electrical decomposition of oxygen in a Sander Laboratory Ozone Generator. Ozone gas phase concentration was monitored by an Anseros Ozomat ozone analyzer.

6.2.2. Materials

Pure herbicides, titanium (IV) isopropoxide (97%) and potassium indigotrisulfonate were purchased from Sigma-Aldrich; while triethylamine (99.5%), hydrochloric acid (37%) and absolute ethanol were from Panreac. A high performance liquid chromatograph (HPLC) was fed with organic solvents from VWR Chemicals and ionic chromatography solutions were prepared with Sigma-Aldrich reagents. All chemicals were used as received. Finally, water from a Milli-Q® water system (Millipore) was used for preparation of all solutions and suspensions.

6.2.3. N-doped titania synthesis

The lab-made photocatalysts were synthesized applying a sol-gel method followed by thermal treatment and calcination. A literature method was carried out in order to synthesize them [27]. Roughly, it starts by dissolving titanium isopropoxide in ethanol, followed by addition of a predetermined amount of nitrogen organic source (in this case triethylamine) to meet the required N:Ti ratio. Afterwards, HCl 0.1M is gradually added to the organic solution to obtain a clear liquid. The precipitation process is completed by autoclaving the mixture at 80°C for 12 h. Then, the suspension is centrifuged at 3500 rpm, and the resultant solid dried overnight at 100°C. Finally, calcination is carried out at 500°C for 4 h with an initial ramp of 10°C min⁻¹. The manufactured photocatalysts were labeled with the general formula TiO₂-1:x, where 1:x means the ratio of Ti atoms to N atoms in the synthesis process.

6.2.4. Catalyst characterization

X-ray photoelectron spectroscopy (XPS) spectra were obtained using XPS K-alpha-Thermo Scientific equipment, working with a K α monochromatic source of Al (1486.68 eV). A value of 284.8 eV for the C 1s peak was taken to calibrate the signals of Ti 2p, O 1s, N 1s peaks. Crystalline phase was analyzed by X-ray diffraction (XRD), in a Bruker D8 Advance diffractometer equipped with a monochromator of Ge 111 K α of Cu (wavelength, 1.5456 Å). Transmission electron microscopy (TEM) analysis was applied using a TEM Tecnai G2 20 Twin-FEI company apparatus (filament LaB₆, voltage 200 kV, magnification up to 1.05 10⁶) while scanning electron microscopy (SEM) was conducted in a Hitachi S-4800 coupled to a secondary electrons detector (acceleration voltage 20 kV).

Diffuse reflectance UV-VIS spectroscopy, used to obtain the catalysts UV-VIS absorbance spectra and band gap values of the catalysts, were completed

with a Jasco V670 UN/VIS/NIR spectrophotometer equipped with an integrating sphere device. BET surface area was quantified through nitrogen adsorption isotherms obtained at 77K with a Quadrasorb instrument (Quantachrome). Samples were treated previously at 150°C for 24h under high vacuum conditions for out degassing the adsorbed gases.

Thermal gravimetry, differential temperature analysis and released gases mass spectrometry (TG-DTA-MS) were performed with Setaram SETSYS Evolution-16 equipment connected to a Prisma™ QMS200 quadrupole mass spectrometer. The operating conditions were: sample loading 28 mg, air flow rate 50 mL min⁻¹ and heating rate of 10°C min⁻¹ from room temperature to 900°C.

6.2.5. Analysis

High performance liquid chromatography (HPLC, Agilent 1100) was used in the analysis of herbicides. The HPLC was equipped with a Kromasil 100 5C18 column. A gradient elution was pumped at a flow rate of 1 mL min⁻¹, and the acetonitrile: acidified water (0.1% H₃PO₄) volume percentages were increased from 10:90 to 50:50 in 12 min. After that, it was kept at 50:50 for 6 min. An engaged wavenumber of 230 nm was considered for conduction.

Short chain organic and inorganic anionic compounds were monitored by ionic chromatography (Metrohm 881 Compact Pro). Total organic carbon (TOC) content was determined by means of a Shimadzu TOC 5000A analyzer which directly injects the aqueous sample.

A method based on the decoloration of 5,5,7-indigotrisulfonate was applied for the determination of dissolved ozone concentration in aqueous solution [28]. A GLP 21+ CRISON pH-meter was used for pH measurement. pH of the media was not adjusted and reactions were conducted at the natural pH after herbicides addition. In toxicity trials, pH was adjusted with H₃PO₄ and NaOH.

Biological oxygen demand after 5 days (BOD₅) was conducted by respirometry. Commercial respirometers OXITOP® were used for the purpose. BOD₅ was determined after the addition of inorganic salts, nutrients and microorganisms from activated sludge to simulate the behavior in a standard residual urban wastewater. A synthetic wastewater representing a secondary treated effluent was prepared [29]. Inoculate was obtained from the local wastewater treatment plant of the city of Badajoz.

6.2.6. Ecotoxicity bioassays with *Daphnia parvula*

For ecotoxicity purposes, the acute toxicity to *Daphnia parvula* was carried out according to US EPA standard procedure [30]. The crustaceans were grown in artificial ponds located at Extremadura University installations.

The analysis started by placing 20 young *D. parvula* into a 100 mL water sample, by means of disposable plastic transfer pipettes. After that, the crustaceans were exposed to 16:8 light: dark photoperiods at room temperature. Surviving organisms were counted at 24 and 48 h, without being fed. The herbicides were dissolved in mineral water (composition: 10.7 mg L⁻¹ HCO₃⁻, 5.3 mg L⁻¹ SO₄²⁻, 19.0 mg L⁻¹ Cl⁻, 2.7 mg L⁻¹ Ca²⁺, 2.7 mg L⁻¹ Mg²⁺, 14.7 mg L⁻¹ Na⁺, and 14.3 mg L⁻¹ SiO₂). In these experiments, pH was adjusted to 7.0±0.1 after extracting samples. Three blank samples without herbicide addition were considered in order to study the mortality due to natural reasons. One photocatalytic ozonation process was carried out; samples at different stages of oxidation extent of the most refractory herbicide were extracted (0, 25, 50, 75, and 100% of initial clopyralid removal). A final sample when TOC removal achieved a steady state level was also analyzed.

The formula proposed by Abbott was used to correct the survival percentage due to natural causes [31]:

$$\%M'_S = \frac{\%M_S - \%M_B}{100 - \%M_B} \quad (6.5)$$

$$\%S'_S = 100 - \%M'_S \quad (6.6)$$

In these equations M_S and M_B denotes mortality without correction in the sample and blank tests, respectively; and, M'_S and S'_S are the sample respective mortality and survival corrected percentages.

6.2.7. Acute fitotoxicity assays

Seeds of *Lactuca Sativa* and *Solanum Lycopersicum* were purchased from Vilmorin® (Batavia blonde of Paris lettuce and cherry tomato, respectively) and used as test plants for acute fitotoxicity assays of water samples extracted at different times of treatment.

Fifteen *L. Sativa* or *S. Lycopersicum* seeds were equally distributed in Petri dishes equipped with paper discs moistened with 4 mL of water sample. The dishes were covered with paraffin plastic in order to avoid liquid evaporation, and incubated in a germination chamber isolated from light at 22±2°C for 120 h. After that period, the root length (L), expressed as the sum of

hypocotyl and radicle, was measured for those seeds whose germination had taken place.

Additionally, a negative control or blank of MilliQ® water and a positive control of H_2O_2 300 mmol L^{-1} were carried out. The validity criteria for the test were an upper 90% of germination and a variation coefficient for the root growth below 30% in negative control experiments. Positive control led to germination of none of the seeds. The percentage root growth was calculated by comparing the radicle lengths for each sample with those observed in the control (L/L_{Blank}).

6.3. RESULTS AND DISCUSSION

6.3.1. Photocatalytic oxidation. Activity of catalysts with different Ti:N ratios

Previously to the application of ozone, some photocatalytic tests were carried out in the presence of oxygen. Different catalysts were synthesized by varying the ratio Ti:N in the manufacturing process. Accordingly, different doping percentages are expected in the lab-made photocatalysts. Doping percentage of titania particles influences the activity of the photocatalyst [32]. Hence, Ti:N ratios from 1:0 to 1:2 were used in the photocatalysis of a mixture of the three herbicides considered in this work.

Figure 6.2 shows the evolution of the normalized concentration of herbicides treated in the presence of different catalysts. Also, the evolution of total organic carbon (TOC) is displayed.

The positive effect of N-doping is observed in Figure 6.2. Regardless of the catalyst nitrogen content, the presence of this anionic dopant improves conversion of the herbicides and the mineralization degree achieved after 180 min of treatment. Optimum N percentage was experienced when the TiO_2 _1:1.6 catalyst was used. The presence of an optimum relies on the influence of opposite effects. On one hand, N doping involves a decrease in the band gap energy and, as a consequence, higher photolytic activity. On the other hand, an increase in particle diameter (lower specific area), formation of TiN (non-transparent), and the number of oxygen vacancies (electron-hole recombination sites) are related to high N doping photocatalysts [33]. In any case, this subject is controversial: some authors claim that N doping decreases particle size while electron-hole recombination is prevented by oxygen vacancies (photoluminescence intensity minimization) [34]. An increase in BET surface area as N percentage reaches a determined value has been reported, values above the optimum lead to a BET area decrease [35]. The mechanisms

of improved photoactivity of N doped titania are beyond the scope of this work.

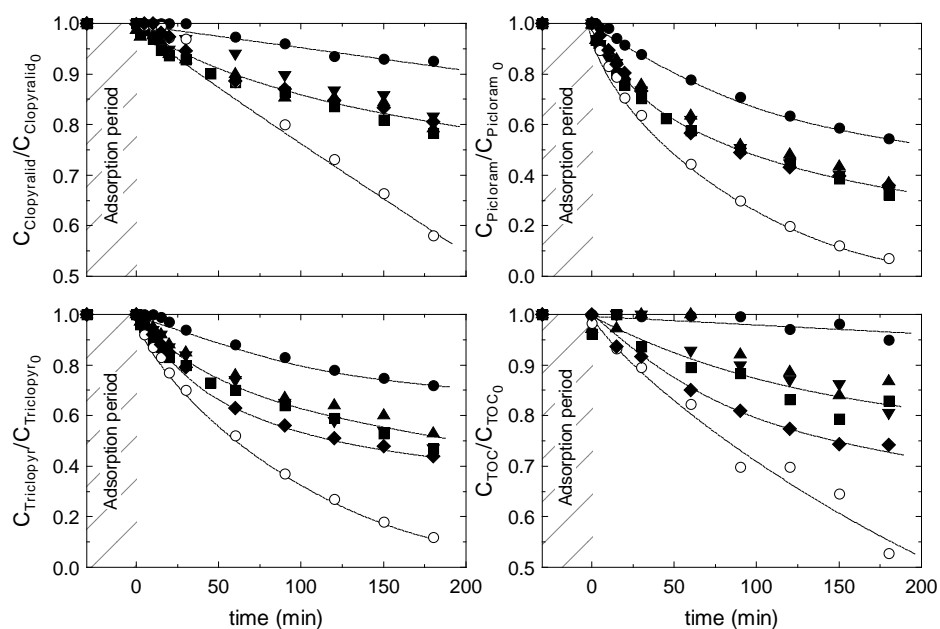


Figure 6.2 Black light photocatalysis of a mixture of clopyralid, picloram and triclopyr. Experimental conditions: $T=20^{\circ}\text{C}$, $V=1.0\text{ L}$; $I=6.86 \cdot 10^{-5}\text{ Einstein L}^{-1}\text{ min}^{-1}$; $\text{pH}=4.0$ (average value), $C_{\text{herbicide}}=5.0\text{ mg L}^{-1}$ (each), $C_{\text{catalyst}}=0.5\text{ g L}^{-1}$. Catalyst: ●, $\text{TiO}_2\text{-1:0}$; ■, $\text{TiO}_2\text{-1:0.4}$; ▲, $\text{TiO}_2\text{-1:0.8}$; ▼, $\text{TiO}_2\text{-1:1.2}$; ○, $\text{TiO}_2\text{-1:1.6}$; ◆, $\text{TiO}_2\text{-1:2}$

Under optimum conditions, after 3 h of reaction, mineralization of the herbicides was 50%. Therefore, in an attempt to improve the extent of TOC conversion, photocatalysis was carried out in the presence of ozone, leading to the photocatalytic ozonation process. For comparison purposes, single ozonation was applied first.

6.3.2. Ozonation and photocatalytic ozonation. Activity of catalyst with different Ti:N ratios

Ozonation of the herbicides mixture (Figure 6.3) confirms the recalcitrant nature of these compounds towards molecular ozone. In fact, in previous work the rate constants between ozone and the herbicides were tested and took values of $20\text{ M}^{-1}\text{ min}^{-1}$ for clopyralid and triclopyr, and $105\text{ M}^{-1}\text{ min}^{-1}$ in the case of picloram [36] TOC remains almost constant showing conversion values in the proximity of 10% after 3 h of ozonation. Dissolved ozone and at the reactor outlet were immediately detected and remained unchanged throughout the process, corroborating the slow regime developed in this

heterogeneous reaction. Accordingly, the system UVA/O₃/TiO₂ was applied using different TiO₂-x catalysts.

Figure 6.3 shows the results obtained in photocatalytic ozonation experiments. As observed, use of ozone in the presence of titania significantly increases the efficiency of herbicides removal and TOC conversion. In this case, however, with the exception of the TiO₂-1:1.6 catalyst, doping of titania particles does not necessarily enhance the rate of abatement of herbicides. Moreover, TiO₂-1:0.8 and TiO₂-1:2.0 display a worse performance than undoped TiO₂-1:0 when herbicides conversion is monitored. The best results, in terms of parent compounds elimination, were experienced with the TiO₂-1:0.4 and TiO₂-1:1.6 catalysts.

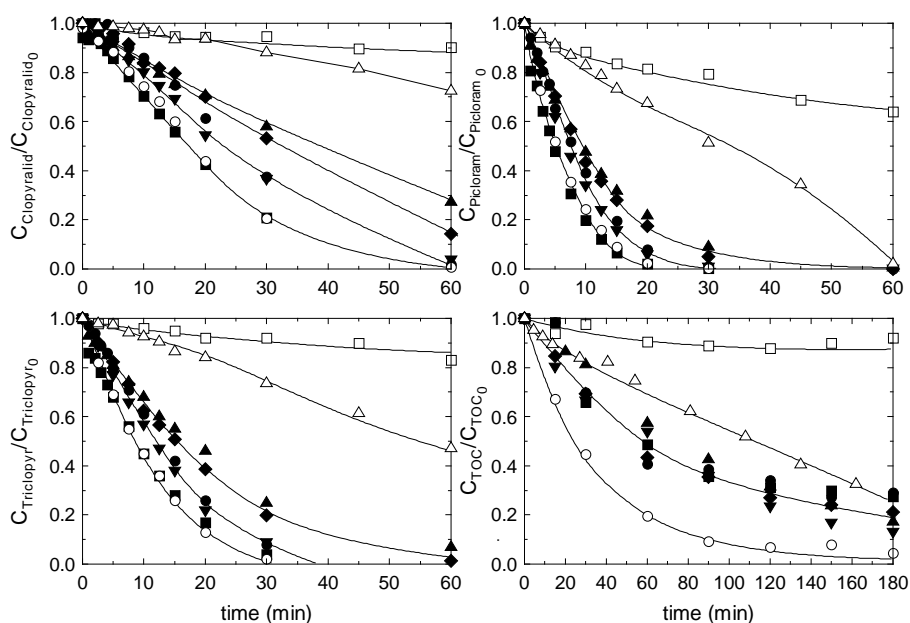


Figure 6.3 Black light photocatalytic ozonation of a mixture of clopyralid, picloram and triclopyr. Experimental conditions: $T=20^{\circ}\text{C}$, $V=1.0\text{ L}$; $I=6.86 \cdot 10^{-5}\text{ Einstein min}^{-1}\text{ L}^{-1}$; $\text{pH}=4.0$ (average value), $C_{\text{herbicide}}=5.0\text{ mg L}^{-1}$ (each), $C_{\text{Catalyst}}=0.5\text{ g L}^{-1}$. \square , Single ozonation; Δ , Photolytic ozonation. Photocatalytic ozonation: Catalyst: \bullet , TiO₂-1:0; \blacksquare , TiO₂-1:0.4; \blacktriangle , TiO₂-1:0.8; \blacktriangledown , TiO₂-1:1.2; \circ , TiO₂-1:1.6; \blacklozenge , TiO₂-1:2.

These two catalysts are capable of achieving >99% conversion of clopyralid, picloram and triclopyr in 60, 20 and 30min, respectively. After 180 min, single ozonation just led to 27, 77, and 44% conversion of the same herbicides. Again, it seems that an optimum in N doping extent does exist. Mineralization of the reaction mixture revealed the higher activity of

TiO₂_1:1.6 compared with the rest of the catalysts and, obviously, single ozonation. For instance, photocatalytic ozonation in the presence of TiO₂_1:1.6 led to 80% mineralization in roughly 60 min, while the rest of the catalysts tested required 180 min on average to achieve the same TOC conversion.

Photocatalytic ozonation in the presence of undoped titania suggests the existence of some synergistic effect when combining the UVA/TiO₂_1:1.0 and O₃ systems. This synergism is particularly visible when TOC evolution is analyzed. Hence, the UVA/TiO₂_1:1.0 system hardly achieved 5% TOC reduction while single ozonation led to just 10% of mineralization (after 180 min). Adding the TOC conversions experienced in individual systems (roughly 15%) is far away from the 80% obtained in the combined process. As stated previously, doping of the titania particles to generate the TiO₂_1:1.6 catalyst increased the final TOC removal to 95% after 180 min treatment. Synergism is also observed with the latter catalyst, experiencing TOC reductions of 10% and 45% over single ozonation and photocatalytic oxidation, respectively, after 3 h.

6.3.3. Photocatalytic ozonation. Stability and characterization of TiO₂_1:1.6 catalyst

Stability of the TiO₂_1:1.6 catalyst (the most active solid) was assessed by recycling the solid through five consecutive runs with no replacement of solid losses during the recovery stages. Recovery of the catalyst by filtration at lab scale led to significant reductions in the catalyst amount used in the following run.

Thus, catalyst concentrations in the 2nd, 3rd, 4th, and 5th runs were reduced to 66%, 46%, 30% and 20% of the amount used in the 1st experiment. As inferred from Figure 6.4, a slight decrease in herbicide removal rate was experienced after the 2nd use. However, this fact was no impediment to achieving 100% conversion of the parent compounds at similar reaction times to those obtained in the first two runs. Analogous behavior was observed when TOC conversion was considered. Hence, 90-95% mineralization of the mixture was obtained after 180 min regardless of the amount of catalyst and reuse. For comparison purposes an empirical pseudo-first-order reaction constant has been calculated and normalized to the catalyst concentration used in each run. Hence, the normalized rate constants were 0.053, 0.089, 0.0767, 0.10 and 0.14 min⁻¹ L g⁻¹, corresponding to the 1st, 2nd, 3rd, 4th and 5th reuses, respectively. These empirical reaction rates have revealed that effectively no apparent deactivation of the catalyst occurs, moreover, some

enhancement of the process can be envisaged likely due to optimization of catalyst concentration in the media. Some theoretical analysis of the reactor geometry and efficiency based on Monte Carlo simulations reveal that optimum catalyst concentration is below 0.1 g L^{-1} to achieve the maximum LVRPA (Local Volumetric Rate of Photon Absorption).

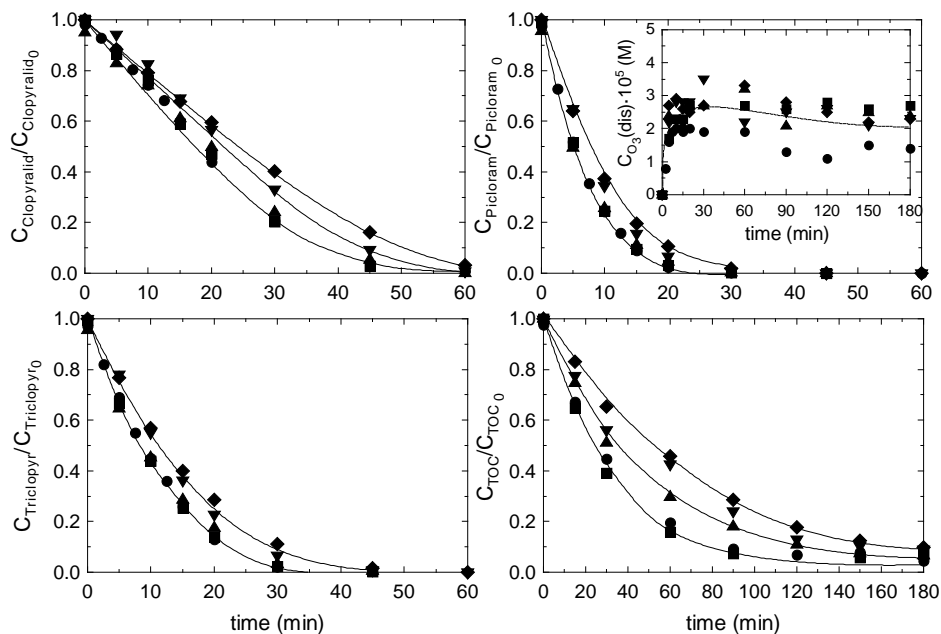


Figure 6.4 Black light photocatalytic ozonation of a mixture of clopyralid, picloram and triclopyr. Experimental conditions: $T=20^{\circ}\text{C}$, $V=1.0 \text{ L}$; $I=6.86 \cdot 10^{-5} \text{ Einstein L}^{-1} \text{ min}^{-1}$; $\text{pH}=4.0$ (average value), $C_{\text{herbicide}}=5.0 \text{ mg L}^{-1}$ (each). $C_{\text{Catalyst}}=\text{TiO}_{2_1:1.6} \text{ (g L}^{-1}\text{)}$: ●, 0.50 1st use; ■, 0.33 2nd use; ▲, 0.23 3rd use; ▼, 0.15 4th use; ◆, 0.10 5th use.

To elucidate the possible reason for the $\text{TiO}_{2_1:1.6}$ higher activity, some preliminary tests were applied to all the manufactured solids.

UV-vis absorption spectra

UV-vis absorption spectra profiles of manufactured catalysts are shown in Figure 6.5. This figure reveals no significant differences in the spectra obtained. Tauc's method to calculate the band gap energy was applied thereafter [37]. Table 6.1 displays the results obtained, confirming that the band gap energies of the solids were quite similar and do not explain the observed differences in activity.

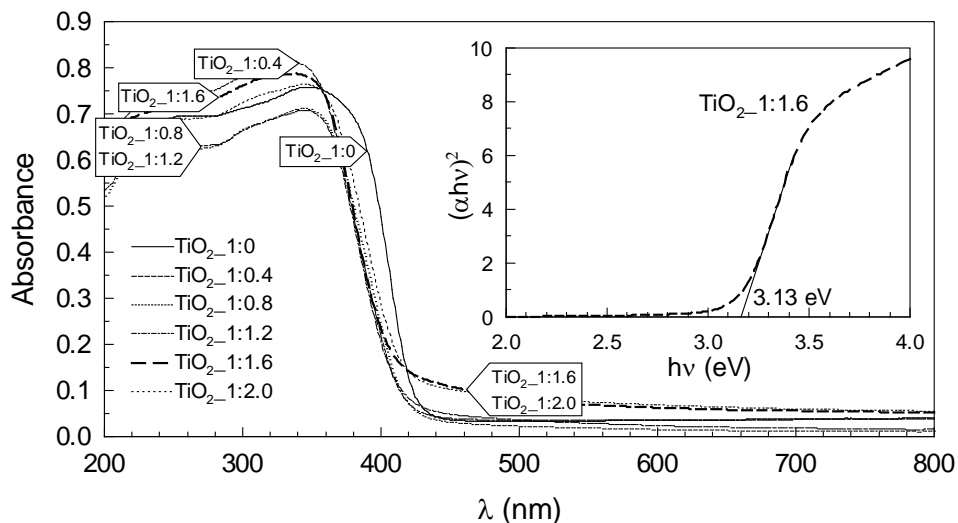


Figure 6.5 UV-vis absorption spectra profiles of catalysts and Tauc's plot corresponding to TiO₂_1:1.6 (inset figure).

Table 6.1 Characterization of manufactured catalysts

Catalyst	Band Gap (eV)	S _{BET} (m ² g ⁻¹)
TiO ₂ _1:0	2.991	14.48
TiO ₂ _1:0.4	3.145	-
TiO ₂ _1:0.8	3.095	11.34
TiO ₂ _1:1.2	3.129	-
TiO ₂ _1:1.6	3.130	34.56
TiO ₂ _1:2.0	3.075	12.98

BET area

The other parameter that has been suggested to contribute to the activity of N doped titania is the increase in surface area. Table 6.1 shows the BET area found in nitrogen adsorption experiments. The displayed results show a higher area for the TiO₂_1:1.6 catalyst that would explain its higher activity [35].

Given the high stability and activity of the TiO₂_1:1.6 catalyst, additional characterization of this solid was carried out by different techniques.

X-ray diffraction

Figure 6.6 shows the XRD pattern of TiO₂_1:1.6 as a function of temperature. As expected, according to the temperature of calcination (500°C), a 100% anatase phase diffractogram was obtained. Higher temperatures involve the partial transformation of anatase to the non-photoactive rutile [32], hence, rutile percentages of 9.4, 15.3 and 24.3% were

obtained at temperatures of 550, 600 and 700°C, respectively. The Scherrer equation was used to estimate the crystal size (D) according to:

$$D = K \frac{\lambda}{\beta \cos \theta} \quad (6.7)$$

where θ is the diffraction angle of the peak selected, β the half-height peak's width (in radians); λ the wavelength of the source of X ray applied (1.5456 Å for Cu radiation); K Scherrer's constant, which depends on the shape of the particles (value of 0.9 if spherical shape is considered). Considering the anatase peak at $2\theta = 25.4^\circ$ a value in the proximity of 13–14 nm was obtained in all diffractograms with the exception of 700°C where a higher value of 29 nm was obtained.

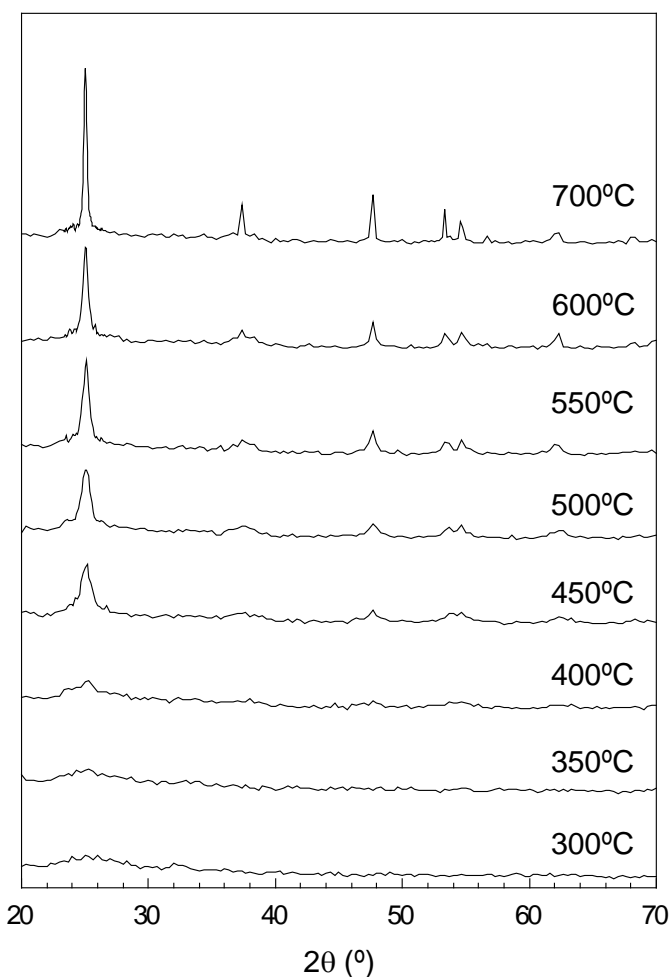


Figure 6.6 XRD pattern diffractograms of $\text{TiO}_2_{1:1.6}$ as a function of temperature

X-ray photoelectron spectroscopy

Three areas of the XPS spectrum were investigated: the Ti 2p, O 1s and N 1s regions (Figure 6.7). The binding energy of N 1s when introduced into the TiO₂ structure extends from 397 to 403 eV. In the spectra of TiO₂_1:1.6, a peak at 400.0 eV is observed.

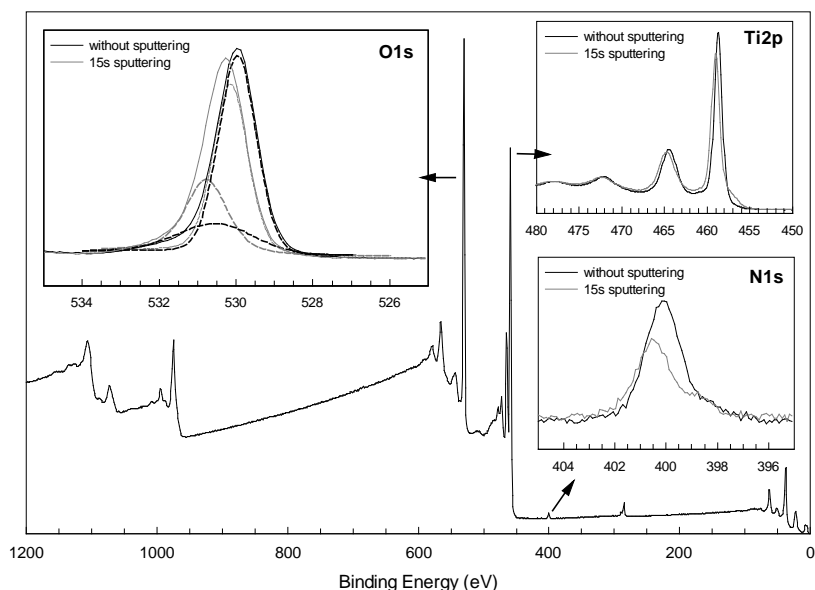


Figure 6.7 XPS spectra of fresh TiO₂_1:1.6 catalyst

Sputtering for 15 s led to cleaning of the superficial layer and the energy of the N 1s peak increased to 400.5 eV. According to the literature, this peak can be attributed to the environment O-Ti-N [33], or the states of nitrogen doped in titania might be various and coexist in the form N-Ti-O and Ti-O-N [27]. O 1s shows a certain asymmetry due to the fact that it has contributions of two peaks, located at 530 and 531 eV. The first one is characteristic of O-Ti-O linkages, while the second one is frequently attributed to O-Ti-N structure [38]. Ti 2p peak observed (results not shown) had a lower binding energy compared with O-Ti-O linkage, which is also indicative of insertion of N in the TiO₂ lattice. Nitrogen content calculated from the spectra revealed values of 1.7 and 0.96%, before and after 15 s of etching, respectively. The Shirley method was applied in order to determinate the baseline of quantified peaks.

Scanning electron microscopy/Transmission electron microscopy

SEM analysis of TiO₂_1:1.6 shows (Figure 5.8) a variety of particle sizes and shapes forming heterogeneous agglomerates. TEM images (Figure 6.8) corroborate the crystal size obtained by XRD. Some images display crystals

showing an octahedral derived shape with the appearance of rhombic {100} and hexagonal {112} faces.

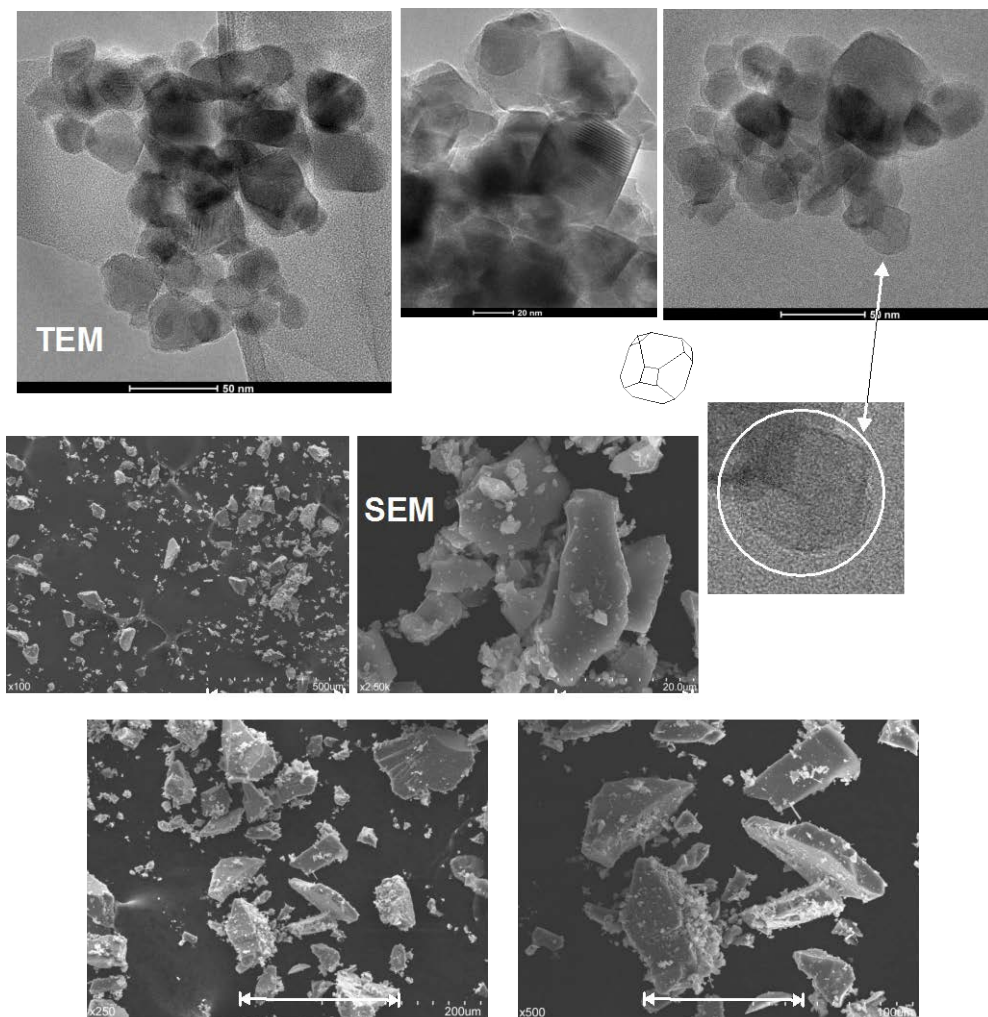


Figure 6.8 SEM/TEM images of fresh TiO_2 _1:1.6 catalyst

Thermal gravimetry-differential temperature analysis-mass spectrometry

Figure 6.9 displays the percentage of mass loss in the characterization run. A linear decrease is experienced up to 500°C. Thereafter a partial stabilization was observed. The mass loss was roughly 24%. The differential thermal analysis reveals two main exothermic variations in energy coinciding with the release of water and carbon dioxide (280 and 440°C).

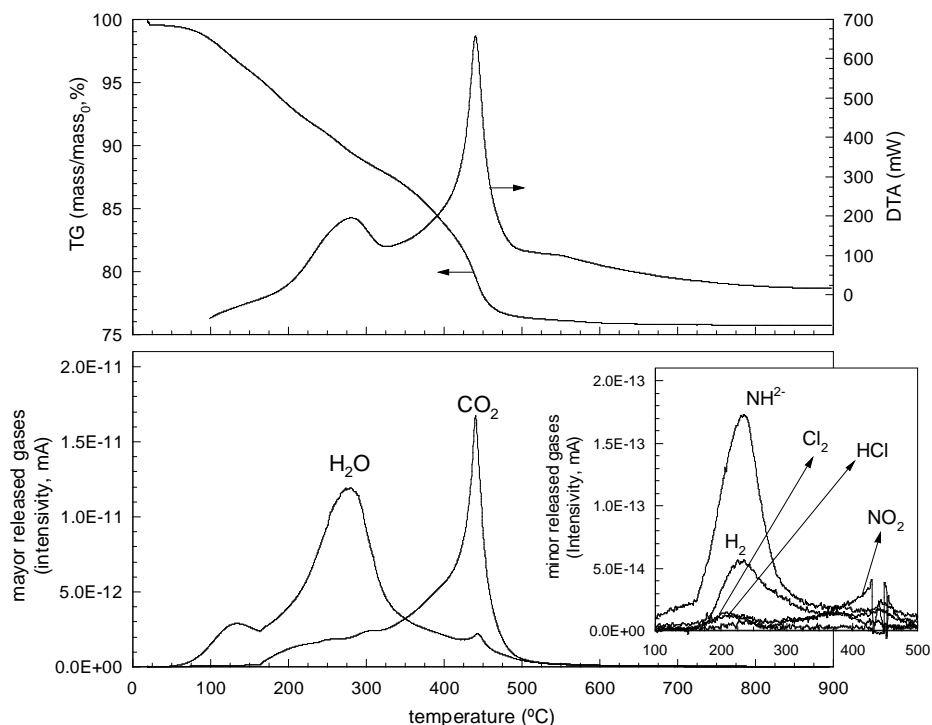


Figure 6.9 TG-DTA-MS results of fresh TiO_2 _1:1.6 catalyst

6.3.4. Photocatalytic ozonation. Toxicity and fitotoxicity of treated samples

Toxicity of the herbicide mixture after photocatalytic ozonation was first tested by monitoring BOD evolution of different samples. BOD tests were carried out by using synthetic water doped with the herbicides and being exposed to the photocatalytic ozonation process. Figure 6.10(A) shows the results. BOD evolution of synthetic water, with and without doping before being treated by photocatalytic ozonation, showed similar trends with a value after 5 days of 19 mg L^{-1} . This might be indicative of the nontoxic nature of the herbicides. Nevertheless, different results were observed after treating the initial compounds by the oxidation process. After 10 min treatment, parent compounds are completely abated, and BOD_5 dropped off to a value of 13 mg L^{-1} , which could be considered as an increase in toxicity. This effect is assumed to be due to the formation of reaction intermediates more toxic than the parent compounds. Maxima in concentrations of organic short chain acids such as acetic, propionic and oxalic acids were detected (embedded figure plot in Figure 6.10 C).

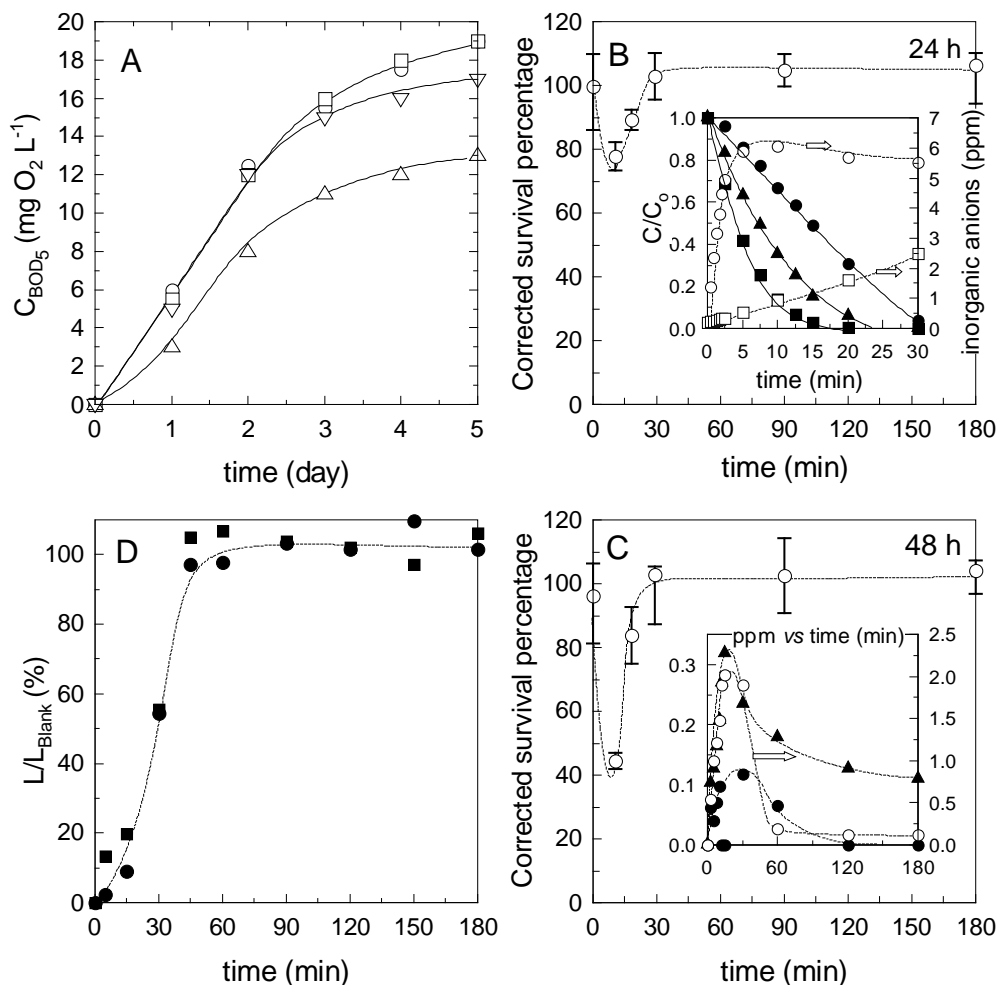


Figure 6.10 Black light photocatalytic ozonation of a mixture of clopyralid, picloram and triclopyr. Experimental conditions: $T=20^{\circ}C$, $V=1.0$ L; $I=6.86 \cdot 10^{-5}$ Einstein $L^{-1} min^{-1}$; $pH=4.0$ (average value), $C_{herbicide}=5.0$ mg L^{-1} (each). $C_{Catalyst}=0.5$ g L^{-1} TiO_2 -1:1.6. **(A)** BOD evolution in synthetic water: \circ , water without herbicides; \square , doped water with 5 mg L^{-1} in each herbicide; \triangle , doped water after 10 min of photocatalytic ozonation; ∇ , doped water after 180 min of photocatalytic ozonation. **(B)** 24 h *D. Parvula* survival percentage after different periods of photocatalytic ozonation. **(Embedded figure:** evolution of \bullet , clopyralid, \blacksquare , picloram, \blacktriangle , triclopyr, \circ , chloride, and \square , nitrate during the experiment). **(C)** 48 h *D. Parvula* survival percentage after different periods of photocatalytic ozonation. **(Embedded figure:** evolution of \bullet , acetic acid, \circ , propionic acid, and \blacktriangle , oxalic acid during the experiment). **(D)** Fitotoxicity evolution of black light photocatalytic ozonation of a mixture of clopyralid, picloram and triclopyr. \bullet , *L. Sativa*; \blacksquare , *S. Lycopersicum*.

Rupture and opening ring of the herbicides take place at an early stage of the process. Chloride profile sustains the previous hypothesis (embedded figure of plot in Figure 6.10 B). After enough time of treatment (180 min), TOC removal reaches a state value. At this point BOD₅ took a value of 17 mg L⁻¹, higher than BOD₅ at 10 min, but lower than the initial value (19 mg L⁻¹).

Since BOD is a general parameter affected by a number of variables, some additional toxicity tests considering the exposure of *D. parvula* were completed. In this case, more samples at initial stages of parent herbicides oxidation were taken and exposed to the crustacean. The first one, which corresponds to a 25% removal of the most recalcitrant herbicide (clopyralid), showed the highest mortality rate. After that, survival rate increases to almost 100% in the sample having 75% clopyralid removal, and remains constant for the rest of the treatment. Again, as BOD₅ suggested previously, a maximum of toxicity appears at the early stage of the photocatalytic ozonation process. Formation of more toxic chloride organic intermediates before the dechlorination to short-chain organic compounds can explain the results. Once the herbicides have been degraded, mortality drops off to a negligible value. It should be highlighted that this absence of toxicity corresponds with a mineralization extent up to 95%. Similar results to those previously discussed were found when fitotoxicity assays were completed (Figure 6.10 D).

6.4. CONCLUSIONS

From the results obtained in this work, the following conclusions can be drawn:

- An optimum amount of triethylamine applied in the synthesis led to the highest activity in photocatalytic oxidation trials. N doping improves titania photoactivity.
- Photocatalytic ozonation considerably improved herbicide and TOC abatement compared with photocatalytic oxidation or single ozonation.
- N doped titanium dioxide with the best photocatalytic behavior showed 100% of anatase phase with a crystal size of 13.5 nm. XPS analysis suggests the formation of O-Ti-N linkage and N content of 1%.
- Photoactivity is maintained after four consecutive runs.
- At the early stages of the herbicide photocatalytic ozonation process, toxicity suffered a significant increase. It disappeared when parent herbicides were completely abated and dechlorination completed.

Acknowledgments

The authors acknowledge the economic support received from *Gobierno de Extremadura* and *CICYT* of Spain through Projects GRU10012 and CTQ2012-35789-C02-01, respectively. Mr. Rafael Rodríguez Solís thanks *Gobierno de Extremadura*, *Consejería de Empleo, Empresa e Innovación*, and *FSE* Funds for his PhD grant (PD12058).

REFERENCES

- [1] Cox C, *Picloram herbicide factsheet*. *J Pestic Reform* 18 (1998) 13-20
- [2] Cox C, *Clopyralid herbicide factsheet*. *J Pestic Reform* 18 (1998) 15-19
- [3] Cox C, *Triclopyr herbicide factsheet*. *J Pestic Reform* 20 (1998) 12-29
- [4] Pang L, Close ME, Watt JPC, Vincent KW, *Simulation of picloram, atrazine, and simazine leaching through two New Zealand soils and into groundwater using HYDRUS-2D*. *J Contam Hydrol* 44 (2000) 19-46
- [5] Liu L-C, Dumas JA, Cacho CL, *Picloram groundwater contamination from pasture use*. *J Agric Univ P R* 81 (1997) 211-218
- [6] Elliott JA, Cessna AJ, Nicholaichuk W, Tollefson LC, *Leaching rates and preferential flow of selected herbicides through tilled and untilled soil*. *J Environ Qual* 29 (2000) 1650-1656
- [7] Diaz R, Loague K, *Assessing the potential for pesticide leaching for the pine forest areas of Tenerife*. *Environ Toxicol Chem* 20 (2001) 1958-1967
- [8] Rivas J, Gimeno G, Borralho T, Carbajo M, *UV-C photolysis of endocrine disruptors. The influence of inorganic peroxides*. *J Hazard Mater* 174 (2010) 393-397
- [9] Agustina TE, Ang HM, Vareek VK, *A review of synergistic effect of photocatalysis and ozonation on wastewater treatment*. *J Photochem Photobiol C* 6 (2005) 264-273
- [10] Fisher MB, Keane DA, Fernández-Ibáñez P, Colreavy J, Hinder SJ, McGuigan KG, Pilla SC, *Nitrogen and copper doped solar light active TiO₂ photocatalysts for water decontamination*. *Appl Catal B: Environ* 130-131 (2013) 8-13
- [11] Peláez M, Cruz AA, Stathatos E, Falaras P, Dionysiou DD, *Visible light-activated N-F-codoped TiO₂ nanoparticles for the photocatalytic degradation of microcystin-LR in water*. *Catal Today* 144 (2009) 19-25.

- [12] Choi H, Antoniou MG, Peláez M, Cruz AA, Shoemaker JA, Dionysiou DD, *Mesoporous nitrogen-doped TiO₂ for the photocatalytic destruction of the cyanobacterial toxin microcystin-LR under visible light*. Environ Sci Technol 41 (2007) 7530-7535
- [13] Sacco O, Vaiano V, Han Ch, Sannino D, Dionysiou DD, *Photocatalytic removal of atrazine using N-doped TiO₂ supported on phosphors*. Appl Catal B: Environ 164 (2015) 462-474
- [14] Vaiano V, Sacco O, Sannino D, Ciambelli P, *Photocatalytic removal of spiramycin from wastewater under visible light with N-doped TiO₂ photocatalysts*. Chem Eng J 261 (2015) 3-8
- [15] Yu J, Wang J, Zhang J, He Z, Liu Z, Ai X, *Characterization and photoactivity of TiO₂ sols prepared with triethylamine*. Mater Lett 61 (2007) 4984-4988
- [16] Westphal K, Saliger R, Jager D, Teevs L, Pruse U, *Degradation of clopyralid by the Fenton reaction*. Ind Eng Chem Res 52 (2013) 13924-13929
- [17] Özcan A, Şahin Y, Koparal AS, Oturan MA, *Degradation of picloram by the electro-Fenton process*. J Hazard Mater 153 (2008) 718-727
- [18] Huston PL, Pignatello JJ, *Degradation of selected pesticide active ingredients and commercial formulations in water by the photo-assisted Fenton reaction*. Water Res 33 (1999) 1238-1246
- [19] Rudyak SS, Solozhenko EG, Soboleva NM, Goncharuk VV, *Destruction of picloram under the effect of ozone and hydrogen peroxide*. Sov J Water Chem Technol 9 (1987) 34-37
- [20] Abramović B, Šojića D, Despotovića V, Vioneb D, Pazzib M, Csanádia J, *A comparative study of the activity of TiO₂ Wackherr and Degussa P25 in the photocatalytic degradation of picloram*. Appl Catal B: Environ 105 (2011) 191-198
- [21] Poullos I, Kositzki M, Kouras A, *Photocatalytic decomposition of triclopyr over aqueous semiconductor suspensions*. J Photochem Photobiol A: Chem 115 (1998) 175-183
- [22] Qamar M, Muneer M, Bahnemann D, *Heterogeneous photocatalysed degradation of two selected pesticide derivatives, triclopyr and daminozid in aqueous suspensions of titanium dioxide*. J Environ Manage 80 (2006) 99-106

- [23] Šojić DV, Anderluh VB, Orčić DZ, Abramović BF, *Photodegradation of clopyralid in TiO₂ suspensions: identification of intermediates and reaction pathways*. J Hazard Mater 168 (2009) 94-101
- [24] Šojić D, Despotović V, Abramović B, Todorova N, Giannakopoulou T, Trapalis C, *Photocatalytic degradation of mecoprop and clopyralid in aqueous suspensions of nanostructured N-doped TiO₂*. Molecules 15 (2010) 2994-3009
- [25] Orellana-García F, Álvarez MA, López-Ramon V, Rivera-Utrilla J, Sánchez-Polo M, Mota AJ, *Photodegradation of herbicides with different chemical natures in aqueous solution by ultraviolet radiation. Effects of operational variables and solution chemistry*. Chem Eng J 255 (2014) 307-315
- [26] Tizaoui C, Mezughi K, Bickley R, *Heterogeneous photocatalytic removal of the herbicide clopyralid and its comparison with UV/H₂O₂ and ozone oxidation techniques*. Desalination 273 (2011) 197-204
- [27] Senthilnathan J, Philip L, *Photocatalytic degradation of lindane under UV and visible light using N-doped TiO₂*. Chem Eng J 161 (2010) 83-92
- [28] Bader H, Hoigne J, *Determination of ozone in water by the indigo method*. Water Res 15 (1981) 449-456
- [29] Erdei L, Arecrachakul N, Vigneswaran S, *A combined photocatalytic slurry reactor-immersed membrane module system for advanced wastewater treatment*. Sep Purif Technol 62 (2008) 382-388
- [30] Environmental Protection Agency, *Methods for Measuring the Acute Toxicity of Effluents and Receiving Water to Freshwater and Marine Organisms*, 5th ed. Washington (2002)
- [31] Abbott WS, *A method of computing the effectiveness of an insecticide*. J Econ Entomol 18 (1925) 265-267
- [32] Carp O, Huisman CL, Reller A, *Photoinduced reactivity of titanium dioxide*. Prog Solid State Chem 32 (2004) 33-177
- [33] Cha J-A, An S-H, Jang H-D, Kim C-S, Song D-K, Kim T-O, *Synthesis and photocatalytic activity of N-doped TiO₂/ZrO₂ visible-light*. Adv Powder Technol 23 (2012) 717-723
- [34] Cong Y, Zhang J, Chen F, Anpo M, *Synthesis and characterization of nitrogen-doped TiO₂ nanophotocatalyst with high visible light activity*. J Phys Chem C 111 (2007) 6976-6982

- [35] Dhanya TP and Sugunan S, *Preparation, characterization and photocatalytic activity of N doped TiO₂*. IOSR J Appl Chem 4 (2013) 27-33
- [36] Solís RR, Rivas FJ, Gimeno O , Pérez-Bote JL, *Photocatalytic ozonation of clopyralid, picloram and triclopyr. Kinetics, toxicity and operational parameters influence*. J Chem Technol Biotechnol 91 (2016) 51-58
- [37] Tauc J, Grigorovici R, Vancu A, *Optical properties and electronic structure of amorphous germanium*. Phys Stat Sol 15 (1966) 627-637
- [38] Chen X, Burda C, *Photoelectron spectroscopic investigation of nitrogen-doped titania nanoparticles*. J Phys Chem B 108 (2004) 15446-15449

CHAPTER SEVEN

PAPER FIVE

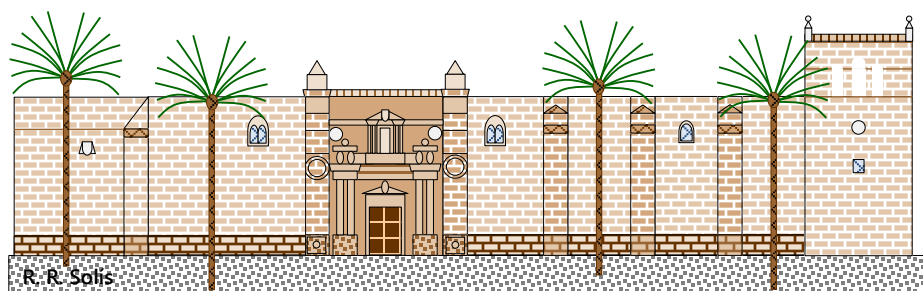
Ozonation, photocatalysis and photocatalytic ozonation of diuron. Intermediates identification

Chem Eng J 292 (2016) 72-81

Rafael R. Solís, F. Javier Rivas, Ana Martínez-Piernas, Ana Agüera

ABSTRACT. Aqueous 3-(3,4-dichlorophenyl)-1,1-dimethylurea (diuron) has been oxidized by ozonation, photocatalysis and photocatalytic ozonation. Diuron degradation takes place via radical pathway through hydroxyl radicals in those systems involving ozone. Diuron elimination in photocatalytic ozonation is not enhanced if compared to single ozonation; however, TOC removal was significantly improved. Specifically, 80% TOC removal in 2 h was reached in photocatalytic ozonation while single ozonation just led to 25% TOC reduction. Photocatalysis required 9 h to reach 25% TOC reduction. Ten transformation by-products generated during the application of the three technologies were tentatively identified by liquid chromatography-quadrupole time-of-flight mass spectrometry (LC-QTOF-MS/MS). Single ozonation and photocatalytic ozonation led to the formation and complete elimination of all by-products. Low weight carboxylic acids evolution suggests that high TOC removal in photocatalytic ozonation is linked to its capacity to oxidize small oxygenated compounds and release of inorganic chloride and nitrate. Toxicity evolution to *Vibrio fischeri* in photocatalytic ozonation displayed an increase in inhibition at the initial stages (>90% of inhibition), followed by a decrease of this parameter as the reaction progressed. The final treated sample shows a lower toxicity than the initial one (55% vs 20%).

KEYWORDS: photocatalytic ozonation, diuron, transformation products, toxicity evolution



Catedral de la Encarnación, Almería

7.1. INTRODUCTION

Intensive agriculture involves a high herbicide demand. The presence of these substances in the environment is alarmingly increasing all over the world. Since herbicides are usually persistent in soil and water, their presence supposes a potential harmful risk in natural ecosystems.

Water resources scarcity is an increasingly problem in many areas of the Earth. Recycling aqueous effluents by new treatment methods is a challenge for the scientific community. Although treating organic/inorganic pollutants by means of different technologies (usually biodegradation) is quite often viable, a variety of them, such as some pesticides, are recalcitrant to conventional biological treatments [1]. For this reason, more powerful oxidizing technologies are required.

Organochlorides are some of the most popular and widely used pesticides. They derive from chlorinated hydrocarbons. The high physical and chemical stability favor their persistence and slow biodegradability in the environment. Diuron ($C_9H_{10}Cl_2N_2O$, 3-(3,4-dichlorophenyl)-1,1-dimethylurea) works by inhibiting the photosynthesis process. Diuron is an organochloride phenylurea herbicide commonly used as pre and post emergent herbicide of a huge variety of both, crop and non-crop areas. Diuron's use is currently approved in the European Union until 2018 [2]. This herbicide, whose presence has been reported in 70% of 100 rives of 27 European Countries with a maximum concentration of $0.826 \mu\text{g L}^{-1}$ [3], appears to be moderately persistent and relatively immobile in water [4]. Moreover, because of its high toxicity, pollution due to this substance is considered as a real environmental hazard. This is evidenced by a recently launched European Directive which includes diuron in the list of priority pollutants in water treatment policy [5].

The harmful presence of phenylurea herbicides in aqueous environments has initiated a considerable research production, including ozone and advanced oxidation processes such as Fenton-based systems, photocatalysis and, ozone combined with UV radiation, catalysts or H_2O_2 [6]. Diuron ozonation has been reported in the literature as an effective technology [7]. Nevertheless, to the author's knowledge, individual diuron photocatalytic ozonation focused on the generated transformation products has not yet been reported.

Photocatalytic ozonation consists in the simultaneous application of ozone and photocatalysis. The process is presented as a promising chemical technology which reaches high mineralization rates. The combination of ozone in photocatalytic systems allows for a synergistic effect based on the high

efficient electron trapping by ozone. Additionally higher amounts of hydroxyl radicals are generated if compared to photocatalysis in the presence of oxygen alone [8]. In spite of being an effective technology, separation of catalyst from the media and energy requirements must be considered at the time of scaling up. In any case, the synergistic effect frequently observed considerably reduces the costs if compared to photocatalysis or ozonation alone [9].

In the last years, photocatalytic efforts have been focused on developing more reliable and efficient photocatalysts which can take benefit of the solar spectrum more effectively [10]. Amongst the main proposed strategies, TiO₂ metal and non-metal doping [11], coupling of oxides to TiO₂ [12], photocatalysts alternative to TiO₂ and supported or easily removable solids [9] and [13] can be listed. In this work, a lab manufactured N-doped titania has been used. N doping improvements on photoactivity and characterization of the solid have previously been studied in-depth in a mixture of three pyridine based herbicides, under photocatalysis and photocatalytic ozonation processes [14]. Moreover, N-doping may be considered as a starting point in catalyst recovering due to the increase in particle size. A higher particle diameter, if compared to commercial formulas, makes easier the recovering process from the effluent. Ozonation and photocatalysis of diuron have been compared to photocatalytic ozonation under UVA radiation when required (maximum of emission at 365 nm).

The aim of the present work has been focused on the identification of the main transformation byproducts formed in photocatalytic ozonation and comparison to those generated under single ozonation or photocatalysis. Final oxidation organic acids evolution has also been monitored in order to explain TOC removal extents. Toxicity evolution to bacteria *Vibrio fischeri* has been studied for the three processes and compared to results of intermediates, organic acids released and TOC evolution.

7.2. MATERIALS AND METHODS

7.2.1. Chemicals

Analytical standard diuron was acquired from Sigma-Aldrich (>98%) and used as received in all experiments. HPLC-grade acetonitrile from VWR Chemicals was used in the HPLC system. Ionic chromatography solutions were prepared from Sigma-Aldrich reagents. Titanium isopropoxide (Sigma-Aldrich, >97%), trimethylamine (Panreac, 99.5%) and HCl (Fischer Scientific, 37%) were used in N doped titania photocatalyst synthesis. Potassium indigo trisulfonate, used in dissolved ozone monitoring, was purchased from Sigma-Aldrich

(99%). Ultrapure water used in all trials was produced in a Milli-Q® academic (Millipore) system.

Chemicals for mobile phase in LC-QTOF-MS analysis (water, >99.9% and acetonitrile, >99.9%) were LC-MS CROMASOLV® from Fluka. Formic acid was used (98%, LC-MS from Fluka) to acidify water.

7.2.2. Experimental setup and procedure

Photoreaction installation was equipped with a 1.0 L volume cylindrical reactor made of borosilicate glass. The reactor was placed into a cylinder pipe (54 cm of height and 31 cm of external diameter) equipped with four black light lamps of 41 cm of length (LAMP15TBL HQPOWER™ 15 W emitting in the range 350–400 nm, maximum at 365 nm). The inner surface was covered with aluminum foil in order to enhance photons reflection. UVA photon flow entering the reaction system was calculated in a previous work by means of ferrioxalate actinometry. Values of 1.77, 3.26, 5.13 and $6.86 \cdot 10^{-5}$ Einstein $L^{-1} \text{ min}^{-1}$ when 1, 2, 3 and 4 lamps, were reported [15]. Additionally, when the aluminum foil covering the internal walls of the installation was substituted by a black surface, the intensity (4 lamps switched on) decreased to $3.60 \cdot 10^{-5}$ Einstein $L^{-1} \text{ min}^{-1}$.

In a typical experiment, 30 L h^{-1} gas flow rate of oxygen, or an oxygen-ozone mixture, was fed to the photoreactor system through a stainless steel diffuser. Solid photocatalyst was added 30 min before starting the reaction, in order to reach the possible adsorption equilibria onto its surface. Samples at different times were extracted and filtered by means of Millex-HA filters (Millipore, $0.45 \mu\text{m}$) before analysis.

Ozone was continuously generated by electrical discharges of pure oxygen in a Sander Laboratory Ozone Generator. An Anseros Ozomat ozone analyzer, the measurement based on 254 nm absorbance, was used to monitor ozone gas phase concentration.

7.2.3. Photocatalyst synthesis

N doped titania photocatalyst was prepared applying a sol-gel method followed by thermal treatment and calcination according to literature and previous works [16] and [14]. Briefly, 12 mL of titanium (IV) isopropoxide were dissolved in 100 mL of ethanol. Next, 9 mL of triethylamine was added. Afterwards, titania was precipitated using 100 mL of HCl 0.1 M. The suspension was thermally treated at 80°C for 12 h. The final residue was dried overnight at 100°C and calcined at 500°C for 4 h (initial ramp of $10^\circ\text{C min}^{-1}$).

7.2.4. Analytical methods

Diuron was analyzed by an Agilent 1100 (Hewlett-Packard) high performance liquid chromatography with UV detection (HPLC-UV). The column used was a Kromasil 100 5C18 (5 μm , 2.1 \times 150 mm). 0.1% H_3PO_4 acidified water (A) and acetonitrile (B) were the mobile phases used. An elution gradient from 50% to 65% of B in 6 min was applied. UV detection was conducted at 243 nm.

Liquid chromatography coupled to a quadrupole time-of-flight mass spectrometer (LC-QTOF-MS) was used to identify and monitor transformation products generated in single ozonation, photocatalytic oxidation and photocatalytic ozonation processes. Chromatographic separation was carried out in an Agilent 1260 Infinity system equipped with a Poroshell 120 EC-C18 (2.7 μm , 4.6 \times 50 mm) column. Pure Milli-Q[®] water (phase A) or acidified water with 0.1% formic acid (for negative and positive ionization modes, respectively), and acetonitrile (phase B) were used as mobile phases. Elution gradient at 0.4 mL min^{-1} flow rate went from 10% A (1 min) to 100% B in 10 min, and kept thereafter for 5 min before returning to initial conditions. Injection was completed with 10 μL . HPLC system was connected to a hybrid quadrupole time-of-flight mass spectrometer TRIPLE TOF 5600 + system (AB Sciex) with an electrospray interface (ESI). Both ESI (+) and ESI (-) modes were considered for unknown transformations products (TPs) identification. The equipment worked via TOF MS survey scan followed by four IDA (Information Dependent Acquisition) TOF MS/MS scans. Alternatively to IDA mode, other tools like 'mass defect filters' and 'include list' for potential candidates were used in order to focus and shorten TPs identification during the acquisition process. Besides, for low intensity TPs, the SWATH[®] tool was considered to obtain MS/MS fragmentation patterns. Scanned mass range was from $m/z = 50$ to 800 Da, either in TOF or MS/MS experiments. An accumulation time of 100 ms was used in each scan. IDA criteria considered dynamic background subtraction. Collision energy of 30 eV with a ± 10 eV spread was used in MS/MS fragmentation. Diverse AB SCIEX software (Analyst TF 1.5, PeakViewTM 2.2 and MasterView 1.1) was used to record and process LC-QTOF-MS data. MasterView processing was also enhanced with potential candidates lists based on computational (*in silico*) prediction tools like University of Minnesota Pathway Prediction System and PathPred [17].

Ionic short chain organic and inorganic anions were monitored by ionic chromatography using a Metrohm 881 Compact Pro ionic connected to MagIC NETTM software.

Total organic carbon (TOC) was determined by a Shimadzu TOC 5000A analyzer. Aqueous dissolved ozone was measured by Bader and Hoigné method [18], the analysis is based on 5,5,7-indigo-trisulfonate decolouration, spectrophotometrically determined at 600 nm.

7.2.5. Ecotoxicity assays

Toxicity evolution was evaluated by means of the bioluminescence bacterium *Vibrio fischeri* inhibition to reaction samples. Microtox 500 was used at room temperature to quantify light emitting decay when exposed to reaction samples extracted at different oxidation times. Luminescence decay was recorded at different exposure times (5, 15 and 30 min) and inhibition percentages were calculated.

7.3. RESULTS

7.3.1. Efficiency of ozonation, photocatalysis and photocatalytic ozonation

Some preliminary experimental series were conducted to assess the efficacy of different oxidation systems on both, diuron and TOC removal. Additionally, the effect of different catalysts (doped, undoped and commercial TiO_2) was also investigated. Experimental conditions such as catalyst load and ozone dose have been chosen according to previous literature [19]. Figure 7.1 shows the results obtained.

Figure 7.1 reveals some interesting aspects. Hence, no appreciable difference in diuron conversion was experienced in runs conducted in the presence of ozone. Single ozonation, catalytic ozonation and photocatalytic ozonation led to similar diuron depletion rates. However, contrarily to the first though, in these systems diuron (and likely TOC) is mainly removed by the action of hydroxyl radicals generated after ozone decomposition. Some simple calculations could corroborate the previous hypothesis.

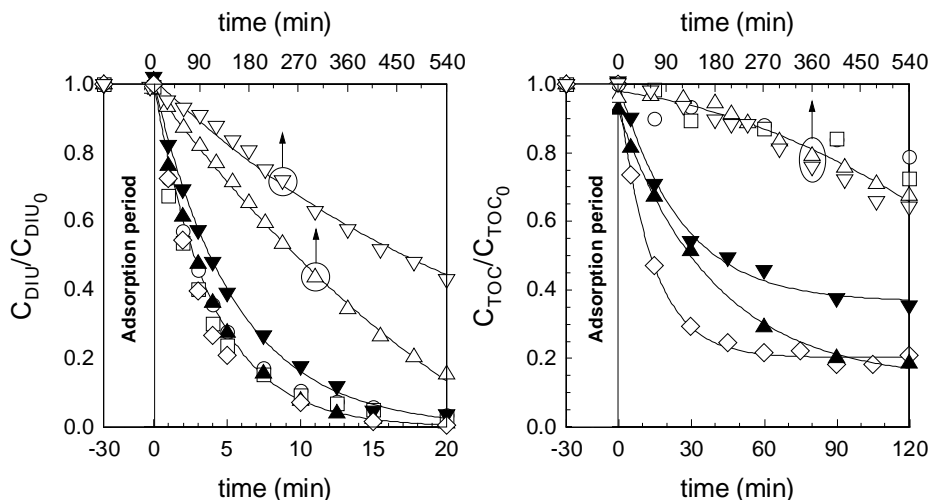


Figure 7.1 Normalized concentration of diuron (left) and TOC removal (right) evolution with time under diverse technologies. Experimental conditions: $V=1.0$ L; $C_{DIU,0}=10$ mg L⁻¹; $Q_G=30$ L h⁻¹; $C_{O_3inlet}=10$ mg L⁻¹ (if applied); $C_{catalyst}=0.5$ g L⁻¹; $pH_0=5.6-6.0$ ○, ozonation; □, catalytic ozonation; ▲, photocatalytic ozonation with N doped TiO₂; ▼, photocatalytic ozonation with undoped TiO₂; ◇, photocatalytic ozonation with Degussa P25 TiO₂; △, photocatalysis with N doped TiO₂; ▽, photocatalysis with undoped TiO₂

If the heterogeneous reaction develops in the slow regime, the following rate expression can be applied:

$$-\frac{dC_{DIU}}{dt} = k_{O_3} C_{DIU} C_{O_3d} + k_{\bullet OH} C_{DIU} C_{\bullet OH} \quad (7.1)$$

where k_{O_3} and $k_{\bullet OH}$ are the second order rate constants of the reactions between diuron and ozone and hydroxyl radicals, respectively. The Hatta number was thereafter calculated to estimate the regime of the reaction. Hatta number (Ha) is defined as:

$$Ha = \frac{\sqrt{C_{DIU} k_{O_3} D_{O_3}}}{k_L} \quad (7.2)$$

D_{O_3} stands for ozone diffusivity in water and k_L is the individual mass transfer coefficient in the liquid phase. Values used to calculate Ha were $D_{O_3} = 1.7 \cdot 10^{-9}$ m² s⁻¹ [20] and $k_L = 5 \cdot 10^{-5}$ m s⁻¹, typical of bubble contactors. When $Ha < 0.03$ slow regime kinetic is developed. If only the reaction of diuron with molecular ozone took place, which can experimentally be tested adding a

hydroxyl radical inhibitor, such as *tert*-butyl alcohol, equation 7.1 would be reduced to:

$$-\frac{dC_{\text{DIU}}}{dt} = k_{\text{O}_3} C_{\text{DIU}} C_{\text{O}_3} \quad (7.3)$$

Since ozone concentration was experimentally measured, equation 7.3 could be numerically solved by applying the simple Euler method:

$$C_{\text{DIU}}^{t+1} = C_{\text{DIU}}^t - (k_{\text{O}_3} C_{\text{DIU}}^t C_{\text{O}_3}^t) \Delta t \quad (7.4)$$

In the previous expression, ozone concentration was adjusted to a third order polynomial leading to:

$$C_{\text{DIU}}^{t+1} = C_{\text{DIU}}^t - (k_{\text{O}_3} C_{\text{DIU}}^t [at^3 + bt^2 + ct + d]) \Delta t \quad (7.5)$$

Figure 7.2 shows the experimental evolution of diuron in absence and presence of *tert*-butyl alcohol. A value of $k_{\text{O}_3} = 19.2 \pm 1.1 \text{ M}^{-1} \text{ s}^{-1}$ ($R^2 > 0.99$) was obtained by considering the ozonation in presence of *tert*-butyl alcohol, where H_a value was always below 0.03. Other authors have reported similar kinetic rate constant values, $14.7 \text{ M}^{-1} \text{ s}^{-1}$ [21] and $16.5 \text{ M}^{-1} \text{ s}^{-1}$ [22], evaluated under competition kinetic methods. As observed from Figure 7.2, the radical pathway of diuron oxidation plays an important role under the operating conditions used in this study.

Moreover, since diuron conversion in the absence of *tert*-butanol does not depend on initial concentration, Figure 7.2 suggests that the concentration curves obey first order kinetics. First order kinetics can be obtained provided that $k_{\text{O}_3} C_{\text{DIU}} C_{\text{O}_3} \ll k_{\cdot\text{OH}} C_{\text{DIU}} C_{\cdot\text{OH}}$ and $C_{\cdot\text{OH}}$ is kept constant during the process, i.e. quasi steady state conditions in hydroxyl radicals concentration applies. Accordingly, equation 7.1 was now solved optimizing the $C_{\cdot\text{OH}}$ to minimize the differences between experimental and calculated DIU depletion profiles. A steady state hydroxyl radical concentration of $7.1 \cdot 10^{-13} \text{ M}$, assuming $k_{\cdot\text{OH}} = 6.6 \cdot 10^9 \text{ M}^{-1} \text{ s}^{-1}$ [22], was found to acceptably model the process. This result allows for elucidating the percentage of indirect diuron removal due to hydroxyl radicals as the ratio:

$$\eta_{\cdot\text{OH}} = \frac{k_{\cdot\text{OH}} C_{\cdot\text{OH}}}{k_{\text{O}_3} C_{\text{O}_3} + k_{\cdot\text{OH}} C_{\cdot\text{OH}}} \times 100 \quad (7.6)$$

This ratio had a minimum around 99% when ozone concentration reached its maximum but DIU conversion was above 99% (see Figure 7.2) which is similar and consistent with previous ozonation works [7].

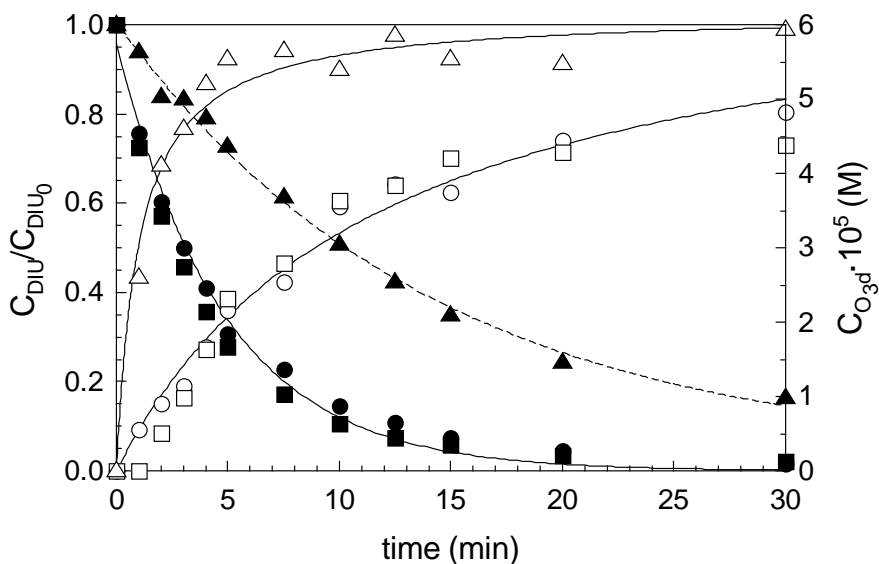


Figure 7.2 Ozonation of diuron. Experimental conditions: $V=1.0$ L; $Q_g=30$ L h^{-1} $C_{O_3inlet}=10$ mg L^{-1} , $pH_0=5.6-6.0$. Ozonation: ●, $C_{DIU,0}=5$ mg L^{-1} ; ■, $C_{DIU,0}=10$ mg L^{-1} . Ozonation with *tert*-butyl alcohol: ▲, $C_{DIU,0}=10$ mg L^{-1} and $C_{t-BOH} = 10^{-2}$ M. Empty symbols correspond to dissolved ozone concentration (C_{O_3d}). Solid lines: normalized diuron model concentration and 3rd order polynomial representing dissolved ozone. Dashed line: normalized diuron model concentration with no radical contribution.

As DIU was mainly eliminated by hydroxyl radicals, photocatalytic ozonation would have been expected to enhance the DIU depletion rate; however, this was not the case. Previous results indicate that hydroxyl radicals generated in the presence of ozone are sufficient to degrade diuron and additional active species from the photocatalytic system do not play a significant role in diuron conversion. Nevertheless, substantial differences were experienced when analyzing TOC results. Figure 7.1 shows a poor 25% mineralization when O_3 or $O_3/N-TiO_2$ was applied for 2 h. Photocatalysis could achieve similar results only after 9 h. Mineralization, however, reached an outstanding (if compared to the rest of systems) 80% after 120 min when photocatalytic ozonation was used. A synergistic effect could therefore be obtained when simultaneously applying the photocatalysis in the presence of ozone. Ozone might improve photocatalytic systems by trapping photo-generated electrons, avoiding, therefore, the undesirable hole-electron

recombination. Additionally, after electron trapping, more active species (mainly radicals) are generated [8]. The extent of synergism can be calculated from:

$$\Lambda_{\text{Synergism}} = \frac{k_{\text{PhotCat-O}_3} - [k_{\text{Ozonation}} + k_{\text{PhotCat}}]}{k_{\text{PhotCat-O}_3}} \times 100 \quad (7.7)$$

where $k_{\text{PhotCat-O}_3}$, $k_{\text{Ozonation}}$ and k_{PhotCat} are empirical pseudofirst order rate constants corresponding to photocatalytic ozonation, single ozonation and photocatalysis, respectively. TOC removal pseudo first order rate constants values obtained from Figure 7.1 were, when N-TiO₂ was applied, $1.66 \cdot 10^{-2} \text{ min}^{-1}$ ($R^2=0.997$), $1.90 \cdot 10^{-3} \text{ min}^{-1}$ ($R^2=0.995$) and $0.8 \cdot 10^{-3} \text{ min}^{-1}$ ($R^2=0.992$), for $k_{\text{PhotCat-O}_3}$, $k_{\text{Ozonation}}$ and k_{PhotCat} respectively. Synergism percentage was calculated to be 83.7%.

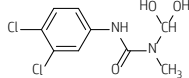
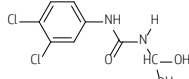
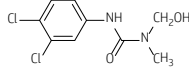
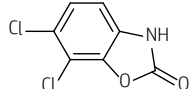
Moreover, Figure 7.1 shows that N doping of TiO₂ improves photoactivity in the photocatalytic ozonation process. Although Figure 7.1 shows no significant differences in diuron removal for undoped and doped catalyst, N-TiO₂ led to higher mineralization rates than undoped TiO₂. Undoped titania achieved 40% TOC reduction after 180 min while N doped TiO₂ led to 80% under the same operating conditions. Physical properties of solids and its photoactivity behavior have previously been discussed [14]. Commercial P25 also exhibits 80% of mineralization.

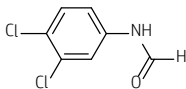
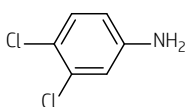
After assessing the efficiency of the different systems under study, in the next stage an attempt was conducted to identify some of the most important transformation products (TPs) generated during their application.

7.3.2. Identification of TPs by LC-QTOF-MS/MS and ionic chromatography

In this work, 10 compounds have been tentatively identified by LC-QTOF-MS/MS. Table 7.1 summarizes, organized in increasing experimental accurate mass value, some of their characteristics such as generating system, retention time and elemental composition of the protonated/deprotonated ions and their fragment ions, obtained by ESI (+) or ESI (-) and Rings plus Double Bonds Equivalent (RDBE).

Table 7.1 Proposed intermediates found by LC-QTOF-MS/MS after diuron oxidation by ozone, photocatalysis and photocatalytic ozonation

Transformation Product	Oxidation Process	Retention time (min)	Experimental Exact Mass (error, ppm)	Ion formula, [M+H] ⁺	Ion formula, [M-H] ⁻	RDBE
	O ₂ /UVA/CAT	9.20	262.9996 (2.19)		C ₉ H ₉ Cl ₂ N ₂ O ₃ ⁻	5.0
	O ₃		216.9940 (2.10)		C ₈ H ₇ Cl ₂ N ₂ O ⁻	5.0
	O ₃ /UVA/CAT		159.9726 (3.25)		C ₆ H ₄ Cl ₂ N ⁺	4.0
TP2			250.9985 (-2.1)	C ₈ H ₈ Cl ₂ N ₂ O ₃ ⁺		5.0
	O ₃	10.64	159.9731 (6.4)	C ₆ H ₄ Cl ₂ N ⁺		5.0
TP3			249.0192 (-2.2)	C ₉ H ₁₁ Cl ₂ N ₂ O ₂ ⁺		5.0
	O ₂ /UVA/CAT	10.63				
	O ₃ /UVA/CAT		159.9715 (-3.6)	C ₆ H ₄ Cl ₂ N ⁺		5.0
TP4	O ₂ /UVA/CAT	10.42	244.9890 (2.21)		C ₉ H ₇ Cl ₂ N ₂ O ₂ ⁻	6.0
			216.9941 (2.56)		C ₈ H ₇ Cl ₂ N ₂ O ⁻	5.0
			187.9675 (2.69)		C ₇ H ₄ Cl ₂ NO ⁻	5.0
	O ₃ /UVA/CAT	10.45	159.9726 (3.25)		C ₆ H ₄ Cl ₂ N ⁺	4.0
			58.0298 (8.80)		C ₂ H ₄ NO ⁻	
			247.0812 (1.3)	C ₉ H ₉ Cl ₂ N ₂ O ₂ ⁺	6.0	
DIU	O ₂ /UVA/CAT	9.62	123.9968 (11.3)		C ₆ H ₅ ClN ⁺	4.0
			60.0444 (-8.9)		C ₂ H ₆ NO ⁺	1.0
			231.0097 (2.2)		C ₉ H ₉ Cl ₂ N ₂ O ⁻	5.0
	O ₃	9.58	185.9519 (3.0)		C ₇ H ₂ Cl ₂ NO ⁻	5.0
			149.9744 (-1.2)		C ₇ HCINO ⁻	5.0
			233.0243 (-2.3)	C ₉ H ₁₁ Cl ₂ N ₂ O ⁺	5.0	
TP5	O ₂ /UVA/CAT	9.20	187.9664 (-3.2)		C ₇ H ₄ Cl ₂ NO ⁺	5.0
			159.9715 (-3.6)		C ₆ H ₄ Cl ₂ N ⁺	4.0
			72.0444 (-7.5)		C ₃ H ₆ NO ⁺	2.0
	O ₃ /UVA/CAT	9.27	216.9941 (2.56)		C ₈ H ₇ Cl ₂ N ₂ O ⁻	5.0
			159.9726 (3.2)		C ₆ H ₄ Cl ₂ N ⁺	4.0
			219.0081 (-4.9)		C ₈ H ₉ Cl ₂ N ₂ O ⁺	5.0
TP6	O ₂ /UVA/CAT	6.44	161.9869 (-5.2)		C ₆ H ₆ Cl ₂ N ⁺	4.0
			127.0183 (-4.5)		C ₆ H ₆ ClN ⁺	4.5
			213.0425 (-2.7)		C ₉ H ₁₀ ClN ₂ O ₂ ⁻	5.0
	O ₃	6.59	167.9858 (3.4)		C ₇ H ₃ ClNO ₂ ⁻	6.0
			139.9909 (4.2)		C ₆ H ₃ ClNO ⁻	N/A
			132.0091 (4.1)		C ₇ H ₂ NO ₂ ⁻	N/A
TP7	O ₂ /UVA/CAT	1.44	215.0582 (-1.1)		C ₉ H ₁₂ ClN ₂ O ₂ ⁺	5.0
			126.9945 (-4.5)		C ₆ H ₄ ClO ⁺	4.0
			72.0440 (-13.0)		C ₃ H ₆ NO ⁺	1.0
	O ₃	1.44	203.0662 (-2.9)		C ₇ H ₁₁ N ₂ O ₅ ⁺	4.0
			185.0566 (1.98)		C ₇ H ₉ N ₂ O ₄ ⁺	3.0
			157.0604 (-5.8)		C ₆ H ₉ N ₂ O ₃ ⁺	3.0
TP8	O ₂ /UVA/CAT	9.54	72.0462 (17.5)		C ₃ H ₆ NO ⁺	2.0
			201.94681 (9.1)		C ₇ H ₂ Cl ₂ NO ₂ ⁻	6.0
			165.9701 (3.12)		C ₇ HCINO ₂ ⁻	N/A

TP9		O_2 /UVA/CAT O_3 O_3 /UVA/CAT	10.44	187.9675 (2.7) 159.9726 (3.2) 116.0142 (4.8)	$C_7H_4Cl_2NO^-$ $C_6H_4Cl_2N^-$ $C_7H_2NO^-$	5.0 4.0 N/A
TP10		O_2 /UVA/CAT O_3 O_3 /UVA/CAT	9.23	159.9726 (1.9) 123.9960 (4.8)	$C_6H_4Cl_2N^-$ $C_6H_3ClN^-$	4.0 5.0

Diuron and some of their TPs were identified in both ESI (-) and ESI (+) modes. From the $[M-H]^-$ ion two fragments were obtained corresponding to the loss of the $-NH(CH_3)_2$ group and further chloride release from the aromatic ring. From the $[M-H]^+$ three fragments were detected, again the loss of the $-NH(CH_3)_2$ group and the two moieties resulting from breakage of the $-CO-NH(CH_3)_2$ side chain. This MS/MS fragmentation pattern may be useful to interpret where the initial molecule has easiness to be oxidized since this are the more likely bounds to be broken by oxidation processes [23].

The first transformation product TP1 was given an ion formula $[C_9H_9Cl_2N_2O_3]^-$. Figure 7.3 shows the product ion spectra and tentative fragment ion structures of some TPs found in this investigation. This molecule could be the result of two hydrogen abstractions by hydroxyl radicals present in the three investigated systems. Hydroxylation of diuron has been reported to occur in photocatalytic systems both in the aromatic ring and $-CH_3$ groups [24] and [25]. However, fragmentation of the precursor led to the loss of a $-CH(OH)_2$ group and further release of the $-CO-NHCH_3-CH(OH)_2$ moiety, suggesting that hydroxyl attack has occurred in one of the external methyl chains. The proposed structure of this transformation product has also been reported in the photo Fenton treatment of a mixture of diuron and linuron [26]. Attack of hydroxyl radicals to N-methylated derivatives of formamide and acetamide has been reported to occur by abstraction of hydrogen from the methyl group [27].

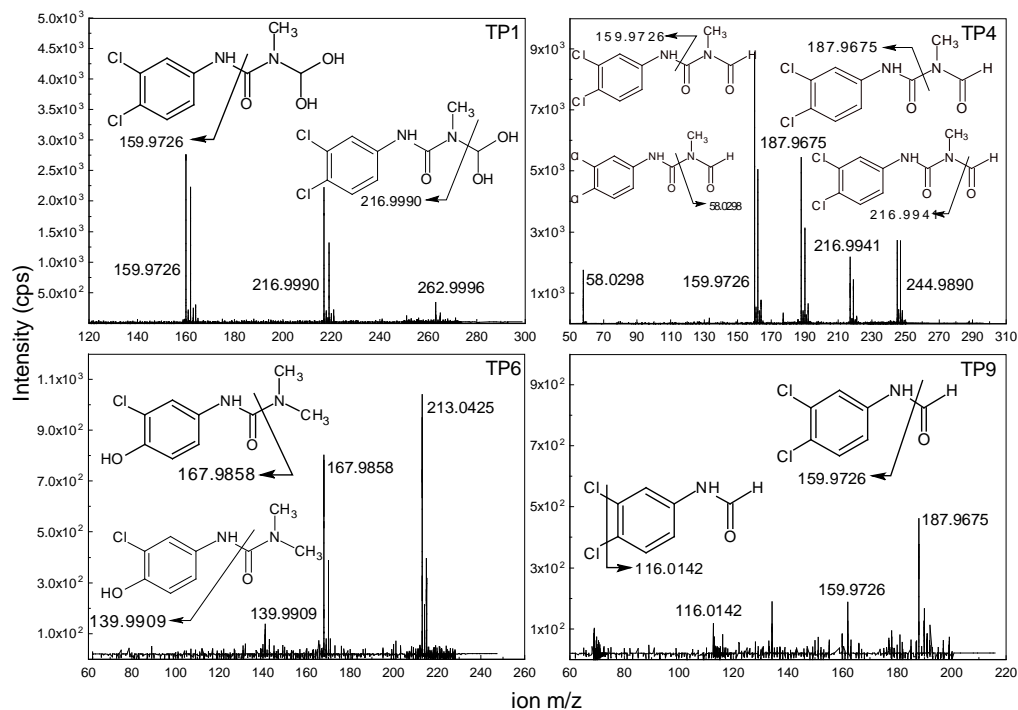


Figure 7.3 MS/MS fragmentation pattern spectra and fragment ion structures of some TPs found in this investigation in ESI (-)

TP2 presents an ion formula $[C_8H_8Cl_2N_2O_3]^+$ obtained in ESI (+) mode. It would result from demethylation of TP1 and further release of a molecule of formaldehyde. Fragmentation of TP2 suggests the presence of the dichlorophenyl structure (loss of the $-CO-NH-CH(OH)_2$ group). The proposed formula would be 3-(3,4-dichlorofenil)-1,1-dihydroxy urea. This compound has also been proposed as an intermediate in the photo Fenton process [26]. In this investigation TP2 was only detected when single ozonation was used. TP2 is also likely to be generated in the photocatalytic ozonation but it must be instantaneously removed from the reaction media, so it could not be detected.

TP3 was identified in those systems using radiation. The ion formula of this compound, $[C_9H_{11}Cl_2N_2O_2]^+$, maintains the same number of carbons than the parent herbicide. Fragmentation of the precursor leads to the detection of an m/z moiety corresponding to the dichloroaniline ion. Accordingly, loss of a $-CO-N(CH_3)CH_2OH$ group is suggested. TP3 formation is previous to TP1, since hydroxylation of methyl group takes place in two steps. The presence of this structure in the photo Fenton and photocatalytic systems has been reported [24], [26] and [28].

TP4 led to 4 fragments in ESI (-) and 2 fragments in ESI (+) modes. The precursor was tentatively assigned in ESI (-) as $[C_9H_7Cl_2N_2O_2]^-$ (or $[C_9H_9Cl_2N_2O_2]^+$ in ESI (+) mode). Fragments in ESI (-) mode indicated losses of $-CO$, $-N(CH_3)CO$ and $-CON(CH_3)CO$ (see Figure 7.3). TP4 is the main byproduct of diuron oxidation detected in photocatalytic [24] and [28], photoFenton [26] and [28] and ozonation [29] and [30] systems.

TP5 was identified in ESI (+) and ESI (-) modes, in both cases fragmentation led to the release of the $-CONHCH_3$ group. The proposed structure of this transformation product is likely to be the result of diuron demethylation, already reported in all the cited works dealing with identification of byproducts of diuron.

TP6 was the only transformation product suggesting the hydroxylation of the aromatic ring by substitution of one of the chloride groups in the parent herbicide. This hypothesis is substantiated by the analysis of the fragments generated from the precursor (see Figure 7.3). Hence, in ESI (-) mode the precursor $[C_9H_{10}ClN_2O_2]^-$ exhibits the typical loss of the $-NH(CH_3)_2$ group, followed by losses of the $-CO$ group or the HCl neutral loss. The absence of the ion 159.9715 ($C_6H_4Cl_2N^+$) found in the rest of TPs that still maintain the dichloroaniline structure, which also indicates the breakage of the ring.

TP7 was only detected in the ozonation process, being the unique transformation product resulting from the aromatic ring opening. Fragmentation of TP7 leads to the release of H_2O , $-COOH$ and $-CO-N(CH_3)_2$ groups. The lower retention time and RDBE value compared to the rest of precursors is consistent with the increased polarity of the proposed structure confirming the suggested structure. No bibliographic reference could be found for this compound. The proposed structure indicates a high degree of oxidation with two acidic groups located in the opened ring (see Table 7.1). It is noteworthy to say that the side chain bounded to the aromatic ring in the original diuron molecule is kept unchanged in TP7, suggesting that multiple hydroxyl attack to the aromatic ring has previously occurred. This is substantiated by a high release of Cl^- during ozonation process (see below in Figure 7.6).

TP8 was only detected in the photocatalytic systems. Moreover, TP8 (together with TP4) accumulates in the reaction media after 540 min of photocatalysis treatment showing a high intensity. TP8 involves the release of one molecule of dimethylamine (or *N,N*-dimethylhydroxylamine) from diuron and further formation of an oxazole like ring. No reference has reported the

formation of this compound; however two ring transformation products have been suggested elsewhere [31].

TP9 structure is the result of the release of the dimethylamine group (or N,N dimethylhydroxyamine) from diuron. Fragmentation of TP9 includes the loss of -CHO in one of the fragments and the two -Cl of the aromatic ring in the other analyzed fragment (Figure 7.3).

Finally, TP10 suggests the formation of dichloroaniline, the typical end product in all kind of incomplete diuron mineralization systems.

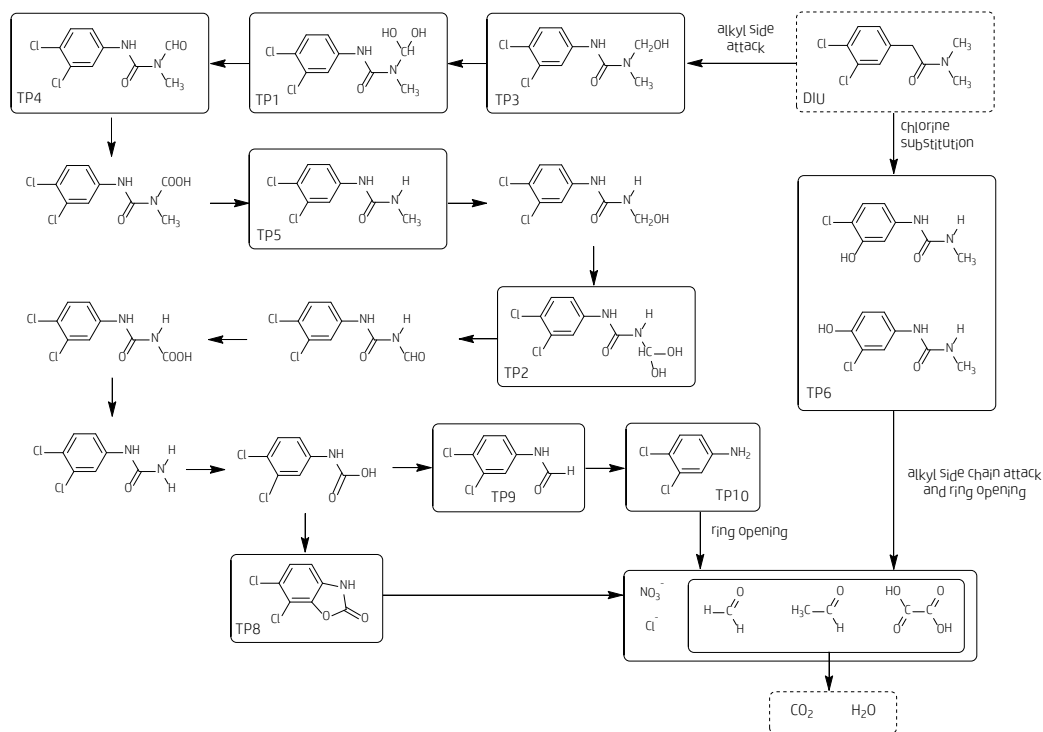


Figure 7.4 Tentative oxidation pathway in diuron oxidation by $\cdot\text{OH}$ radical attack. TPs detected are highlighted in boxes

Based on the structures found in this work and results presented in literature [24], [27] and [28], Figure 7.4 summarizes the proposed mechanism pathway degradation by $\cdot\text{OH}$ radical attack. Since direct ozonation is negligible if compared to $\cdot\text{OH}$ radical pathway, TPs formation is assumed to be the consequence of hydroxyl radicals reactions. Two different routes have been considered, the attack and oxidation of the alkyl side chain and the substitution of chlorine by OH groups. However, other authors include the $\cdot\text{OH}$ attack to aromatic rings and simultaneous substitution of chlorine by $\cdot\text{OH}$,

oxidation of alkyl chain and $\cdot\text{OH}$ attack to aromatic rings [28]; reactions that have not been considered in this work.

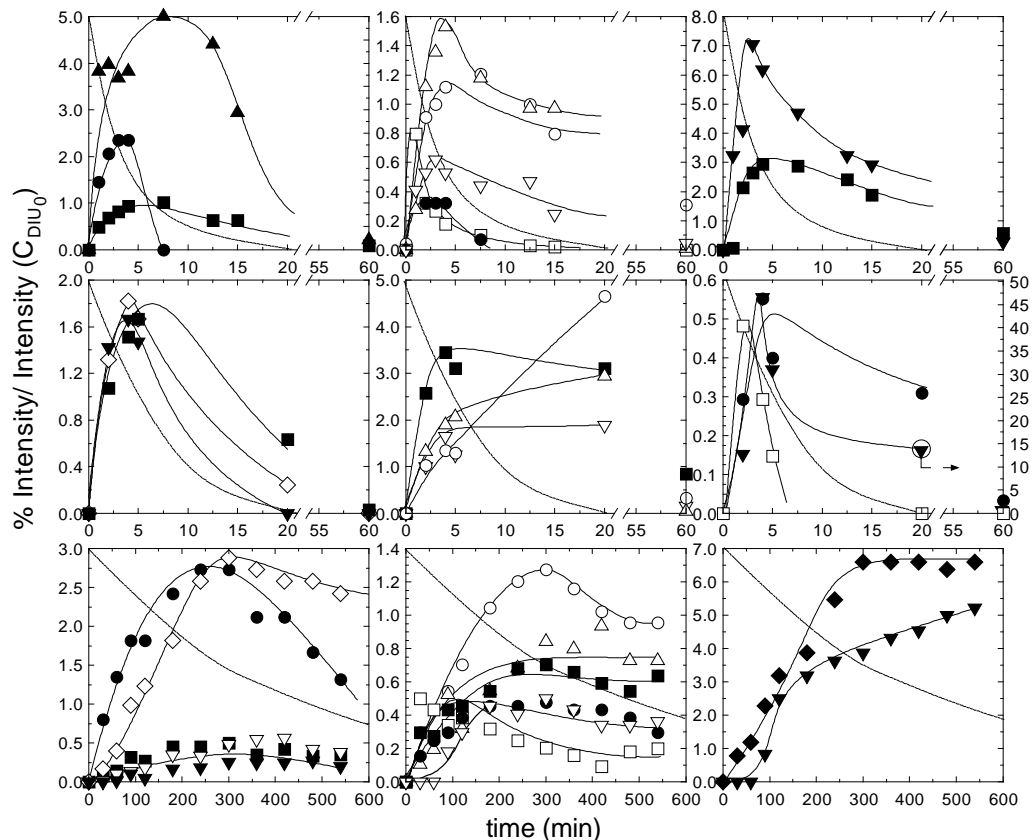


Figure 7.5 Evolution of normalized intensity of TPs related to maximum intensity of DIU at time zero in the ozonation (top), photocatalytic ozonation (middle) and photocatalysis (bottom) of diuron. Symbols: ∇ , TP1; \blacktriangle , TP2; \diamond , TP3; \blacktriangledown , TP4; \blacksquare , TP5; \bullet , TP6; \blacklozenge , TP8; \triangle , TP9; \circ , TP10. (Dashed lines: Intensity in ESI (+) mode, solid line: Intensity in ESI (-) mode, thick dashed line: DIU evolution)

Figure 7.5 shows the evolution of normalized intensity of TPs related to maximum intensity of diuron at time zero. Normalized intensity percentage is not necessarily proportional to concentration in the same proportion for all compounds, i.e. peak intensity highly depends on analytical operating conditions and easiness of ionization of the TP. However, this parameter could give an approximated idea of the amount of TP generated and its evolution with time. Accordingly, from Figure 7.5 some hypothesis can be derived. Hence, in the ozonation process, based on peak intensity, TP2 and TP4 are the

transformation products showing a higher transient concentration in the media with a maximum located in the range 5-7.5 min and 2.5-5 min for TP2 and TP4, respectively.

Photocatalytic ozonation is characterized by the apparent high selectivity of the process towards TP4 formation, achieving a peak intensity of roughly 45% of the initial diuron intensity. Also, if compared to the ozonation process, maximum in concentration for some TPs are shifted from the range 2.5-7.5 min to values above 20 min. Thus, TP1, TP9 and TP10 show increasing intensities from 0 to 20 min.

The photocatalysis was the least efficient system. Diuron and TPs were detected even after 540 min of reaction. TP8 and TP4 were the TPs presenting a higher intensity. The first one was only detected in this system.

Figure 7.6 displays the evolution of some typical low weight organic acids that accumulate in the media after applying advanced oxidation systems. Also nitrate and chloride profiles are shown. As observed, chloride appears in the three systems almost from the beginning, suggesting that hydroxylation of diuron aromatic ring immediately takes place coinciding with the hydroxyl attack to the chain attached. Also it has to be pointed out that, when ozone is present, chloride concentration linearly increases from the initial state until diuron has disappeared, thereafter a second slower period of chloride accumulation occurs due to chloride release from intermediates. Nitrate follows a similar pattern in the ozonation process although a short lag period previous to its detection was found. This lag period was more evident in the photocatalytic ozonation. In this process nitrates were not detected until diuron was completely depleted. Thereafter nitrate concentration linearly increased up to the values predicted from the initial diuron concentration. The higher mineralization capacity of the photocatalytic ozonation, if it is compared to single ozonation, is the capacity of oxidizing small oxygenated molecules. This fact is patent after observing the concentration profiles of formic acid in both systems. Formic acid reached a value of 1.16 mg L^{-1} after 180 min of ozonation, followed by a clear upward trend, while this compound presented a maximum of around 1.03 mg L^{-1} in photocatalytic ozonation at 30 min sharply decreasing its concentration to 0.05 mg L^{-1} at 120 min. In opposition to single ozonation, photocatalytic ozonation is capable of removing formic acid. Finally, it should be mentioned the absence of nitrates in the photocatalytic process which agrees with the fact that nitrogen derivatives of diuron are still present in solution.

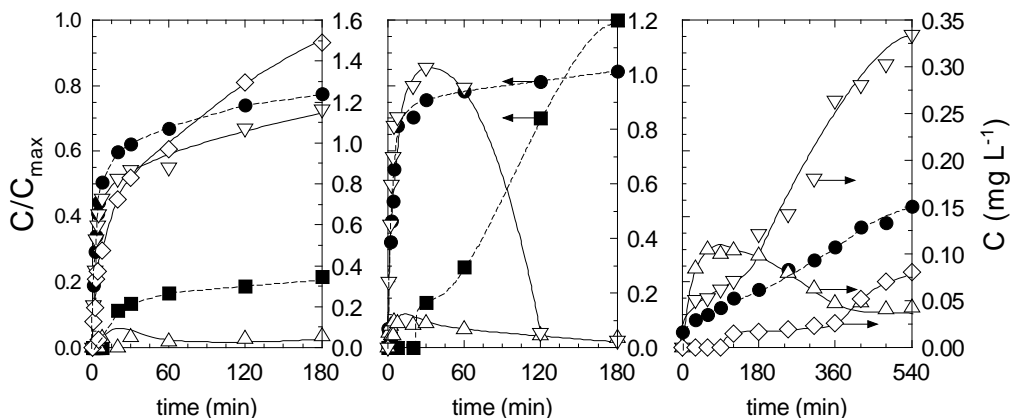


Figure 7.6 Anionic and short chain organic acids evolution during ozonation (left), photocatalytic ozonation (middle) and photocatalysis (right). Experimental conditions as in Figure 7.1. Left y-axis (dashed lines): ●, chloride normalized to maximum chloride concentration; ■, nitrate normalized to maximum nitrate concentration. Right y-axis (solid lines): ▲, acetic acid; ▽, formic acid; ◇, oxalic acid

7.3.3. Evolution of toxicity to *Vibrio fischeri*

Toxicity of TPs towards *V. fischeri* was assessed at different times of exposure in samples taken along the reaction period in single ozonation, photocatalysis and photocatalytic ozonation runs. Figure 7.7 depicts the inhibition percentage as a function of time. This figure shows diverse trends when using different systems. With the exception of photocatalysis, a slight increase in toxicity at the initial stages of the oxidation followed by a decrease in toxicity as the reaction proceeds is observed. This tendency is related to a higher toxicity from initial intermediates. As low weight oxygenated species are being formed, toxicity tends to be reduced. In relation to diuron toxicity, Gatidou and co-workers [32] reported an EC_{50} value of 9.2 mg L^{-1} after 30 min of exposition to *V. fischeri*.

Although ozonation and photocatalytic ozonation display similar toxicity responses with a maximum (>90% inhibition at 30 min of exposure) followed by decrease; some slight differences could be extracted. Hence, photocatalytic ozonation exhibits lower inhibition values at the final stage of the process, when small organic acids and TOC are removed from the media. After 3 h of treatment ozonation decreased the inhibition percentage to 55% while photocatalytic ozonation reduced it to 20%. The maximum inhibition reached might be due to the higher toxicity of intermediates compared to diuron, especially TP10 (3,4-dichloroaniline) which is the most toxic transformation product [33] and [34]. Moreover, photocatalytic ozonation clearly reaches its

maximum in toxicity at 5 min, while ozonation requires 15-20 min. This delay supports the idea that maximum of toxicity matches maximum of TPs formation in each oxidation technology, discussed previously.

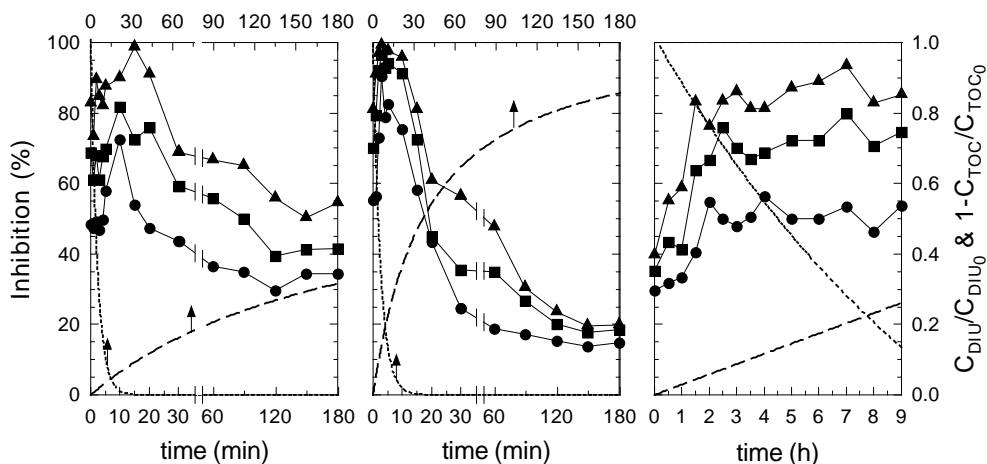


Figure 7.7 Toxicity evolution to *V. fischeri* during ozonation (left), photocatalytic ozonation (middle) and photocatalysis (right) at different exposure times. Experimental conditions: $V=1.0$ L; $C_{DIU,0}=10$ mg L⁻¹; $Q_G=30$ L h⁻¹; $C_{O_3inlet}=10$ mg L⁻¹; (if applied); $C_{N-TiO_2}=0.5$ g L⁻¹; $pH_0=5.6-6.0$. Exposure time (min): ●, 5; ■, 15; ▲, 30. (Dotted lines: normalized DIU concentration, dashed lines: normalized TOC removal)

In the case of photocatalysis, the inhibition profile steadily increases through the process because of the incomplete oxidation of intermediates. According to Figure 7.5, photocatalysis is the technology displaying the highest values of TPs intensity. This explains why after 9 h of treatment inhibition percentage reaches 85% (30 min of exposure).

7.4. CONCLUSIONS

Diuron has a low rate constant towards molecular ozone, accordingly, oxidation processes involving ozone take place via hydroxyl radical, this latter pathway supposes above 99%. Photocatalytic ozonation does not significantly improve parent compound removal. However, high TOC removal rates are reached by this system, showing an outstanding 83% of synergism in TOC removal if compared to single ozonation and photocatalysis.

Transformation products derived from ozonation, photocatalysis and photocatalytic ozonation are quite similar since the radical pathway plays an important role in the three systems. In processes in the presence of ozone,

TPs maximum formation were observed once diuron was abated, afterwards they were utterly removed. Photocatalytic ozonation displayed high selectivity to TP4 formation (N-[(3,4-dichlorophenyl)carbamoyl]-N-methylformamide).

High mineralization rates linked to photocatalytic ozonation are due to the high capacity of oxidizing small oxygenated organics. Chloride evolution suggests that hydroxylation of diuron takes place coinciding with hydroxyl radical attack. Inorganic nitrogen was not displayed until diuron was completely depleted.

Toxicity evolution to *V. fischeri* during photocatalytic ozonation showed an increase at the initial oxidation stage (>90%) decreasing thereafter as the reaction progresses. Ozonation displayed a lower ability to decrease the inhibition percentage after reaching the maximum in toxicity. Photocatalysis gradually increased the toxicity to the bacteria.

Photocatalytic ozonation has a powerful capacity of generating radicals making possible the oxidation of organic pollutants, with high environmental concern. This is the origin of the observed higher mineralization rate if compared to single ozonation or photocatalysis.

Acknowledgements

Authors thank economic support received from *Gobierno de Extremadura* and *CICYT* of Spain through Projects GRU10012 and CTQ2012-35789-C02-01, respectively. Mr. Rafael Rodríguez Solís also thanks *Gobierno de Extremadura*, *Consejería de Empleo, Empresa e Innovación*, and *FSE* Funds for his Ph.D. Grant (PD12058).

REFERENCES

- [1] Gavrilescu M, *Fate of pesticides in the environment and its bioremediation*. Eng Life Sci 5 (2005) 497-526
- [2] Commission Directive 2008/91/CE of 29 September 2008 amending Council Directive 91/414/EEC to include diuron as active substance, Official Journal of the European Union 262 (2008) 31-32
- [3] Loos R, Gawlik BM, Locore G, Rimaviute E, Contini S, Bidoglio G, *EU-wide survey of polar organic persistent pollutants in European river water*, Environ Pollut 157 (2009) 561-568
- [4] Pesticide Properties Database. University of Hertfordshire, UK. <http://sitem.herts.ac.uk/aeru/ppdb/en/index.htm>, 2016 (last accessed 01.02.16)

- [5] EU Directive 2013/39/EU of the European Parliament and The Council of 12, Amending Directives 2000/60/EC and 2008/105/EC as regards priority substances in the field of water policy, Official Journal of the European Union 226 (2013) 1-17
- [6] Ribeiro AR, Nunes OC, Pereira MFR, Silva AMT, *An overview on the advanced oxidation processes applied for the treatment of water pollutants defined in the recently launched directive 2013/39/EU*, Environ Int 75 (2015) 33-51
- [7] Rosal R, Rodríguez A, Perdigón-Melón JA, Petre A, García-Calvo E, Gómez MJ, Agüera A, Fernández-Alba AR, *Occurrence of emerging pollutants in urban wastewater and their removal through biological treatment followed by ozonation*, Water Res 44 (2006) 578-588
- [8] Agustina TE, Ang HM, Vareek VK, *A review of synergistic effect of photocatalysis and ozonation on wastewater treatment*, J Photochem Photobiol C Photochem Rev 6 (2005) 264-273
- [9] Xiao J, Xie Y, Cao H, *Organic pollutants removal in wastewater by heterogeneous photocatalytic ozonation*, Chemosphere 121 (2015) 1-17
- [10] Malato S, Fernández-Ibáñez P, Maldonado M, Blanco J, Gernjak W, *Decontamination and disinfection of water by solar photocatalysis: recent overview and trends*, Catal Today 147 (2009) 1-59
- [11] Peláez M, Nolan NT, Pillai SC, Seery MK, Falaras P, Kontos AG, Dunlop PSM, Hamilton JWJ, Byrne JA, O'Shea K, Entezari MH, Dionysiou DD, *A review on the visible light active titanium dioxide photocatalysts for environmental applications*, Appl Catal B Environ 125 (2012) 331-349
- [12] Dagherir, Droguí P, Rober D, *Modified TiO₂ for environmental photocatalytic applications: a review*, Ind Eng Chem Res 52 (2013) 2581-3599
- [13] Hernández-Alonso MD, Fresno F, Suárez S, Coronado JM, *Development of alternative photocatalysts to TiO₂: challenges and opportunities*, Energy Environ Sci 2 (2009) 1231-1257
- [14] Solís RR, Rivas FJ, Gimeno O, Pérez-Bote JL, *Photocatalytic ozonation of pyridine-based herbicides by N-doped titania*, J Chem Technol Biotechnol 91 (2016) 1998-2008
- [15] Rivas J, Solís RR, Gimeno O, Sagasti J, *Photocatalytic elimination of aqueous 2-methyl-4-chlorophenoxyacetic acid in the presence of*

- commercial and nitrogen-doped TiO₂*, Int J Environ Sci Technol 12 (2015) 513-526
- [16] Senthilnathan J, Philip L, *Photocatalytic degradation of lindane under UV and visible light using N-doped TiO₂*, Chem Eng J 161 (2010) 83-92
- [17] Bletsou AA, Jeon J, Hollender J, Archontaki E, Thomaidis NS, *Targeted and non-targeted liquid chromatography-mass spectrometric workflows for identification of transformation products of emerging pollutants in the aquatic environment*, Trends Anal Chem 66 (2015) 32-44
- [18] Bader H, Hoigné J, *Determination of ozone in water by the indigo method*, Water Res 15 (1981) 449-456
- [19] Solís RR, Rivas FJ, Gimeno O, Pérez-Bote JL, *Photocatalytic ozonation of clopyralid, picloram and triclopyr. Kinetics, toxicity and influence of operational parameters*, J Chem Technol Biotechnol 91 (2016) 51-58
- [20] Johnson PN, Davis RA, *Diffusivity of Ozone in Water*, J Chem Eng Data 41 (1996) 1485-1487
- [21] Laet J de, Maouala-Makata P, Dore M, *Constantes cinétiques de réaction de l'ozone moléculaire et des radicaux hydroxyles sur quelques phenyl-ureas et acetamides (rate constants of ozone and hydroxyl radicals with several phenyl-ureas and acetamides)*, Environ Technol 17 (1996) 707-716
- [22] Benítez FJ, Real FJ, Acero JL, García C, *Kinetics of the transformation of phenyl-urea herbicides during ozonation of natural waters: rate constants and model predictions*, Water Res 41 (2007) 4073-4084
- [23] Agüera A, Gómez Ramos MM, Fernández-Alba AR, *Chemical Evaluation of Water Treatment Processes by LC-(Q)TOF-MS: Identification of Transformation Products*, in: A.R. Fernández-Alba (Ed.), *TOF-MS within Food and Environmental Analysis*, Comp Anal Chem, 2012, 61-109
- [24] López MC, Fernández MI, Rodríguez S, Santaballa JA, Steenken S, Vulliet E, *Mechanisms of direct and TiO₂-photocatalysed UV degradation of phenylurea herbicides*, ChemPhysChem 6 (2005) 2064-2074
- [25] Carrier M, Besson M, Guillard C, Gonze E, *Removal of herbicide diuron and thermal degradation products under catalytic wet Air oxidation conditions*, Appl Catal B Environ 91 (2009) 275-283
- [26] Farré MJ, Brosillon S, Domenech X, Peral J, *Evaluation of the intermediates generated during the degradation of Diuron and Linuron herbicides by the photo-Fenton reaction*, J Photochem Photobiol A 189 (2007) 364-373

- [27] Hayon E, Ibata T, Lichtin NN, Simic M, *Sites of attack of hydroxyl radicals on amides in aqueous solution. II. Effects of branching alpha to carbonyl and to nitrogen*, J Am Chem Soc 93 (1971) 5388-5394
- [28] Malato S, Cáceres J, Fernández-Alba AR, Piedra L, Hernando MD, Agüera A, Vial J, *Photocatalytic treatment of diuron by solar photocatalysis: evaluation of main intermediates and toxicity*, Environ Sci Technol 37 (2003) 2516-2524
- [29] Feng J, Zheng Z, Luan J, Zhang J, Wang L, *Degradation of diuron in aqueous solution by ozonation*, J Environ Sci Health Part B 43 (2008) 576-587
- [30] Ramírez-Zamora RM, Seux R, *Identificación du diuron et identificación de quelques sous produits de la reaction*, Rev Sci de l'eau 12 (1999) 545-560
- [31] Pradittakan W, Sadudeewong E, Apichatsanee K, Vangnai AS, Pavarajarn V, *Comparative study of photocatalytic degradation of diuron on titanium dioxide and zinc oxide nanoparticles*, in: Proceedings of Chemeca 2011: Engineering a better world, Sydney, 2011, ISBN: 978-0858259225
- [32] Gatidou G, Stasinakis AS, Iatrou EI, *Assessing single and joint toxicity of three phenylurea herbicides using Lemna minor and Vibrio fischeri bioassays*, Chemosphere 119 (2015) S69-S74
- [33] Bonnet JL, Bonnemoy F, Dusser M, Bohatier J, *Assessment of the potential toxicity of herbicides and their degradation products to nontarget cells using two microorganisms, the bacteria Vibrio fischeri and the ciliate Tetrahymena pyriformis*, Environ Toxicol 22 (2007) 78-91
- [34] Tixier C, Bogaerts P, Sancelme M, Bonnemoy F, Twagilimana L, Cuer A, Bohatier J, Veschambre H, *Fungal biodegradation of a phenylurea herbicide, diuron: structure and toxicity of metabolites*, Pest Manage Sci 56 (2000) 455-462

CHAPTER EIGHT

PAPER SIX

Monoperoxysulfate photocatalysis under 365 nm radiation. Direct oxidation and monoperoxysulfate promoted photocatalysis of the herbicide tembotrione

J Environ Manag 181 (2016) 385-394

Rafael R. Solís, F. Javier Rivas, Mercedes Tierno

ABSTRACT. Oxone® (potassium monoperoxysulfate, MPS) has been used to oxidize the herbicide tembotrione in aqueous solution. Tembotrione elimination kinetics by MPS direct oxidation has been studied. The influence of the main operating variables affecting the process (MPS concentration, temperature and pH) has been evaluated. The process follows 2/3 and first orders in MPS and tembotrione concentrations, respectively. Optimal pH is located around circumneutral conditions. MPS decomposition in the presence of 365 nm UVA radiation and titanium dioxide has also been studied. The system MPS/UVA/TiO₂ significantly improves tembotrione and mineralization rate abatement if compared to runs conducted in the absence of MPS. Tembotrione total abatement was achieved in 20 min when 0.05 g L⁻¹ of titania and 10⁻⁴ M of Oxone® were used. TOC conversion was roughly 70% in 90 min under similar operating conditions. An experimental design (Plackett-Burman) has been considered to study the influence of the main variables affecting tembotrione photocatalytic oxidation promoted by MPS.

KEYWORDS: tembotrione, monoperoxysulfate, oxone, photocatalysis, UVA radiation



8.1. INTRODUCTION

As a consequence of increasing population needs, pesticides are used in intensive farming around the world. Uncontrolled use of pesticides supposes an alarmingly hazard for the environment and human health. Triketone herbicides, such as sulcotrione, mesotrione or tembotrione, are 4-hydroxyphenylpyruvate dioxygenase (HPPD) inhibitors, which act blocking the HPPD indispensable enzyme in plant growth. Thus, the plant develops leaf bleaching followed by necrosis and death [1]. Since some weeds developed resistance to traditional herbicides and because pesticide legislation became more restrictive to classical herbicides, HPPD inhibitors were brought to North American and European markets as the newest class herbicides in the late 1990s and 2000s. Tembotrione (TEMB), 2-[2-chloro-4-mesyl-3-((2,2,2-trifluoroethoxy)methyl)benzoyl]cyclohexane-1,3-dione, was launched in 2007 by Bayer CropScience (Laudis®) to control different types of grass and broadleaf weeds during the early to mid-post-emergence of field corn [2]. Although TEMB is mostly used in popcorn crop, sweet corn and seed corn fields; other applications, like in sorghum and soyabean, are still under consideration. In 2013, the global demand of the tembotrione market was 267.4 tons and it is expected to reach a market value of US\$51.2 million by 2020 [3]. Since tembotrione is one of the newest herbicides released, little is known about the effects on the environment; however, its use is currently approved in the European Union [4].

Pesticides, as an example of organic and emerging contaminant, are not properly removed in conventional biological wastewater treatment. Amongst the Advanced Oxidation Processes applied to herbicides management, photocatalysis has raised a great interest, particularly if considering the use of solar radiation which reduces the environmental impact if compared to other technologies. To the authors' knowledge, not many works have dealt with the oxidation of tembotrione in water. Although chlorination [5], photolysis [6-8], Fenton process [9] and other Advanced Oxidation Processes [10,11] have been reported in the elimination of triketone herbicides, few of them include tembotrione in their research.

Oxone® is a chemical manufactured by DuPont. This compound is a triple salt rich in monoperoxysulfate ($2\text{KHSO}_5 \cdot \text{KHSO}_4 \cdot \text{K}_2\text{SO}_4$). Monoperoxysulfate (MPS) is considered an alternative to other chemical oxidants because of several advantages. It is a homogeneous oxidant whose activity is higher than other traditional oxidants like hydrogen peroxide. MPS decomposes into sulfate and hydroxyl radicals. Sulfate radicals present a higher standard

reduction potential compared to hydroxyl radicals (2.5–3.1 V at neutral pH versus 1.8–2.7 V depending on the pH). Moreover, MPS decomposition is easily promoted by transition metals [12] or by heterogeneous catalysts [13–15], UV radiation [16, 17] or heat [18]. Furthermore, MPS is usually labelled as an environmentally-friendly oxidant, as it does not generate toxic byproduct after its application. MPS research has recently been focused on the removal of phenols [19,20], pharmaceutical compounds [21,22], herbicides [23], chlorinated compounds [24], and disinfection [25]. However, to date, few works have integrated the use of MPS as oxidant promoter in photocatalysis [26–28].

Since previous experiments revealed the direct reaction between oxone and tembotrione, in this work, this herbicide has been oxidized in the presence of MPS. The most influencing variables in the process such as MPS concentration, temperature and pH, have been studied. In order to improve mineralization extent, MPS was used as a promoter in the photocatalytic tembotrione oxidation using TiO_2 . Previously, MPS decomposition under 365 nm UVA radiation has been assessed. MPS photocatalytic oxidation of tembotrione has been studied. A Plackett-Burman experimental design has been completed to examine the weight of the main variables of the process (MPS, tembotrione concentration and catalyst load).

8.2. EXPERIMENTAL

8.2.1. Materials

Analytical standard tembotrione (PESTANAL[®], CAS 335104-84-2) was purchased from Sigma-Aldrich and was used as received in all the experiments. Oxone[®] and the rest of chemicals were acquired from Sigma-Aldrich. Acetonitrile from VWR Chemicals was used in HPLC determination of tembotrione. All solutions were prepared with ultrapure water from a Milli-Q[®] academic (Millipore) system. Commercial TiO_2 Degussa P25 (70% anatase and 30% rutile) was the photocatalyst used in heterogeneous experiments (average particle size of 30 nm and BET surface area of $50 \text{ m}^2 \text{ g}^{-1}$).

8.2.2. Analytical methods

Tembotrione was quantified by means of an Agilent 1100 (Hewlett-Packard) high performance liquid chromatography system with UV detection (HPLC-UV). A Kromasil 100 5C18 (5 mm, 2.1x150 mm) column was connected. The mobile phase was a 50:50 (A:B) mixture of 0.1% H_3PO_4 acidified water (A) and acetonitrile (B). UV detection was conducted at 250 nm. Relative error of HPLC determination, expressed as relative standard deviation of a sample of

5 mg L⁻¹ of tembotrione which was analyzed 10 times, was found to be 0.46%. Moreover the limit of detection of the calibration curve [29] was 54.5 µg L⁻¹.

Tembotrione mineralization was monitored by analyzing the total organic carbon (TOC) in a Shimadzu TOC 5000A analyzer. 1.31% of relative error was obtained (5 mg L⁻¹ of tembotrione which corresponds to 2.5 mg L⁻¹ of TOC) and the limit of detection of the calibration curve was 114 µg L⁻¹.

MPS concentration evolution was analyzed spectrophotometrically by a colorimetric method based on N,N-diethyl-p-phenylenediamine (DPD) oxidation [30], with a relative error of 3.44%. pH of the reaction media was adjusted and controlled by means of a Radiometer Copenhagen pH-meter (HPM82).

8.2.3. Photoreactor setup and experimental procedure

The reaction system, whose scheme is depicted in Figure 8.1, consisted of a cylindrical 1.0 L borosilicate photoreactor. The glass reactor was located in the middle of a 31cm external diameter pipe of 54 cm height. The reactor was magnetically stirred by an IKA® RCT basic stirrer equipped with temperature control. In order to maximize photons reflection, the internal wall of the pipe was covered by aluminum foil. Four black light lamps of 41 cm height (LAMP15TBL HQPOWER™ manufactured by Velleman®) were evenly placed and attached to the internal wall of the pipe. Each lamp, which a nominal power of 15 W, mainly emits radiation within the range 350-400 nm with a maximum located at 365 nm. UVA photon flow was determined in a previous work by means of ferrioxalate actinometry. Values of 1.77, 3.26, 5.13 and 6.86 10⁻⁵ Einstein L⁻¹ min⁻¹ with 1, 2, 3 and 4 lamps switched on, were obtained [31]. Moreover, the intensity decreased to 3.65 10⁻⁵ Einstein L⁻¹ min⁻¹ when the aluminum foil covering the internal wall was substituted by a black surface (4 lamps switched on).

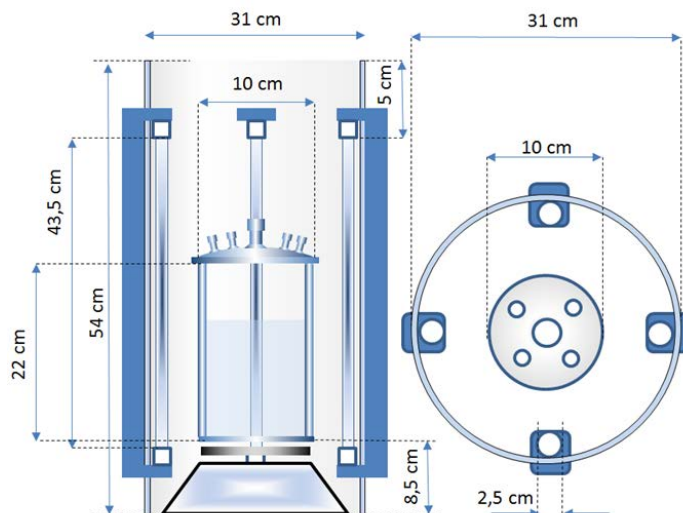


Figure 8.1 Frontal and top views of the photoreactor setup

In all experiments 5 mg L^{-1} of initial tembotrione was used. This abnormally high concentration was used to be able to monitor TOC evolution. Homogeneous experiments of MPS oxidation were carried out with the lamps switched off, under stirring and control of temperature. Less than 10 mL of MPS was added from a high concentrated solution to start the reaction. Steadily samples were withdrawn from the reactor and quenched with $\text{Na}_2\text{S}_2\text{O}_3$ 0.5 M (10 μL per 10 mL of sample). When required, pH was controlled by NaOH or HCl addition. Heterogeneous photocatalytic experiments were carried out in the same way, in this case, in order to reach the tembotrione adsorption equilibria onto titanium dioxide (if any), each trial was preceded by 30 min of stirring under absence of radiation. Millex-HA filters (Millipore, $0.45 \mu\text{m}$) were used to remove the catalyst before analysis.

8.3. RESULTS AND DISCUSSION

8.3.1. Monoperoxysulfate promoted experiments in the absence of light and photocatalyst

Influence of initial Oxone® concentration

A series of preliminary experiments was carried out to investigate the potential oxidation of tembotrione by monoperoxysulfate as a sole oxidizing agent. The capability of monoperoxysulfate as oxidant in the absence of any decomposition promoter has been reported previously by some authors [21].

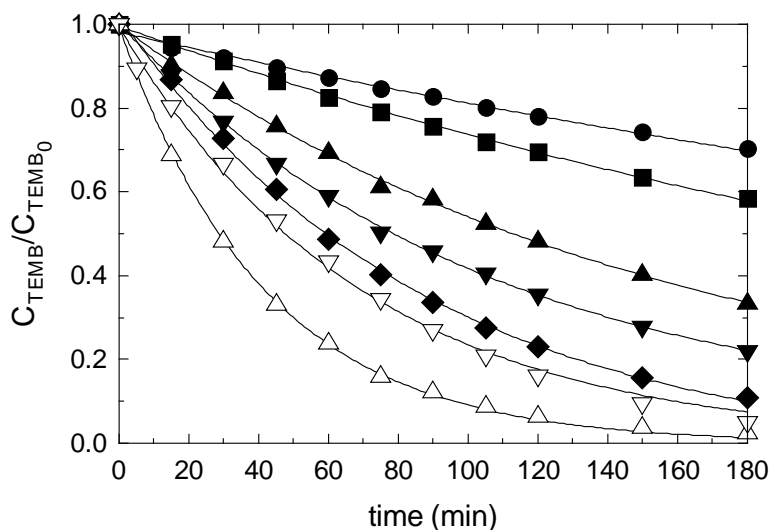


Figure 8.2 Oxone[®] oxidation of tembotrione. Influence of the initial Oxone[®] concentration. Experimental conditions: $T=25^{\circ}\text{C}$; $V=1.0\text{ L}$; $\text{pH}=3.1$; $C_{\text{TEMB},0}=5\text{ mg L}^{-1}$ (average value); $C_{\text{Oxone},0} \cdot 10^4(\text{M})$: ●, 1.05; ■, 2.52; ▲, 5.0; ▼, 10.0; ◆, 25.1; ▽, 50.0; △, 10.0 (in the presence of UVA light). Solid lines correspond to pseudofirst order kinetics fitting, $R^2>0.99$ in all cases

Figure 8.2 shows the evolution of normalized tembotrione concentration in experiments conducted in the presence of initial Oxone[®] concentrations in the range $1.0\text{--}50 \cdot 10^{-4}\text{ M}$. As inferred from the figure, tembotrione is eliminated at acceptable rates by apparently following exponential pseudofirst order kinetics. In these experiments, however, no TOC reduction was appreciated, suggesting the absence or insufficient generation of powerful free radicals species. Addition to double bonds is normally associated to direct attack of monoperoxysulfate to organic molecules [32].

In the worst case, initial tembotrione concentration is at least 20 times lower than monoperoxysulfate concentration. Accordingly, it can be assumed that Oxone[®] concentration will remain practically constant along the oxidation experiments. Also, as stated previously, monoperoxysulfate likely adds to any tembotrione double bond in the molecule. Since this compound presents several positions of potential attack, a generic n -th order was assumed regarding Oxone[®] concentration. As a consequence, the following kinetic expression was assumed to describe the process:

$$-\frac{dC_{\text{TEMB}}}{dt} = k C_{\text{TEMB}} C_{\text{Oxone}}^n \quad (8.1)$$

where k is a rate constant depending on temperature and pH. If Oxone® concentration remains constant:

$$-\frac{dC_{\text{TEMB}}}{dt} = k C_{\text{Oxone}_0}^n C_{\text{TEMB}} = k_{\text{Obs}} C_{\text{TEMB}} \quad (8.2)$$

After integration:

$$\ln \frac{C_{\text{TEMB}_0}}{C_{\text{TEMB}}} = k_{\text{Obs}} t \quad (8.3)$$

Values of k_{Obs} were obtained after plotting the left side member in equation 8.3 versus time, leading to values of 0.113 ± 0.002 , 0.179 ± 0.005 , 0.364 ± 0.012 , 0.506 ± 0.015 , 0.754 ± 0.014 , $1.278 \pm 0.020 \text{ h}^{-1}$ in experiments completed in the presence of 1.05, 2.52, 5.0, 10.0, 25.1, and 50.0 10^{-4} M of Oxone® initial concentration, respectively.

The order regarding Oxone® concentration could be obtained after applying natural logarithms to k_{Obs} :

$$k_{\text{Obs}} = k C_{\text{Oxone}_0}^n \quad (8.4)$$

$$\ln(k_{\text{Obs}}) = \ln(k) + n \ln(C_{\text{Oxone}_0})$$

An adequate plot of equation 8.4 led to a value of $n = 0.62 \pm 0.03$ ($\sim 2/3$) and $k = 22.2 \pm 1.43 \text{ M}^{-0.62} \text{ h}^{-1}$ ($R^2 = 0.99$) at pH 3.1.

Influence of temperature

Temperature influence was investigated in the interval 25–60°C. Experiments were conducted in the presence of 10^{-3} M in Oxone®. Figure 8.3 shows the results obtained. Once again pseudofirst order kinetics regarding tembotrione concentration could acceptably describe the process. In this case, calculated k_{Obs} values were 0.506 ± 0.015 , 1.26 ± 0.04 , 2.29 ± 0.08 , and $4.29 \pm 0.06 \text{ h}^{-1}$, corresponding to experiments completed at 25, 40, 50, and 60°C, respectively.

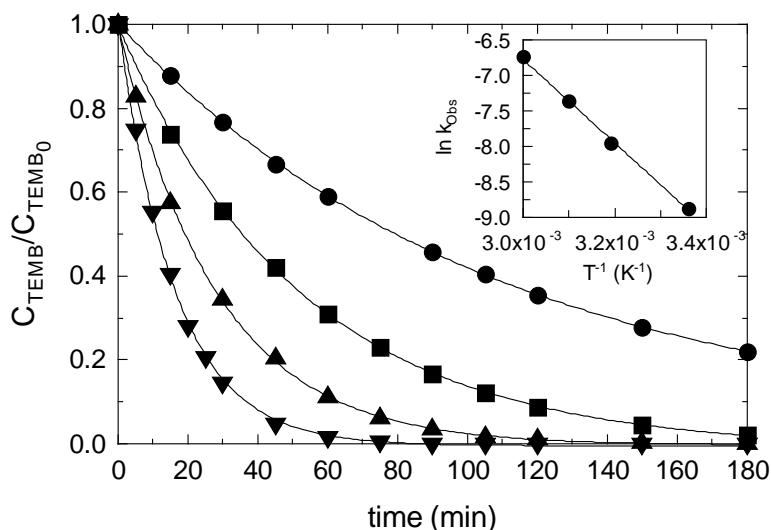


Figure 8.3 Oxone® oxidation of tembotrione. Influence of temperature. Experimental conditions: $C_{Oxone,0} = 10^{-3}$ M; $V = 1.0$ L; $pH = 3.1$; $C_{TEMB,0} = 5$ mg L $^{-1}$ (average value); T (°C): ●, 25; ■, 40; ▲, 50; ▼, 60. (Inset: Arrhenius plot). Solid lines correspond to pseudofirst order kinetics fitting, $R^2 \sim 0.999$ in all cases.

Although heat could activate the decomposition of MPS into radicals, monoperoxysulfate is poorly activated at temperatures below 80°C [33]. Accordingly, any effect observed by an increase in temperature will only be related to changes in the value of the direct rate constant.

Assuming Arrhenius behavior in the observed rate constant:

$$k_{obs} = AC_{Oxone_0}^n e^{-\frac{E_A}{RT}} \quad (8.5)$$

$$\ln(k_{obs}) = \ln(AC_{Oxone_0}^n) - \frac{E_A}{R} \frac{1}{T}$$

where R is the universal gas constant, E_A is the activation energy of the process and A , the pre-exponential factor. A plot of equation (8.5) is shown in the inset of Figure 8.3. From this plot, the activation energy of the process was calculated to be 50.1 ± 0.1 kJ mol $^{-1}$.

Again, no significant TOC reduction was experienced regardless of the temperature used.

Influence of pH

pH is an important parameter in monoperoxysulfate oxidation mediated processes [21]. This aspect was assessed by completing an experimental series at different pHs in the range 3-12. Figure 8.4 shows the results obtained.

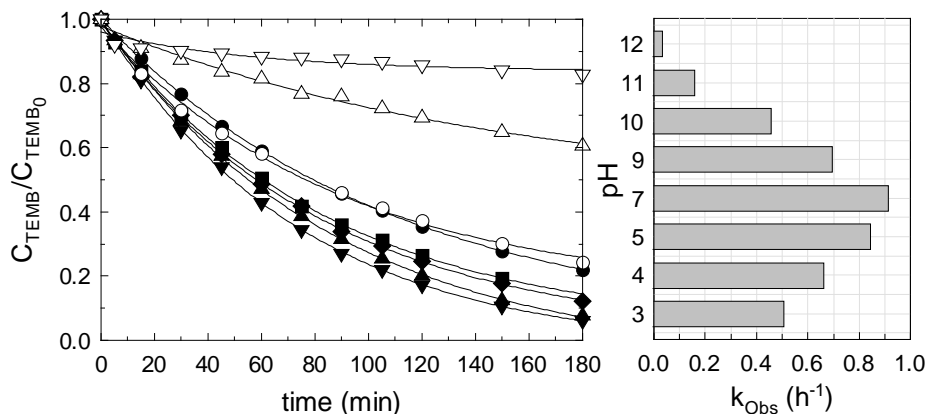


Figure 8.4 Oxone® oxidation of tembotrione. Influence of pH. Experimental conditions: T=25°C; C_{Oxone,0}=10⁻³ M; V=1.0 L; C_{TEMB,0}=5 mg L⁻¹ (average value); pH: ●, 3.1; ■, 4.0; ▲, 5.0; ▼, 7.0; ◆, 9.0; ○, 10.0; △, 11.0; ▽, 12.0. (Right figure: observed rate constant as a function of pH). Solid lines correspond to pseudofirst order kinetics fitting, R²>0.99 in all cases.

Figure 8.4 reveals an optimum in pH around 7.0. Two effects could be considered to explain these results. Hence, monoperoxysulfate has a second acid dissociation pK_a of roughly 9.4 while tembotrione presents a pK_a of 3.2. It seems that the anionic form of tembotrione is more reactive than the molecular form, that is, increasing the pH above 3 up to circumneutral conditions favors the process since the oxidant remains as HSO₅⁻. Contrarily, if pH is increased above 7-8, monoperoxysulfate dissociates and the predominant species is SO₅²⁻, which, apparently, reacts with the ionic form of tembotrione at a lower rate than the protonated form. No mineralization of the parent compound was observed no matter the working pH used.

As stated previously, no TOC reduction could be achieved by using monoperoxysulfate as the only oxidant agent. In an attempt to improve the process, UVA light was applied to the reaction media (see Figure 8.2). As seen in Figure 8.2, tembotrione depletion was slightly improved if compared to the run conducted in the dark under similar conditions. This improvement could be associated to partial Oxone® decomposition due to UVA light absorption (not probable because Oxone® does not absorb at 365 nm) or the generation of

some intermediates acting as sensitizers of the photolysis (tembotrione does not absorb UVA light). In any case, no mineralization of the herbicide could be detected.

8.3.2. Oxone[®] promoted tembotrione photocatalysis

In an attempt to accelerate the parent compound removal and simultaneously increase mineralization, some experiments were conducted in the presence of Oxone[®] and Degussa P25 titania applying UVA light at 365 nm. For comparison purposes, some nonpromoted experiments were also carried out.

Figure 8.5 shows the evolution of the normalized tembotrione concentration in experiments conducted in the presence of titania at two different pHs. As observed, the process is significantly improved both in terms of tembotrione abatement rate and mineralization extent if compared to the application of Oxone[®] as the unique oxidant.

When pH is not adjusted, the non-promoted photocatalysis of tembotrione leads to total parent compound abatement in roughly 90 min while if 10^{-4} M of Oxone[®] is added, this time is reduced to 20 min and pH does not exert a significant effect in tembotrione abatement when monoperoxysulfate is not added to the reaction media, however some inhibition was observed in Oxone[®] promoted experiments when increasing the pH from 3.1 to 7. pH effect is associated to several parameters such as reagents pK_a and also the point of zero charge of titania which influences the adsorption extent.

The extent of synergism ($\Lambda_{\text{Synergism}}$) reached during tembotrione oxidation could be calculated as follows:

$$\Lambda_{\text{Synergism}} (\%) = \frac{k_{\text{OxonePhotoCat}} - (k_{\text{PhotoCat}} + k_{\text{Oxone}})}{k_{\text{OxonePhotoCat}}} \times 100 \quad (8.6)$$

where $k_{\text{OxonePhotoCat}}$, k_{PhotoCat} and k_{Oxone} represent the empirical pseudofirst order rate constant corresponding to photocatalytic oxidation promoted with Oxone[®], without Oxone[®] and the direct reaction with Oxone[®], respectively. Table 8.1 shows the results of synergism. Hence, promoted photocatalytic oxidation cannot be explained as the sum of photocatalytic and direct oxidation processes, reaching higher synergism values for tembotrione at acidic pH.

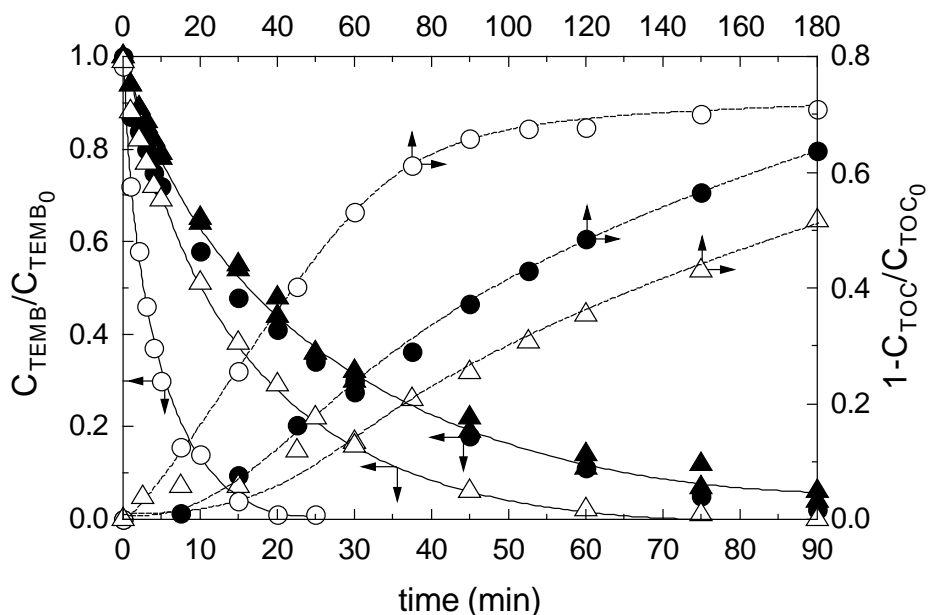


Figure 8.5 Photocatalysis of tembotrione in the presence of titania P25. Influence of Oxone[®] addition at different pHs. Experimental conditions: T=25°C; V=1.0 L; C_{TEMB,0}=5 mg L⁻¹ (average value); C_{TiO2}=0.05 g L⁻¹. Symbols: ●, pH=3.1 and C_{Oxone,0}=0 M; ○, pH=3.1 and C_{Oxone,0}=10⁻⁴ M; ▲, pH=7.0 and C_{Oxone,0}=0 M; △, pH=7.0 and C_{Oxone,0}=10⁻⁴ M. Solid lines correspond to pseudofirst order kinetics fitting, R²>0.99 in all cases.

It is also noteworthy to highlight the mineralization extent achieved. A maximum of roughly 70% after 3 h of treatment was experienced when 0.05 g L⁻¹ of titania were used in the presence of Oxone[®] with no pH adjustment. Once again, a synergistic effect is appreciated in TOC removal (see Table 8.1).

In this section some experiments were conducted in the presence of free radical scavengers (results not shown) at a high concentration of Oxone[®] (10⁻³ M) in order to prove their inhibitory effect if any. Contrarily to Oxone[®] photocatalysis, partial inhibition of the process was experienced at pH=7 suggesting the presence of radicals in solution. Methanol showed a higher scavenging capacity than *tert*-butanol. If a sufficiently high scavenger concentration is used (0.01 M), both alcohols lead to similar results, reducing the pseudofirst order reaction rate constant from roughly 16 h⁻¹ to 6.3 h⁻¹.

Table 8.1 Experimental pseudofirst order rate constant (h^{-1}) of tembotrione and TOC removal obtained from Figure 8.5

	Tembotrione				TOC			
	$k_{OxonePhotoCat}$ (R^2)	$k_{PhotoCat}$ (R^2)	k_{Oxone} (R^2)	$\Delta_{Synergism}$ (%)	$k_{OxonePhotoCat}$ (R^2)	$k_{PhotoCat}$ (R^2)	k_{Oxone} (R^2)	$\Delta_{Synergism}$ (%)
Uncontrolled pH	12.69 (0.994)	2.33 (0.984)	0.11 (0.994)	80.8	0.78 (0.996)	0.36 (0.996)	0	53.8
pH=7	3.69 (0.999)	1.82 (0.983)	0.22 ^a	44.7	0.25 (0.992)	0	0	-

^a Obtained theoretically from equation 8.4 knowing k_{obs} at pH=7 and 10^{-3} M of Oxone®

8.3.3. Tembotrione photocatalysis in the presence of Oxone®. Experimental design

A final effort was made to optimize the promoted photocatalytic process by completing a Plackett-Burman experimental design (ED) with three factors and two center points. The three factors were the initial concentrations of Oxone® and herbicide concentration plus the amount of catalyst added to the reaction media. Although pH exerts a high influence in the process, in order to reduce the disadvantages associated to a pH adjusting step in a real application, this parameter has not been considered in the experimental design.

Table 8.2 shows the factor values of the ED. The observed pseudo first order rate constant of tembotrione abatement was considered as the response of the process.

The regression of the data was completed by codifying the values of the factors between -1 and 1 corresponding to the minimum and maximum values used. A freeware Excel addin was used in the process.

By considering a linear plus interaction regression, the best output of the tembotrione abatement rate constant and the corresponding ANOVA analysis is shown in Table 8.3.

Table 8.2 Plackett-Burman experimental design and responses

Experiment	C_{TiO2} ($g L^{-1}$)	$C_{Oxone} \cdot 10^4$ (M)	$C_{TEMB,0}$ ($mg L^{-1}$)	k_{TEMB} (min^{-1})	$k_{TOC} \cdot 10^2$ (min^{-1})	$k_{Oxone} \cdot 10^2$ (min^{-1})
1	0.05	13	4.65	0.23	1.07	0.23
2	0.50	0.083	1.23	0.08	0.46	1.68
3	0.05	0.083	1.22	0.20	1.22	2.03
4	0.10	1.0	2.42	0.23	1.02	1.83

5	0.10	1.1	2.43	0.23	0.64	1.37
6	0.50	13	1.29	0.79	0.68	0.70
7	0.05	12	4.60	0.23	0.81	0.17
8	0.50	0.083	5.12	0.04	0.63	0.59
9	0.50	14	4.59	0.25	0.64	0.46
10	0.05	0.14	5.11	0.06	0.44	1.01
11	0.05	0.11	1.27	0.29	1.44	1.54
12	0.50	0.13	3.66	0.04	0.18	1.11
13	0.05	12	0.88	0.98	1.61	0.79
14	0.50	13	0.88	1.01	1.05	0.45

Table 8.3 Modelling of tembotrione abatement and mineralization in the Oxone® promoted photocatalysis system.

$$k_{\text{TEMB}}^{-1} = b_0 + b_1 C_{\text{TiO}_2} + b_2 C_{\text{Oxone}} + b_3 C_{\text{TEMB}} + b_4 C_{\text{TiO}_2} C_{\text{Oxone}} + b_5 C_{\text{Oxone}} C_{\text{TEMB}}$$

	Model parameters (k_{TEMB}^{-1})	Model parameters p-value·10 ²	ANOVA analysis	Value
b₀	7.853	0.002	R ²	0.941
b₁	2.575	1.277	R _{adj}	0.905
b₂	-5.876	0.022	Durbin Watson d	2.06
b₃	3.512	0.779	Sum of Squares (regression)	911
b₄	-2.782	0.973	Sum of Squares (residuals)	56.7
b₅	-2.650	2.877	F _{Signif} (Regression)	0.941

As inferred from Table 8.3, tembotrione abatement is acceptably modelled showing an R²_{adj} of 0.905, i.e. all the terms in the model are significant. Under the operating conditions investigated, titania and tembotrione concentrations show a negative effect in the pseudofirst order rate constant while Oxone® exerts a positive influence. An optimum in titania concentration was experimentally observed in the proximity of 0.05 g L⁻¹, coinciding with theoretical calculations of the LVRPA (Local Volumetric Rate of Photon Absorption) by means of Monte Carlo simulations (results not shown). The negative effect observed at higher titania concentrations is normally associated to a “shielding” effect, however, this aspect is at least controversial and is not substantiated by theoretical calculations. Likely, the negative effect observed is related to particle agglomeration leading to a lower surface exposed to radiation and tembotrione adsorption.

Figure 8.6 compares the values of k_{TEMB}^{-1} calculated and experimentally obtained. Also using the model parameters, some validation reactions completed at different titania concentrations and 10^{-4} M in Oxone® have been simulated and compared to model results. The simulation acceptably predicts the tembotrione removal profiles in runs not used in the experimental design. Some discrepancies were observed in the reaction completed with 0.05 g L^{-1} of titania; however, given the complexity of the system, these differences can be assumed within the uncertainty of the process variables.

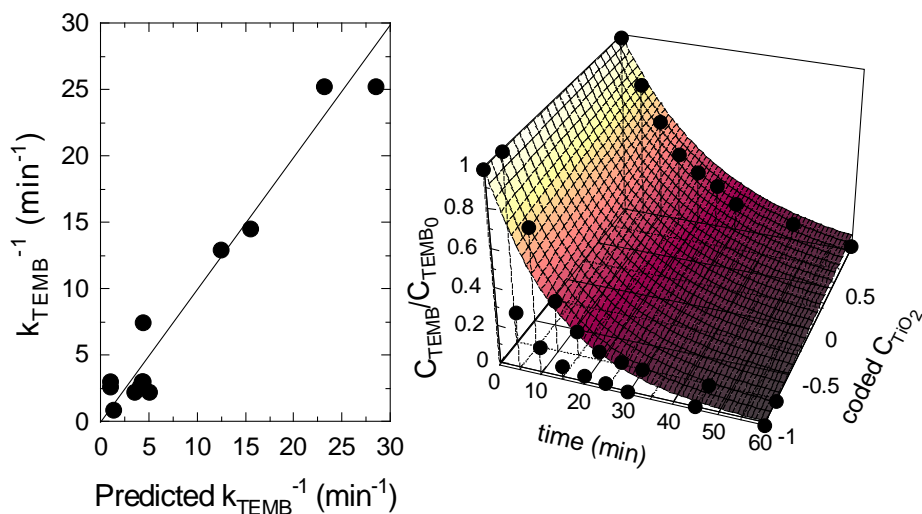


Figure 8.6 Oxone® promoted photocatalysis of tembotrione in the presence of titania P25. Left: comparison of experimental and model calculations. Right: Influence of titania concentration from model calculations. Experimental conditions: $T=25^\circ\text{C}$; $V=1.0 \text{ L}$; $\text{pH}=3.1$; $C_{\text{Oxone},0}=10^{-4} \text{ M}$, $C_{\text{TEMB},0}=5 \text{ mg L}^{-1}$ (●, experimental results at different titania concentrations)

8.4. CONCLUSIONS

Use of Oxone® seems to be a suitable alternative to oxidize organic aqueous contaminants. Direct tembotrione MPS oxidation follows 2/3 and first order in MPS and tembotrione concentrations, respectively. pH exerts an important effect since MPS and tembotrione pK_a 's do affect the process. 50.1 kJ mol^{-1} of activation energy was found to describe temperature influence on rate constant, according to Arrhenius definition.

MPS improves photocatalytic oxidation of tembotrione in both, parent compound and mineralization rate. The experimental design carried out shows that under the operating conditions investigated; titania and

tembotrione concentrations show a negative effect in the pseudofirst order rate constant while initial concentration of Oxone® exerts a positive influence.

Acknowledgments

Authors thank economic support received from *Gobierno de Extremadura* and *CICYT* of Spain through Projects GRU10012 and CTQ2012-35789-C02-01, respectively. Mr. Rafael Rodríguez Solís also thanks *Gobierno de Extremadura*, *Consejería de Empleo, Empresa e Innovación*, and *FSE Funds* for his Ph.D. grant (PD12058).

REFERENCES

- [1] Sutton P, Richards CL, Buren L, Glasgow L, *Activity of mesotrione on resistant weeds in maize*. *Pest Manag Sci* 58 (2002) 981-984
- [2] Tarara G, Fliege R, Desmarteau D, Kley C, Peters B, *Environmental fate of tembotrione*. *Bayer Crop Sci J* 62 (2009) 63-78
- [3] Transparency Market Research USA & Canada, 2015. *Global Tembotrione Market to Be Driven by Usage in Glyphosate-resistant Weed Control*. <http://www.transparencymarketresearch.com/article/global-tembotrione-market.htm> (last accessed 01-04-2016)
- [4] European Union, *Commission implementing decision of 10 April 2012 allowing Member States to extend provisional authorizations granted for the new active substances amisulbrom, chlorantraniliprole, meptyldinocap, pinoxaden, silver thiosulfate and tembotrione*. *Official J Eur Union* 102 (2012) 15-16
- [5] Tawk A, Deborde M, Labanowski J, Gallard H, *Chlorination of the β -triketone herbicides tembotrione and sulcotrione: kinetic and mechanistic study, transformation products identification and toxicity*. *Water Res* 76 (2015) 132-142
- [6] Calvayrac C, Bontemps N, Nougá-Bissoué A, Romdhane S, Coste CM, Cooper JF, *Photolysis of tembotrione and its main by-products under extreme artificial conditions: comparison with another β -triketone herbicide*. *Sci Total Environ* 452-453 (2013) 227-232
- [7] Trivella A, Stawinoga M, Dayan FE, Cantrell CL, Mazellier P, Richard C, *Photolysis of natural β -triketonic herbicides in water*. *Water Res* 78 (2015) 28-36
- [8] Halle AT, Richard R, *Simulated solar light irradiation of mesotrione in natural waters*. *Environ Sci Technol* 40 (2006) 3842-3847

- [9] Bensalah N, Khodary A, Abdel-Wahab A, *Kinetic and mechanistic investigations of mesotrione degradation in aqueous medium by Fenton process*. J Hazard Mater 189 (2011) 479-485
- [10] Jović M, Manojlović D, Stanković D, Dojčinović B, Obradović B, Gašić U, Roglić G, 2013. *Degradation of triketone herbicides, mesotrione and sulcotrione, using advanced oxidation processes*. J Hazard Mater 260 (2013) 1092-1099
- [11] Murati M, Oturan N, Aaron JJ, Dirany A, Tassin B, Zdravkovski Z, Oturan MA, *Degradation and mineralization of sulcotrione and mesotrione in aqueous medium by the electro-Fenton process: a kinetic study*. Environ Sci Pollut Res 19 (2012) 1563-1573
- [12] Sun J, Li X, Feng F, Tian X, *Oxone/Co²⁺ oxidation as an advanced oxidation process: comparison with traditional Fenton oxidation for treatment of landfill leachate*. Water Res 43 (2009) 4363-4369
- [13] Anipsitakis GP, Stathatos E, Dionysiou DD, *Heterogeneous activation of oxone using Co₃O₄*. J Phys Chem B 109 (2005) 13052-13055
- [14] Su S, Guo W, Leng Y, Yi C, Ma Z, *Heterogeneous activation of Oxone by Co_xFe_{3-x}O₄ nanocatalysts for degradation of rhodamine B*. J. Hazard Mater 244-245 (2013) 736-742
- [15] Yao Y, Xu C, Qin J, Wei F, Rao M, Wang S, *Synthesis of magnetic cobalt nanoparticles anchored on graphene nanosheets and catalytic decomposition of orange I*. Ind Eng Chem Res 52 (2013) 17341-17350
- [16] Fernández J, Maruthamuthu PA, Kiwi J, *Photobleaching and mineralization of Orange II by oxone and metal ions involving Fenton like chemistry under visible light*. J Photochem Photobiol A 161 (2004) 185-192
- [17] Rivas FJ, Gimeno O, Borralho T, Carbajo M, *UV-C radiation based methods for aqueous metoprolol elimination*. J Hazard Mater 179 (2010) 357-362
- [18] Gao YQ, Gao NY, Deng Y, Yin DQ, Zhang YS, Rong WL, Zhou SD, *Heat activated persulfate oxidation of sulfamethoxazole in water*. Desalination. Water Treat 56 (2015) 2225-2233
- [19] Anipsitakis GP, Dionysiou DD, González MA, *Cobalt-mediated activation of peroxymonosulphate and sulphate radical attack on phenolic compounds. Implications of chloride ions*. Environ Sci Technol 40 (2006) 1000-1007

- [20] Ji F, Li C, Deng L, *Performance of CuO/Oxone system: heterogeneous catalytic oxidation of phenol at ambient conditions*. Chem Eng J 178 (2011) 239-243
- [21] Rivas FJ, Gimeno O, Borallho T, *Aqueous pharmaceutical compounds removal by potassium monopersulfate. Uncatalyzed and catalyzed semicontinuous experiments*. Chem Eng J 192 (2012) 326-333
- [22] Deng J, Shao Y, Gao N, Tan C, Zhou S, Hu X, *CoFe₂O₄ magnetic nanoparticles as a highly active heterogeneous catalyst of oxone for the degradation of diclofenac in water*. J Hazard Mater 262 (2013) 836-844
- [23] Romero A, Santos A, Vicente F, González C, *Diuron abatement using activated persulfate: effect of pH, Fe(II) and oxidant dosage*. Chem Eng J 162 (2010) 257-265
- [24] Cong J, Wen G, Huang T, Deng L, Ma J, 2015. *Study on enhanced ozonation degradation of para-chlorobenzoic acid by peroxymonosulfate in aqueous solution*. Chem Eng J 264 (2015) 399-403
- [25] Anipsitakis GP, Tufano TP, Dionysiou DD, *Chemical and microbial decontamination of pool water using activated potassium peroxymonosulfate*. Water Res 48 (2008) 2899-2910
- [26] Malato S, Blanco J, Richter C, Braun B, Maldonado MI, *Enhancement of the rate of solar photocatalytic mineralization of organic pollutants by inorganic oxidizing species*. Appl Catal B Environ 17 (1998) 347-356
- [27] Gimeno O, Carbajo M, López MJ, Melero JA, Beltrán FJ, Rivas FJ, *Photocatalytic promoted oxidation of phenolic mixtures: an insight into the operating and mechanistic aspects*. Water Res 41 (2007) 4672-4684
- [28] Shukla PR, Wang S, Ang HM, Tade MO, *Photocatalytic oxidation of phenolic compounds using zinc oxide and sulfate radicals under artificial solar light*. Sep Purif Technol 70 (2010) 338-344
- [29] Miller JN, Miller JC, *Statistics and Chemometrics for Analytical Chemistry*, sixth ed. Pearson, Harlow 2010
- [30] Fukushima M, Tatsumi T, *Effect of hydroxypropyl- β -cyclodextrin on the degradation of pentachlorophenol by potassium monopersulfate catalyzed with iron(III)-porphyrin complex*. Environ Sci Technol 39 (2005) 9337-9342
- [31] Rivas J, Solís RR, Gimeno O, Sagasti J, *Photocatalytic elimination of aqueous 2-methyl-4-chlorophenoxyacetic acid in the presence of*

commercial and nitrogen-doped TiO₂. Int J Environ Sci Technol 12 (2015) 513-526

- [32] Renganathan R, Maruthamuthu PJ, *Kinetics and mechanism of oxidation of aromatic aldehydes by peroxomonosulfate*. Chem Soc Perkin Trans 11 (1986) 285-289
- [33] Yang S, Wang P, Yang X, Shan L, Zhang W, Shao X, Niu R, *Degradation efficiencies of azo dye Acid Orange 7 by the interaction of heat, UV and anions with common oxidants: persulfate, peroxymonosulfate and hydrogen peroxide*. J Hazard Mater 179 (2010) 552-558

CHAPTER NINE

PAPER SEVEN

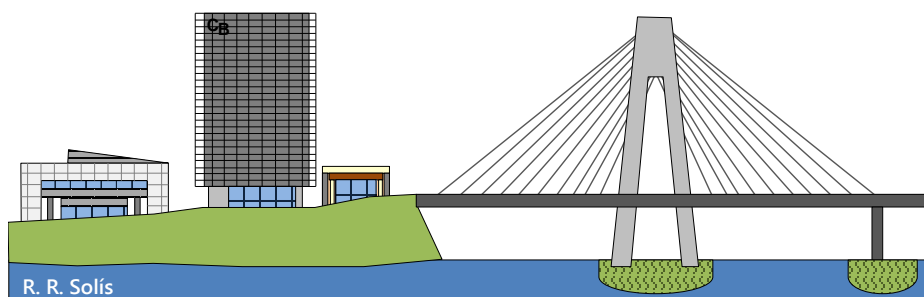
Removal of aqueous metazachlor, tembotrione, tritosulfuron and ethofumesate by heterogeneous monoperoxysulfate decomposition on lanthanum-cobalt perovskites

Appl Catal B Environ 200 (2017) 83-92

Rafael R. Solís, F. Javier Rivas, Olga Gimeno

ABSTRACT. This study reports LaCoO_3 perovskite oxide activity in the removal of aqueous herbicides (metazachlor, tembotrione, tritosulfuron and ethofumesate) by means of potassium monoperoxysulfate (MPS) decomposition. The influences of initial MPS concentration and catalyst load have been assessed. MPS is instantaneously absorbed onto the perovskite surface where this species decomposes. Thus, MPS breakage leads to the formation of powerful oxidizing radicals which react with herbicides in solution. Tritosulfuron was the most recalcitrant compound towards this technology. Catalyst stability was tested by means of consecutive reuse cycles. No appreciable loss of activity was experienced. Experiments in the presence of *tert*-butyl alcohol, methanol and carbonate outlined the importance of radicals in herbicides degradation. Finally, synthesized LaCoO_3 was characterized. Scanning and transmission electron microscopy showed the presence of nanosized material, mostly spherical shaped, with $15.20 \text{ m}^2 \text{ g}^{-1}$ of BET area. LaCoO_3 perovskite structure was corroborated by diverse techniques such as X-ray fluorescence (La:Co atomic ratio of 1:1), X-ray photoelectron spectroscopy (surface Co(III) and La(III)), and X-ray diffraction (rhombohedral LaCoO_3 phase).

KEYWORDS: LaCoO_3 perovskite, oxone, monoperoxysulfate, herbicides, oxidation



R. R. Solís

Biblioteca Pública Bartolomé J. Gallardo, Edificio Badajoz Siglo XXI y Puente Real, Badajoz

9.1. INTRODUCTION

Farming uses large amounts of herbicides which usually run off into water resources. Therefore, a large list of different herbicides and pesticides is frequently detected in surface waters as micropollutants [1,2]. These discharges suppose a great environmental impact causing undesirable effects on non-targeted species. Metazachlor ($C_{14}H_{16}ClN_3O$, CAS 67129-08-2, METAZ) belongs to chloroacetamide family, tembotrione ($C_{17}H_{16}ClF_3O_6S$, CAS 335104-84-2, TEMB) is a synthetic β -triketone, tritosulfuron ($C_{13}H_9F_6N_5O_4S$, CAS 142469-14-5, TRITO) is a sulfonylurea and ethofumesate ($C_{13}H_{18}O_5S$, CAS 26225-79-6, ETHO) is an example of benzofuran selective systemic herbicide. All of them are commonly applied as pre and post-emergence control of diverse weeds in a wide variety of crops. Table 9.S1 shows some of their most important properties. Although the majority of these herbicides are relatively new in use, their occurrence in water is being screened at $ng\ L^{-1}$ or even $\mu g\ L^{-1}$ levels [1-5].

Oxone[®] ($2KHSO_5 \cdot KHSO_4 \cdot K_2SO_4$) is the commercial name of the main source of potassium monoperoxysulfate (MPS), which is considered a versatile and environmentally friendly oxidant used for bleaching, cleaning and disinfection. MPS is attracting attention due to its capacity of producing sulfate radicals which have some advantages over hydroxyl radical, such as higher oxidation potential, higher selectivity and effectiveness; wider pH range for reaction and higher half-life [6]. MPS can be activated by means of temperature [7], UV radiation [8], and metallic catalysts [7]. Hence, cobalt is catalogued as one of the best transition metal in the homogeneous activation of MPS [9]. However, homogeneous catalysis requires the further removal of the catalyst, especially in those cases where the active substance presents toxic properties. Actually, cobalt shows toxicity and causes health problems at very low concentrations, leading to the development of asthma, pneumonia and cardiomyopathy [10]. As a consequence, developing heterogeneous catalysts containing cobalt for MPS activation seems to be a challenging and promising alternative. Nevertheless, acid conditions usually lead to cobalt leaching. Thus, this latter aspect has to be taken into account.

A number of previous studies have investigated the heterogeneous catalytic decomposition of MPS using cobalt oxides such as CoO and Co_3O_4 [11], spinel cobalt ferrite ($CoFe_2O_3$) [12], and cobalt supported onto diverse materials like different oxides (TiO_2 , MgO, Al_2O_3 , SiO_2 , MnO_2 or ZnO) or activated carbon [6]. In a high number of cases, problems associated to cobalt leaching have been experienced.

Perovskite oxides derive from the ABO_3 structure, where the A cation is larger than the B cation. $LaXO_3$ perovskite oxides have been demonstrated to be active in wet peroxide oxidation processes [13]. Lanthanum perovskites have successfully been used in catalytic ozonation [14] and some H_2O_2 and/or UV mediated processes [15]. Nevertheless, to author's knowledge, no attention to $LaCoO_3$ as a MPS activator has been paid. The present study reports the use of $LaCoO_3$ perovskite oxide in MPS activation. $LaCoO_3$ has been synthesized, and the solid characterized by means of nitrogen isotherm adsorption, scanning and transmission electron microscopy, X-ray photoelectron spectroscopy, X-ray fluorescence and X-ray diffraction. $LaCoO_3$ and MPS combination has been applied to a mixture of four herbicides in water (metazachlor, tembotrione, tritosulfuron and ethofumesate). The effectiveness of $LaCoO_3$ and MPS combination has been studied varying MPS concentration, catalyst load and solution pH, which are the main operating variables. Cobalt leaching has also been considered at different operating pHs. Catalyst reusability and radical scavenger presence have also been assessed.

9.2. EXPERIMENTAL

9.2.1. Materials

Analytical herbicide Pestanal[®] standards were purchased from Sigma-Aldrich[®]. Oxone[®] was acquired from Sigma-Aldrich[®]. Lanthanum (III) nitrate hexahydrate (>99.99%) from Aldrich[®], cobalt (II) acetate tetrahydrate (>98%) from Sigma-Aldrich[®] and citric acid (99%) from Aldrich[®] were used for perovskite synthesis. The rest of chemicals were purchased from Sigma-Aldrich and used as received. Acetonitrile from VWR Chemicals was used in HPLC determination of herbicides in water. All solutions were prepared with ultrapure water from a Milli-Q[®] academic (Millipore) system (18.2 M Ω cm).

9.2.2. Catalyst synthesis and characterization

$LaCoO_3$ perovskite was synthesized in the presence of citric acid as complexing organic agent [16]. In a typical synthesis run, $La(NO_3)_3 \cdot 6H_2O$ and $Co(CH_3COO)_2 \cdot 4H_2O$ with a molar ratio La:Co=1:1 were dissolved in 400 mL of ultrapure water. After 1 h mixing under magnetic agitation, 100 mL of citric acid in excess (twice the stoichiometrically needed for each metal [16]) was slowly added. The resultant solution was heated at 100°C to remove water excess, drying thereafter the obtained pinkish gel. The solid was grinded and calcined at 700°C for 7 h. This catalyst was used in all experiments.

pH of point of zero charge (pH_{pzc}) was obtained by mass titration method [17]. Briefly, a solution of HNO_3 0.1 M was prepared and pH adjusted until

value of 3 with NaOH 0.1 M. Different containers with increasing amounts of solid (0.05, 0.1, 0.5, 1, 5, 10 and 20%) were filled with 15 mL of solution. Solutions were kept under stirring and pH was measured after 48 h of equilibria. A plot of pH versus solid fraction (%) gives a curve which tends asymptotically to pH_{pzc} value.

BET surface area was quantified by means of nitrogen adsorption isotherms obtained at 77 K with a Quadrasorb instrument (Quantachrome). Prior to analysis, samples were treated at 150°C for 24 h under high vacuum conditions.

Scanning Electron Microscopy (SEM) was conducted in a Hitachi-S-4800 coupled to a secondary electrons detector (acceleration voltage 20 kV) while Transmission Electron Microscopy (TEM) analysis was applied using a TEM Tecnai G2 20 Twin-FEI company apparatus (filament LaB6, voltage 200 kV, magnification up to $1.05 \cdot 10^6$).

X-ray Photoelectron Spectroscopy (XPS) spectra were obtained using a XPS K-alpha-Thermo Scientific device, working with a $K\alpha$ monochromatic source of Al (1486.68 eV). A value of 284.8 eV for the C 1s peak was taken to calibrate the signals of the rest peaks. High resolution of XPS spectra for La 3d, Co 2p and O 1s were recorded.

The XRF measurements were carried out by a sequential wavelength dispersive X-Ray Fluorescence (WDXRF) spectrometer (S8 Tigger, Bruker) equipped with an X-ray tube of rhodium anode operating at 60 kV, and 170 mA.

Thermal Gravimetry, Differential Temperature Analysis and released gases Mass Spectrometry (TG-DTA-MS) was performed with a Setaram SETSYS Evolution-16 equipment connected to a Prisma™ QMS200 quadrupole mass spectrometer. The operation conditions were: sample loading 21 mg, air flow rate 50 mL min^{-1} and heating rate of $10^\circ\text{C min}^{-1}$ from room temperature to 800°C.

Crystalline phases were analyzed by X-Ray Diffraction (XRD), in a Bruker D8 Advance diffract meter equipped with a monochromator of Ge 111 $K\alpha$ of Cu (wavelength, 1.5456 Å). A temperature chamber complemented the installation in order to obtain diffractograms through temperature variation.

9.2.3. Experimental setup and procedure

The experimental reaction system basically consisted of a 1.0 L borosilicate cylindrical glass vessel. It was magnetically stirred by an IKA® RCT stirrer

equipped with temperature control. The reactor was filled with 1.0 L of herbicides (1 mg L⁻¹ of each) water solution. pH was adjusted by NaOH addition (10 or 1 M). In order to start the reaction, a small volume (less than 10 mL) of a high concentrated MPS solution was initially added, and pH was thereafter readjusted. Previously, to achieve the adsorption equilibrium, the solution was kept under stirring for 30 min. Samples were regularly extracted at different times and filtered with Millex-HA filters (Millipore, 0.45 µm). HPLC samples were quenched with Na₂S₂O₃ 0.5 M (10 µL per 1 mL of sample).

9.2.4. Analytical methods

Herbicides were analyzed by an Agilent 1100 (Hewlett-Packard) High Performance Liquid Chromatography equipped with UV detection (HPLC-UV). The column used was a Kromasil 100 5C18 (5 µm, 2.1x150 mm). A mobile phase composed by 0.1% H₃PO₄ acidified water (A) and acetonitrile (B) was pumped at a flow rate of 1 mL min⁻¹, with an isocratic percentage composition of 55:45 A:B. UV detection was conducted at 220 nm. Observed retention times were 6.4, 11.3, 12.5 and 14.9 min for metazachlor, tembotrione, tritosulfuron, and ethofumesate, respectively. Figure 9.S1 shows a typical example of chromatogram.

MPS concentration evolution was analyzed spectrophotometrically by a colorimetric method based on N,N-diethyl-p-phenylenediamine (DPD) oxidation [18].

Cobalt leaching was quantified by means of atomic absorption, using a Varian SpectrAA Series 140 instrument. Alternatively, this metal was also analyzed spectrophotometrically by the zincon method [19].

pH of the reaction media was monitored, adjusted and controlled by means of a Crison GLP 21+ pH meter, whose electrode was submerged into the reactor.

9.3. RESULTS AND DISCUSSION

9.3.1. Operating variables influence

pH influence and cobalt leaching

As stated in the introduction section, one of the main drawbacks in using heterogeneous catalysts containing transition metals is the deactivation of the catalyst due to leaching of these metals into the water bulk [20]. Additionally, homogeneous catalysis of dissolved metals may mislead to the interpretation of the results obtained. Accordingly, a first experimental series was conducted

at different pH operating conditions. In addition to parent compound removal, leached cobalt was also monitored in these experiments.

Figure 9.1 shows the results obtained when pH 3, 5, 7, and 9 were used. Previous to these experiments, blank runs demonstrated the negligible reactivity of monoperoxysulfate alone towards individual herbicides (the exception was tembotrione). However, some conversion was obtained in all herbicides when treated with MPS simultaneously (likely, tembotrione partial conversion generates some species capable of reacting with the rest of herbicides).

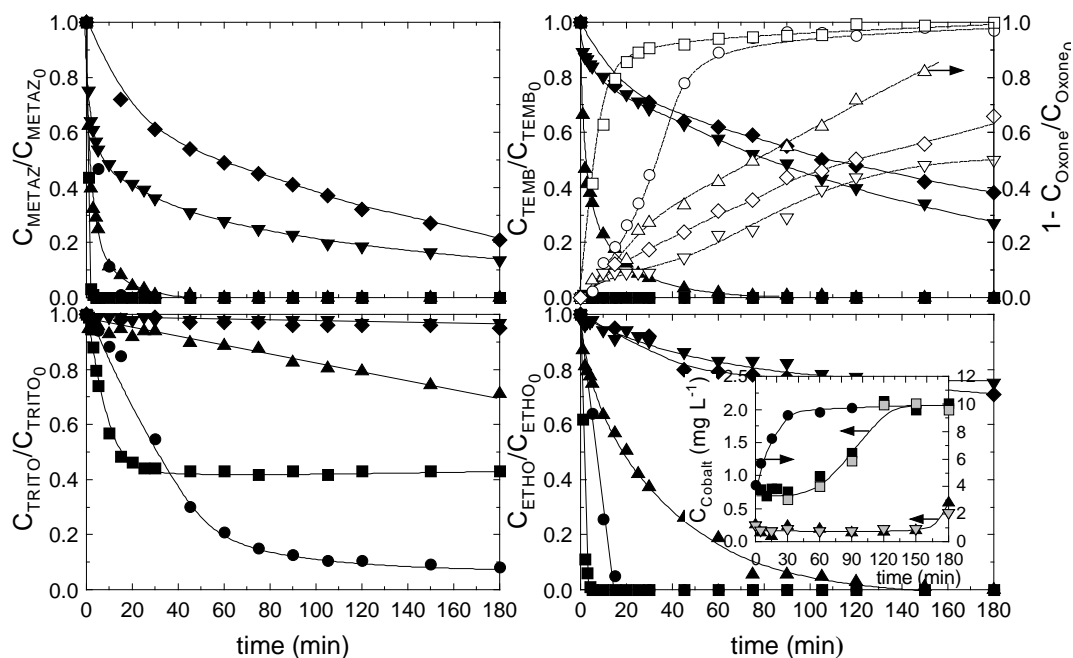


Figure 9.1 Oxone® mediated elimination of a mixture of herbicides in the presence of LaCoO_3 . Influence of pH. Experimental conditions: $C_{\text{Herbicide}}=1 \text{ mg L}^{-1}$ each, $C_{\text{LaCoO}_3}=0.5 \text{ g L}^{-1}$, $T=20^\circ\text{C}$. $C_{\text{Oxone},0}=1.0 \cdot 10^{-4} \text{ M}$, pH: ●, 3.0; ■, 5.0; ▲, 7.0; ▼, 9.0; ◆, 7.0, homogeneous contribution. Open symbols in top right figure: Oxone® conversion. **Inset figure:** leached cobalt (grey filled symbols correspond to atomic absorption analysis, black ones were spectrophotometrically obtained).

As observed in Figure 9.1, the system is more effective at low pH. Hence, instantaneous 100% conversion (less than 1 min) of metazachlor, tembotrione and ethofumesate was experienced when pH values in the range 3-5 were used. Tritosulfuron was the most recalcitrant compound, requiring more than 100 min to achieve 90% elimination. Inset in Figure 9.1 depicts the

evolution of cobalt in water. At the sight of the figure, a significant leaching of cobalt to water bulk was obtained when the working pH was 3. The concentration of this transition metal was as high as 4 mg L^{-1} even before the addition of Oxone[®], (leached during the 30 min adsorption period). Under these conditions, the homogeneous reaction predominates over the heterogeneous path. Moreover, as the reaction progresses, the concentration of cobalt reaches values in the proximity of 10 mg L^{-1} . Oxone[®] is easily decomposed in the presence of dissolved cobalt leading to radical species [11]. Hence, monoperoxysulfate concentration rapidly decreases at pH 3 and 5. As a consequence, tritosulfuron abatement comes to a halt when Oxone[®] conversion reaches roughly 90%. Homogeneous catalyzed Oxone[®] decomposition rate is favored at alkaline conditions [21], explaining why the peroxide is faster removed at pH 5 than at pH 3, even when cobalt concentration is lower at the more basic pH. Monoperoxysulfate decomposition orders regarding Co^{2+} and H^+ concentrations are 1 and -1 , respectively [22]. Accordingly, a 5-10 fold increase in dissolved cobalt concentration exerts a lower influence than a 100-fold decrease in protons. At circumneutral or basic pH, leached cobalt concentration is quite low (below 0.2 mg L^{-1} or $3.4 \cdot 10^{-6} \text{ M}$). The homogeneous contribution was analyzed at neutral pH by carrying out an experiment in the presence of 0.2 mg L^{-1} of cobalt, which is the observed cobalt lixiviated at this pH. The results revealed that herbicide conversions were similar to those obtained in a blank run in the presence of Oxone[®] and absence of cobalt and catalyst.

pH reduces cobalt leaching and decreases monoperoxysulfate abatement. The pH_{pzc} value of the catalyst was found to be 9.08 (Figure 9.S2). This explains the ability of the catalyst to adsorb anions, such as monoperoxysulfate, at acidic or neutral pH since its surface is positively charged. The low MPS decomposition at $\text{pH}=9$ is likely related to its second acid dissociation $\text{pK}_a=9.4$.

Oxone concentration

Taking into account the results obtained in the previous section, in order to avoid cobalt leaching and limit this study to the heterogeneous catalysis, next experiments were conducted at pH 7, a compromise between leached cobalt and reaction rate. The influence of the initial Oxone[®] concentration was studied in the range 10^{-4} - 10^{-3} M . Figure 9.2 shows the results obtained in this experimental series. As inferred from this figure, Oxone[®] concentration above $5 \cdot 10^{-4} \text{ M}$ led to the instantaneous removal of metazachlor, tembotrione and ethofumesate while tritosulfuron required almost one hour to completely disappear when $5 \cdot 10^{-4} \text{ M}$ in Oxone[®] was used. As stated previously,

experiments in the absence of perovskite did show some reactivity of Oxone® towards the herbicides when simultaneously treated.

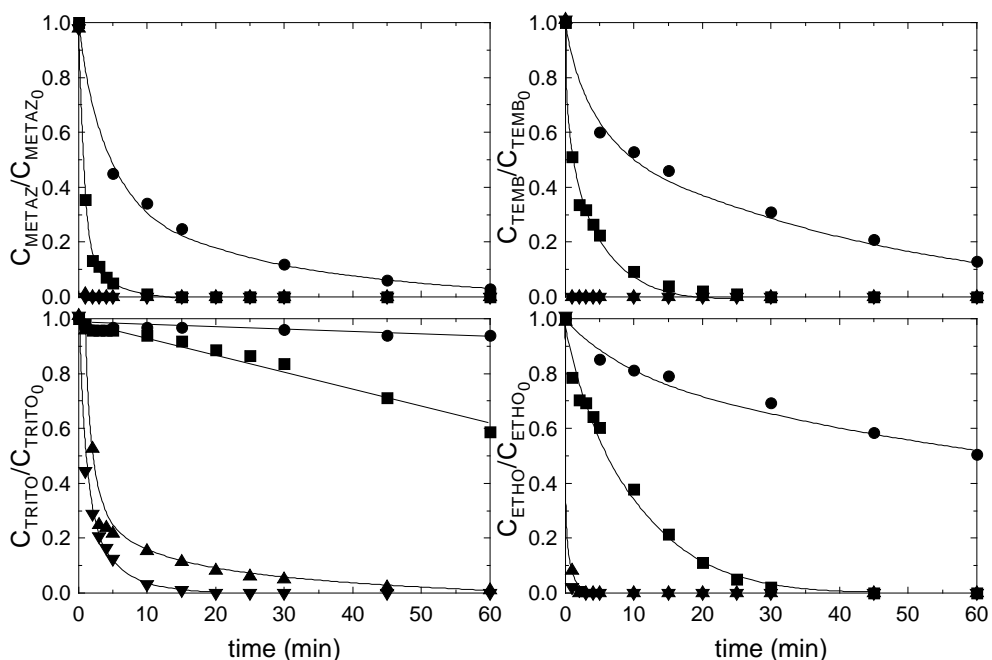


Figure 9.2 Oxone® mediated elimination of a mixture of herbicides in the presence of LaCoO_3 . Influence of initial Oxone® concentration. Experimental conditions: $C_{\text{Herbicide}}=1 \text{ mg L}^{-1}$ each, $\text{pH}=7$, $C_{\text{LaCoO}_3}=0.5 \text{ g L}^{-1}$, $T=20^\circ\text{C}$. $C_{\text{Oxone},0}\cdot 10^4 \text{ (M)}$: ●, 1.0; ■, 2.0; ▲, 5.0; ▼, 10

An analysis of Oxone® uptake (measured as moles of monoperoxysulfate consumed per mol of herbicide abated, see Figure 9.3), applied to the two runs conducted with the lowest oxidant concentration revealed an efficient consumption of the oxidant up to values of 60-70% of total herbicides conversion; thereafter, the stoichiometric coefficient sharply increased by following an exponential growth, likely due to the accumulation of intermediates competing for the active oxidizing species generated.

From a practical point of view, conversion values below 70% are recommended provided that the effluent can be further polished in a biological step or fulfill the regulatory laws of direct discharge. At this point, it should be pointed out that 70% total conversion involves the complete elimination of metazachlor and tembotrione and 80% removal of ethofumesate. Tritosulfuron, being the most recalcitrant compound only achieves a scarce 10% oxidation.

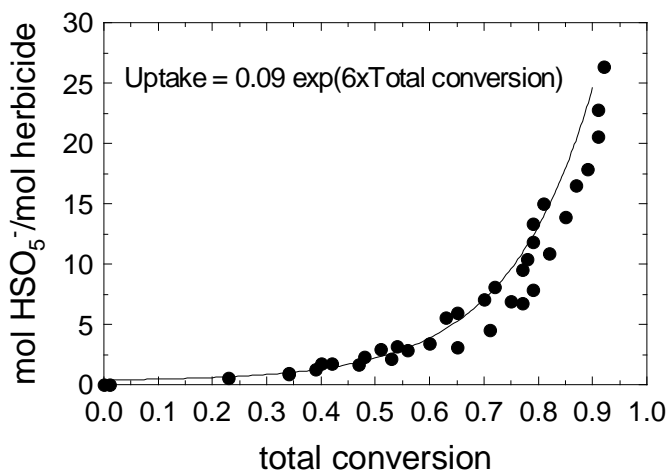


Figure 9.3 Oxone[®] mediated elimination of a mixture of herbicides in the presence of LaCoO₃. Monoperoxysulfate uptake as a function of total conversion. Experimental conditions: $C_{\text{Herbicide}} = 1 \text{ mg L}^{-1}$ each, $\text{pH} = 7$, $C_{\text{LaCoO}_3} = 0.5 \text{ g L}^{-1}$, $T = 20^\circ\text{C}$. $C_{\text{Oxone},0} = 1.0 - 2.0 \cdot 10^{-4} \text{ M}$

Catalyst concentration influence

An additional experimental series was conducted at different perovskite concentrations by maintaining the rest of operating variables constant. Figure 9.4 depicts the results obtained when 10^{-4} M in Oxone[®] was used. As a rule of thumb, perovskite amount exerts a positive influence on herbicides conversion, although global differences are minor when analyzing the results of total herbicide abatement achieved when 0.5, 1.0 and 1.5 g L^{-1} of catalyst were used (see bottom-right inset of Figure 9.4 which depicts total conversion versus time).

Once more, Figure 9.4 confirms the recalcitrance of tritosulfuron if compared to the reactivity of the rest of herbicides. The shape of the curves revealed a fast initial period (first 2-3 min) where herbicide concentration sharply decreases. Thereafter, the removal rate slows down resembling first order like kinetics. A priori, this behavior cannot be attributed to a fast adsorption of herbicides. Hence, previous to each experiment, the herbicides solution is stirred in the presence of perovskite for 30 min with negligible change in their aqueous concentration.

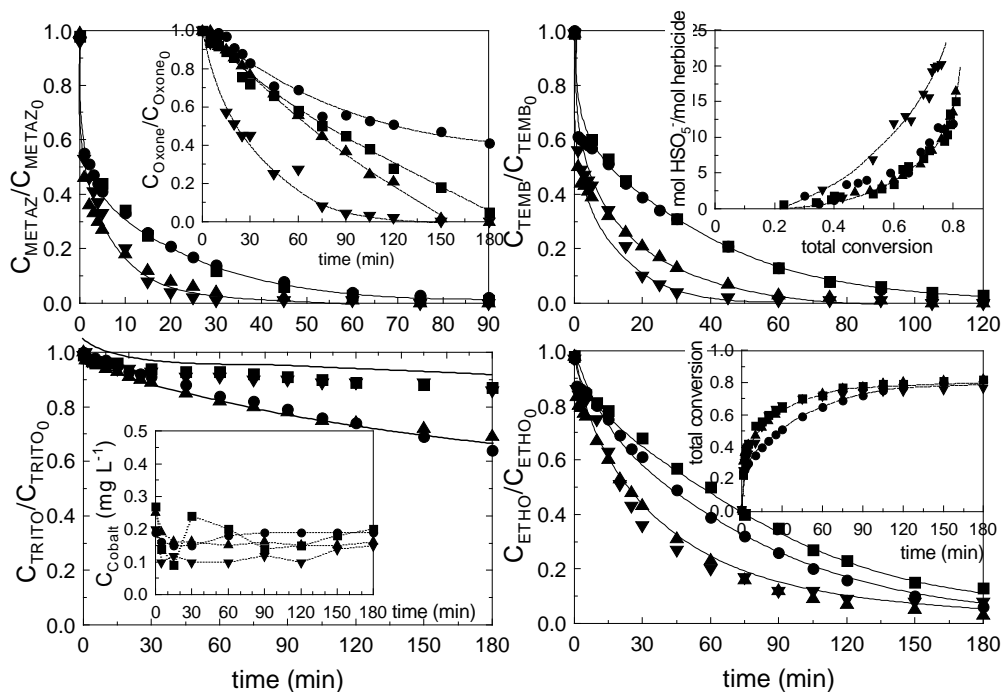
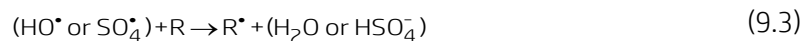
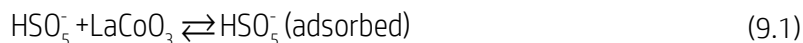


Figure 9.4 Oxone® mediated elimination of a mixture of herbicides in the presence of LaCoO₃. Influence of perovskite concentration. Experimental conditions: $C_{Herbicide}=1 \text{ mg L}^{-1}$ each, pH=7, T=20°C. $C_{Oxone,0}=1.0 \cdot 10^{-4} \text{ M}$, C_{LaCoO3} (g L⁻¹): ●, 0.25; ■, 0.50; ▲, 1.0; ▼, 1.5. **Inset Figures:** top-left, Oxone® normalized concentration; top-right, monoperoxysulfate uptake; bottom-left, cobalt leached; bottom-right, total herbicide conversion.

On the one hand, the rise of catalyst load does significantly affect the rate of decomposition of monoperoxysulfate (top-left inset of Figure 9.4) which denotes the role played by the catalyst in the formation of radicals. On the other hand, a high amount of solid seems to negatively affect the monoperoxysulfate efficient uptake (top-right inset of Figure 9.4). Hence, a slightly higher consumption of Oxone® was experienced when 1.5 g L⁻¹ of LaCoO₃ was used, not leading to an appreciable improvement in herbicides total conversion if compared to results obtained when lower solid concentrations were used.

Additionally, the bottom-left inset of Figure 9.4 shows that the amount of cobalt leached was negligible, below 0.2 mg L⁻¹, and constant regardless of the initial perovskite concentration or elapsed reaction time. This small amount suggests a high stability of the catalyst which was thereafter checked

by conducting some runs using the same recovered catalyst. From the experimental results obtained previously the following simplified mechanism is proposed, taking monoperoxysulfate and organic matter (represented as R) into account:



Hence, the fast adsorption of monoperoxysulfate until equilibrium would lead to the instantaneous generation of radicals and fast removal of herbicides. Thereafter, a chain radical mechanism would evolve accounting for the second slower stage. The second stage would be controlled by the rate of organic radical reactions.

Catalyst stability

To ascertain the stability of the catalyst, six consecutive runs were conducted by recycling the catalyst used. As observed in Figure 9.5, the solid maintains its activity even in the last run. This fact is also corroborated if considering the monoperoxysulfate depletion profile shown in the embedded plot. No appreciable cobalt leaching was experienced in these experiments.

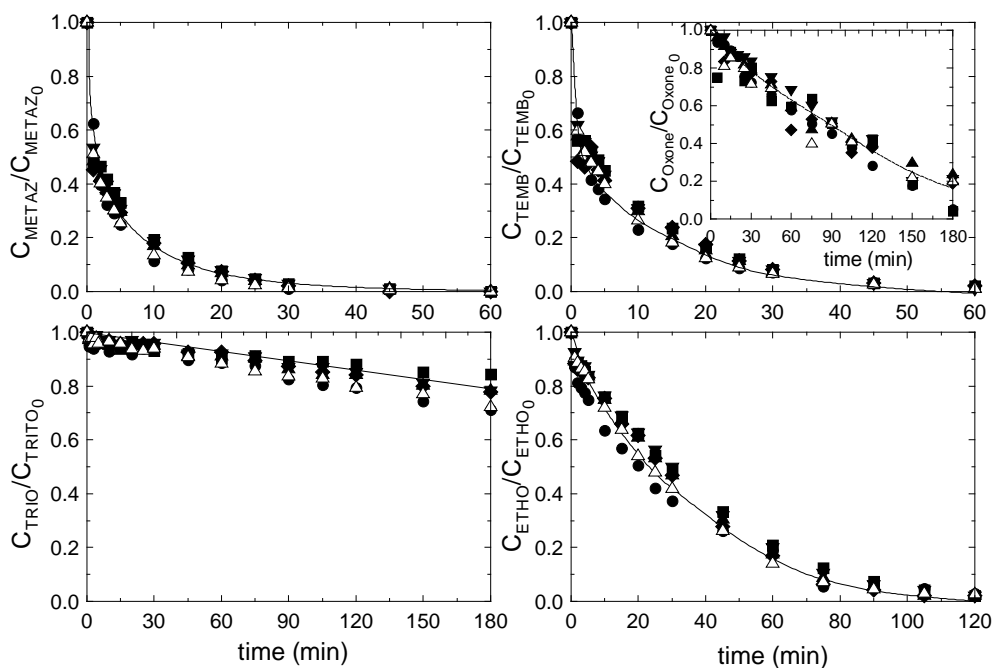
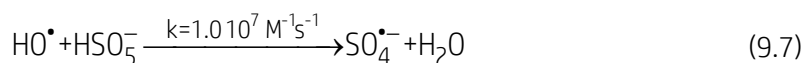


Figure 9.5 Oxone® mediated elimination of a mixture of herbicides in the presence of LaCoO₃. Influence of perovskite reuse. Experimental conditions: C_{Herbicide}=1 mg L⁻¹ each, pH=7, T=20°C. C_{Oxone,0}=1.0 10⁻⁴ M, C_{LaCoO3}=0.5 g L⁻¹. ●, Fresh catalyst; ■, 1st reuse; ▲, 2nd reuse; ▼, 3rd reuse; ◆, 4th reuse; △, 5th reuse. **Inset Figure:** Oxone® normalized evolution

Scavengers influence

The influence of radical scavengers was assessed by using *tert*-butyl alcohol (t-BuOH), Methanol (MeOH) and carbonates which react with hydroxyl and sulfate radicals with second order rate constants of 6 10⁸ M⁻¹s⁻¹ [23] and 4 10⁵ M⁻¹s⁻¹ [24], 9.7 10⁸ M⁻¹s⁻¹ [25] and 3.2 10⁶ M⁻¹s⁻¹ [26], and 8.5 10⁶ M⁻¹s⁻¹ [27] and 9.1 10⁶ M⁻¹s⁻¹ [28], respectively.

Figure 9.6 reveals some interesting aspects. Hence, *tert*-butyl alcohol, a well-known hydroxyl radical scavenger, has no significant influence in the monoperoxysulfate decomposition rate onto the perovskite surface. This fact suggests that monoperoxysulfate is not decomposed by free hydroxyl radicals found in the solution bulk according to:



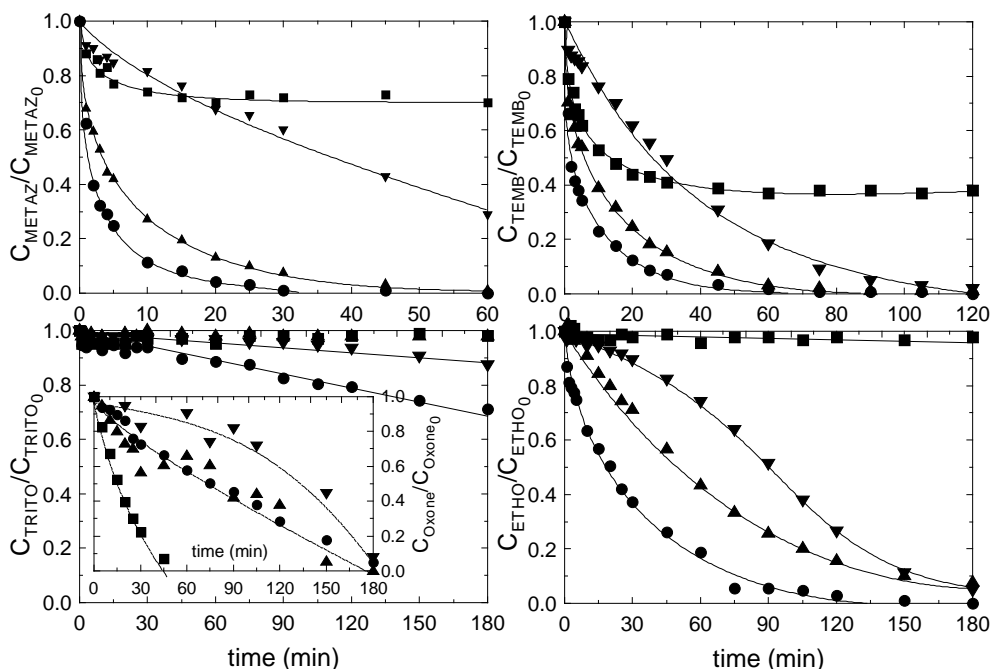


Figure 9.6 Oxone® mediated elimination of a mixture of herbicides in the presence of LaCoO_3 . Influence of scavengers presence. Experimental conditions: $C_{\text{Herbicide}}=1 \text{ mg L}^{-1}$ each, $\text{pH}=7$, $T=20^\circ\text{C}$. $C_{\text{Oxone},0}=1.0 \cdot 10^{-4} \text{ M}$, $C_{\text{LaCoO}_3}=0.5 \text{ g L}^{-1}$, Scavenger: ●, No scavenger; ■, Methanol 10^{-2} M ; ▲, *tert*-butanol 10^{-2} M ; ▼, Carbonates $5 \cdot 10^{-3} \text{ M}$. **Inset Figure:** Oxone® normalized evolution

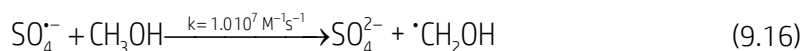
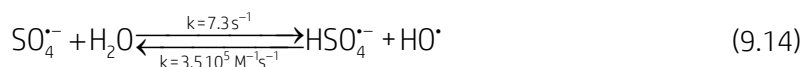
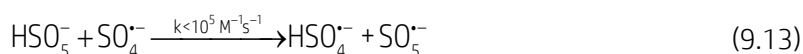
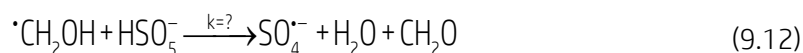
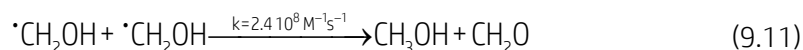
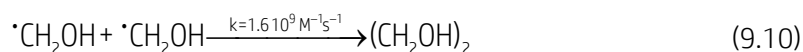
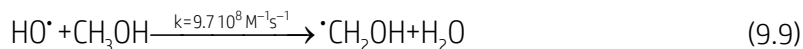
These results could be expected since herbicides compete with the promoter to trap the HO^\bullet species (Reaction 9.3) showing second order rate constants around 2-3 orders of magnitude higher. Accordingly, by considering the total herbicide concentration (roughly $12 \mu\text{M}$) and an average second order rate constant of $5 \cdot 10^9 \text{ M}^{-1}\text{s}^{-1}$, the ratio of the above competing reactions would be:

$$\text{Ratio} = \frac{k_{\text{HO}^\bullet, \text{herbicides}} C_{\text{herbicides}}}{k_{\text{HO}^\bullet, \text{HSO}_5^-} C_{\text{HSO}_5^-}} \approx \frac{5 \cdot 10^9 \times 1.2 \cdot 10^{-5}}{110^7 \times 2.0 \cdot 10^{-5}} \approx 30 \quad (9.8)$$

However, the presence of the tertiary alcohol partially inhibits the removal rate of the herbicides, suggesting that HO^\bullet species are present in solution.

Given the particular effect of MeOH addition, this reaction was conducted by triplicate. The reproducibility of the results confirmed a fast inefficient monoperoxysulfate depletion leading to a significant inhibition of herbicides removal. The inhibition is likely related to suppression not only of HO^\bullet but also of sulfate radicals due to their reactions with methanol. Additionally,

monoperoxysulfate would tentatively be decomposed by reacting with hydroxymethyl radicals (Equation 9.12) initiating an inefficient chain mechanism in terms of herbicides removal. Additionally, the aforementioned hypothesis would sustain why tembotrione is less affected since this compound directly reacts with monoperoxysulfate. The mechanism supporting these facts obeys the following reactions [22, 28]:



Carbonates negatively affect herbicides removal rates, likely due to radical scavenging. However, contrary to MeOH, monoperoxysulfate is decomposed to a lower extent if compared to the experiments in the absence of scavengers. The explanation can be associated to two potential effects, on one hand by partially avoiding the reactions of radicals and monoperoxysulfate; and on the other hand, the most probable cause may be that carbonates could negatively affect the adsorption of Oxone® onto the perovskite surface impeding its decomposition.

9.3.2. Catalyst characterization

Figure 9.53 reports results of nitrogen adsorption isotherm. As it could be observed, LaCoO₃ provides a type II isotherm, which is characteristic of non-porous or macroporous materials. In this kind of isotherm unrestricted

monolayer and multilayer adsorption may take place. Multipoint BET surface area fitting (see Figure 9.S3 inset) in the range p/p_0 0.1-0.35 led to a specific surface area of $15.20 \text{ m}^2 \text{ g}^{-1}$, which is indicative of a non-porous material ($R=0.998$). It might prove the fact of a nanosized material. From this linear regression is also possible to obtain the C constant ($C=5.592$), which is related to the affinity and interaction of the solid with the adsorbate; and therefore, the heat of the process.

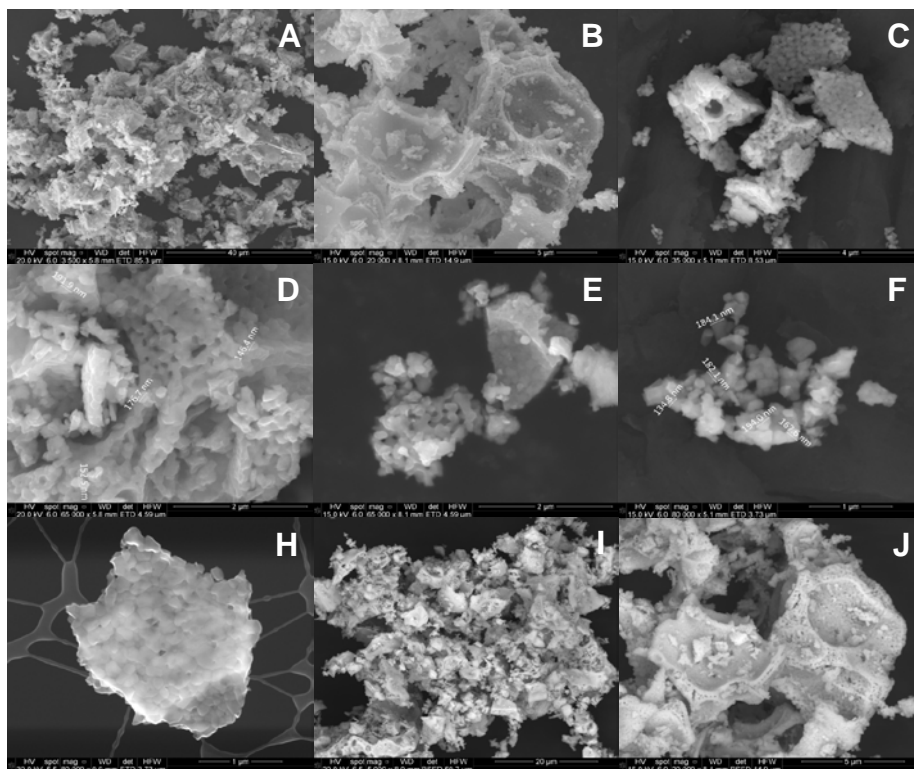


Figure 9.7 LaCoO_3 powder SEM images obtained using secondary electrons (A-H) and backscattered electrons (I and J)

LaCoO_3 powder was also studied by means of Scanning Electron Microscopy (SEM). Diverse micrographs are summarized in Figure 9.7. Firstly, main images, which are obtained from secondary electrons, verify the existence of homogeneous nanosized spherical particles, which are in the range 15-18 nm. This fact has been reported in literature [29,30]. However, these particles seem to form bigger agglomerates (100-200 nm). Actually, some structures are made of these spherical particles, strongly linked to each other, where it is difficult to distinguish them. In others, the spherical aggregates are weakly linked. The biggest structures might have followed a pattern before grinding the powder in the synthesis process, as it could be

discerned in some images. Secondly, from BackScattered Electrons (BSE) pictures (images I and J in Figure 9.7), it is possible to analyze the homogeneity in terms of composition of the sample. Thus, the contrast in the image produced is determined by the distribution of different chemical phases in the sample. Accordingly, high homogeneity was observed, leading to the idea of one phase oxide composition. Thirdly, an Energy Dispersive X-ray (EDX, Figure 9.54) analysis led to an elemental composition, expressed as atomic percentage, 22.12 ± 0.55 , 23.60 ± 1.31 , 54.28 ± 1.82 for La, Co and O, respectively.

Wavelength Dispersive X-Ray Fluorescence (WDXRF) was also applied to calculate the proportion between cobalt and lanthanum (Fig. S5). Without taking oxygen into account, 49.45 ± 0.02 and $50.54 \pm 0.02\%$ of atomic La and Co was found, respectively (proportion La:Co=1.00:1.02).

TEM analysis confirmed the morphology and size particle observed in SEM. Results are shown in Figure 9.56. In this figure it is possible to observe that spherical particles illustrated in SEM micrographs are likely to be composed by smaller aggregates, whose size is inferior to 100 nm in some cases. Despite what is reported in others LaCoO_3 works [31,32], a clear crystal phase could not be confirmed from TEM analysis.

XPS technique was employed to analyze LaCoO_3 surface properties. Figure 9.8 depicts general and high resolution spectra of La3d, Co2p and O1s regions. In Co2p region two peaks can be appreciated, whose maximums are located at 794.8 and 779.9 eV. These values correspond to $\text{Co}2p_{1/2}$ and $\text{Co}2p_{3/2}$, respectively. $\text{Co}2p_{3/2}$ binding energy highly coincides with conventional value reported on Co_2O_3 and LaCoO_3 [33,34], where Co(III) state dominates. Furthermore, absence of satellite peaks ensures that the perovskite catalyst exclusively contains trivalent cobalt. La3d shows two regions with two peaks each one, corresponding to $\text{La}3d_{5/2}$ (834.5 and 837.6 eV) and $\text{La}3d_{3/2}$ (851.2 and 854.8 eV). These values again ensure the presence of La (III) as it is observed in La_2O_3 [29]. XPS spectrum of O1s level presents two high features at 531.2 and 528.7 eV. The lower value could be attributed to oxide state, O^{2-} , characteristic of perovskite oxide network; while the higher value mainly represents the existence of hydroxyl groups in the surface, or adsorbed oxygen arising from atmospheric exposure [29,35,36]. The atomic superficial percentages, after a Shirley type background subtraction were 15.05, 11.48 and 57.25 for La, Co and O, respectively. These values differ from atomic ratios reported by EDX and XRF techniques, leading to a higher O proportion. Since XPS is a superficial analysis, the reason of this

behavior may be originated from the presence of hydroxylated groups onto the surface of the solid.

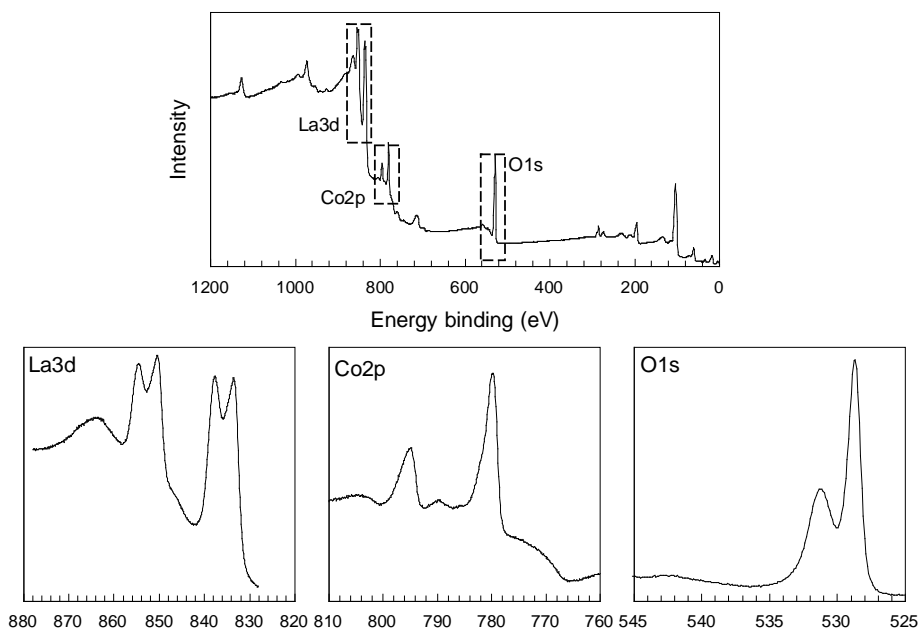


Figure 9.8 XPS of LaCoO_3 . General and high resolution spectra of La3d, Co2p and O1s

In order to assess the effect of temperature during the process of calcination, a sample dried at 105-110°C before being annealing was characterized by means of Thermal Gravimetry, Differential Temperature Analysis and released gases Mass Spectrometry (TG-DTA-MS) and X-ray Diffraction (XRD). TG spectrum (Figure 9.9) shows a weak and continuous weigh loss up to 120°C due to water desorption and condensation of hydroxyl groups, being accompanied with a slightly exothermic peak at 157°C. Firstly, from this temperature until ~320°C, H_2O and CO_2 are continuously released. In a second stage, at 347°C a maximum of CO_2 release and an exothermic DTA peak are appreciated. This fact is the result of organic species burning and solid-state reaction. At this temperature a change in TG rate is also observed. DTA peak keeps increasing until 480°C, sharply decreasing at 500°C, when combustion is supposed to be finished. After 500°C, no significant changes in TG, DTA and released gases are appreciated. A final 71.3% of mass loss is observed. In this loss, 15.76% is associated to H_2O and 79.9% corresponds to CO_2 . A final 4.35% is due to minor gases which accompany the two CO_2 release steps. H_2 is appreciated in the second and most important release of CO_2 . Mass 58 may be identified as an acetone derivate. The simultaneous release of mass 15 may correspond to methyl fragments. A very low intensity

mass 36 is observed, which might be tentatively identified as a sulfur derivative.

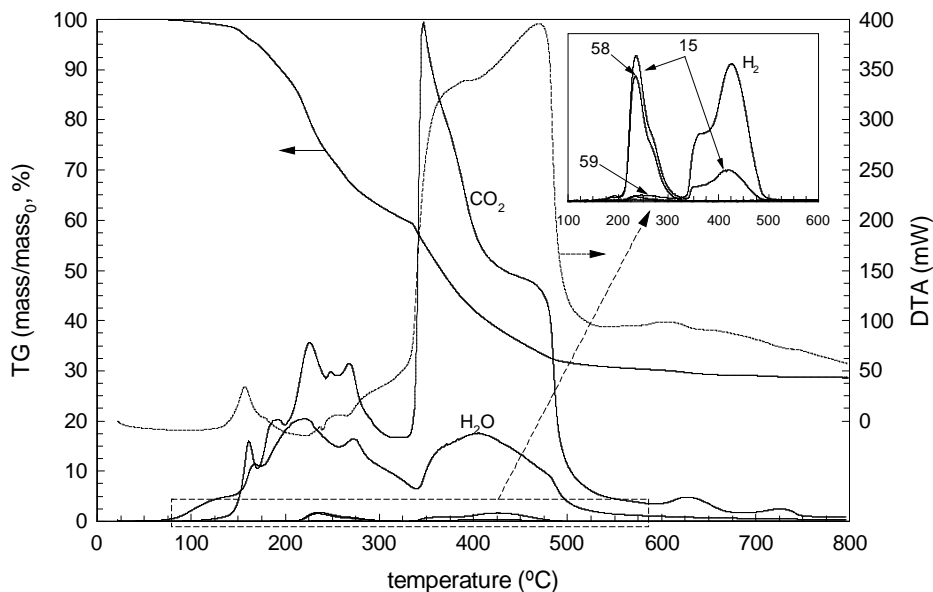


Figure 9.9 TG-DTA-MS of uncalcined LaCo_3 powder

XRD in a thermal untreated sample was carried out, in order to assess the effect of temperature in LaCoO_3 structure formation. Results are depicted in Figure 9.10. During the calcination process rhombohedral LaCoO_3 perovskite-type symmetry is formed [29,30,34]. At low temperatures, e.g. 600°C , a semiquantitative analysis outlines $\text{Co}(\text{OH})_2$ (hexagonal, 18.9%), Co_3O_4 (cubic, 9.6%), $\text{La}_2\text{O}_2\text{CO}_3$ (hexagonal, 11.3%), La_2O_3 (cubic, 2.3%), CoCO_3 (rhombohedral, 48.5%) and $\text{La}(\text{OH})_3$ (hexagonal, 9.4%) as the main species. Hydroxides and carbonated precursors are likely to be responsible for LaCoO_3 formation. As temperature increases, the intensity of the starting patterns gradually diminishes and the peaks of perovskite structure increase. Thus, at 800°C the sample is composed mainly by LaCoO_3 (rhombohedral, 83.6%), and small amounts of La_2O_3 (hexagonal, 8.5%) and Co_3O_4 (cubic, 7.9%).

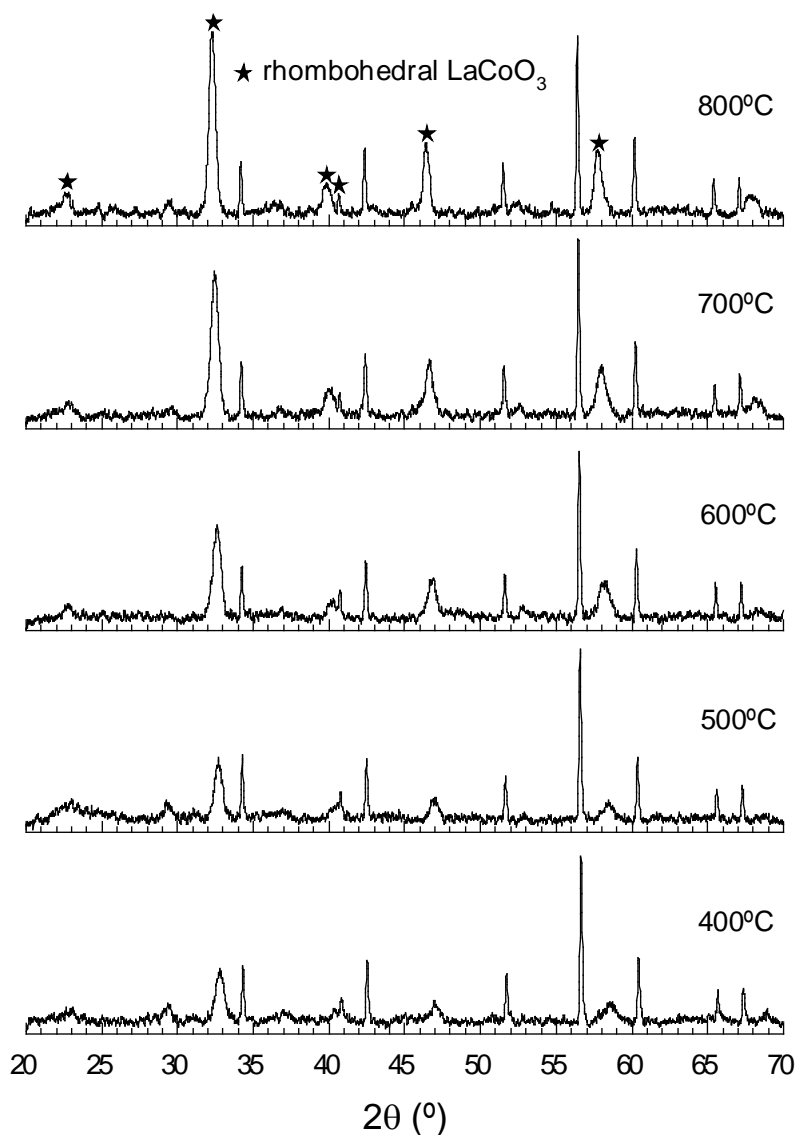


Figure 9.10 XRD patterns of LaCoO₃ precursor during calcination process

9.4. CONCLUSIONS

LaCoO₃ shows a high activity with unappreciated cobalt leaching at neutral or basic pH. While acidic conditions accelerate the process due to homogeneous contribution from cobalt leaching, basic pH also worsens MPS decomposition rate. Furthermore, catalyst stability was analyzed by means of consecutive recycling uses and no significant loss in removal rate activity was

experienced. pH and stability highly concern the nature of water which is suitable to be considered for this technology. Herbicides as micropollutants are frequently screened in natural water resources, whose pH is usually around circumneutral conditions. Thus, natural waters with a low content of organic matter and neutral or slightly basic pH are recommended.

Oxone® concentration up to 10^{-4} M led to a complete elimination of herbicides, being tritosulfuron the most recalcitrant compound. Experiments in the presence of *tert*-butyl alcohol indicate that MPS decomposes onto the perovskite surface. The technology seems to be suitable for removing organic pollutants even at mg L^{-1} concentrations.

Solid LaCoO_3 settles down easily which is an advantage if compared to other catalysts. Moreover, since load does not significantly improve reaction rate, a low concentration would be enough for activating MPS decomposition, facilitating its recovering from the solution.

SEM and TEM techniques reveal the formation of nanosized particles, mainly spherical shaped. A poor $15.20 \text{ m}^2 \text{ g}^{-1}$ BET area was found and LaCoO_3 perovskite presence was remarked by diverse techniques such as X-ray Fluorescence (La:Co atomic ratio of 1:1), X-ray Photoelectron Spectroscopy (surface Co(III) and La(III)), and X-ray Diffraction (rhombohedral LaCoO_3 phase). TG-DTA-MS and XRD corroborated the formation of perovskite at temperatures higher than 700°C .

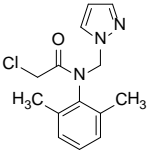
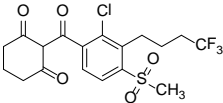
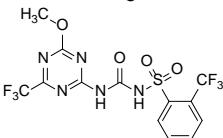
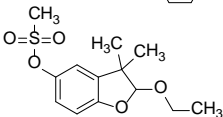
Future work should be focused on assessing the possibilities of this perovskite catalyst in combination with some photocatalysts. Adding radiation might enhance MPS decomposition and radicals' production.

Acknowledgements

Authors thank economic support received from *Gobierno de Extremadura* and *CICYT* of Spain through Projects GRU10012 and CTQ2012-35789-C02-01, respectively. Mr. Rafael Rodríguez Solís also thanks *Gobierno de Extremadura*, *Consejería de Empleo, Empresa e Innovación*, and FSE Funds for his Ph.D. grant (PD12058). Catalyst characterization was provided by Facility of Analysis and Characterization of Solids and Surfaces of SAIUEx (financed by *UEX*, *Junta de Extremadura*, *MICINN*, *FEDER* and *FSE*).

Supplementary data

Table 9.S1 Herbicides properties (from the Pesticide Properties Database, <http://sitem.herts.ac.uk/aeru/ppdb/en/index.htm>)

Herbicide	Molecule Structure	Formula	CAS	pK _a	Water solubility (mg L ⁻¹)
Metazachlor		C ₁₄ H ₁₆ ClN ₃ O	67129-08-2	N/A	450
Tembotrione		C ₁₇ H ₁₆ ClF ₃ O ₆ S	335104-84-2	3.18	71000
Tritosulfuron		C ₁₃ H ₉ F ₆ N ₅ O ₄ S	142469-14-5	4.69	78.3
Ethofumesate		C ₁₃ H ₁₈ O ₅ S	26225-79-6	N/A	50

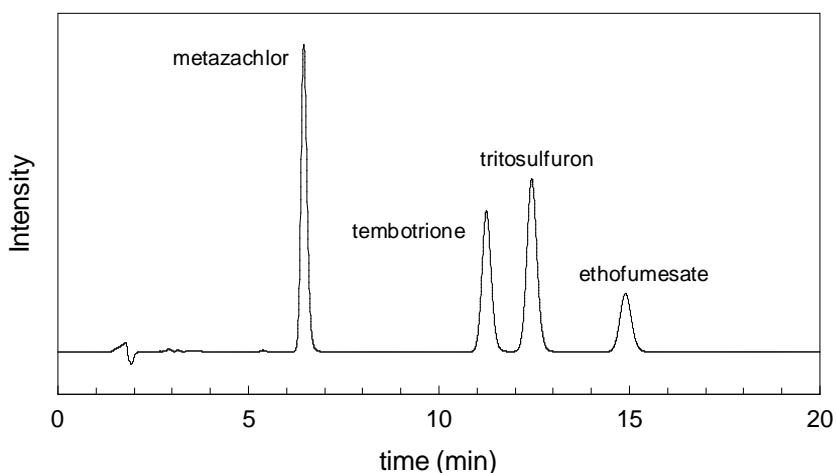


Figure 9.S1 HPLC-UV chromatogram of a mixture of metazachlor (5.010 mg L⁻¹), tembotrione (5.010 mg L⁻¹), tritosulfuron (5.005 mg L⁻¹) and ethofumesate (5.005 mg L⁻¹) in water. Chromatographic analysis conditions: mobile phase 45% ACN-50% H₂O (0.1% H₃PO₄), flow rate 1 mL min⁻¹, injection volume 100 μL, UV conduction at 220 nm

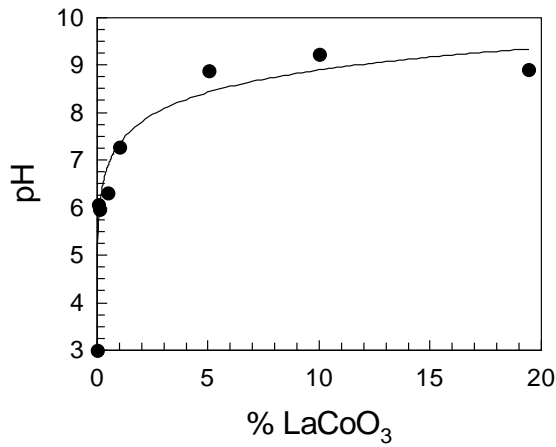


Figure 9.52 pH_{pzc} of fresh $LaCoO_3$ determination by mass titration method

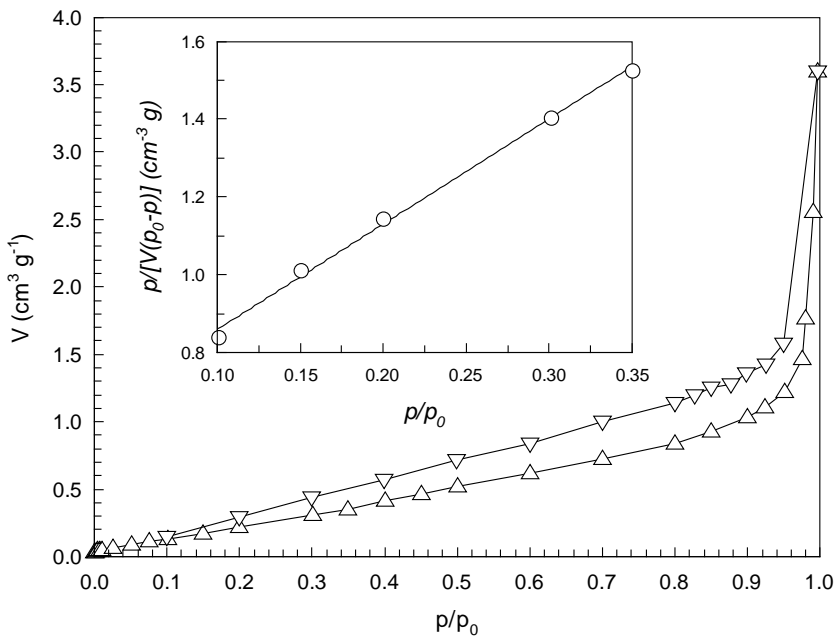


Figure 9.53 Nitrogen isotherm adsorption and desorption of fresh $LaCoO_3$ powder.
Inset Figure: BET equation representation

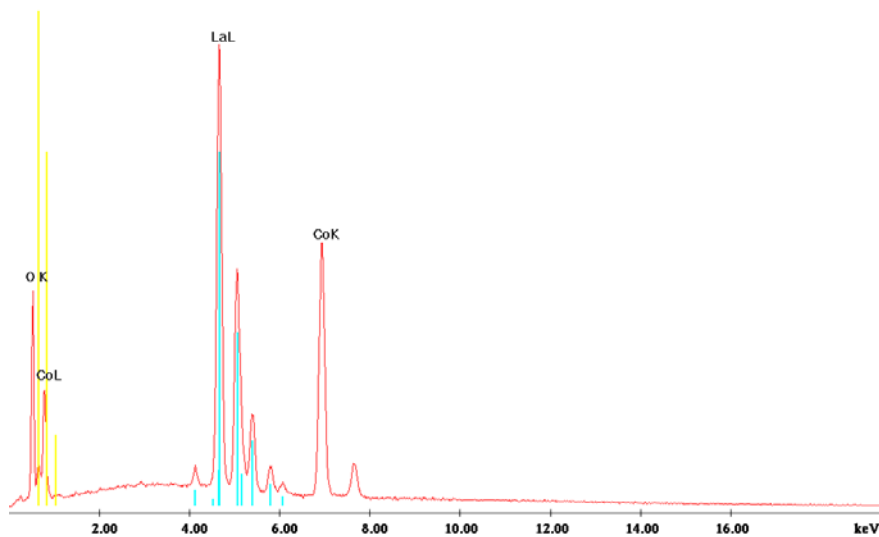


Figure 9.S4 Example of EDX (30kV) analysis spectrum of fresh LaCoO_3

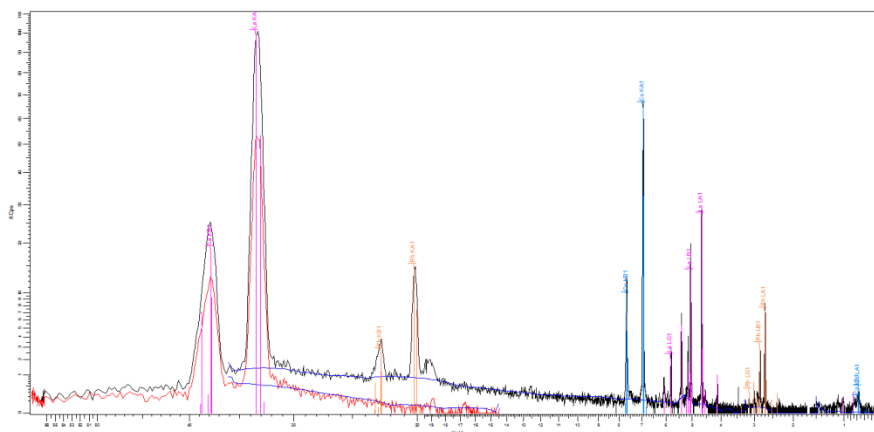


Figure 9.S5 Example of WDXRF spectrum of fresh LaCoO_3

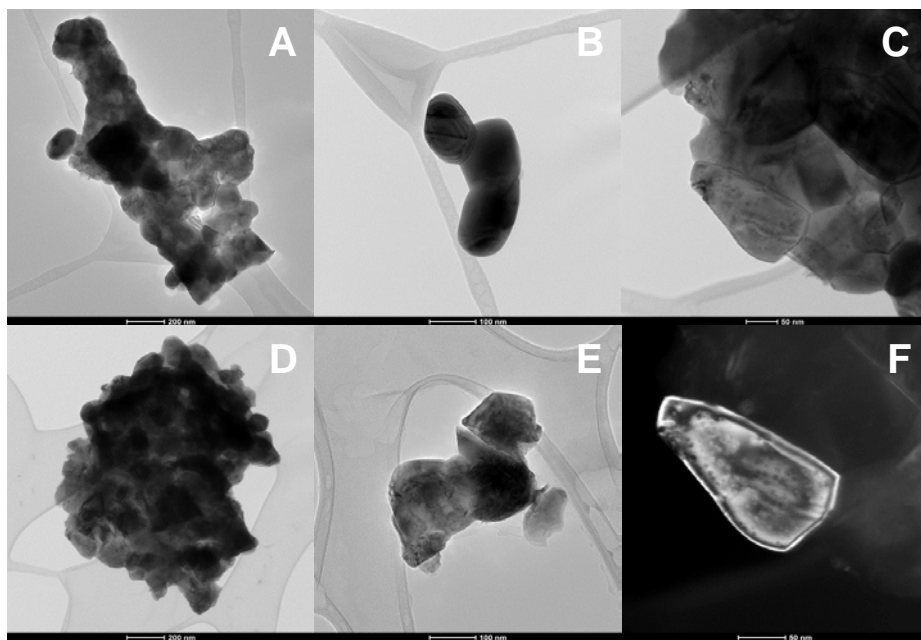


Figure 9.56 TEM images of fresh LaCoO_3 powder

REFERENCES

- [1] Reemtsma T, Alder L, Banasiak U, *Emerging pesticide metabolites in groundwater and surface water as determined by the application of a multimethod for 150 pesticide metabolites*. *Water Res* 47 (2013) 5535-5545
- [2] Moschet C, Wittmer I, Simovic J, Junghans M, Piazzoli A, Singer H, Stamm C, Leu C, Hollender J, *How a complete pesticide screening changes the assessment of surface water quality*. *Environ Sci Technol* 48 (2014) 5423-5432
- [3] Vryzas Z, Vassiliou G, Alexoudis C, Papadopoulou-Mourkidou E, *Spatial and temporal distribution of pesticide residues in surface waters in northeastern Greece*. *Water Res* 43 (2009) 1-10
- [4] Herrero-Hernández E, Andrades MS, Álvarez-Martín A, Pose-Juan E, Rodríguez-Cruz MS, Sánchez-Martín MJ, *Occurrence of pesticides and some of their degradation products in waters in a Spanish wine region*. *J Hydrol* 486 (2010) 234-245

- [5] Silva E, Daam MA, Cerejeira MJ, *Aquatic risk assessment of priority and other river basin specific pesticides in surface waters of Mediterranean river basins*. Chemosphere 135 (2015) 394-402
- [6] Hu P, Long M, *Cobalt-catalyzed sulfate radical-based advanced oxidation: a review on heterogeneous catalysts and applications*. Appl Catal B Environ 181 (2016) 103-117
- [7] Gao YQ, Gao NY, Deng Y, Yin DQ, Zhang YS, Rong WL, Zhou SD, *Heat-activated persulfate oxidation of sulfamethoxazole in water*. Desalination Water Treat 56 (2015) 2225-2233
- [8] Yang S, Wang P, Yang X, Shan L, Zhang W, Shao X, Niu R, *Degradation efficiencies of azo dye Acid Orange 7 by the interaction of heat, UV and anions with common oxidants: Persulfate, peroxymonosulfate and hydrogen peroxide*. J Hazard Mater 179 (2010) 552-558
- [9] Anipsitakis GP, Dionysiou DD, *Radical Generation by the Interaction of Transition Metals with Common Oxidants*. Environ Sci Technol 38 (2004) 3705-3712
- [10] Barceloux DG, *Cobalt*. Clin Toxicol 37 (1999) 201-216
- [11] Anipsitakis GP, Stathatos E, Dionysiou DD, *Heterogeneous Activation of Oxone Using Co_3O_4* . J Phys Chem B 109 (2005) 13052-13055
- [12] Ren Y, Lin L, Ma J, Yang J, Feng J, Fan Z, *Sulfate radicals induced from peroxymonosulfate by magnetic ferrosin MFe_2O_4 ($M = Co, Cu, Mn, and Zn$) as heterogeneous catalysts in the water*. Appl Catal B Environ 165 (2015) 572-578
- [13] Tarana OP, Ayusheev AB, Ogorodnikova OL, Prosvirin IP, Isupova LZ, Parmon VN, *Perovskite-like catalysts $LaBO_3$ ($B = Cu, Fe, Mn, Co, Ni$) for wet peroxide oxidation of phenol*. Appl Catal B Environ 180 (2016) 86-93
- [14] Carbajo M, Beltrán FJ, Gimeno O, Acedo B, Rivas FJ, *Ozonation of phenolic wastewaters in the presence of a perovskite type catalyst*. Appl. Catal. B: Environ. 74 (2007) 203-210
- [15] Rivas FJ, Carbajo M, Beltrán F, Gimeno O, Frades J, *Comparison of different advanced oxidation processes (AOPs) in the presence of perovskites*. Appl Catal B Environ 155 (2008) 407-414
- [16] Sotelo JL, Ovejero G, Martínez F, Melero Ja, Milieni A, *Catalytic wet peroxide oxidation of phenolic solutions over a $LaTi_{1-x}Cu_xO_3$ perovskite catalyst*. Appl. Catal. B: Environ. 47 (2004) 281-294

- [17] Noh JS, Schwarz JA, *Effect of HNO₃ treatment on the surface acidity of activated carbons*. Carbon 28 (1990) 675-682
- [18] Fukushima M, Tatsumi K, *Effect of Hydroxypropyl-β-cyclodextrin on the Degradation of Pentachlorophenol by Potassium Monopersulfate Catalyzed with Iron(III)-Porphyrin*. Complex Environ Sci Technol 39 (2005) 9337-9342
- [19] Ghasemi J, Ahmadi Sh, Torkestani K, *Simultaneous determination of copper, nickel, cobalt and zinc using zincon as a metallochromic indicator with partial least squares*. Anal Chim Acta 487 (2003) 181-188
- [20] Shukla P, Sun H, Wang S, Ang HM, Tadé MO, *Nanosized Co₃O₄/SiO₂ for heterogeneous oxidation of phenolic contaminants in wastewater*. Sep Purif Technol 77 (2011) 230-236
- [21] Rivas J, Gimeno O, Carbajo M, Borrvalho T, *Catalytic Decomposition of Potassium Monopersulfate. Influence of Variables*. World Acad Sci Eng Technol 57 (2009) 218-222
- [22] Gimeno O, Rivas J, Carbajo M, Borrvalho T, *Catalytic Decomposition of Potassium Monopersulfate. The Kinetics*. World Acad Sci Eng Technol 57 (2009) 223-226
- [23] Wolfenden BS, Willson RL, *Radical-cations as reference chromogens in kinetic studies of one-electron transfer reactions: pulse radiolysis studies of 2,2'-azinobis-(3-ethylbenzthiazoline-6-sulphonate)*. J Chem Soc Perkin Trans II (1982) 805-812
- [24] Eibenberger H, Steenken S, O'Neill P, Schulte-Frohlinde D, *Pulse radiolysis and electron spin resonance studies concerning the reaction of SO₄.^{•-} with alcohols and ethers in aqueous solution*. J Phys Chem 82 (1978) 749-750
- [25] Buxton GV, Greenstock CL, Helman WP, Ross AB, *Critical Review of rate constants for reactions of hydrated electrons, hydrogen atoms and hydroxyl radicals (•OH/•O⁻ in Aqueous Solution*. J Phys Chem Ref Data 17 (1988) 513-886
- [26] Buxton GV, Elliot AJ, *Rate constant for reaction of hydroxyl radicals with bicarbonate ions*. Int J Radiat Appl Instrum C Radiat Phys Chem 27 (1986) 241-243
- [27] Dogliotti L, Hayon E, *Flash photolysis of per[oxydi]sulfate ions in aqueous solutions. The sulfate and ozonide radical anions*. J Phys Chem 71 (1967) 2511-2516

- [28] Ulanski P, Sonntag C, *The OH radical-induced chain reactions of methanol with hydrogen peroxide and with peroxodisulfate*. J Chem Soc 2 (1999) 165-168
- [29] Natile MM, Ugel E, Maccato C, Glisenti A, *LaCoO₃: Effect of synthesis conditions on properties and reactivity*. Appl Catal B Environ 72 (2007) 351-362
- [30] Predoana L, Malic B, Kosec M, Carata M, Caldararu M, Zaharescu M, *Characterization of LaCoO₃ powders obtained by water-based sol-gel method with citric acid*. J Eur Ceram Soc 27 (2007) 4407-4411
- [31] Xiong G, Zhi ZL, Yang X, Lu L, Wan X, *Characterization of perovskite-type LaCoO₃ nanocrystals prepared by a stearic acid sol-gel process*. J Mater Sci Lett 16 (1997) 1064-1068
- [32] Wang Y, Yang x, Lu L, Wang X, *Experimental study on preparation of LaMO₃ (M=Fe, Co, Ni) nanocrystals and their catalytic activity*. Termochim Acta 443 (2006) 225-230
- [33] Yamada Y, Yano K, Honga D, Fukuzumi S, *LaCoO₃ acting as an efficient and robust catalyst for photocatalytic water oxidation with persulfate*. Phys Chem Chem Phys 14 (2012) 5753-5760
- [34] Yang Z, Huang Y, Dong B, Li HL, Shi SQ, *Sol-gel template synthesis and characterization of LaCoO₃ nanowires*. Appl Phys A 84 (2006) 117-122
- [35] Wang Y, Ren J, Wang Y, Zhang F, Liu X, Guo Y, Lu G, *Nanocasted Synthesis of Mesoporous LaCoO₃ Perovskite with Extremely High Surface Area and Excellent Activity in Methane Combustion*. J Phys Chem C 112 (2008) 15293-15298
- [36] Armelao L, Bandoli G, Barreca D, Bettinelli M, Bottaro G, Caneschi A, *Synthesis and characterization of nanophasic LaCoO₃ powders*. Surf Interface Anal 34 (2002) 112-115

CHAPTER TEN

PAPER EIGHT

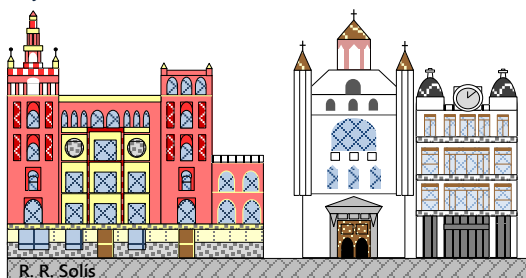
Synergism between monoperoxysulfate and $\text{LaCoO}_3\text{-TiO}_2$ photocatalysis for oxidation of herbicides. Operational variables and catalyst characterization assessment

J Chem Technol & Biotechnol DOI: 10.1002/jctb.5228

Rafael R. Solís, F. Javier Rivas, Olga Gimeno, Jose-Luis Pérez-Bote

ABSTRACT. BACKGROUND. This paper reports the use of novel coupled $\text{LaCoO}_3\text{-TiO}_2$ as photocatalyst with double route of monoperoxysulfate (MPS) activation. Firstly, as a photocatalyst due to titania; and secondly, through MPS heterogeneous decomposition onto LaCoO_3 particles. Thus, photocatalytical activity was tested for removing a mixture of four herbicides of different recalcitrance (metazachlor, tembotrione, tritosulfuron and ethofumesate). RESULTS. The presence of light and MPS highly enhances herbicides rate removal. 3.5-5 times of increase were appreciated because of UVA light. Oxidant concentration, catalyst load, pH and temperature were assessed. Herbicides were completely oxidized depending on the operational variables and their recalcitrant nature. 55% of TOC conversion was reached using Oxone® $5 \cdot 10^{-4}$ M. Phytotoxicity assays denoted no inhibition after 180 min of treatment (~80% of initial inhibition). Solid properties of Co/Ti=0.1:1 ratio were studied by means of SEM (LaCoO_3 aggregates linked to a variety of shapes and sizes of TiO_2), XRF (6.1% of LaCoO_3), XPS (superficial Co^{3+} , La^{3+} and Ti^{4+}), XRD (anatase, rutile and rhombohedral LaCoO_3) and UV-vis reflectance (visible range absorption and bandgap of 2.88 eV for TiO_2). CONCLUSIONS. Catalysts based on $\text{LaCoO}_3\text{-TiO}_2$ combined to MPS seem to be suitable for removing organic pollutants, with a moderate conversion of TOC and elimination of toxicity.

KEYWORDS: photocatalysis, advanced oxidation, environmental remediation, heterogeneous catalysis, oxidation, decontamination



R. R. Solís

Plaza de la Soledad, Badajoz

10.1. INTRODUCTION

Aqueous contaminants represent an environmental hazard since most of them are persistent and not easily removed by themselves in natural ecosystems. Pesticides are frequently detected in watercourses at low levels that risk non-compliance with European water framework Directive 2000/60/EC [1] drawn up to protect all surface and ground waters [2,3]. Metazachlor (METAZ, C₁₄H₁₆ClN₃O, CAS 67129-08-2), tembotrione (TEMB, C₁₇H₁₆ClF₃O₆S, CAS 335104-84-2), tritosulfuron (TRITO, C₁₃H₉F₆N₅O₄S, CAS 142469-14-5) and ethofumesate (ETHO, C₁₃H₁₈O₅S, CAS 26225-79-6) are three different pesticides, with a relatively new presence in herbicide's market, which are used as pre and post-emergence herbicide to control a broad spectrum of broad-leaved and grassy weeds in crops, ornamental trees and shrubs. All of them, except tembotrione, are labelled as carcinogens. Moreover, tritosulfuron and ethofumesate seem to have mutagenic action, and tritosulfuron is also an endocrine disrupter [4]. Some of them, like ethofumesate, have been recently detected in surface and ground water [5] or soil [6].

Management of organic aqueous pollutants is a matter of concern to water companies that need to develop new and specific technologies for that purpose. Conventional biological treatment seems to be inefficient due to the organic recalcitrant nature of these substances [7,8]. That is why alternative technologies such as chemical oxidation through Advanced Oxidation Processes are required. Monoperoxysulfate (MPS) is an oxidant which is attracting attention recently. This substance can be used as a promoter of sulfate radicals which present diverse advantages upon hydroxyl radical generation. Sulfate radical has a higher oxidation potential, more selectivity through electron transfer to chemicals that contains unsaturated bonds or aromatic rings, wider range of pH work in contrast to Fenton's chemistry, and higher half-life period which improves contact with the target compound. Furthermore, MPS decomposition provide both, sulfate and hydroxyl radicals [9].

MPS by itself is poorly capable of attacking organic compounds at some points such as double bonds or aromatic rings [10]; however its decomposition promoted by homogeneous or heterogeneous catalysts, temperature, UV radiation, or ultrasound, considerably improves the elimination rate of organic pollutants. Homogeneous catalysis has the disadvantage of catalyst elimination and recycling after reaction, especially in those cases where its presence is undesirable, e.g. toxicological concerns.

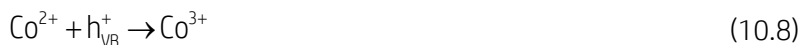
Some alternatives have been recently suggested. Heterogeneous catalysis combined with or without radiation [11,12], has raised attention of diverse researching groups, mainly focusing on cobalt oxides [13]. Among them, heterogeneous combination with photocatalysts, such as titanium dioxide [14, 15] is drawing attention due to enhancement in MPS decomposition. Cobalt inserted into the titania lattice acts as active center in MPS decomposition [11]:



Photocatalytic decomposition of MPS can also be launched under the presence of radiation [15]:



Moreover electrons generated in photocatalytic processes contribute to regenerate the original oxidation state of cobalt, minimizing electron-hole recombination [15]:



Thus, a powerful reaction-chained mechanism is triggered, generating sulfate and hydroxyl radicals from photocatalytic reaction and Fenton-like heterogeneous reactions. It should be highlighted that few new catalysts different from cobalt oxide have been coupled to TiO_2 [16,17].

This study reports the performance of lanthanum cobalt perovskite coupled to titania ($\text{LaCoO}_3\text{-TiO}_2$) as a new catalyst which combines heterogeneous and photocatalytic decomposition of MPS. The MPS catalytic decomposition through catalytic reactions (10.1) and (10.2) using LaCoO_3 has been studied in a previous work, proving its high effectiveness, stability and low cobalt leaching under circumneutral pH range [18]. The purpose of the

current work is to combine heterogeneous cobalt activity of LaCoO₃ and photocatalytic activity of TiO₂ in order to enhance the oxidation of organics pollutants, in this case a mixture of four new herbicides with high environmental concern. LaCoO₃:TiO₂ proportion influence on catalytic activity has been studied, being Co/Ti=0.1:1 chosen for the rest of the study. Main operational parameters such as MPS concentration, catalyst load, pH and temperature affecting herbicides' removal were considered. Catalyst stability was evaluated in consecutive runs of reusing. Phytotoxicity assays were carried out in order to assess the toxicological aspects of remaining TOC. Finally, main superficial properties of Co/Ti=0.1:1 ratio were analyzed through diverse techniques: SEM, XRF, XPS and UV-vis diffuse reflectance.

10.2. EXPERIMENTAL

10.2.1. Chemicals

All chemicals used were analytical grade and were used as received. Herbicides standards (purity >99%) were purchased from Sigma-Aldrich®. Oxone®, monoperoxysulfate compound (2KHSO₅·KHSO₄·K₂SO₄, CAS 37222-66-5), was obtained from Sigma-Aldrich®. Chemicals used in catalyst synthesis were pure grade. Acetonitrile from VWR Chemicals was used in HPLC determination of herbicides in water. All solutions were prepared with ultrapure water from a Milli-Q® academic (Millipore) system (resistivity 18.2 MΩ cm).

10.2.2. Catalyst synthesis and characterization

LaCoO₃-TiO₂ was prepared in two different steps. Firstly, LaCoO₃ perovskite was synthesized in the presence of citric acid as complexing organic agent [19]. In a typical synthesis run, La(NO₃)₃·6H₂O and Co(CH₃COO)₂·4H₂O with a molar ratio La:Co=1:1 were dissolved in 400 mL of ultrapure water. After 1 hour of mixing under magnetic agitation, 100 mL of citric acid in excess, twice the stoichiometrically needed for each metal, was slowly added. The resultant solution was heated at 100°C to remove water excess, drying thereafter the obtained pinkish gel. The solid was grinded and calcined at 700°C for 5 hours.

LaCoO₃-TiO₂ heterojunction was prepared by hydrothermal precipitation of a titanium organic precursor in the presence of the previous synthesized perovskite. Titanium isopropoxide was dissolved in 2-propanol and a fixed amount of LaCoO₃ was added under stirring to meet a specific LaCoO₃:TiO₂ molar ratio. Afterwards, ultrapure water was gradually dropped into the above suspension. The precipitation of titanium dioxide was completed by

autoclaving the mixture at 80°C for 12 h. The resultant suspension was centrifuged at 3500 rpm and the solid washed with water and 2-propanol. Finally, the solid dried overnight at 100°C, was calcined at 500°C for 4 hours under air atmosphere (initial ramp, 10°C min⁻¹).

Mass titration method was considered to estimate pH of point of zero charge (pH_{pzc}) [20]. A solution of pH=3 was prepared by adding NaOH 0.1 M to a HNO₃ 0.1 M solution. Different glass bottles of 30 mL of capacity were filled in with 15 mL of the above solution, and different amounts of catalyst were added to meet a certain solid mass percentage (0.05, 0.10, 0.50, 1.00, 2.50, 5.00 and 10.00%). After 48 hours of equilibrium in a shaking water bath (25°C, 100 rpm), pH was measured. A plot of pH versus solid percentage gives a curve whose asymptote tends to be pH_{pzc} value.

Scanning electron microscopy (SEM) was conducted in a QUANTA 3D FEG (FEI) coupled to secondary and backscattered electrons detectors (acceleration voltage 20 kV).

XPS K-alpha-Thermo Scientific device was used for obtaining X-ray photoelectron spectroscopy (XPS) spectra, working with a K α monochromatic source of Al (1486.68 eV). 284.8 eV for C1s peak was taken to calibrate the signals of the rest peaks. High resolution of XPS spectra for La3d, Co2p, Ti2p and O1s were recorded.

Atomic concentration of La, Co and Ti were quantified by X-ray fluorescence (XRF) in a sequential Wavelength Dispersive X-ray Fluorescence (WDXRF) spectrometer (S8 Tigger, Bruker) equipped with an X-ray tube of rhodium (60 kV, 170 mA).

Crystalline phase composition was analyzed by X-ray diffraction (XRD), in a Bruker D8 Advance diffract meter equipped with a monochromator of Ge 111 K α of Cu (wavelength, 1.5456 Å).

Diffuse reflectance UV-Vis spectra was performed by using a Varian-Agilent UV-Vis-NIR Cary 5000 spectrophotometer, equipped with an integrating sphere device.

10.2.3. Photoreactor and procedure

Experimental photoreactor setup consisted of a cylindrical glass vase (10 cm of diameter and 22 cm of height) in which 1.0 L of herbicides mixture (1 mg L⁻¹) was loaded. The reactor was magnetically stirred and thermally controlled by using an IKA® RCT basic stirrer. The installation was completed with a 31 cm external diameter pipe of 54 cm of height, being the reactor

located in the centre. Four tubular black light lamps (41 cm of height, LAMP15TBL HQPOWER™ manufactured by Velleman®, 15 W of nominal power) were equidistantly distributed and attached to the internal wall of the pipe, which was foiled by aluminum foil. Every lamp mainly emits radiation within the range 350-400 nm, with a maximum placed at 365 nm. Figure 10.S1, available in supplementary information, provides a scheme of the photoreaction system and Figure 10.S2 the emission spectrum of UVA lamp.

Previous to the experiment, pH (Crison GLP 21+) was adjusted to the specific value and 30 min of stirring without MPS was carried out in order to achieve the adsorption equilibrium of organic compounds onto catalyst surface (if any). A small volume (less than 10 mL) of a concentrated MPS solution was added in order to meet the MPS initial concentration and to start the reaction. pH was quickly readjusted. Samples were extracted at different times and filtered with Millex-HA filters (Millipore, 0.45 µm). HPLC and TOC samples were quenched with Na₂S₂O₃ 0.5 M (10 µL per 1 mL of sample).

10.2.4. Analytical methods

MPS concentration was spectrophotometrically quantified by means of a method based on N,N-diethyl-p-phenylenediamine (DPD) oxidation [21].

Herbicides aqueous concentration were analyzed by liquid chromatography in a HPLC Agilent 1100 equipped with UV detection. A Kromasil 100 5C18 column (5µm, 2.1x150 mm) was used, and a mobile phase composed by 0.1% H₃PO₄ acidified water (A) and acetonitrile (B) was pumped at a flow rate of 1 mL min⁻¹, with an isocratic percentage composition of 55:45 A:B. UV detection was conducted at 220 nm.

Total Organic Carbon (TOC) content was determined by means of a Shimadzu TOC-V_{CSH} 5000A analyzer which directly injects the aqueous sample.

The Ionic Chromatographic system was a Methrom® 881 Compact IC pro equipped with a 800 Dosino, chemical suppression, autosampler (863 Compact autosampler) and conductivity detector. The stationary phase was an anionic exchange column (MetroSep A Supp 5).

Cobalt in solution was measured through atomic absorption in a Varian SpectrAA Series 140 device.

Phytotoxicity assays were carried out with seeds of *Lactuca Sativa* as test plant (*Romana Bionda Degli Ortolani*, Vilmorin®). Fifteen seeds were equally

distributed into Petri dishes equipped with paper discs moistened with 4 mL of sample. Parafilm was used to cover the dishes in order to avoid liquid evaporation, and the seeds were incubated in a germination chamber, isolated from light at 22°C during 120 hours. After that, the root length of each germinated root was measured (L), expressed as the sum of hypocotyl and radicle. The percentage root growth was calculated by comparing the radicle lengths for each sample with those observed in the control (L_0), done with ultrapure water.

10.3. RESULTS & DISCUSSION

10.3.1. Effect of the ratio $\text{LaCoO}_3\text{:TiO}_2$

Different catalysts were tested varying the ratio of the perovskite to titanium dioxide. Also, pure TiO_2 and LaCoO_3 were also used as control runs to have a reference in activity. The first case represents the conventional photocatalytic process in the presence of a promoter. The second case reveals the capacity of the perovskite to decompose monoperoxy sulfate. Figure 10.1 shows the results obtained.

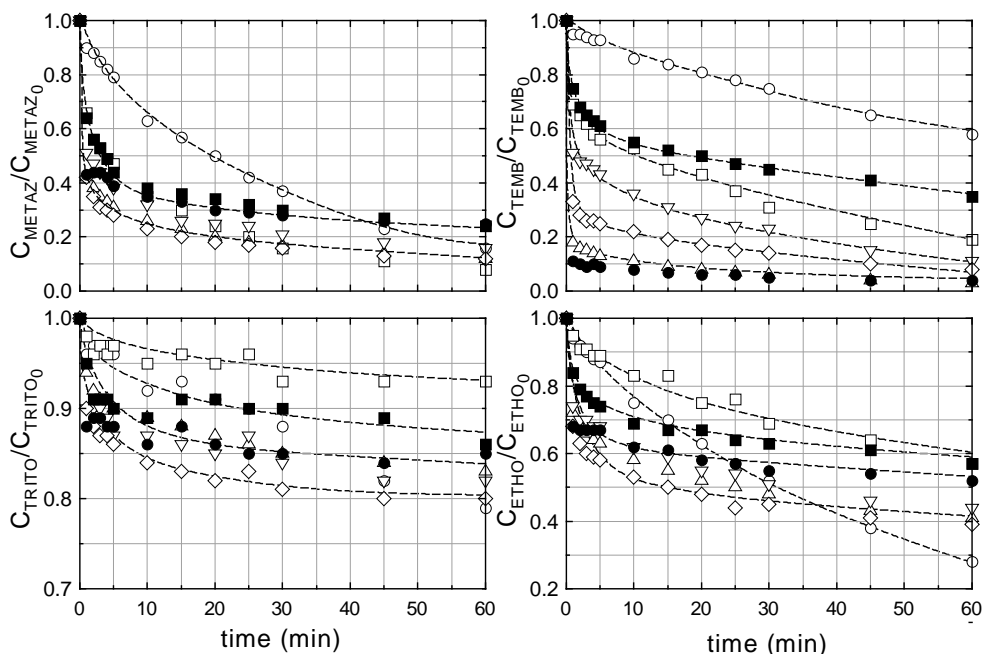


Figure 10.1 Oxone[®] promoted photocatalytic elimination of herbicides. $\text{LaCoO}_3\text{-TiO}_2$ ratio influence. Experimental conditions: $C_{\text{Herbicide}}=1.0 \text{ mg L}^{-1}$ each, $\text{pH}=7.0$, $T=15\text{-}20^\circ\text{C}$, $C_{\text{CAT}}=0.5 \text{ g L}^{-1}$, $C_{\text{Oxone}}=1.0 \cdot 10^{-4} \text{ M}$. Ratio Co/Ti : \circ , 0:1; \square , 0.05:1; Δ , 0.1:1; ∇ , 0.25:1; \diamond , 0.5:1; \bullet , 0.75:1; \blacksquare , 1:0.

At the sight of Figure 10.1, depending on the herbicide the optimum catalyst is different. As a rule of thumb, catalysts with Co:Ti ratios in the range 0.1:1 to 0.5:1 show a higher activity than the rest of solids tested. Titanium dioxide displays moderate activity with the exception of ethofumesate. In the latter case, TiO₂ leads to the highest herbicide conversion after 60 minutes (around 70% conversion of the initial ethofumesate concentration). Tembotrione is one of the most reactive herbicides tested, in this case, even monoperoxysulfate in the absence of radiation and catalyst is capable of oxidize the herbicide.

Additionally, no matter the ratio Co:Ti used, a fast initial period in herbicide elimination was experienced followed by a second slower stage. An analysis of Oxone® evolution (results not shown) reveals that the slow stage does not coincide with monoperoxysulfate total depletion. A potential explanation could be a shortage in dissolved oxygen that would prevent the propagation of the free radical mechanism through organoperoxides radical formation-decomposition [22]. Also, electron-hole recombination is favored in the absence of oxygen. As a consequence, a new experimental series was conducted by injecting an oxygen stream to the reaction media.

Figure 10.2 illustrates that oxygen has no influence in the process with the exception of tembotrione. In this latter case the concentration of O₂ exerts a positive influence, however, given the high reactivity of tembotrione and the residual improvement obtained in terms of total conversion of herbicides, it was decided to continue this study in the absence of oxygen, avoiding, therefore, additional costs associated to the process.

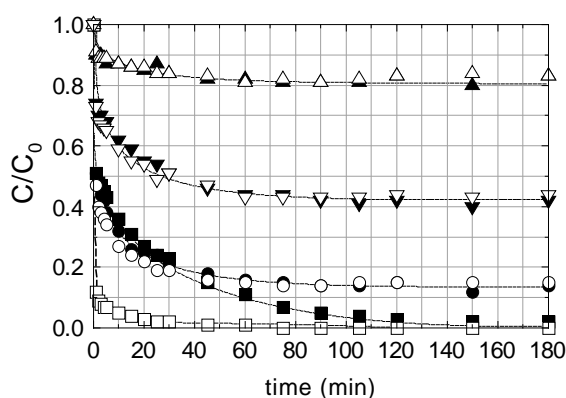


Figure 10.2 Oxone® promoted photocatalytic elimination of herbicides. Oxygen bubbling effect. Experimental conditions: $C_{\text{Herbicide}}=1.0 \text{ mg L}^{-1}$ each, $\text{pH}=7.0$, $T=15\text{-}20^\circ\text{C}$, $C_{\text{CAT}}=0.5 \text{ g L}^{-1}$, $C_{\text{Oxone}}=1.0 \cdot 10^{-4} \text{ M}$, Ratio Co/Ti=0.25:1. ●○, Metazachlor; ■□, Tembotrione; ▲△, Tritosulfuron; ▼▽, Ethofumesate. (Open symbols: oxygen bubbling, Solid symbols: air bubbling)

10.3.2. Monoperoxysulfate concentration effect

Given the results obtained in the previous section, the catalyst with a ratio Co:Ti of 0.1 was thereafter used in the rest of experiments. This catalyst represents a compromise between conversion achieved and low cobalt content to avoid leaching of this transition metal.

The next experimental series was conducted at different initial Oxone® concentrations and keeping constant the rest of operating variables. Additionally, some control runs have also been conducted.

Figure 10.3 illustrates the results obtained. For comparison purposes, from the same figure, the role played by Oxone® alone is shown. At this point it should be highlighted that in a previous work [23], only tembotrione presented some reactivity towards Oxone® in experiments carried out individually. However, when treating the four herbicides simultaneously, conversions of 78, 53, 3 and 21% in metazachlor, tembotrione, tritosulfuron and ethofumesate were experienced after 180 min. It seems that either species formed in the oxidation of tembotrione by Oxone® have the capacity to co-oxidize the rest of herbicides or/and at pH=7, herbicides are more reactive towards monoperoxysulfate than at pH=3 used in the reference. A first approximation to monoperoxysulfate oxidation kinetics can be accomplished by considering a second order reaction:

$$-\frac{dC_{\text{herbicide}}}{dt} = k_{\text{MPS}} C_{\text{herbicide}} C_{\text{MPS}} \quad (10.9)$$

Where $C_{\text{Herbicide}}$ and C_{MPS} mean the concentration of herbicide and MPS, respectively, and k_{MPS} the second order pseudo rate constant. Applying equation 10.9 to experiments displayed in Figure 10.3 led to k_{Oxone} values of 75.1 ± 7.3 , 50.2 ± 5.2 , 2.0 ± 0.6 , and $15.1 \pm 1.8 \text{ M}^{-1} \text{ min}^{-1}$ (corresponding to metazachlor, tembotrione, tritosulfuron, and ethofumesate removal, respectively), where herbicides concentration was monitored in mg L^{-1} and MPS concentration in mol L^{-1} . Given the values of k_{MPS} , the most recalcitrant compound is tritosulfuron while the most reactive is metazachlor. Notice that in individual experiments metazachlor did not react with monoperoxysulfate at pH=3.

The presence of light and MPS involves a considerable enhancement of the process. This improvement is not the consequence of the direct activation of monoperoxysulfate by UVA radiation. At 365 nm nor MPS nor the herbicides

absorb radiation (see Supplementary Material, Figure 10.S2). Likely, herbicides act as sensitizers of the photoreaction initiating the mechanism of photodecomposition of monoperoxysulfate. Again, for comparison purposes the global process was modeled by a second order expression, similar to Equation 10.9 leading to values of the rate constant of $k_{MPS,UVA}=0.350\pm 0.04 \cdot 10^3$, $0.175\pm 0.028 \cdot 10^3$, 8.5 ± 1.1 , and $75\pm 5 \text{ M}^{-1} \text{ min}^{-1}$ (metazachlor, tembotrione, tritosulfuron, and ethofumesate). As inferred from these values, the presence of light increased the reactivity in the range of 3.5-5 times if compared to experiments in the absence of radiation. LaCoO₃ does not have photocatalytic activity by itself, fact that was proved by carrying out an experiment in absence of MPS (results not shown). In a similar way, TiO₂ shows is capable of oxidizing herbicides at similar rate constant to direct oxidation with Oxone[®], as it can be appreciated in Figure 10.3.

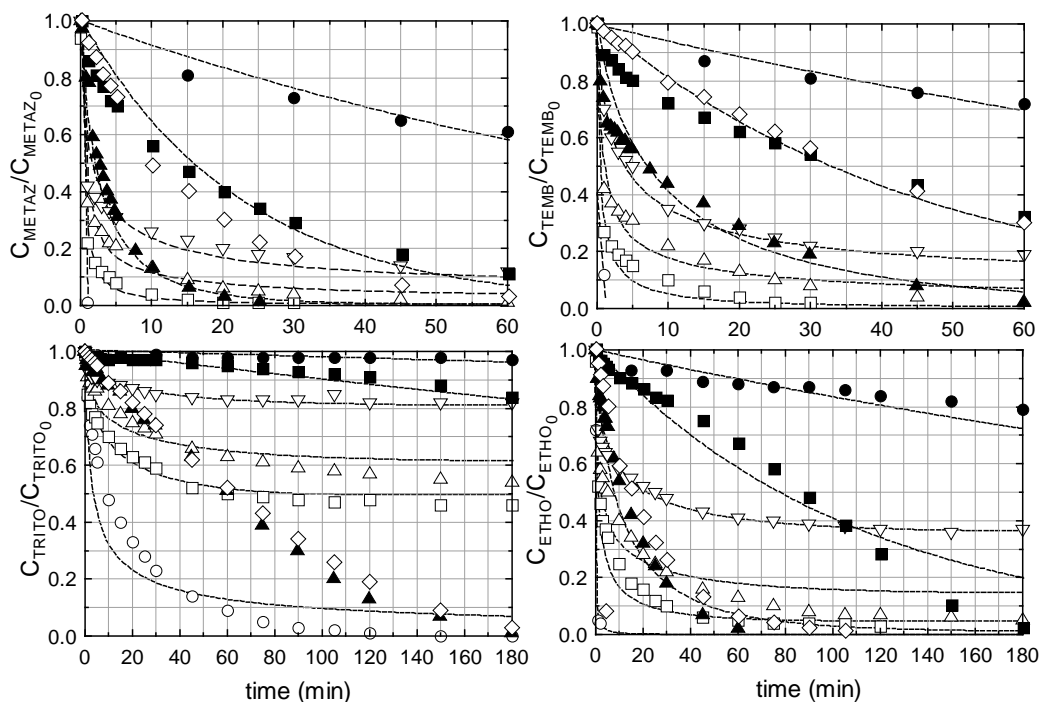


Figure 10.3 Oxone[®] promoted photocatalytic elimination of herbicides. Oxone[®] concentration influence. Experimental conditions: $C_{\text{Herbicide}}=1.0 \text{ mg L}^{-1}$ each, $\text{pH}=7.0$, $T=15\text{-}20^\circ\text{C}$, $C_{\text{CAT}}=0.5 \text{ g L}^{-1}$, $\text{Ratio Co/Ti}=0.1:1$, $C_{\text{Oxone}} \cdot 10^4 \text{ (M)}$: \circ , 5.0; \square , 2.0; Δ , 1.5; ∇ , 1.0; \bullet , 1.5 (no UVA, no catalyst); \blacksquare , 1.5 (no catalyst); \blacktriangle , 5.0 (Ratio Co/Ti=0:1); \diamond , 0 (Ratio Co/Ti=0:1)- Dashed lines: theoretical calculations with $n=0.8$

When the $\text{LaCoO}_3\text{-TiO}_2$ catalyst was added to the reaction media, MPS concentration exerted a positive influence in herbicides removal rate. An initial concentration of the promoter of $5 \cdot 10^{-4}$ M led to the instantaneous removal of three of the four compounds, tritosulfuron was eliminated after roughly 2 hours. Maximum TOC conversion after 180 min was 55%. At the sight of the profiles obtained and the low TOC reduction, accumulation of intermediates is likely to occur impeding the adsorption of reactants onto the catalyst surface and competing for oxidizing species. Moreover, curve shapes rule out the development of simple second order kinetics. Accordingly, a rough empirical approximation to the kinetics of the process would consider that the rate of any herbicide removal would be proportional to the amount of the parent compound, catalyst load and the concentration of reactive species, and inversely proportional to the amount of intermediates generated. Some of the previous parameters have not been monitored in this study, however, for comparison purposes a pseudoempirical model can be proposed by considering that oxidizing species are proportional to MPS concentration and intermediates accumulation is proportional to reaction time:

$$-\frac{dC_{\text{herbicide}}}{dt} = k(T, \text{CAT}, \text{UVA}, \text{pH}) \frac{C_{\text{herbicide}} (\sum C_{\text{oxidants}})}{\sum C_{\text{intermediates}}} \approx$$

$$\approx k(T, \text{CAT}, \text{UVA}, \text{pH}) \frac{C_{\text{herbicide}} C_{\text{MPS}}}{t^n} \quad (10.10)$$

In equation 10.10, herbicides concentration has been measured in mg L^{-1} and MPS in mol L^{-1} . Time in minutes is powered to “n”. The rate constant is a function of temperature, catalyst load, UVA radiation and geometry of the reactor, and likely, of pH. Applying the Euler approximation to the derivative term:

$$C_{i+1, \text{herbicide}} = C_{i, \text{herbicide}} - \left(k(T, \text{CAT}, \text{UVA}, \text{pH}) \frac{C_{i, \text{herbicide}} \sum C_{i, \text{oxidants}}}{\sum C_{i, \text{intermediates}}} \right) \Delta t \approx$$

$$\approx C_{i, \text{herbicide}} - \left(k(T, \text{CAT}, \text{UVA}, \text{pH}) \frac{C_{i, \text{herbicide}} C_{i, \text{PMS}}}{t_i^n} \right) \Delta t \quad (10.11)$$

Where C_i is the concentration at time i and C_{i+1} refers to the concentration at time $i+\Delta t$. The optimization process that minimized the squared difference between calculated and experimental concentrations led to values of n in the

range 0.5-0.8, however, for comparison purposes in terms of reactivity of herbicides, in this first series, this parameter was fixed to 0.8 in all experiments. The rate constants k were $4.8 \pm 0.1 \cdot 10^3$, $3.9 \pm 0.2 \cdot 10^3$, $5.9 \pm 1.1 \cdot 10^2$, and $2.6 \pm 0.3 \cdot 10^3 \text{ M}^{-1} \text{ min}^{-0.2}$, corresponding to metazachlor, tembotrione, tritosulfuron, and ethofumesate removal, respectively. As seen in Figure 10.3, equation 10.10 is a suitable tool to compare the reactivity of the different herbicides under a variety of experimental conditions. In this case, the most reactive substance is metazachlor while tritosulfuron is almost 10 times more recalcitrant than the former.

The presence of cobalt in the catalyst is of paramount importance. Hence, Figure 10.3 displays how, under similar experimental conditions, the removal rate of herbicides diminishes when only TiO₂ was present if compared to the similar experiment completed with the LaCoO₃-TiO₂ catalyst. Also, the accumulation of intermediates affects to a lower extent the conversion of the herbicides at higher reaction times. As a consequence, when TiO₂ was used, the curve profiles were different to those experienced when the LaCoO₃-TiO₂ catalyst was employed. Hence, the initial oxidation rate was slower in TiO₂ based experiments. However, this reaction rate did not suffer a sharp decrease at higher reaction times as in the case of the perovskite based solid. An expression similar to equation 10.10 was adopted to model the process. With the exception of tritosulfuron, the model led to acceptable results. As deduced from the curve shapes the value of "n" decreased from 0.8 to 0.4 indicating the lower effect of intermediates on catalyst activity. Simultaneously, the values of the rate constants also diminished to values of $2.2 \pm 0.6 \cdot 10^3$, $1.0 \pm 0.08 \cdot 10^3$, and $0.95 \pm 0.04 \cdot 10^3 \text{ M}^{-1} \text{ min}^{-0.6}$ for metazachlor, tembotrione, and ethofumesate, respectively.

10.3.3. Influence of catalyst concentration

The influence of catalyst concentration was investigated in the range 0.05 to 0.5 g L⁻¹. Figure 10.4 depicts the results obtained. As inferred from the figure, no significant influence was observed and herbicide conversion was almost similar regardless of the amount of catalyst used in the interval studied. Catalyst dosage did affect the MPS decomposition rate. Hence, the higher amount of catalyst, the faster decomposition of monoperoxysulfate. However, as stated previously, this decomposition does not lead to a better performance in terms of herbicides or TOC removal.

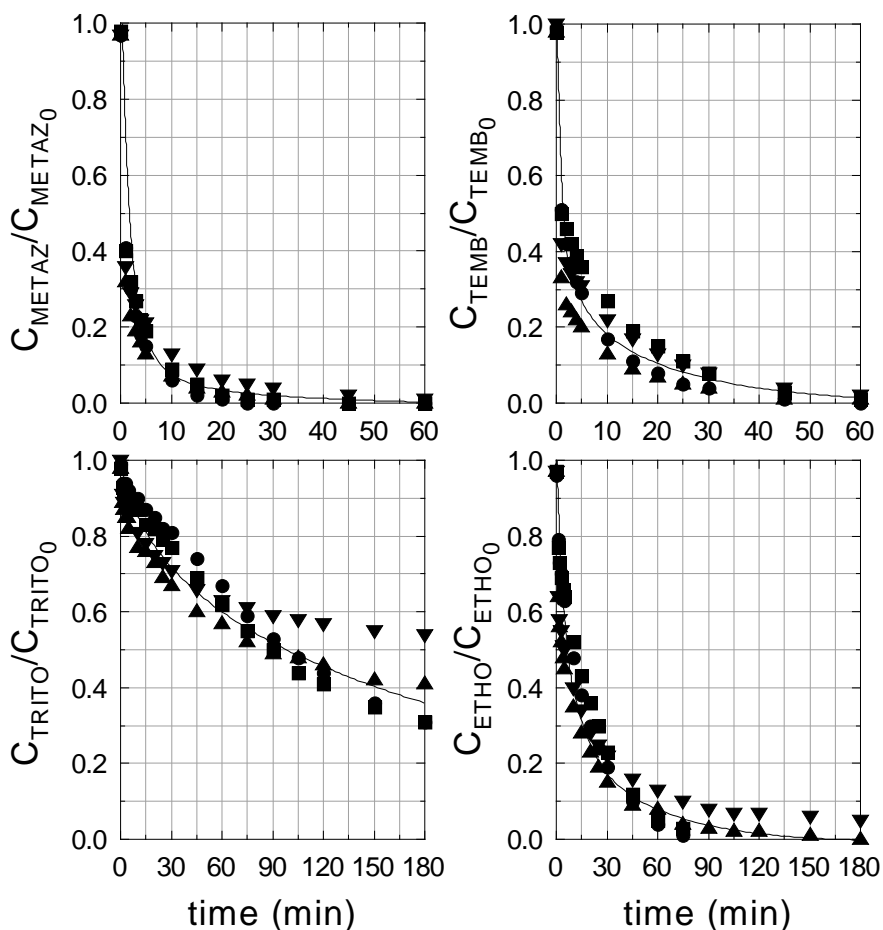


Figure 10.4 Oxone[®] promoted photocatalytic elimination of herbicides. Catalyst load influence. Experimental conditions: $C_{Herbicide}=1.0 \text{ mg L}^{-1}$ each, $\text{pH}=7.0$, $T=15\text{--}20^\circ\text{C}$, $\text{Ratio Co/Ti}=0.1:1$, $C_{Oxone^{\circledast}}=1.5 \cdot 10^{-4} \text{ M}$, $C_{CAT} \text{ (g L}^{-1}\text{)}$: ●, 0.05; ■, 0.10; ▲, 0.25; ▼, 0.50

10.3.4. pH influence

pH influence was assessed from slightly acidic conditions ($\text{pH}=5$) to slightly basic conditions ($\text{pH}=8$). pH plays a notorious role in the chemistry of monoperoxysulfate decomposition. Figure 10.5 shows the results obtained. As observed, pH exerts a notorious influence in the herbicides removal rate. Total organic carbon elimination, however, was similar regardless of the pH (roughly 30% conversion after 180 min).

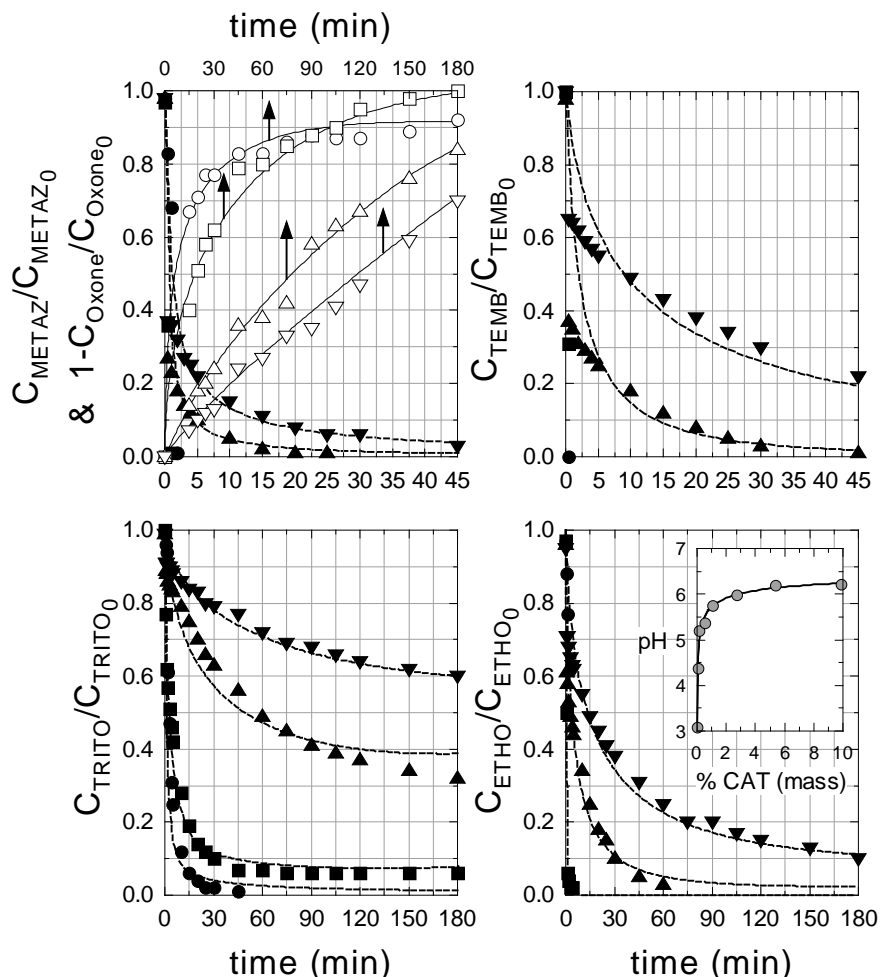


Figure 10.5 Oxone[®] promoted photocatalytic elimination of herbicides. pH influence. Experimental conditions: $C_{\text{Herbicide}}=1.0 \text{ mg L}^{-1}$ each, $T=15\text{-}20^\circ\text{C}$, Ratio Co/Ti=0.1:1, $C_{\text{Oxone}}=1.5 \cdot 10^{-4} \text{ M}$, $C_{\text{CAT}}=0.5 \text{ g L}^{-1}$, pH: ●, 5; ■, 6; ▲, 7; ▼, 8. Open symbols correspond to Oxone[®] conversion. Dashed lines: Theoretical calculations with $n=0.5\text{-}0.8$. **Inlet bottom-right figure:** pH_{pzc} determination

As inferred from Figure 10.5, the best conditions were obtained at the lowest pH used. One of the reasons to explain the results could be the influence of leached cobalt into solution. Cobalt above the detection limit of the analytical procedure used was only detected at pH=5. Under these conditions the maximum amount of Co^{2+} was 0.8 mg L^{-1} ($1.4 \cdot 10^{-5} \text{ M}$) at 180 min. Some experiments carried out in homogenous mode revealed that this small amount was insufficient to explain the effect of pH and/or the

activity of the tested catalyst. In most cases, equation 10.10 could acceptably simulate the curve profiles obtained. The optimum value of n was 0.8 for metazachlor and 0.5 for the rest of herbicides. pH negatively affected the values of k . Table 10.1 shows the values obtained as a function of pH.

Table 10.1 Rate constants (10^{-3}) calculated for herbicides elimination ($M^{-1} \text{ min}^{-1}$) as a function of pH ($n = 0.8$ for metazachlor and $n = 0.5$ for the rest of compounds).

pH	metazachlor	tembotrione	tritosulfuron	ethofumesate
5	-	-	4.6 ± 0.1	-
6	-	-	2.8 ± 0.1	9.0 ± 0.3
7	6.0 ± 0.3	3.1 ± 0.4	0.55 ± 0.08	2.1 ± 0.2
8	4.1 ± 0.4	1.2 ± 0.4	0.22 ± 0.02	0.95 ± 0.12

The tendency here obtained coincides with those reported when the perovskite LaCoO_3 was used in the presence of Oxone® to treat these herbicides [18]. Apparently, the dissociation degree of monoperoxysulfate ($\text{pK}_a=9.4$) highly influences its decomposition onto the catalyst surface. The catalyst has a point of zero charge around 6.22, suggesting that the solid presents low affinity towards negative ionic species.

10.3.5. Temperature influence

The effect of temperature was investigated by using two different initial MPS concentrations, 1.0 and $1.5 \cdot 10^{-4}$ M. Figure 10.6 illustrates the results obtained in experiments completed with the lowest MPS concentration in the range 30-50°C. Insets contain the Arrhenius plot derived from calculated rate constants.

As expected, temperature exerts a positive influence in the process; however, the values of the activation energy obtained are not excessively high, indicating that this parameter does not produce notable modifications in the efficacy of the process, at least in the range of temperatures investigated. Calculated activation energies were 14.7 ($R^2=0.96$), 20.5 ($R^2=0.96$), 20.5 ($R^2=0.98$) and, 28.7 ($R^2=0.99$) kJ mol^{-1} corresponding to metazachlor, tembotrione, tritosulfuron, and ethofumesate, respectively. Higher temperatures (above 80°C) might lead to the thermal decomposition of MPS into radicals. In this case, temperature influence could be different [24].

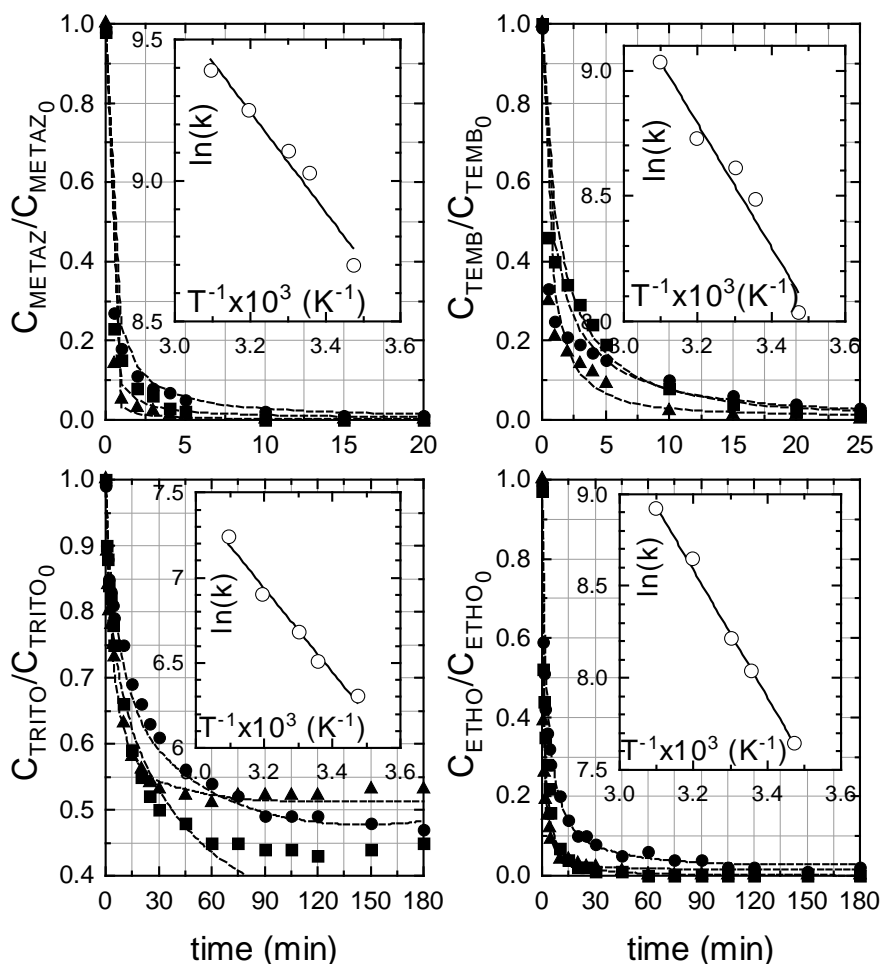


Figure 10.6 Oxone[®] promoted photocatalytic elimination of herbicides. Temperature influence. Experimental conditions: $C_{\text{Herbicide}}=1.0 \text{ mg L}^{-1}$ each, $\text{pH}=7$, $\text{Ratio Co/Ti}=0.1:1$, $C_{\text{Oxone}}=1.0 \cdot 10^{-4} \text{ M}$, $C_{\text{CAT}}=0.5 \text{ g L}^{-1}$, $T \text{ (}^\circ\text{C)}$: ●, 30; ■, 40; ▲, 50. Inset figures: Arrhenius plot. Dashed lines: Theoretical calculations with $n = 0.5-0.8$

10.3.6. Catalyst stability

Catalyst stability was assessed by conducting several consecutive experiments using the same recycled catalyst after filtration and drying. Figure 10.7 shows the evolution of Oxone[®] decomposition with time in the aforementioned experiments. The calculated reaction rate constant according to equation 10.10 is also depicted for each cycle. At the sight of Figure 10.7, a slight decrease in monoperoxysulfate decomposition rate can be envisaged as

the number of reuses is augmented; however, this reduction is not translated to a deterioration of the process efficiency. Actually, with the exception of tritosulfuron, calculated rate constants maintain, or even increase, the values obtained when fresh catalyst was used. In the case of tritosulfuron, the rate constant is reduced from the control run (fresh catalyst) to the first cycle; thereafter, this constant does not suffer any appreciable change. The reason is unclear and needs further work; in all cases leached cobalt was negligible.

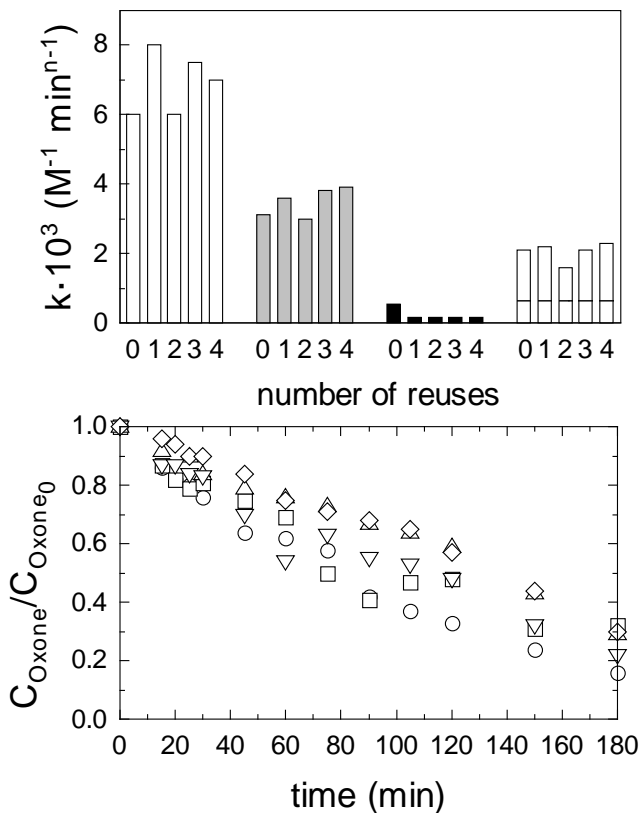


Figure 10.7 Oxone® promoted photocatalytic elimination of herbicides. Catalyst stability. Experimental conditions: $C_{\text{Herbicide}}=1.0 \text{ mg L}^{-1}$ each, $\text{pH}=7$, $\text{Ratio Co/Ti}=0.1:1$, $C_{\text{Oxone}}=1.5 \cdot 10^{-4} \text{ M}$, $C_{\text{CAT}}=0.5 \text{ g L}^{-1}$, $T=20^\circ\text{C}$. **Top figure:** calculated k value with $n=0.8$ (metazachlor) and $n=0.5$ (rest) according to equation 10.10: white bars, metazachlor; grey bars, tembotrione; black bars, tritosulfuron; striped bars, ethofumesate. **Bottom figure:** oxone® decomposition, number of reuses: \circ , initial; \square , 1st reuse; Δ , 2nd reuse; ∇ , 3rd reuse; \diamond , 4th reuse

10.3.7. Phytotoxicity evolution

Previous experiments have revealed that herbicides can be easily removed from water if adequate conditions are applied. However, no total mineralization of the samples could be achieved. Accordingly, this section was

devoted to assess the potential phytotoxicity of the accumulated intermediates during the photocatalytic oxidation in presence of Oxone[®].

Hence, a series of experiments were conducted in the presence of radiation and different amounts of Oxone[®]. Thereafter, seeds of *Lactuca Sativa* were germinated as described in the experimental section. Figure 10.8 illustrates the results of root length obtained when germinating the seeds in water obtained at different reaction times. As observed, when no treatment is applied (time zero), root growth only achieves ~20% (~80% of inhibition) of the root length obtained with pure water. As the reaction exposure increases, phytotoxicity almost disappears. Hence, the higher the initial MPS amount used, the faster the phytotoxicity decreases. With the exception of the run conducted with the lowest MPS concentration, all samples did show no phytotoxicity after 180 min of treatment.

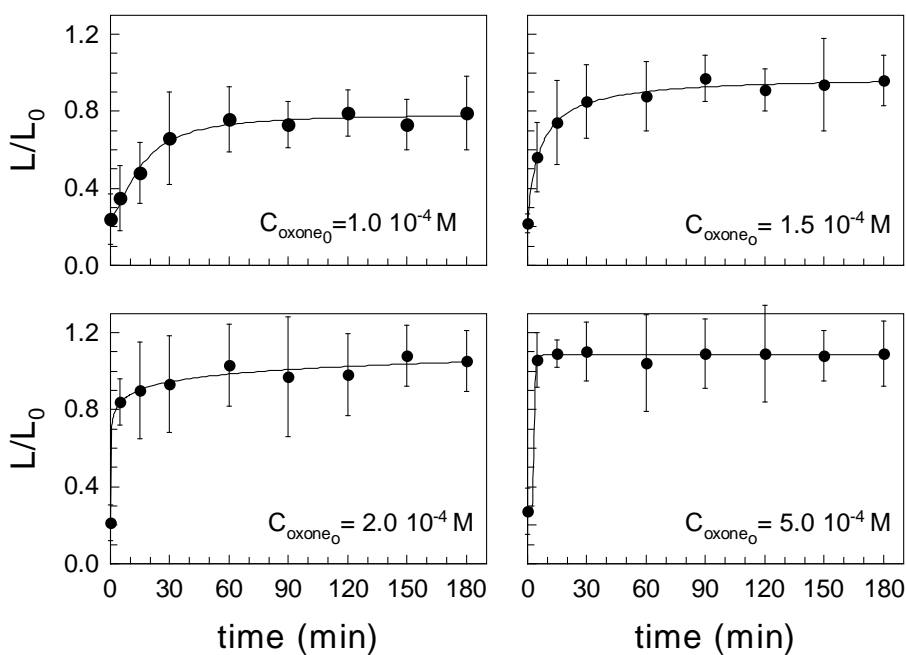


Figure 10.8 Oxone[®] promoted photocatalytic elimination of herbicides. Phytotoxicity evolution. Experimental conditions: $C_{\text{Herbicide}} = 1.0 \text{ mg L}^{-1}$ each, $\text{pH} = 7$, Ratio $\text{Co/Ti} = 0.1:1$, $C_{\text{CAT}} = 0.5 \text{ g L}^{-1}$, $T = 20^\circ\text{C}$. Variation of phytotoxicity (expressed as normalized root length) during treatment time and Oxone[®] concentration.

Although organic intermediates have not been measured in this work, some ionic species were detected and monitored throughout the reaction by ionic chromatography. In this sense, several aspects can be highlighted.

Hence, the F-C bond is hardly broken in $-CF_3$ substituents; the amount of free fluoride found in most cases was below the 10% of the maximum concentration that could be released. Nitrates were found at maximum concentrations around 18% of the highest concentration that could be found. This quantity coincides with the amount of nitrates that would be generated from the two amine groups in tritosulfuron, i.e. nitrogen in the heterocycle seems to be difficult to be converted to inorganic nitrate. Amongst small organic acids, acetic, formic, succinic and muconic acids were tentatively detected. Figure 10.9 shows the evolution of acetic and formic acids.

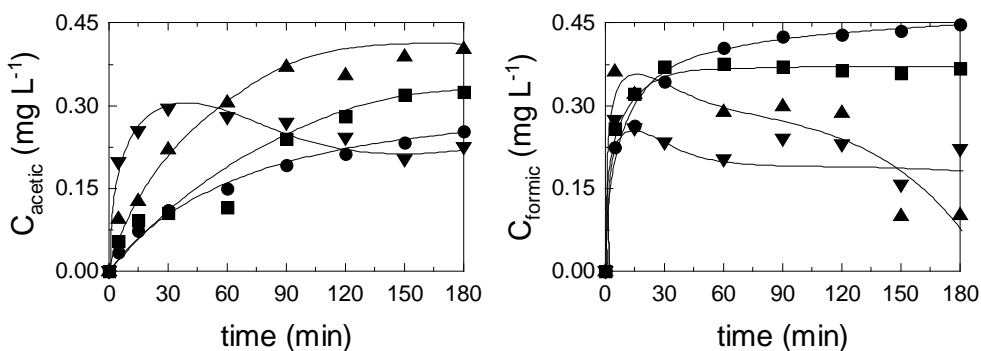


Figure 10.9 Oxone[®] promoted photocatalytic elimination of herbicides. Evolution of released acetic and formic acids. Experimental conditions: $C_{\text{Herbicide}}=1.0 \text{ mg L}^{-1}$ each, $T=15\text{-}20^\circ\text{C}$, Ratio $\text{Co/Ti}=0.1:1$, $C_{\text{CAT}}=0.5 \text{ g L}^{-1}$, $\text{pH}=7$, $C_{\text{Oxone}} 10^4 \text{ (M)}$: ●, 1.0; ■, 1.5; ▲, 2.0; ▼, 5.0

10.3.8. Catalyst characterization

Once the performance of the catalyst was assessed, the catalyst with the ratio $\text{Co/Ti}=0.1:1$ used in most of experiments was characterized by means of several techniques. Figure 10.10 summarizes some of the SEM images obtained. A, B and C pictures were obtained with secondary electron detection, while A', B' and C' are their corresponding images acquired with BackScattered Electron (BSE). More detailed pictures can be observed in supplementary information, Figure 10.S3. From Figure 10.10 can be appreciated a variety of sizes (from 20 to less than $5 \mu\text{m}$) and shapes likely due to irregularity of titania particles. From BSE images brighter particles outstand from the rest. These highlighted regions, which usually correspond to heavy elements, represent aggregates of smaller spherical LaCoO_3 particles. Energy Dispersive X-ray (EDX) analysis led to the confirmation of composition (Table 10.S1), enabling the corroboration that the darkest particles of BSE images belong to titania while the brightest correspond to perovskite.

X-ray Fluorescence (XRF) technique made possible to obtain global percentages of each element, and not only superficial. In this way, mass percentage of each element, without considering oxygen, were 80.41, 12.63 and 5.72 for Ti, La and Co, respectively. In a LaCoO_3 structure atomic mass relation between composition percentages of La and Co is $\text{La/Co}=2.36$, while in the synthesized $\text{LaCoO}_3\text{-TiO}_2$ this relation is 2.20. This near proportion might be considered as a proof of perovskite presence. Moreover, if it is considered that for a 10% of LaCoO_3 in the structure of the catalyst, mass percentage of La must be 20.55; a 6.1% of molar perovskite is found in the synthesized solid.

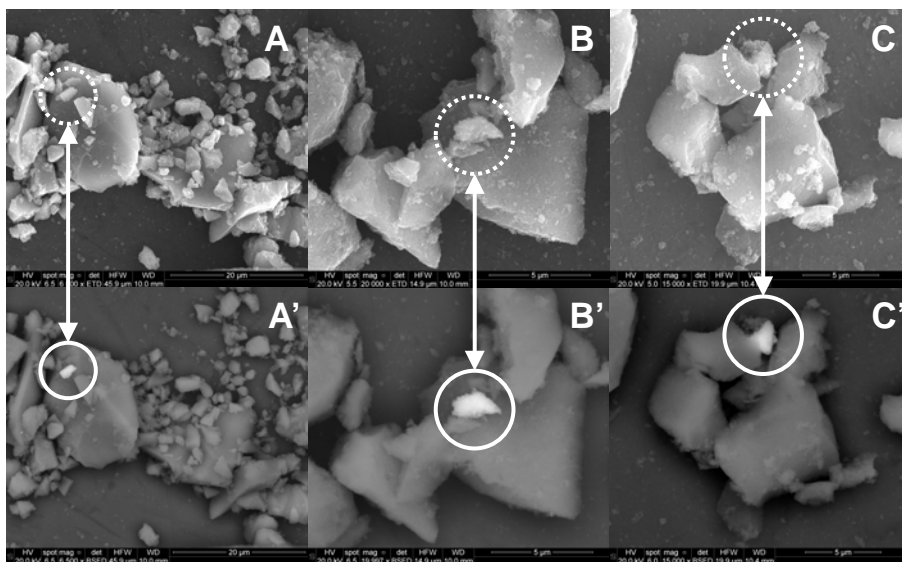


Figure 10.10 SEM images of $\text{LaCoO}_3\text{-TiO}_2$ ($\text{Co/Ti}=0.1:1$) obtained from secondary electron (A, B and C) and their corresponding's from backscattered electron (A', B' and C')

Surface composition and oxidation state of each element were analyzed by means of XPS. Figure 10.11 summarizes the results of general spectrum and high resolution spectra for La3d, Co2p, Ti2p and O1s. On one hand, Co and La present trivalent oxidation states. Co2p image depicts two peaks at 794.1 and 779.4 eV, corresponding to $\text{Co}2p_{1/2}$ and $\text{Co}2p_{3/2}$ respectively. The value observed for $\text{Co}2p_{3/2}$ matches with that observed in cobalt oxides such as Co_2O_3 [25] and LaCoO_3 [26], where Co(III) is the main oxidation state. La3d presents two regions ($\text{La}3d_{5/2}$ and $\text{La}3d_{3/2}$), containing two peaks each one whose values are 834.7 and 839.0 eV for $\text{La}3d_{5/2}$ region; and, 851.4 and 856.0 eV for $\text{La}3d_{3/2}$. These values are consistent with that expected for trivalent La in LaCoO_3 network [27]. On the other hand, Ti2p peak showed the

typical value when XPS is carried out in TiO_2 . Thus, Figure 10.11 illustrates a symmetrical $\text{Ti}2p_{3/2}$ peak whose maximum is located at 458.8 eV. Finally, $\text{O}1s$ presents a completely symmetrical peak at 529.9 eV, associated to O^{2-} state, which outlines the absence of hydroxylated groups onto the surface. A quantitative surface analysis, after Shirley's background subtraction, led to the following composition expressed as atomic percentages: 59.3 of O, 21.5 of Ti, 3.1 of La, and 4.36 of Co.

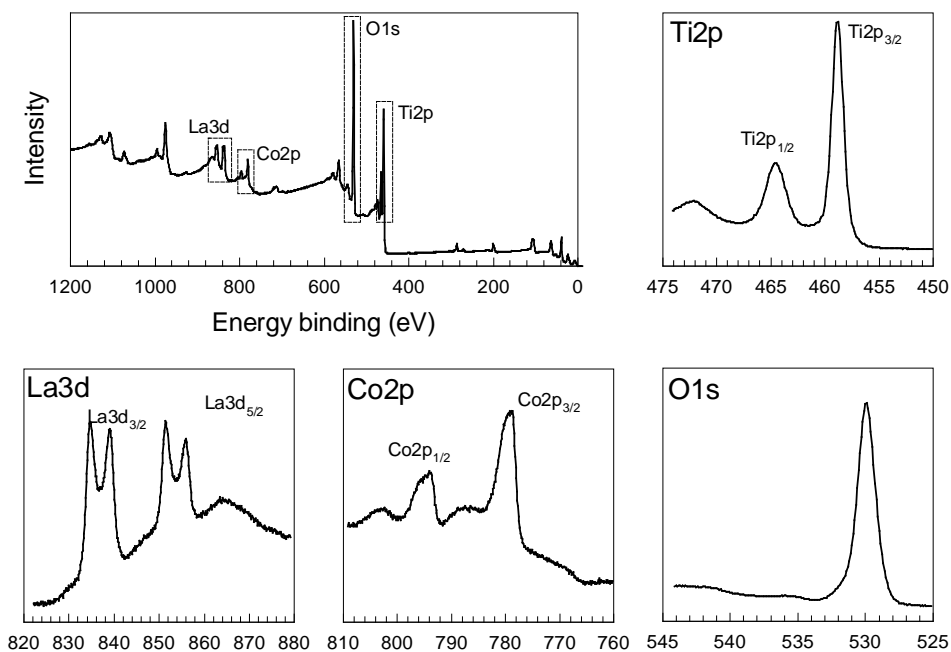


Figure 10.11 XPS spectra of $\text{LaCoO}_3\text{-TiO}_2$ (Co/Ti=0.1:1)

XRD technique was applied in order to study the nature of crystalline phases present in the catalyst. XRD patterns are presented in Figure 10.12. Anatase and rutile were identified as the main TiO_2 phases, being anatase 73.1% of all TiO_2 . LaCoO_3 presence was confirmed as rhombohedral crystalline structure, as well as small amounts of cubic Co_3O_4 .

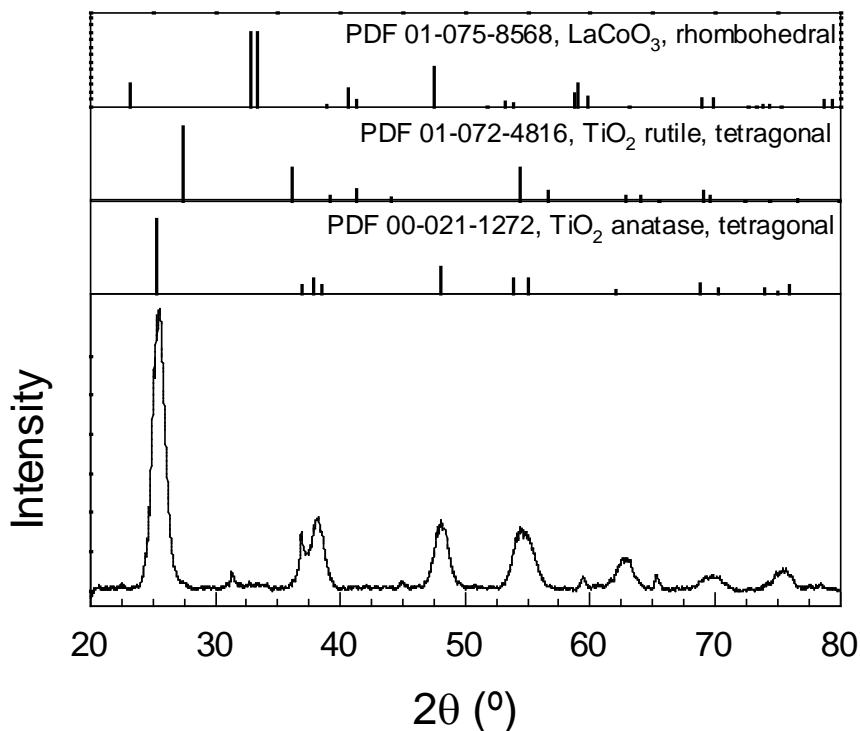


Figure 10.12 XRD diffractogram of LaCoO₃-TiO₂ (Co/Ti=0.1:1)

Finally, optical absorbance was applied by means of diffuse reflectance UV-vis technique. Figure 10.13 illustrates the spectra obtained and the corresponding Tauc's plot for bandgap determination. At first sight, absorption efficiency considerably increases in the visible range due to perovskite presence. Moreover, the LaCoO₃-TiO₂ presents two different absorption regions, whose bandgaps are 2.88 and 1.81 eV, being attributed to TiO₂ and LaCoO₃ respectively. Cobalt oxides combined with TiO₂ frequently has two bandgaps [16]. Titania synthesized by hydrothermal methods usually presents values around 3.2 eV, not showing visible light absorption. Although a slight decrease of bandgap might be consequence of cobalt [15, 28] or lanthanum doping [29], in this case this value drops to 2.88 eV, far from being explained by this effect. Presence of transition metal oxides coating TiO₂ has been reported to shift bandgap value of TiO₂ [30]. Therefore, LaCoO₃ in the lattice of titania may be the origin of the bandgap decrease for TiO₂ reported in this study.

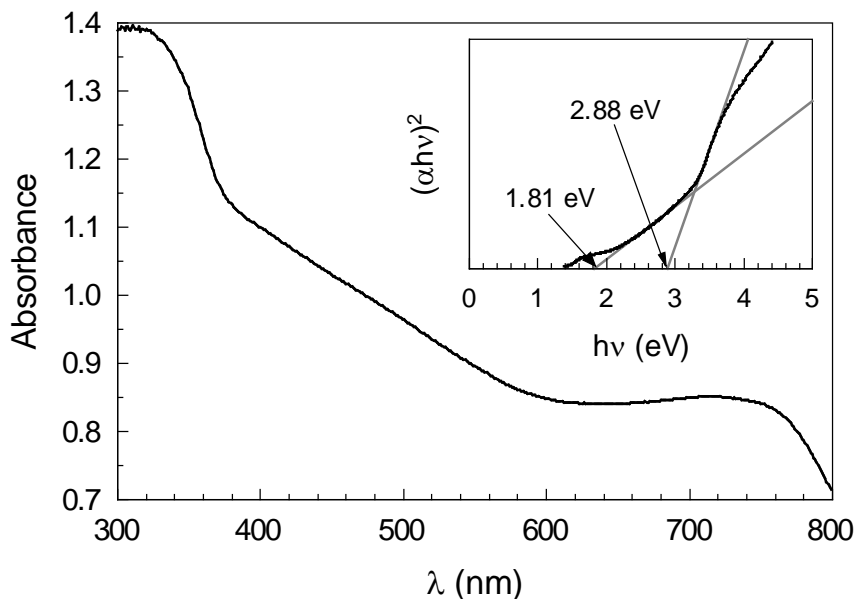


Figure 10.13 Diffuse reflectance UV-vis spectra of $\text{LaCoO}_3\text{-TiO}_2$ (Co:Ti=0.1:1). **Inset figure:** Tauc's plot for bandgap determination

10.4. CONCLUSIONS

Catalysts based on $\text{LaCoO}_3\text{-TiO}_2$ seem to be suitable for removing organic pollutants through combination of photocatalytic and heterogeneous decomposition of monoperoxysulfate. Co/Ti ratio of 0.1:1 is enough to reach enhanced degradation rates if compared to bare titania or pure perovskite. From all variables assessed, oxone[®] concentration is the most influential, making possible to remove almost instantaneously herbicides at concentration up to $5 \cdot 10^{-4}$ M of oxone[®]. Tritosulfuron was 10 times more recalcitrant than the rest. Maximum mineralization extent was found to be 55% ($5 \cdot 10^{-4}$ M oxone[®], 3 hours of treatment), with low release of fluorine (~10%) and nitrate (~18%). Nevertheless, phytotoxicity assays of *Lactuca Sativa* germination pointed out almost complete disappearance of growth inhibition. Thus, the higher MPS amount used, the faster phytotoxicity decreases during treatment.

$\text{LaCoO}_3\text{-TiO}_2$ (ratio Co/Ti=0.1:1) characterization by SEM indicated a heterogeneous variety of TiO_2 size and LaCoO_3 aggregates which seem to be made of smaller spheres. XRF technique led to quantification of roughly 6% of LaCoO_3 in the solid. Superficial XPS highlighted the oxidation states of Co^{3+} , La^{3+} , Ti^{4+} , O^{2-} and absence of hydroxyl groups. A high increase in absorption in the visible range is appreciated in UV-vis spectra, with bandgaps of 2.88 and 1.81 eV due to TiO_2 and LaCoO_3 particles, respectively.

Supplementary Material

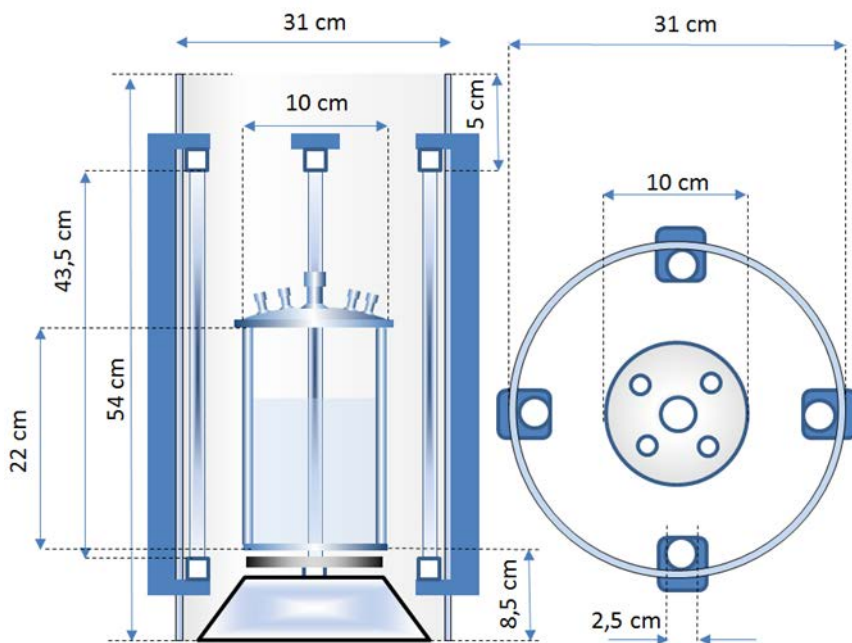


Figure 10.S1 Scheme of the photoreactor setup

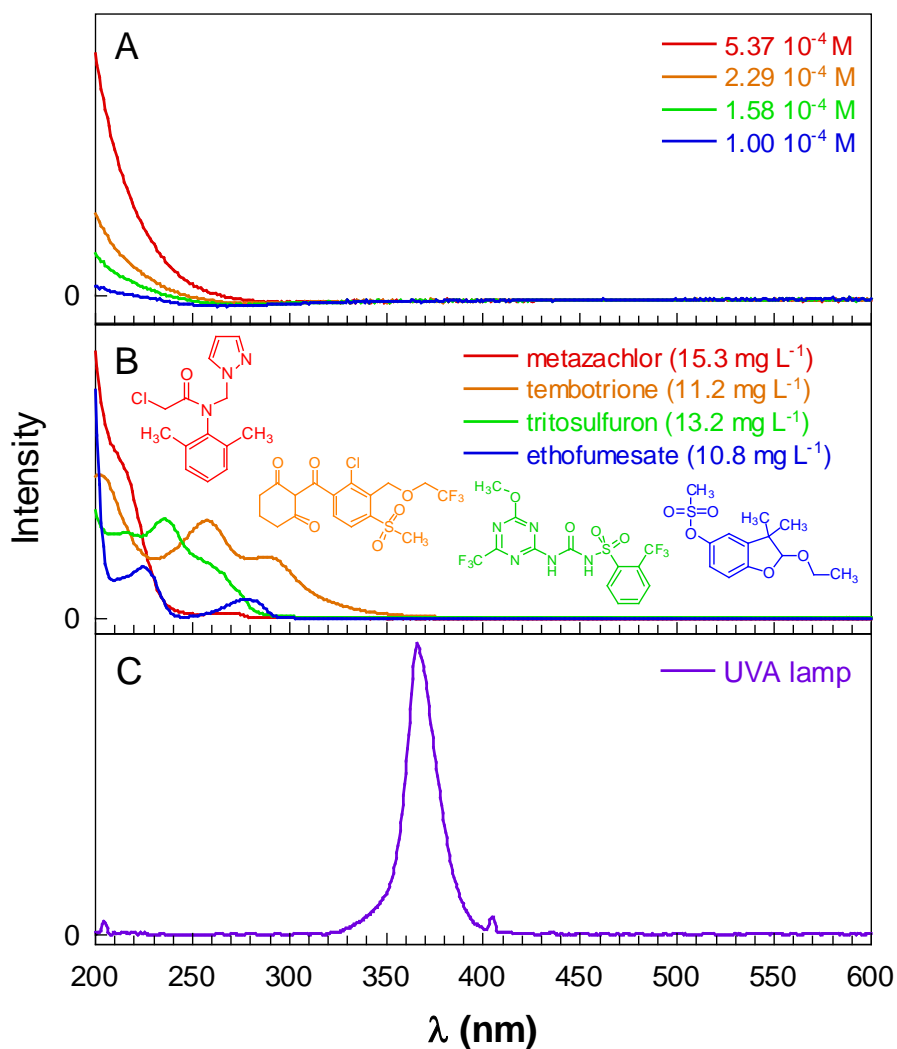


Figure 10.S2 Absorption spectra of Oxone® at different concentrations (A), absorption spectra of herbicides (B) and UVA lamp emission spectra (C)

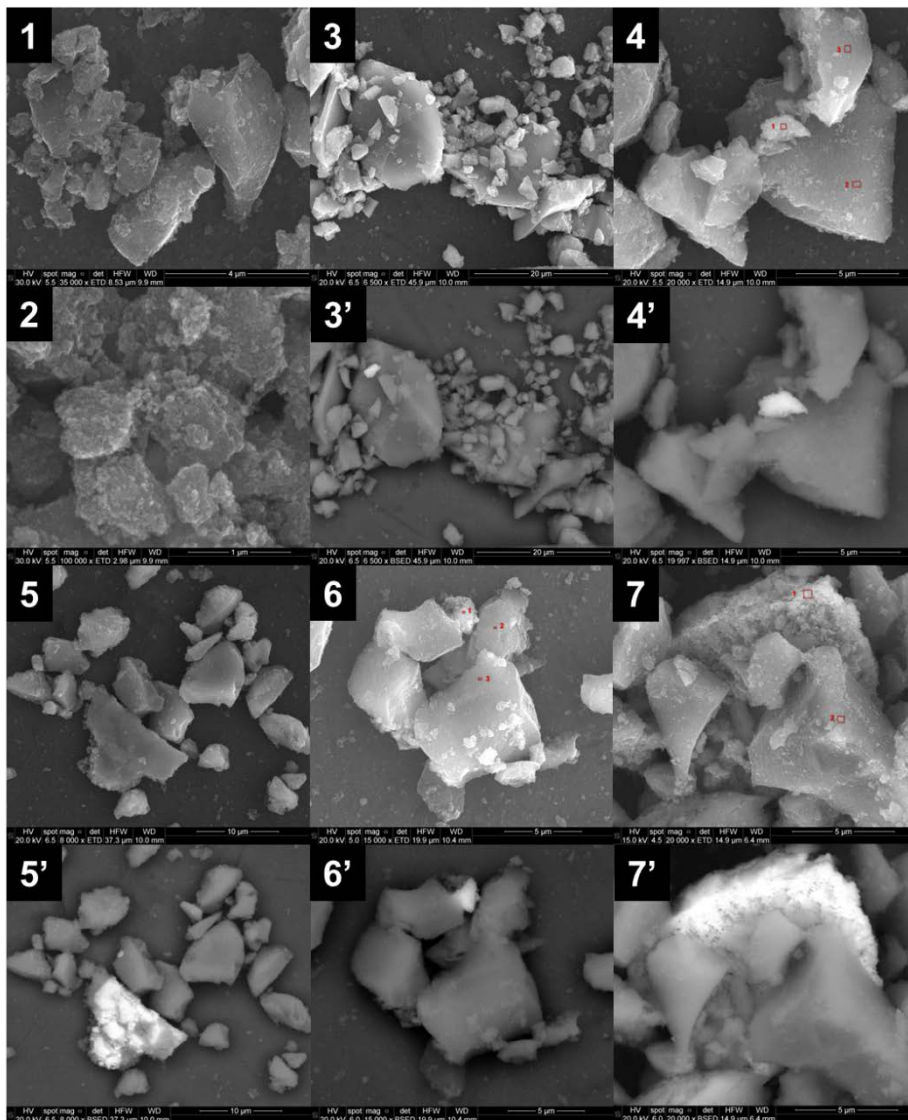


Figure 10.S3 Extended selection of SEM images of $\text{LaCoO}_3\text{-TiO}_2$ (Co/Ti=0.1:1) acquired from secondary electron (1 to 7) and from backscattered electron (3' to 7')

Table 10.S1 Semiquantitative EDX determination of $\text{LaCoO}_3\text{-TiO}_2$ (Co/Ti=0.1:1)

SEM image (from Figure 10.S2)	Point	% atomic			
		O	Ti	La	Co
4	1	67.31	20.34	9.64	2.72
	2	75.65	24.35	-	-
	3	78.55	21.45	-	-
6	1	65.12	14.34	12.38	8.16
	2	72.20	26.37	-	1.44
	3	75.29	23.71	-	1.00
7	1	43.41	6.34	23.03	8.27
	2	54.28	42.12	-	1.42

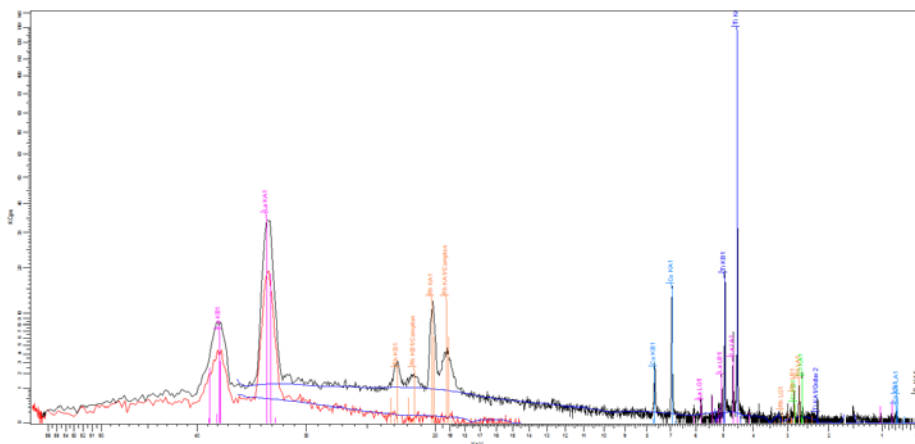


Figure 10.S4 XRF spectra of $\text{LaCoO}_3\text{-TiO}_2$ (Co/Ti=0.1:1)

Acknowledgements

Authors thank economic support received from *Junta de Extremadura*, *CICYT* of Spain and *FEDER* funds through Projects GRU15033 and CTQ2015/64944-R, respectively. Mr. Rafael Rodríguez Solís also acknowledges *Gobierno de Extremadura*, *Consejería de Empleo Empresa e Innovación*, and *FSE* Funds for his Ph.D. grant (PD12058). Catalyst characterization was provided by Facility of Analysis and Characterization of Solids and Surfaces of *SAIUEx* (financed by *UEx*, *Junta de Extremadura*, *MICINN*, *FEDER* and *FSE*).

REFERENCES

- [1] *Directive of the European Parliament and of the council 2000/60/EC establishing a framework for community action in the field of water policy.* Official Journal C513, 23/10/2000
- [2] Loos R, Gawlik BM, Locoro G, Rimaviciute E, Contini S, Bidoglio G. *EU-wide survey of polar organic persistent pollutants in European river waters.* Environ Pollut 157 (2009) 561-568
- [3] Loos R, Locoro G, Comero S, Contini S, Schwesig D, Werres F, Balsaa P, Gans O, Weiss S, Blaha L, Bolchi M, Gawlik BM. *Pan-European survey on the occurrence of selected polar organic persistent pollutants in ground water.* Water Res 44 (2010) 4115-4126
- [4] Pesticide Properties DataBase (PPDB). University of Hertfordshire, UK. <http://sitem.herts.ac.uk/aeru/ppdb/en/index.htm>, 2016 (last accessed 15.07.16)
- [5] Herrero-Hernández E, Andrades MS, Álvarez-Martín A, Pose-Juan E, Rodríguez-Cruz MS, Sánchez-Martín MJ. *Occurrence of pesticides and some of their degradation products in waters in a Spanish wine region.* J Hydrol 486 (2013) 234-245
- [6] Pose-Juan E, Sánchez-Martín MJ, Andrades MS, Rodríguez-Cruz MS, Herrero-Hernández E. *Pesticide residues in vineyard soils from Spain: Spatial and temporal distributions.* Sci Total Environ 514 (2015) 351-358
- [7] Loos R, Carvalho R, António DC, Comero S, Locoro G, Tavazzi S, Paracchini B, Ghiani M, Lettieri T, Blaha L, Jarosova B, Voorspoels S, Servaes K, Haglund P, Fick J, Lindberg RH, Schwesig D, Gawlik BM. *EU-wide monitoring survey on emerging polar organic contaminants in wastewater treatment plant effluents.* Water Res 47 (2013) 6475-6487
- [8] Martínez Bueno MJ, Gomez MJ, Herrera S, Hernando MD, Agüera A, Fernández-Alba AR. *Occurrence and persistence of organic emerging contaminants and priority pollutants in five sewage treatment plants of Spain: Two years pilot survey monitoring.* Environ Pollut 164 (2012) 267-273
- [9] Hu P, Long M. *Cobalt-catalyzed sulfate radical-based advanced oxidation: A review on heterogeneous catalysts and applications.* Appl Catal B Environ 181 (2016) 103-117
- [10] Renganathan R, Maruthamuthu PJ. *Kinetics and mechanism of oxidation of aromatic aldehydes by peroxomonosulphate.* J Chem Soc, Perkin Trans 2 11 (1986) 285-289

- [11] Yang Q, Choi H, Dionysiou DD. *Nanocrystalline cobalt oxide immobilized on titanium dioxide nanoparticles for the heterogeneous activation of peroxymonosulfate*. Appl Catal B Environ 74 (2007) 170-178
- [12] Yang Q, Choi H, Chen Y, Dionysiou DD. *Heterogeneous activation of peroxymonosulfate by supported cobalt catalysts for the degradation of 2,4-dichlorophenol in water: The effect of support, cobalt precursor, and UV radiation*. Appl Catal B Environ 77 (2008) 300-307 (2008)
- [13] Anipsitakis GP, Dionysiou DD. *Radical Generation by the Interaction of Transition Metals with Common Oxidants*. Environ Sci Technol 38 (2004) 3705-3712
- [14] Chen Q, Ji F, Liu T, Yan P, Guan W, Xu X. *Synergistic effect of bifunctional Co-TiO₂ catalyst on degradation of Rhodamine B: Fenton-photo hybrid process*. Chem Eng J 229 (2013) 57-65
- [15] Chen Q, Ji F, Guo Q, Fan F, Xu X. *Combination of heterogeneous Fenton-like reaction and photocatalysis using Co-TiO₂ nanocatalyst for activation of KHSO₅ with visible light irradiation at ambient conditions*. J Environ Sci 26 (2014) 2440-2450
- [16] Sathishkumar P, Mangalaraja RV, Anandana S, Ashokkumar M. *CoFe₂O₄/TiO₂ nanocatalysts for the photocatalytic degradation of Reactive Red 120 in aqueous solutions in the presence and absence of electron acceptors*. Chem Eng J 220 (2013) 302-310
- [17] Chan KH, Chu W. *Degradation of atrazine by cobalt-mediated activation of peroxymonosulfate: Different cobalt counteranions in homogenous process and cobalt oxide catalysts in photolytic heterogeneous process*. Water Res 43 (2009) 2513-2521
- [18] Solís RR, Rivas FJ, Gimeno O. *Removal of aqueous metazachlor, tembotrione, tritosulfuron and ethofumesate by heterogeneous monopersulfate decomposition on lanthanum-cobalt perovskites*. Appl Catal B Environ 200 (2017) 83-92
- [19] Sotelo JL, Ovejero G, Martínez F, Melero JA, Milieni A. *Catalytic wet peroxide oxidation of phenolic solutions over a LaTi_{1-x}Cu_xO₃ perovskite catalyst*. Appl Catal B: Environ 47 (2004) 281-294
- [20] Noh JS, Schwarz JA. *Effect of HNO₃ treatment on the surface acidity of activated carbons*. Carbon 28 (1990) 675-682 (1990)
- [21] Fukushima M, Tatsumi K. *Effect of Hydroxypropyl-β-cyclo-dextrin on the Degradation of Pentachlorophenol by Potassium Monopersulfate Catalyzed with Iron(III)-Porphyrin Complex*. Environ Sci Technol 39 (2005) 9337-9342
- [22] Rivas FJ, Beltrán FJ, Carvalho F, Álvarez PM. *Oxone-Promoted Wet Air Oxidation of Landfill Leachates*. Ind Eng Chem Res 44 (2005) 749-758

- [23] Solís RR, Rivas FJ, Tierno M. *Monopersulfate photocatalysis under 365 nm radiation. Direct oxidation and monopersulfate promoted photocatalysis of the herbicide tembotrione*. J Environ Manage 181 (2016) 385-394
- [24] Yang S, Wang P, Yang X, Shan L, Zhang W, Shao X, Niu R. *Degradation efficiencies of azo dye Acid Orange 7 by the interaction of heat, UV and anions with common oxidants: persulfate, peroxymonosulfate and hydrogen peroxide*. J Hazard Mater 179 (2010) 552-558
- [25] McIntyre NS, Cook MG. *X-ray photoelectron studies on some oxides and hydroxides of cobalt, nickel, and copper*. Anal Chem 47 (1975) 2208-2213
- [26] Yang Z, Huang Y, Dong B, Li HL, Shi SQ. *Sol-gel template synthesis and characterization of LaCoO₃ nanowires*. Appl Phys A Mater Sci Process 84 (2006) 117-122
- [27] Natile MM, Ugel E, Maccato C, Glisenti A. *LaCoO₃: Effect of synthesis conditions on properties and reactivity*. Appl Catal B Environ 72 (2007) 351-362
- [28] Jiang P, Xiang W, Kuang J, Liu W, Cao W. *Effect of cobalt doping on the electronic, optical and photocatalytic properties of TiO₂*. Solid State Sci 46 (2015) 27-32
- [29] Liqiang J, Xiaojun S, Baifu X, Baiqi W, Weimin C, Honggang F. *The preparation and characterization of La doped TiO₂ nanoparticles and their photocatalytic activity*. J Solid State Chem 177 (2004) 3375-3382
- [30] Pozan GS, Isleyen M, Gokcen S. *Transition metal coated TiO₂ nanoparticles: Synthesis, characterization and their photocatalytic activity*. Appl Catal B Environ 140-141 (2013) 537-545

CHAPTER ELEVEN

PAPER NINE

Integrated aerobic biological-chemical treatment of winery wastewater diluted with urban wastewater. LED based photocatalysis in the presence of monoperoxysulfate

Submitted for publication

Rafael R. Solís, F. Javier Rivas, Leonor C. Ferreira, Antonio Pirra, José A. Peres

ABSTRACT. The aim of this research is to develop a combined biological + chemical process in order to achieve the degradation of biodegradable and recalcitrant organic content of Winery Wastewater (WW). In this sense, a biological oxidation by diluting WW with simulated urban wastewater is carried out by applying activated sludge. Acclimation of sludge to Diluted Winery Wastewater (DWW) was first applied, and afterwards some aspects of paramount importance concerning biological oxidation were evaluated. Moreover, parameters of sedimentation design were also studied. After DWW has been biologically oxidized (40-50% of COD removal in 8 hours), chemical processes based on UVA-LEDs radiation, monoperoxysulfate (MPS) and photocatalysts were applied in order to complete oxidation of the remaining COD and complete oxidation of the polyphenols, which were poorly degraded by means of activated sludge. From the all options tested, the combination of UVA, MPS and a novel $\text{LaCoO}_3\text{-TiO}_2$ composite, with double route of MPS decomposition through heterogeneous catalysis and photocatalysis, reached the best results (95% of polyphenol degradation, and additional 60% of COD removal). MPS concentration and pH effect in this process were assessed.

KEYWORDS: winery wastewater, polyphenols, monoperoxysulfate, LEDs, photocatalysis, perovskites, titania



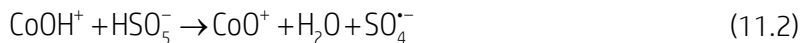
11.1. INTRODUCTION

Wine industry is one of the largest marketplaces in agricultural production all around the world, with a global production of ~265 million of hL in 2015 [1]. Over 50% of wine production is focused on Mediterranean European countries, where it supposes a high impact activity for their economies. It is estimated that 1.2 liters of wastewater are produced per liter of wine processed [2]; however, this value strongly depends on the size and disposal practices of each cellar.

Wastewater produced in winery industry is mainly the result of wine processing (grape reception, fermentation steps, filtrations, tank transfers and bottling), cleaning activities (tanks, floors and equipment), disposable wine and product losses [3,4]. The effluent generated generally is rich in alcohols (methanol, ethanol and glycerol), sugars, organic acids (acetic, tartaric, propionic), aldehydes, phenolic compounds, fermentation products, soaps and detergents resulting from cleaning operations [4,5]. Thus, winery effluents present high values of Chemical Oxygen Demand (COD), reaching values over 25 g L^{-1} at acidic conditions (pH below 4 during vintage period). Although the majority of organic content is biodegradable, biorecalcitrant or toxic contribution of some compounds, i.e. polyphenols, joint to an inadequate proportion C:N:P, make difficult in some cases to yield an acceptable purification degree by just applying biological treatments.

Recently, the addition of Advanced Oxidation Processes (AOPs) as a post-treatment of biological processes seems to show promising COD reductions and it was found to be the most effective combination, yielding the highest removal rates [3]. While AOPs are focused on the use of hydroxyl radical (HO^\bullet), which unselectively oxidize organic matter, this work considers the use of sulfate radical ($\text{SO}_4^{\bullet-}$) which overcomes some interesting advantages [6]. Monoperoxysulfate (HSO_5^- , MPS) is commonly used as promoter of sulfate radicals. Although persulfate presents a higher oxidation potential (2.01 versus 1.82 V), MPS seems to develop better oxidation activity of organic compounds [7]. MPS can be easily activated by means of heat, UV radiation [8,9] or homogeneous catalysis in presence of some metallic species such as Co(II), Fe (II), Ru (III) [10,11], being Co(II) the most active catalyst. Cobalt triggers MPS decomposition by means of a Fenton-Like mechanism that can be summarized in the equations [12]:





Homogeneous catalysis requires the further removal of the catalyst, especially in those cases where the active substance, i.e. cobalt, presents toxic properties. Consequently, the development of heterogeneous catalysts emerges as solution.

Recently, LaXO_3 perovskite oxides have proved their high capacity to promote the heterogeneous catalytic decomposition of MPS [13], LaCoO_3 showing the highest activity [14,15]. Other option for heterogeneous activation of MPS is photocatalysis. MPS decomposition can be achieved photocatalytically, using a semiconductor in which MPS can be reduced by excited photoelectrons coming from the conduction band [16]:



MPS traps electrons, avoiding the undesirable recombination of the photogenerated hole-electron pair. Recently, the option of coupling cobalt oxides to photocatalysts like TiO_2 is gaining attention since electrons generated in photocatalytic process contribute to regenerate the original oxidation state of cobalt, minimizing therefore the electron-hole recombination [17,18]:



Hence, two heterogeneous routes of MPS activation, via photocatalysis and heterogeneous Fenton-Like, are launched.

The objective of the research here presented is the use of a combined biological-chemical treatment of a real Winery Wastewater from a local cellar of Douro valley (Portugal). Not only main aspects concerning biological treatment such as efficiency of mineralization and Monod kinetic growth of biomass are studied; but also sedimentation parameters design of the generated sludge are evaluated. After that, the biologically treated effluent

was further oxidized by combining UVA-LEDs radiation, monoperoxysulfate and photocatalysis based on $\text{LaCoO}_3\text{-TiO}_2$, whose ability to decompose MPS into free radicals seems to be promising [19]. Diverse combinations of LEDs, MPS and photocatalysts (commercial P25, lab-made TiO_2 , LaCoO_3 and $\text{LaCoO}_3\text{-TiO}_2$) were conducted for comparison purposes. UVA/MPS/ $\text{LaCoO}_3\text{-TiO}_2$ was significantly the most efficient, in which optimal conditions were 10 mM of MPS concentration and circumneutral pH.

11.2. EXPERIMENTAL SECTION

11.2.1. Reagents

All chemicals used were analytical grade and were used as purchased. Monoperoxysulfate was obtained from Merck ($2\text{KHSO}_5\cdot\text{KHSO}_4\cdot\text{K}_2\text{SO}_4$). Solutions were prepared with distilled or ultrapure water (18.2 M Ω cm).

11.2.2. Wine Wastewater and analytical procedures

The Wine Wastewater (WW) used in this study came from a local cellar located in the Douro Region (Amarante, Portugal), collected during wine harvest. Raw wastewater was filtered with paper, stored at 4°C and characterized as received. Due to the high content of volatiles, aeration overnight was carried out. Table 11.1 shows the results of characterization before and after removal of volatile content.

Table 11.1 Characterization of Wine Wastewater (WW)

Parameter	Raw WW	WW after volatile removal
COD (g L^{-1})	139.25 ± 2.55	63.1 ± 1.1
TOC (g L^{-1})	44.500 ± 0.150	26.49 ± 0.30
BOD ₅ (g L^{-1})	42.5 ± 2.5	27.0 ± 1.0
Total polyphenols (mg L^{-1}) ^a	438 ± 1	622 ± 2
A ₂₅₄ ^b	2.58	2.88
pH	3.43	4.01
Conductivity ($\mu\text{S cm}^{-1}$)	2.43 ± 0.04	4.32 ± 0.09
Turbidity	453 ± 33	527 ± 34

^a Expressed as phenol

^b Measured in a 1 cm path quartz cell after dilution (1:10)

Chemical Oxygen Demand (COD) was analyzed by means of dichromate reflux oxidation method in a Hach® COD block heater (COD reactor, model 45600) followed by colorimetric determination in a DR/2400 Hach® spectrophotometer.

Biological Oxygen Demand after five days (BOD₅) was conducted by respirometric method, using BOD seed capsules of ColeParmer® as inoculum and OxiTop® respirometers.

Total polyphenols content was quantified by the Folin-Ciocalteu method, using phenol as the standard to express the results [20].

Total Organic Carbon (TOC) and Inorganic Carbon (IC) content were determined by a Shimadzu TOC-L_{CSH} analyzer with Non-Dispersive InfraRed (NDIR) detection, equipped with ASI-L autosampler.

Turbidity was achieved in a 2100N IS Hach® turbidimeter based on the nephelometric measurement procedure. pH was measured in a Jenway 3510 pH meter, whose electrode was immersed into the solution when pH was controlled during the reaction. Conductivity was measured in a Crison® 524 conductimeter equipped with graphite cell and automatic compensation of temperature.

11.2.3. Biological treatment with activated sludge

Activated sludge from the local Urban Wastewater Treatment Plant (UWWTP) of the city of Vila Real (Portugal), designed for 60,000 equivalent inhabitants (AdTMAD, Águas de Trás-os-Montes e Alto Douro, Portugal), was used as inoculum in the aerobic biological treatment. Sludge was taken from the recirculation line after the secondary settling tank (8.75 g L⁻¹ of Total Suspended Solids and 6.81 g L⁻¹ Volatile Suspended Solids), and used immediately after being collected.

Given the high organic load of the aerated wastewater, this effluent was first diluted with a synthetic wastewater whose composition simulated the properties normally found in urban wastewater. The resulting wastewater was named as Diluted Wine Wastewater (DWW).

The sludge of the UWWTP was first acclimated to the DWW by decreasing the amounts of glucose and glutamic acid from the synthetic wastewater and increasing the amount of the organic load coming from the DWW [21] until reaching an initial COD content of roughly 1400-1500 mg L⁻¹ (see Table 11.2). Apart from considering the joint treatment of urban and industrial effluents, the objective of using a synthetic wastewater was also to provide the mineral content required by microorganisms in the activated sludge (wine wastewater does not contain a sufficient amount of salts for the sludge to proceed with the biodegradation). The resultant effluent pH was adjusted to 7.0±0.5. Thereafter, a 5.0 L cylindrical reactor equipped with aeration was inoculated with activated sludge in order to have a final concentration of 1-2 g L⁻¹ of Total Suspended Solids (TSS) in the reactor. A total volume of 5.0 L was treated in each biodegradation assay. Consecutive reactions in batch mode were completed, keeping the same biomass after each use. Samples at different

times were extracted and filtrated with glass microfiber filters (Whatman® Reeve Angel™, grade 403). The filtrate was used in COD, TOC and polyphenols analysis, while the glass fiber with the filtrated activated sludge was used in the determination of Total Suspended Solids (TSS) and Volatile Suspended Solids (VSS). Sedimentation analysis was also carried out at different times by taking one liter of sample in a graduated glass cylinder. Aeration was controlled to have up to 2.5 mg L⁻¹ of dissolved oxygen and enough agitation.

Table 11.2 Planning of acclimation and reactions of biological treatment with DWW

Components (mg L ⁻¹)	Reaction time (days)							
	1	2	3	4	5	6	7	8
Glucose	150	112.5	75	37.5	-	-	-	-
Glutamic acid	100	75	50	25	-	-	-	-
K ₂ HPO ₄					138			
KH ₂ PO ₄					69			
NH ₄ Cl					52			
MgSO ₄ ·7H ₂ O					26			
FeSO ₄ ·7H ₂ O					1			
ZnSO ₄ ·7H ₂ O					1			
MnSO ₄ ·7H ₂ O					1			
CaCl ₂					7			
NaHCO ₃					83.2			
Amount of WW (mL/L)	0	6	12	18	24	24	24	24
Percentage of DWW	0	25	50	75	100	100	100	100
COD	172.8	548	847	1252	1636	1427	1406	1465
TOC	81.7	207.1	323.6	490	644.9	558.6	561.8	570.7

11.2.4. LED photoreactor system

Diluted Wine Wastewater pretreated by biological oxidation was thereafter considered in photocatalysis oxidation experiments using sulfate radicals. The experimental setup consisted in a photosource of 12 InGaN LEDs lamps (Roithner APG2C1-36E LEDs, nominal consumption of 1.4 W each) emitting within the range 360-380 nm (maximum located at 368 nm). The resultant UVA irradiance was 85 W m⁻². LEDs system was located on the top of the glass reactor, perfectly mixed through magnetic stirring. Figure 11.1 depicts a scheme of the photocatalytic setup. The irradiance absorbed in the 500 mL reactor, quantified by means of ferryxalate-polyoxometalate actinometry [22], was 2.45 10⁻⁶ Einstein L⁻¹ s⁻¹.

Experiments in batch mode were carried out by adding the photocatalyst and a required amount of monoperoxysulfate (Oxone®, 2KHSO₅·KHSO₄·K₂SO₄). As photocatalyst was considered a lanthanum-cobalt perovskite coupled to titania, previously studied. Catalysts synthesis and characterization belongs to previous works [15,19]. pH was adjusted after

Oxone® addition by adding NaOH 10 M. Samples were extracted and filtered with Millipore® Millex-GV (PVDF 0.22 μm) at different times for COD, TOC and polyphenols analyses.

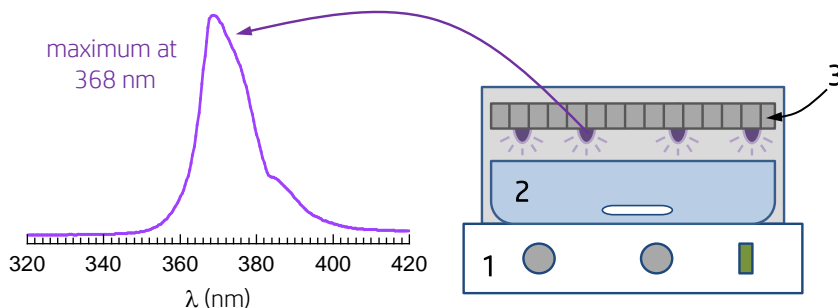


Figure 11.1 Photocatalytic setup installation and UVA-LEDs emission spectra (1: magnetic stirrer, 2: glass photoreactor, 3: UVA-LED photoirradiation system)

11.3. RESULTS AND DISCUSSION

11.3.1. Aerobic Biological treatment of DWW

As stated previously, given the high content in polyphenols, activated sludge was acclimated to DWW for eight consecutive days by increasing the percentage of DWW from 0 % (first day) to 100% (fifth day). Four replicates under the last conditions (100% DWW) were completed in days 5 to 8. Figure 11.2 shows the evolution of COD and TOC in acclimation experiments. As observed, once the activated sludge was acclimated, the biological process was capable of reducing around 45-50% of the initial COD content in 8 hours of reaction. Similar results were obtained when considering TOC abatement, suggesting the conversion of the organic matter directly to carbon dioxide and water. Reduction in polyphenols (results not shown) was around 50-55% at the end of the process.

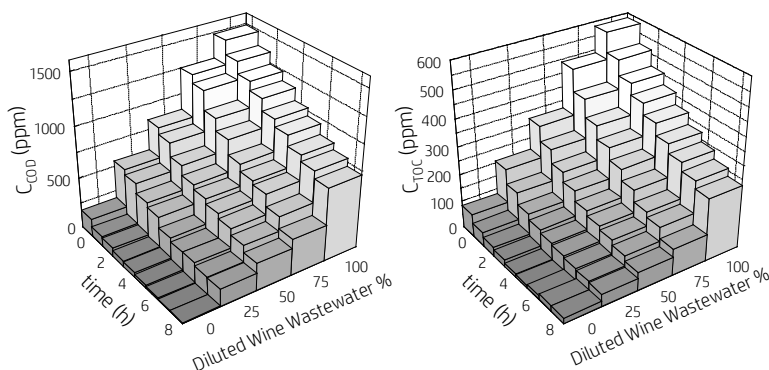


Figure 11.2 Acclimation of microorganism to aerobic biodegradation of DWW at increasing doses of the wastewater

The path of the wastewater biodegradation can be assessed by determining the evolution of the Average Oxidation State of Carbon (AOSC) and the efficiency through partial oxidation (μ_{partox}). These parameters are defined as follows [23]:

$$\Delta(\text{AOSC}) = \text{AOSC} - \text{AOSC}_0 = 4 \left[\frac{\text{COD}_0 - \text{COD}}{\text{TOC}_0 - \text{TOC}} \right] \frac{M_C}{M_{O_2}} \quad (11.9)$$

$$\mu_{\text{partox}} = \frac{\text{COD}_{\text{partox}}}{\text{COD}_0 - \text{COD}} \quad (11.10)$$

where

$$\text{COD}_{\text{partox}} = \frac{\text{TOC}[\Delta(\text{AOSC})]}{4} \frac{M_{O_2}}{M_C} \quad (11.11)$$

In equations 11.9 to 11.11 the subindex “0” denotes conditions at time zero and M_C and M_{O_2} are the molecular weight of carbon and oxygen respectively. Theoretically, the closer the value of μ_{partox} to 1, the higher the extension of the oxidation to generate oxygenated intermediates instead of total mineralization to carbon dioxide. Contrarily, a value of μ_{partox} close to 0 indicates that no partial oxidation proceeds and just complete conversion to CO_2 is occurring [24]. Applying equation 11.10 to the average results obtained with 100% of DWW led to a μ_{partox} value of -0.03 ± 0.06 , close to the minimum value for this parameter of 0.

Substrate consumption in a biological process measured as COD or TOC abatement can be associated to two possible routes. Hence, COD (or TOC) may be the carbon supply of the biomass to grow up, or, alternatively, is the source of energy required to maintain cell activity. Accordingly, the following equation can be used [21]:

$$-\frac{dC_{\text{Substrate}}}{dt} = \frac{1}{Y_{\text{VSS}/\text{Substrate}}} \mu C_{\text{VSS}} + m C_{\text{VSS}} \quad (11.12)$$

where $C_{\text{Substrate}}$ is the substrate concentration (COD or TOC), t is time, C_{VSS} is the biomass concentration expressed as the amount of volatile suspended solids per liter, m is the maintenance energy coefficient, μ the specific growth rate of biomass defined in equation 11.13 and $Y_{\text{VSS}/\text{Substrate}}$ the heterotrophic yield coefficient, defined in equation 11.14, relating substrate consumption and increase in biomass concentration during the exponential growth phase.

$$\mu = \mu_{\text{Max}} \frac{C_{\text{Substrate}}}{K_s + C_{\text{Substrate}}} \quad (11.13)$$

$$Y_{\text{VSS/Substrate}} = \frac{C_{\text{VSS}} - C_{\text{VSS}_0}}{C_{\text{Substrate}_0} - C_{\text{Substrate}}} \quad (11.14)$$

Expression 11.13 is Monod equation where μ_{max} represents the maximum specific growth rate and K_s is the saturation constant.

In the exponential growth phase of biological batch experiments, substrate consumption is associated to formation of new microorganism, and therefore, as a consequence, the term $m \cdot C_{\text{VSS}}$ can be assumed negligible. Since $Y_{\text{VSS/Substrate}}$ almost remains constant during the exponential growth ($Y_{\text{VSS/COD}} = 0.3-0.35$), equation 11.12 can be analytically integrated leading to:

$$\left(\Psi + Y_{\text{VSS/COD}} K_s \right) \ln \left[\frac{\Psi - Y_{\text{VSS/COD}} C_{\text{COD}}}{C_{\text{VSS}_0}} \right] - Y_{\text{VSS/COD}} K_s \ln \frac{C_{\text{COD}}}{C_{\text{COD}_0}} = \mu_{\text{max}} \Psi t \quad (11.15)$$

where the parameter Ψ is defined as:

$$\Psi = C_{\text{VSS}_0} + Y_{\text{VSS/COD}} C_{\text{COD}_0} \quad (11.16)$$

Moreover, since the value of K_s is normally small [25], equation 11.15 becomes:

$$\ln \left[\frac{\Psi - Y_{\text{VSS/COD}} C_{\text{COD}}}{C_{\text{VSS}_0}} \right] = \mu_{\text{max}} t \quad (11.17)$$

A plot of the left hand side of equation 11.17 *versus* time should lead to a straight line of slope μ_{max} . Figure 11.3 shows the results of the linear regression applied to COD abatement in experiments conducted with 100% of DWW. The value of μ_{max} found was $0.0119 \pm 0.0011 \text{ h}^{-1}$, similar to the value reported when wastewater from table olive manufacturing industries was treated after dilution with urban wastewater [21] following a similar kinetic approach.

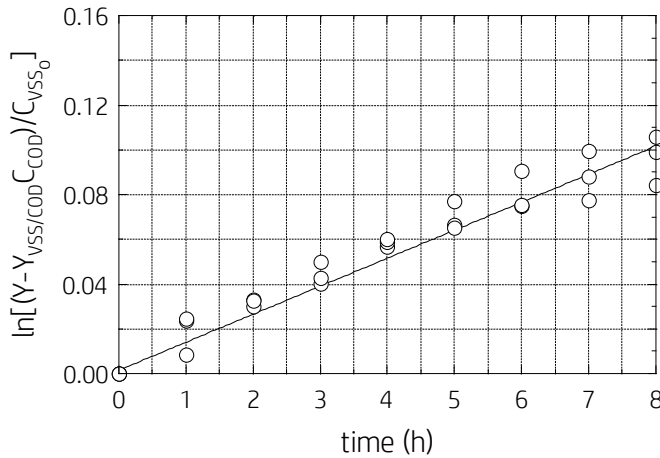


Figure 11.3 Kinetics of the aerobic biodegradation of DWW. Validation of equation 11.17

One of the crucial parameters in conventional activated sludge processes is the secondary settling stage to recirculate the sludge. Hence, settling properties of activated sludge are of paramount importance. Figure 11.4 (left) shows the evolution of the interface clarified water-sludge blanket as a function of time in sedimentation experiments conducted with activated sludge after the biodegradation took place. The previous plot can be fitted to the model proposed by [26]:

$$h(t, h_0) = \frac{\alpha C_{VSS_0} h_0}{\beta} + \left[h_0 - \frac{\alpha C_{VSS_0} h_0}{\beta} \right] \exp\left(-\frac{\beta}{X_0 h_0} t \right) \quad (11.18)$$

where t stands for time, $h(t, h_0)$ is the sludge height at time t ; h_0 the initial sludge height; α and β the adjustable parameters for the sedimentation process and C_{VSS_0} the initial volatile solid concentration. The adjustable parameters were: $\alpha = 2.09 \text{ cm min}^{-1}$ and $\beta = 18,026 \text{ mg L}^{-1} \text{ cm min}^{-1}$. ($R^2 \approx 0.99$). Solid concentration as a function of height can be obtained by [27]:

$$C_{VSS}(t, h) = \frac{C_{VSS_0} h_0}{h(t, h_0) - \left[\alpha - \frac{\beta}{C_{VSS_0} h_0} h(t, h_0) \right] t} \quad (11.19)$$

In case of effluents with a high content in solids ($>500 \text{ mg L}^{-1}$), the solid flow rate fed to the clarifier per surface unit, ($\text{kg m}^{-2} \text{ day}^{-1}$) is the criteria in clarifiers design.

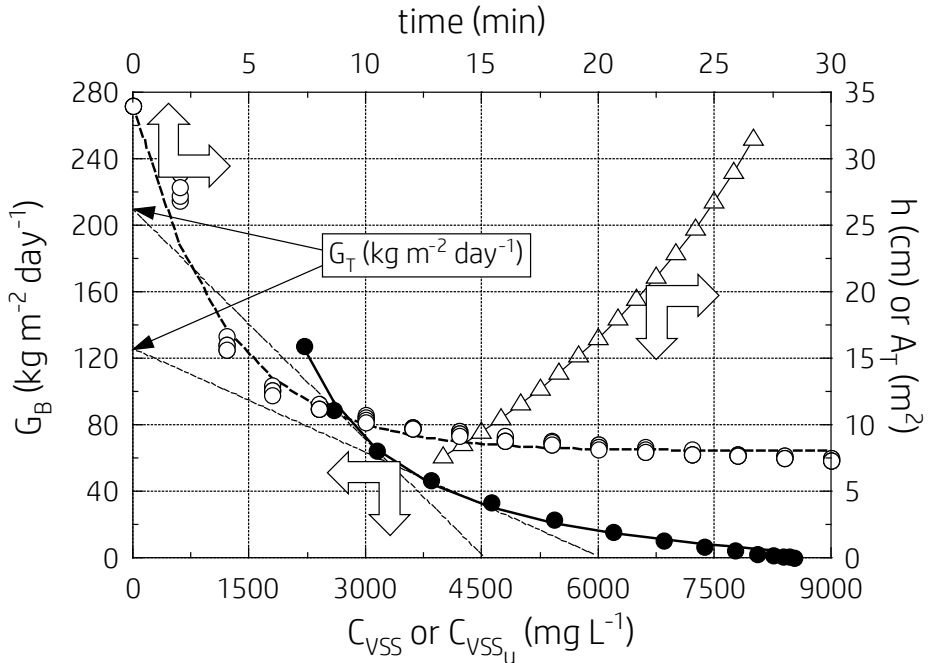


Figure 11.4 Settling properties of activated sludge ($C_{VSS_0} = 2.04 \text{ g L}^{-1}$). \circ , water sludge interface height vs time (long dashed line: fitted curve); \bullet , G_B vs C_{VSS} (solid line: fitted curve), Δ , Clarifier area A_T vs C_{VSS_u}

A graphical method can be used in the design of clarifiers [28]. Hence, G_B is defined as the solid flow rate in the clarifier due to gravity and is given by:

$$G_B = C_{VSS} v_{h(t,h_0)} \quad (11.20)$$

where $v_{h(t,h_0)}$ is the settling velocity corresponding to a sludge height of concentration C_{VSS} .

$$v_{h(t,h_0)} = -\frac{\beta}{X_0 h_0} \left[h_0 - \frac{\alpha C_{VSS_0} h_0}{\beta} \right] \exp\left(-\frac{\beta}{X_0 h_0} t \right) \quad (11.21)$$

The plot G_B vs C_{VSS} is shown in Figure 11.4. A simple exponential correlation of the type $G_B = K \cdot C_{VSS}^n - \phi C_{VSS}$ was used to fit experimental data (fitting parameters: K , n and ϕ). Designing a continuous settling tank does depend on the compacting index, γ . This parameter is the ratio solid concentration fed (C_{VSS_0}) to solid concentration in the concentrated sludge (C_{VSS_u}) withdrawn from the tank. Thus, if $\gamma = 4$ the sludge should have a solid concentration of $C_{VSS_u} \approx 8000 \text{ mg L}^{-1}$. The graphical methodology consists of plotting the tangent to the G_B curve containing the point $(C_{VSS_u}, 0)$. The Y-axis

intercept of this tangent gives the value of G_T , accounting for the global solid flow rate ($G_T = G_B + G_U$) due to gravity (G_B) plus the one due to the movement resulting from sludge outlet at the clarifier bottom (G_U). Hence, if $\gamma = 4$, this value is approximately $G_T = 123.6 \text{ kg m}^{-2} \text{ day}^{-1}$. The area required for the clarifier is given by $A_T = Q_0 C_{VSS,0} G_T^{-1}$, where Q_0 stands for the volumetric flow rate fed to the settling tank. Hence, if Q_0 is given a generic value of $1000 \text{ m}^3 \text{ day}^{-1}$, $A_T = 16.5 \text{ m}^2$, that is, the diameter of a cylindrical clarifier should be 4.5 m approximately. Figure 11.4 illustrates the value of A_T as a function of the $C_{VSS,u}$ for a generic value of $Q_0 = 1000 \text{ m}^3 \text{ day}^{-1}$.

11.3.2. Chemical post-treatment of biologically processed DWW

After the activated sludge process, DWW still shows an unacceptable COD content, impeding the direct discharge of this effluent to the environment. Accordingly, several options were contemplated based on the use of UVA radiation generated by LEDs technology in the presence of a radical promoter (monoperoxysulfate, MPS) and a solid catalyst.

Some preliminary control/blank experiments were first carried out. Hence, the potential photolysis and monoperoxysulfate oxidation (in the presence or absence of a cobalt based perovskite) were initially assessed. Figure 11.5 (up) shows the results obtained. As observed from this figure, none of the system tested was capable of efficiently reduce the COD or TOC levels to values suitable for direct discharge into natural water streams. Nevertheless, phenolic content could be partially eliminated when monoperoxysulfate was added to the reaction media, the efficacy rising to 100% abatement in less than 10 minutes if the perovskite LaCoO_3 was present to decompose the inorganic peroxide.

The next stage was to investigate the photocatalytic process in the absence of radical promoters and the promoted photolysis in the absence of catalyst. Accordingly, two more experiments were conducted by applying UVA radiation in the presence of a labmade photocatalyst (composite of LaCoO_3 and TiO_2) or in the presence of sodium monoperoxysulfate. Figure 11.5 (bottom) shows the low efficiency of the UVA/ LaCoO_3 - TiO_2 system both in terms of COD and TOC reduction. Better results were, however, obtained when UVA radiation was used in the presence of monoperoxysulfate. In this latter case COD and polyphenol conversions were roughly 40% and 90%, respectively.

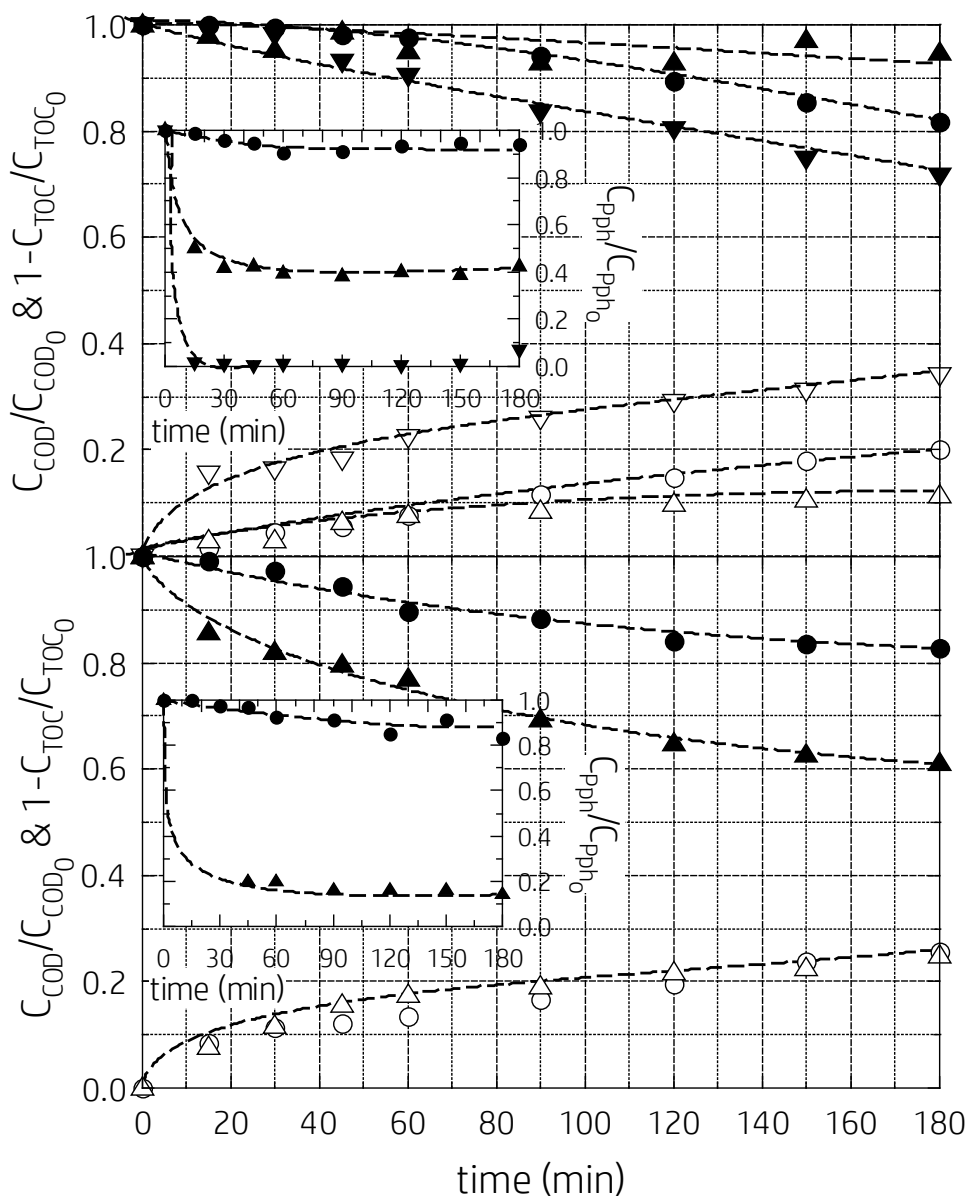


Figure 11.5 Chemical treatment of biologically processed DWW at pH 7. Time evolution of normalized COD (solid symbols) and TOC conversion (open symbols). **Inset figures:** phenolic content. **Up figure:** ●, UVA radiation; ▲, MPS oxidation (0.01 M); ▼, LaCo₃-TiO₂ (0.5 g L⁻¹)/MPS (0.01 M). **Bottom figure:** ●, UVA/LaCo₃-TiO₂ (0.5 g L⁻¹); ▲, UVA/MPS (0.01 M)

In an attempt to improve the process, different options were contemplated. Figure 11.6 (up) depicts the time evolution of COD, TOC and polyphenol content in experiments conducted by irradiating DWW with UVA in the presence of commercial or manufactured TiO_2 and monoperoxydisulfate as promoter. Unexpectedly, no significant differences were found if compared these results with those obtained in the absence of TiO_2 (i.e. MPS promoted photolysis). The systems UVA/ TiO_2 and UVA/MPS when integrated in a more complex technology do not add up their actions, likely due to easy abatement of non-recalcitrant COD by the promoted photolysis so the photocatalysis does not play any significant role. Given the previous results, it was decided to incorporate a solid to the system capable of decomposing MPS such as perovskite type catalysts [15,19]. Hence the systems UVA/MPS/ LaCoO_3 , UVA/MPS/ LaCoO_3 - TiO_2 and UVA/MPS/ LaFeO_3 - TiO_2 were investigated. Figure 11.6 (bottom) shows the results corresponding to this experimental series. At the sight of this figure, the system UVA/MPS/ LaCoO_3 - TiO_2 seems to be the best option in terms of COD conversion and mineralization. Under the conditions used in the experiment with the system UVA/MPS/ LaCoO_3 - TiO_2 , the percentage of COD that suffered partial oxidation rose to 16% after 180 min, however, in the first hour almost all the removed COD was converted to CO_2 .

No significant differences were obtained when considering phenolic content abatement; in this sense the previous three systems tested were able to instantaneously reduce this parameter to values below 5% in a few minutes (results not shown). At this point it can be noticed that inorganic carbon with an initial concentration of roughly 100 mg L^{-1} was efficiently eliminated from the reaction media, suggesting the potential scavenging effect of carbonates if a radical mechanism was developed. To assess this later hypothesis, one more experiment was completed with the system UVA/MPS/ LaCoO_3 - TiO_2 by first removing the carbonate content (acidification + stripping). This experiment did show no significant differences in terms of COD and TOC evolution while inorganic carbon gradually increased from 0 to 35 mg L^{-1} in the interval 0-45 min, thereafter linearly decreasing its concentration to 17 mg L^{-1} after 180 min of treatment. This result suggests that if the process occurs through a radical mechanism, the scavenging nature of carbonates is neutralized by the potential oxidizing action of generated radical carbonates.

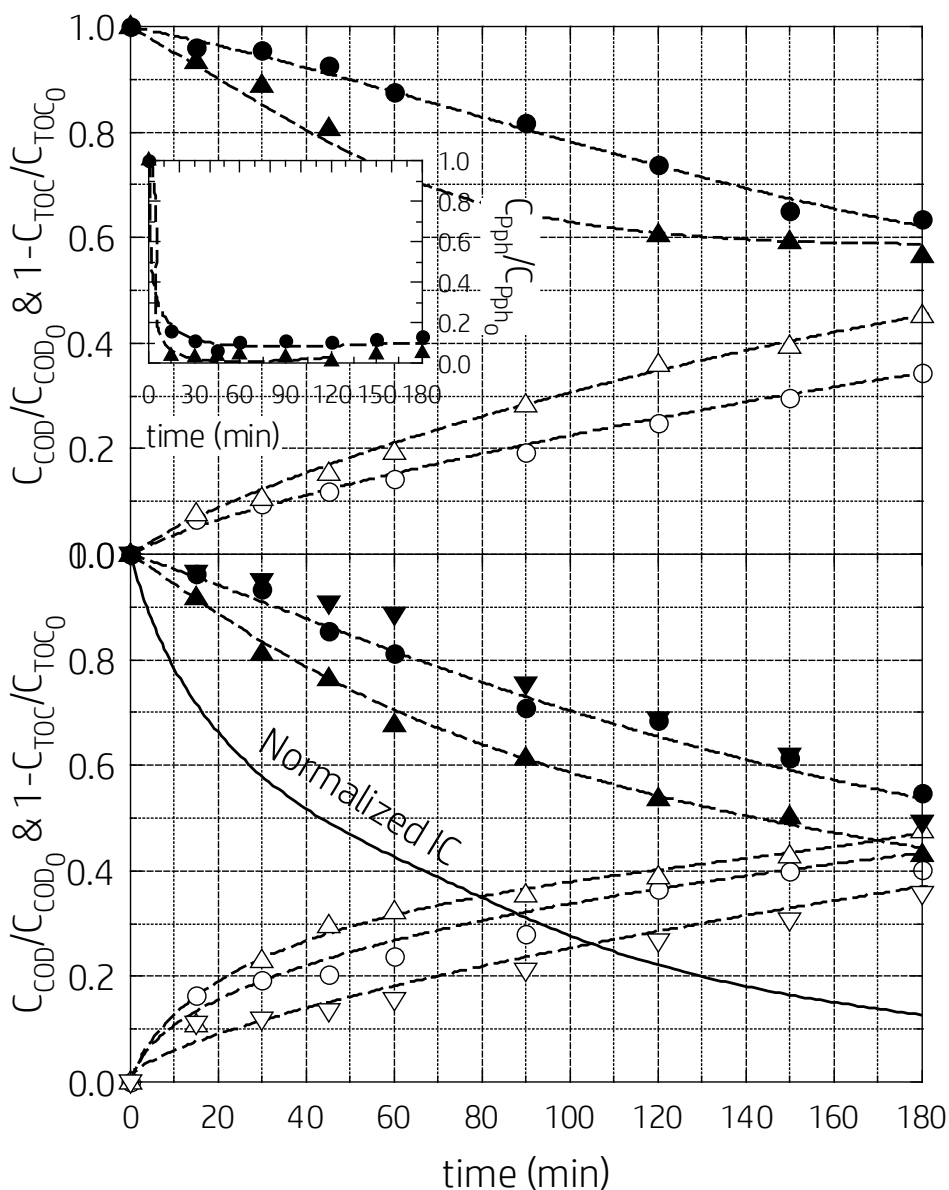


Figure 11.6 Chemical treatment of biologically processed DWW at pH 7. Time evolution of normalized COD (solid symbols) and TOC conversion (open symbols). **Inset figure:** phenolic content. Normalized inorganic carbon=solid line. **Up figure:** ●, UVA/MPS (0.01 M)/P-25 (0.5 g L⁻¹); ▲, UVA/MPS (0.01 M)/TiO₂ (0.5 g L⁻¹). **Bottom figure:** ●, UVA/MPS (0.01 M)/LaCoO₃ (0.5 g L⁻¹); ▲, UVA/MPS (0.01 M)/LaCoO₃-TiO₂ (0.5 g L⁻¹); ▼, UVA/MPS (0.01 M)/LaFeO₃-TiO₂ (0.5 g L⁻¹)

In a final attempt to increase the efficiency of the system UVA/MPS/LaCoO₃-TiO₂, some experiments were conducted at different initial amounts of MPS or different pH. For comparison purposes a simple first order reaction rate was calculated in these experiments. Given the complexity of the photocatalytic mechanism, data from first order kinetics are a mere comparison tool, with no valuable meaning in terms of kinetics. Figure 11.7 reveals how a high concentration of monoperoxysulfate reduces the efficiency of the process in terms of COD removal, likely due to the scavenging character of MPS towards generated radicals if used in excess, according to:



Additionally, no significant effect was experienced when working in the pH range 5-7, however basic pHs (i.e. pH=9) negatively influenced the process. At high pHs, monoperoxysulfate dissociates (second acid dissociation pK_a of roughly 9.4), so apparently, the SO_5^{2-} species is less effective in the process.

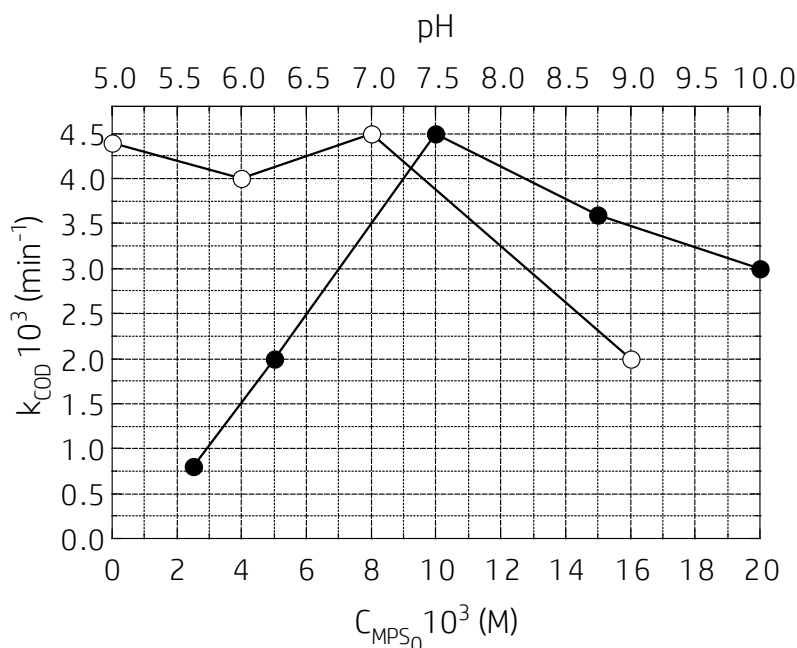


Figure 11.7 Monoperoxysulfate promoted photocatalysis of biologically processed DWW by UVA/MPS/LaCoO₃-TiO₂ (0.5 g L⁻¹). Influence of initial MPS concentration and pH on pseudo first order rate constant of COD abatement. ●, MPS influence at pH 7; ○, pH influence with $C_{\text{MPS},0} = 0.01 \text{ M}$

11.4. CONCLUSIONS

Biological treatment of Diluted Winery Wastewater (DWW) takes place by direct conversion of TOC to CO₂, as the efficiency through partial oxidation of AOSC theory denotes ($\mu_{\text{partox}} \approx 0$). Although the joint of DWW and simulated urban wastewater reached 45–50% of COD degradation in 8 hours, biological treatment by itself seems to be insufficient if applied in small dimensions biological reactors. This is the case of cellars of small village where vine is produced. This issue can easily be resolved by coupling a chemical oxidation process such as photocatalysis using MPS.

Among the chemical processes tested, based on LEDs, MPS and photocatalysis, the photocatalytic decomposition of MPS on LaCoO₃-TiO₂ composite attained the best results. Photocatalysis with TiO₂ did not improve the results observed during photolytic decomposition of MPS. However, LaCoO₃-TiO₂ highly improved COD conversion and mineralization, appreciating a direct conversion of COD into CO₂. Polyphenols, which were only removed in a 50% extent during biological treatment, were almost instantaneously oxidized in chemical processes (95% in UVA/MPS/LaCoO₃-TiO₂ system). The presence of carbonate in this system outlines that the mechanism of scavenging might be neutralized by the potential oxidizing action of generated radical carbonates. Initial MPS concentration in the UVA/MPS/LaCoO₃-TiO₂ system highlights that an increase of this variable exerts a positive effect until reach an optimum value (10⁻² M), after what it slightly starts to be negative. Concurrently, working at basic pH conditions results negative due to the dissociation of HSO₅⁻ into SO₅²⁻ (pK_a=9.4).

Acknowledgements

Authors thank the economic support received from *Gobierno de Extremadura* (GRU15033) and *MINECO* of Spain (CTQ2015/64944-R and *red FOTOCAT* CTM2015-71054-REDT), cofinanced with *FEDER* funds.

Mr. Rafael Rodríguez Solís acknowledges *Gobierno de Extremadura*, *Consejería de Empleo Empresa e Innovación*, and *FSE* Funds for his Ph.D. grant (PD12058).

Authors also acknowledges the funding provided by the project INTERACT (Integrative Research in Environment, Agro-Chains and Technology) NORTE-01-0145-FEDER-000017 and Project INNOVINE & WINE (Innovation Platform of Vine and Wine) NORTE-01-0145-FEDER-000038 (Portugal).

Finally, authors would like to express their gratitude to Águas de Trás-os-Montes e Alto Douro (AdTMAD) for providing activated sludge sample from the urban wastewater treatment plant of Vila Real (Portugal).

REFERENCES

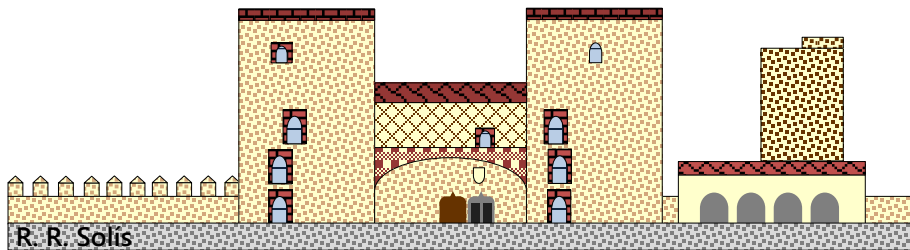
- [1] IOVW, International Organisation of Vine and Wine. 2016 World Vitiviniculture Situation. OIV Statistical Report on World Viticulture, **2016**
- [2] Vlyssides AG, Barampouti EM, Mai S. *Wastewater characteristics from Greek wineries and distilleries*. Water Sci Technol 51 (**2005**) 53-60
- [3] Ioannou LA, Li Puma G, Fatta-Kassinou D. *Treatment of winery wastewater by physicochemical, biological and advanced processes: A review*. J Hazard Mater 286 (**2015**) 343-368
- [4] Kyzas GZ, Symeonidou MP, Matis KA. *Technologies of winery wastewater treatment: a critical approach*. Desalin Water Treat 57 (**2016**) 3372-3386
- [5] Mosse KPM, Patti AF, Christen EW, Cavagnaro TR. *Review: Winery wastewater quality and treatment options in Australia*. Aust J Grape Wine Res 17 (**2011**) 111-122
- [6] Hu P, Long M. *Cobalt-catalyzed sulfate radical-based advanced oxidation: A review on heterogeneous catalysts and applications*. Appl Catal B: Environ 181 (**2016**) 103-117
- [7] Chen X, Wang W, Xiao H, Hong C, Zhu F, Yao Y, Xue Z. *Accelerated TiO₂ photocatalytic degradation of Acid Orange 7 under visible light mediated by peroxymonosulfate*. Chem Eng J 193-194 (**2012**) 290-295
- [8] Yang S, Wang P, Yang X, Shan L, Zhang W, Shao X, Niu R. *Degradation efficiencies of azo dye Acid Orange 7 by the interaction of heat, UV and anions with common oxidants: Persulfate, peroxymonosulfate and hydrogen peroxide*. J Hazard Mater 179 (**2010**) 552-558
- [9] Antoniou MG, de la Cruz AA, Dionysiou DD. *Degradation of microcystin-LR using sulfate radicals generated through photolysis, thermolysis and e-transfer mechanisms*. Appl Catal B: Environ 96 (**2010**) 290-298
- [10] Anipsitakis GP, Dionysiou DD. *Radical generation by the interaction of transition metals with common oxidants*. Environ Sci Technol 38 (**2004**) 3705-3712
- [11] Rodríguez-Chueca J, Amor C, Silva T, Dionysiou DD, Li Puma G, Lucas MS, Peres JA. *Treatment of winery wastewater by sulphate radicals: HSO₅⁻/transition metal/UV-A LEDs*. Chem Eng J 310 (**2017**) 473-483
- [12] Anipsitakis GP, Dionysiou DD. *Degradation of organic contaminants in water with sulfate radicals generated by the conjunction of peroxymonosulfate with cobalt*. Environ Sci Technol 37 (**2003**) 4790-4797

- [13] Lin K-YA, Chen YC, Lin YF. *LaMO₃ perovskites (M=Co, Cu, Fe and Ni) as heterogeneous catalysts for activating peroxymonosulfate in water*. Chem Eng Sci 160 (2017) 96-105
- [14] Pang X, Guo Y, Zhang Y, Xu B, Qi F. *LaCoO₃ perovskite oxide activation of peroxymonosulfate for aqueous 2-phenyl-5-sulfobenzimidazole degradation: Effect of synthetic method and the reaction mechanism*. Chem Eng J 304 (2016) 897-907
- [15] Solís RR, Rivas FJ, Gimeno O. *Removal of aqueous metazachlor, tembotrione, tritosulfuron and ethofumesate by heterogeneous monopersulfate decomposition on lanthanum-cobalt perovskites*. Appl Catal B: Environ 200 (2017) 83-92
- [16] Malato S, Blanco J, Richter C, Braun B, Maldonado MI. *Enhancement of the rate of solar photocatalytic mineralization of organic pollutants by inorganic oxidizing species*. Appl Catal B: Environ 17 (1998) 347-356
- [17] Chen Q, Ji F, Liu T, Yan P, Guan W, Xu X. *Synergistic effect of bifunctional Co-TiO₂ catalyst on degradation of Rhodamine B: Fenton-photo hybrid process*. Chem Eng J 229 (2013) 57-59
- [18] Chen Q, Ji F, Guo J, Fan J, Xu X. *Combination of heterogeneous Fenton-like reaction and photocatalysis using Co-TiO₂ nanocatalyst for activation of KHSO₅ with visible light irradiation at ambient conditions*. J Environ Sci 26 (2014) 2440-2450
- [19] Solís RR, Rivas FJ, Gimeno O, Pérez-Bote JL. *Synergism between peroxymonosulfate and LaCoO₃-TiO₂ photocatalysis for oxidation of herbicides. Operational variables and catalyst characterization assessment*. J Chem Technol Biotechnol (2017) doi: 10.1002/jctb.5228
- [20] Box JD. *Investigation of the Folin-Ciocalteu phenol reagent for the determination of polyphenolic substances in natural waters*. Water Res 17 (1983) 511-525
- [21] Rivas FJ, Beltrán FJ, Álvarez P, Frades J, Gimeno O. *Joint aerobic biodegradation of wastewater from table olive manufacturing industries and urban wastewater*. Bioprocess Eng 23 (2000) 283-286
- [22] Lee J, Kim J, Choi W. *Ferrioxalate-polyoxometalate system as a new chemical actinometer*. Environ Sci Technol 41 (2007) 5433-5438
- [23] Gimeno O, Rivas FJ, Beltrán FJ, Carbajo M. *Photocatalytic Ozonation of Winery Wastewaters*. J Agric Food Chem 55 (2007) 9944-9950
- [24] Hellenbrand R, Mantzavinos D, Metcalfe IS, Livingston AG. *Integration of Wet Oxidation and Nanofiltration for Treatment of Recalcitrant Organics in Wastewater*. Ind Eng Chem Res 36 (1997) 5054-5062
- [25] Bailey JE, Ollis DF. *Biochemical engineering fundamentals*. McGraw Hill, New York, 1997

- [26] Renko E, Sirviö H. *Optimal sampling design for a sludge blanket interface settling model*. Water Res 31(1997) 1148-1154.
- [27] Renko E. *Modelling hindered batch settling Part II: A model for computing solids profile of calcium carbonate slurry*. Water SA 24 (1998) 331-336
- [28] Ramalho RS. Tratamiento de aguas residuales. Reverté, Barcelona, 1996

CHAPTER TWELVE

CONCLUSIONS



Palacio de los Condes de la Roca, Badajoz

After the results have been presented, and the specific conclusions of each piece of research have been drawn, the following general conclusions can be inferred.

From the paper one, '*Photocatalytic elimination of aqueous 2-methyl-4-chlorophenoxyacetic acid in the presence of commercial and nitrogen-doped TiO₂*', where the development of N-doped titania for photocatalytic oxidation of MCPA was investigated, it was proved that nitrogen doping enhances the photocatalytic oxidation of the herbicide MCPA if compared to the undoped synthesized titania. An optimum in N doping percentage can be foreseen. Nitrogen organic compound such as urea as doping agent displayed the best results, comparable to triethylamine. Calcination temperature resulted crucial since up to 600°C the undesirable rutile crystalline phase starts to be formed. A mechanistic approach to the process carried out by adding scavengers, reveals the importance of free radicals in MCPA photocatalytic degradation. Specifically, the importance of the formation of the organic radicals derived from the oxidation of adsorbed MCPA in the surface of the photocatalyst.

Paper two was focused on the photocatalytic ozonation of MCPA using commercial TiO₂, Degussa P25 ('*Photocatalytic ozonation of 4-chloro-2-methylphenoxyacetic acid and its reaction intermediate 4-chloro-2-methyl phenol*'). MCPA is easily oxidized by single ozonation or any combination of light, ozone and TiO₂. Due to this fact, photocatalytic ozonation slightly improved the MCPA degradation rate. However, it did lead to a significant mineralization of initial TOC content (maximum observed, 60 %) at acceptable rates. The main intermediate observed in photocatalytic processes of MCPA oxidation was 4-chloro-2-methyl phenol (CMP), which was steadily removed from the media due to its high reactivity with molecular ozone. Although TiO₂ concentration does not affect MCPA removal rate, TOC conversion is dependent on the amount of solid used since TiO₂ is undoubtedly related to its capacity to catalyze the ozonolysis process. Identified intermediates during photocatalytic ozonation were mainly oxygenated species derived from parent compound after losing some of the substituting groups or opening the aromatic ring leading to aliphatic oxygenated compounds. These intermediates did not present appreciable acute toxicity toward *D. parvula* and *C. pipiens* larvae after the oxidation treatment. It was necessary to carry out oxidation trials with high content of MCPA to appreciate acute toxicity at low oxidation times, which was removed as the oxidation proceeded.

Paper three, entitled '*Photocatalytic ozonation of clopyralid, picloram and triclopyr. Kinetics, toxicity and influence of operational parameters*', explores

the use of photocatalytic ozonation, using commercial TiO_2 , Degussa P25, as the oxidation technique in pollutants refractory to single ozonation. Pyridinic herbicides, highly recalcitrant towards ozone, were easily degraded in systems able to produce radical species. The combination of ozone and photocatalysis in this case did considerably enhance herbicide abatement rate and mineralization extent, if compared to moderately refractory compound like MCPA which only presents a notorious synergism effect in mineralization. Similarly to what was observed for MCPA, TOC conversion is not negatively affected by an increase in the initial herbicide concentration in photocatalytic ozonation process. Newly, this fact suggests the development of autocatalytic routes. Although a slight decrease in herbicide removal rate after several reuses was experienced, commercial titania photocatalyst keeps its mineralization activity. Mineralization analysis was accompanied with study of inorganic species release. It was observed that, chlorine immediately accumulates in the reaction media, suggesting that dechlorination is supposed to occur in the first stages of the photocatalytic ozonation process, probably due to the attack of radical species. Toxicity evolution of photocatalytic ozonation process demonstrates the effectiveness of the technology in removing possible toxic intermediates leading to refractory carboxylic acids such as formic, acetic and oxalic.

Photocatalytic ozonation of pyridinic herbicides was further studied in paper four using synthesized nitrogen doped TiO_2 (*Photocatalytic ozonation of pyridine-based herbicides by N-doped titania*). Nitrogen doping improved bare titania photoactivity, appreciating an optimum amount of doping agent. As noticed in the previous work, both herbicide and TOC abatement showed synergistic improvement if compared to photocatalytic oxidation or single ozonation. Concerning to toxicity evolution, photocatalytic ozonation displayed a significant increase at the early stages of the herbicide oxidation. It disappeared when parent herbicides were completely abated, and dechlorination accomplished.

Paper five (*Ozonation, photocatalysis and photocatalytic ozonation of diuron. Intermediates identification*), dealing with the identification of transformation products of processes involving photocatalysis and or ozone, states the similarity of the nature of intermediates during these processes due to the low rate constant of diuron towards molecular ozone. Photocatalytic ozonation does not significantly improve the parent compound removal, since hydroxyl radical produced in single ozonation results enough to degrade the parent compound. However, high TOC removal rates were reached by this system, showing an outstanding synergism in TOC removal (83%). Actually,

high mineralization rates linked to photocatalytic ozonation are due to the high capacity of oxidizing small oxygenated organics, as the analysis of the released organic acid revealed. Regarding intermediates analysis, transformation products derived from ozonation, photocatalysis and photocatalytic ozonation were quite similar since the radical pathway plays an important role in the three systems. However, in processes involving ozone, intermediates maximum formation were observed once diuron was abated, afterwards they were utterly removed. To finish with this piece of research, toxicity evolution to *V. Fischeri* during photocatalytic ozonation showed an increase at the initial oxidation stage (>90%), decreasing thereafter as the reaction progressed. Ozonation displayed a lower ability to decrease the inhibition percentage after reaching the maximum in toxicity, while photocatalysis gradually increased the toxicity to the bacteria.

In a second part of this dissertation, the research was focused on the use of monoperoxysulfate (MPS) as oxidant agent or promoter of radical species. From paper 6, entitled '*Monoperoxysulfate photocatalysis under 365 nm radiation. Direct oxidation and MPS promoted photocatalysis of the herbicide tembotrione*', it is concluded that monoperoxysulfate is a suitable alternative to oxidize organic aqueous pollutants. pH exerts an important effect in MPS oxidation chemistry due to its pK_a 's, being positive the neutral-acidic interval. In relation to photocatalytic oxidation in presence of monoperoxysulfate as promoter, the presence of MPS improved the parent compound and mineralization rates. MPS concentration exerts an important and positive effect in the process.

Heterogeneous decomposition of monoperoxysulfate seems to be an attractive way to generate radicals, as the results of chapter 9 stated ('*Removal of aqueous metazachlor, tembotrione, tritosulfuron and ethofumesate by heterogeneous monoperoxysulfate decomposition on lanthanum-cobalt perovskites*'). Thus, lanthanum-cobalt perovskite has a high activity with unappreciated cobalt leaching at circumneutral pH conditions. However, acidic conditions strongly produce cobalt leaching, a negative aspect for environmental purposes. Basic conditions, negatively affected the monoperoxysulfate decomposition chemistry. So, this technology would only be appropriate in treating effluents with a low content of organic matter and at neutral or slightly basic pH. MPS concentration up to $2 \cdot 10^{-4}$ M and small loads of catalyst were enough to produce decontamination of pollutants at mg L^{-1} level.

The combination of heterogeneous and photocatalytic decomposition of monoperoxysulfate into radicals significantly improves the effect of removal of aqueous organic pollutants. Chapter 10, '*Synergism between monoperoxysulfate and LaCoO₃-TiO₂ photocatalysis for oxidation of herbicides. Operational variables and catalyst characterization assessment*', proves that catalysts based on LaCoO₃-TiO₂, achieves that behavior. A molar ratio LaCoO₃:TiO₂ of 0.1:1 is adequate to reach that goal. Once again, initial monoperoxysulfate concentration is the most influential variable. A maximum mineralization extent of 55% was reached with 10⁻³ M of monoperoxysulfate. Although a complete mineralization is not achieved, phytotoxicity pointed out almost complete disappearance at the end of the process; appreciating that the higher MPS amount used, the faster phytotoxicity decreases.

Photocatalytic processes seem to be an interesting alternative for biological + chemical oxidation processes of Diluted Winery Wastewater (DWW), as shown in Chapter 11, '*Integrated aerobic biological-chemical treatment of winery wastewater diluted with urban wastewater. LED based photocatalysis in the presence of monoperoxysulfate*'. This piece of research also highlights the direct conversion of TOC to CO₂ during biological oxidation treatment. Among the chemical processes tested, based on LEDs, MPS and photocatalysis, the photocatalytic decomposition of MPS on LaCoO₃-TiO₂ composite attained the best results (95% in UVA/MPS/LaCoO₃-TiO₂ system). An increase in the initial MPS concentration exerts a positive effect until reach an optimum value (10⁻² M), after what it slightly starts to be negative. Concurrently, working at basic pH conditions results negative due to the dissociation of HSO₅⁻ into SO₅²⁻.